The Role of NRAS in Acute Myeloid Leukaemia

Thesis submitted in accordance with the requirements of the University of Liverpool for the degree of Doctor in Philosophy

By

Fiona Marie Healy

Declaration

I declare that this thesis has been written solely by myself and that it has not been submitted, in whole or in part, in any previous application for a degree. Except where states otherwise the work presented is entirely my own. The work was carried out under the supervision of Prof. David MacEwan and Dr. John Woolley.

This PhD has been carried out between September 2019-September 2023. This encompassed the COVID-19 pandemic, resulting in some laboratory access limitations due to lockdowns and short periods of self-isolation.

Fiona Healy

September 2023

Abstract

Acute Myeloid Leukaemia (AML) is a highly heterogenous blood cancer, caused by sustained proliferation of immature myeloid blast cells. Prognosis is poor, particularly in older patients, who comprise the majority of cases. Frontline chemotherapy regimens comprise cytarabine and daunorubicin, followed by stem cell transplant. However, relapse is common, and transplants are not suitable for elderly patients. Thus, it is crucial to understand and develop specific therapeutics against leukaemic drivers, to reduce toxicity and relapse potential. This includes the successful use of FLT3 inhibitors including FDA-approved Gilteritinib, and Quizartinib, currently in Phase III clinical trials. However, resistance is emerging against these inhibitors, and has previously been somewhat attributed to NRAS mutations, amongst others. Mutations within the Ras superfamily of proteins are often highly oncogenic, and NRAS mutations acting as a leukaemic driver in approximately 10% of *de novo* AML patients, and increases following relapse. Thus, it is crucial to understand the risk individual NRAS mutations pose, particularly following relapse, to ultimately ameliorate this risk. This thesis explores three common AML-relevant NRAS mutations, namely G12C, G12D and Q61K, and also NRAS wild-type. Using *in vitro* overexpression and gene editing techniques, effects of these NRAS mutants were studied at a genotypic and phenotypic level. Whilst all mutants conferred a proliferative advantage and increased leukaemogenic capacity in AML, there were differences seen in the pathways underpinning these, as well as the effects that each of these mutants have on drug sensitivity. Indeed, NRAS Q61K over-expression appeared to convey the greatest level of drug resistance. Overall, this work gives a novel perspective on the importance of NRAS mutations in AML, and identifies potential therapeutic avenues for future AML patients, as a means of improving prognosis.

Acknowledgements

There are countless people I wish to thank for getting me through this journey, who have supported me no matter how difficult things got. These include the people thanked below, and so many more.

Firstly, I would like to thank my supervisor, Prof Dave MacEwan. Thank you, Dave, for your support throughout my studies, from a second-year undergraduate to a final-year PhD student. I've loved being a part of the MacEwan lab, and have learned so much. You've always put a positive spin on the most negative of results, and supported me in my ventures even when things aren't going to plan. You've given me the freedom to explore so many avenues of research, and seize fantastic opportunities and embrace challenges within our lab and beyond.

I would also like to thank my secondary supervisor, Dr John Woolley. Thank you for your help, support and guidance with the various research projects you've enabled me to be a part of. I've loved exploring projects beyond the scope of my own, whilst having the support and backing to bring in my own work and ideas to everything we've done.

I also wish to thank the Institute of Translational Medicine at the University of Liverpool, who have funded my PhD. It has been fantastic to pursue this line of research for the last four years, and I am extremely grateful for the opportunity to have done this.

Dr Vanessa Marensi has been a huge support to me throughout my PhD, inspiring me to keep pursuing ideas and 'tell the story'. Thank you, Vanessa, for pushing me and challenging me to think about what the data means, and how we can do things together to get a paper out there! Your dedication and work ethic are inspiring, and your kindness and support both personally and professionally has meant so much throughout the years.

To all my lab colleagues, thank you for your constant words of empathy and care. The MacEwan lab has always been a great place to work, full of passion for what we do. My fellow lab PhD students past and present, Taha, Fatma, Hamdah, Seham, Nisa and Srishti, – it's been wonderful to share in this journey with you! To our wider lab – Emma, James, Paul, Lekh, Medina, Francisca and all of the first floor past and present – whether we're solving problems over a cup of tea or putting the world to rights over a Friday drink, your friendship and support has meant so much throughout all of this.

Thank you to my incredible support network outside of the lab too. Ash, you have kept me sane, smiling and encouraged for even the smallest achievement, keeping me going for the final push to the end. Lucy, Alice, Jess and Gloria – you have always listened to my many lab tales from an outside view and always provided a much-appreciated distraction when required!

Finally, thank you especially to my parents, my brother Connor, my grandparents and my extended family. You have always been so supportive and caring throughout my entire PhD – from the joys of the successes to the stresses of failures and back again. Your faith in me that I could reach the end of this has carried me through, and I couldn't have done it without your unending encouragement, kindness and love. Thank you for everything, always.

Some of the work in this thesis has been previously published in the following publications:

Healy FM, Prior IA, & MacEwan DJ (2022). The importance of Ras in drug resistance in cancer. British Journal of Pharmacology 179: 2844-2867 [Review].

Griffin JM, **Healy FM**, Dahal LN, Floisand Y, & Woolley JF (2022). Worked to the bone: antibody-based conditioning as the future of transplant biology. J Hematol Oncol 15: 65. [Review]

Table of Contents

Declaration 1
Abstract 2
Acknowledgements 3
Some of the work in this thesis has been previously published in the following publications: 4
Table of Contents 5
List of Tables 10
List of Figures 11
Abbreviations 16
1 Introduction 21
1.1 Haematopoiesis 21
1.1.1 Haematopoietic stem cells and the bone marrow niche 22
1.1.2 Clonal haematopoiesis 24
1.2 Acute Myeloid Leukaemia (AML) 27
1.2.1 AML Mutational Signature 28
1.2.2 Classifying AML 29
1.2.3 The AML Niche 33
1.2.4 Current Therapeutic Options for AML 34
1.3 Drug Resistance 37
1.3.1 Cancer Stem Cells 38
1.3.2 Leukaemic Stem Cells 39
1.3.3 Drug-Resistant AML 40
1.4 The Ras Superfamily 44
1.4.1 The Structure of Ras 44
1.4.2 Ras Trafficking 47
1.4.3 Oncogenic Ras 48
1.4.4 Targeting Oncogenic Ras Therapeutically 49
1.4.5 Ras in AML 55
1.4.5.1 Ras in AML Drug Resistance 57
1.5 Gene Editing 59
1.5.1 Mega-nucleases 60
1.5.2 Zinc Finger Nucleases (ZFNs) 60
1.5.3 Transcription Activator-Like Effector Nucleases (TALENs) 61
1.5.4 Clustered Regularly Interspaced Palindromic Repeats (CRISPR) 61
1.5.5 Therapeutic Gene Editing 63
1.6 Thesis Hypothesis and Aims 64
2 Materials and Methods 67
2.1 Buffers 67
2.2 Purchased Reagents and Kits 69
2.3 Cell lines 72

2.4 Antibodies 74
2.5 Plasmids 76
2.6 Cell Culture 77
2.7 Cryopreservation of cells 78
2.8 Preparation of Competent *E. coli* Cells 78
2.9 Ligation 79
2.10 Transformation and Purification of Plasmids 79
2.11 Restriction Digest 80
2.12 Polymerase Chain Reaction 80
2.13 Agarose Gel Electrophoresis 81
2.14 Gel Extraction/PCR Clean-up 82
2.15 Transient Transfection 82
2.16 CRISPR-Cas9 Gene Editing – *NRAS* Gene Knock-out 83
2.17 CRISPR-Cas9 Gene Editing – NRAS G12D Mutation Reversal 83
2.18 Generation and Concentration of Lentivirus 85
2.19 Lentiviral Transduction 86
2.20 Selection of Transduced Cells 86
2.21 Sorting of GFP+ Transduced Cells 87
2.22 Subcloning of Transduced cell lines 87
2.23 Western Immunoblotting 88
2.24 Ras Activity Assay 89
2.25 Cytotoxicity Assays 89
2.26 Colony Forming Assays 90
2.27 Cell Proliferation Assay – Trypan Blue 90
2.28 Cell Proliferation Assay – Carboxyfluorescein Succinimidyl Ester (CFSE) 91
2.29 Cell Cycle Analysis – 7-Aminoactinomycin D (7AAD) Staining 91
2.30 Quantitative PCR 92
2.31 Immunofluorescence 92
2.32 Cell Surface Staining 93
2.33 RNA Extraction and Quality Check 94
2.34 Genomic DNA Extraction 94
2.35 Transcriptomic Analysis by RNASeq 95
2.35.1 Quality Control and Gene Expression Quantification 95
2.35.2 Differential Expression and Functional Analysis 96
2.36 Statistical Analysis 97
3 Characterisation of NRAS in Cell Lines 99
3.1 Introduction 99
3.2 Aims and Hypothesis 100
3.3 Results 101

3.3.1 *NRAS* Genotype in AML cell lines 101
3.3.2 Ras transcript abundance in AML Cell Lines 105
3.3.3 Ras-Mediated Signalling in AML Cell Lines 107
3.3.4 Pharmacological Inhibition of Ras-mediated signalling in wild-type and drug-resistant cell lines 110
3.3.5 Over-expression of NRAS Mutants *in vitro* 113
3.3.5.1 Construct Generation 113
3.3.5.2 Phenotypic Effects of NRAS Mutant Over-expression in Healthy and Cancerous Contexts 117
3.3.5.3. Signalling Alterations of NRAS Mutant Over-expression in Healthy and Cancerous Contexts 119
3.3.6 CRISPR-Cas9-mediated Knock-out of NRAS in a Healthy and Cancerous Context 120
3.3.6.1 Component Generation 120
3.3.6.2 Confirmation of Gene Editing 125
3.3.6.3. Phenotypic Effects of CRISPR-Cas9-Mediated *NRAS* Knock-Out 127
3.4 Discussion 129
4 Using CRISPR-Cas9 to Revert Drug-Induced Mutations 134
4.1 Introduction 134
4.2 Aims and Hypothesis: 136
4.3 Results: 139
4.3.1 Generation of Cas9-expressing cell lines 139
4.3.1.1 Optimisation of a lentiviral transduction protocol in haematopoietic cell lines: 139
4.3.1.2 Transduction of AML cell lines 146
4.3.1.3 Validation of Inducible Cas9 expression 146
4.3.1.4 Optimisation of Doxycycline-Mediated Induction 148
4.3.1.5 Establishing a pure population of inducible Cas9-expressing cells 149
4.3.2 CRISPR-Mediated Editing of NRAS G12D 150
4.3.2.1 Generation of CRISPR Component Vectors 150
4.3.2.2 Transduction of CRISPR Components into MV4-11-DR 156
4.3.2.3 Sorting of Transduced Cells 157
4.3.2.4 Identification of Mutated Cells by PCR 158
4.3.2.5 Identification of Mutated Cells by qPCR 160
4.3.2.6 Sequencing of Transduced Clones 161
4.4 Discussion 162
5 Effects of NRAS Overexpression in Acute Myeloid Leukaemia 165
5.1 Introduction: 165
5.2 Aims and Hypothesis: 166
5.3. Results 167
5.3.1 Generation of NRAS over-expressing cell lines 167

5.3.2 Proliferative Potential 169
5.3.3 Cell cycle analysis 172
5.3.4 Colony Forming Potential 173
5.3.5 Drug Sensitivity 175
5.3.6 Signalling Alterations 179
5.3.6 Detecting Transcriptomic Alterations 181
5.3.6.1 Quality Control of RNASeq Samples 181
5.3.7.2 Identification of Global Transcriptomic Profile Alterations 182
5.3.6.3 Identification of AML Transcriptomic Profile Alterations 185
5.3.6.4 Identification of Most Altered Genes 186
5.3.6.5 Identification of Altered Pathways by Transcriptomics 192
5.3.6.6 NRAS-mediated Haematopoietic Alterations 197
5.4 Discussion 209
6. Discussion 212
6.1 Genotype Heterogeneity in NRAS-mediated AML 212
6.2 Differential NRAS Expression 217
6.3 NRAS-Mediated Signalling Pathway Alterations 220
6.3.1 Ras Signalling in a Transiently Transfectable Context 220
6.3.2 Ras Signalling in AML 221
6.4 NRAS-Mediated Proliferation 226
6.5 NRAS-mediated Cell Cycling 229
6.6 NRAS-mediated Colony Forming Potential 231
6.7 Impacts of NRAS mutants on haematopoiesis 233
6.8 Effects of NRAS over-expression on oxidative phosphorylation 235
6.9 Intracellular Localisation of NRAS Mutants 238
6.10 The AML Therapeutic Landscape 238
6.11 Ras-targeting therapeutics 249
6.12 The Future for NRAS Therapeutics in AML – Potential Novel Targets 253
6.13 Novel Direct Ras-Targeting Therapeutics 255
6.14 Methodological Limitations 256
6.14.1 Lentiviral Component delivery 256
6.14.2 *In vitro* NRAS over-expression 258
6.14.3 *In vitro NRAS* knock-out 260
6.14.4 Inducible Cas9 262
6.14.5 Promoter selection 264
6.14.6 Guide RNA sequences 264
6.14.7 Promoting homology directed repair 265
6.14.8 Puromycin selection 269
6.14.9 Subcloning of mutated cells 270

6.14.10 Identification of successfully edited clones 272
6.14.11 Identification of pathway alterations by Western immunoblotting 273
6.14.12 Understanding stemness potential 275
6.14.13 Modelling the true leukaemic context 276
6.15 Final conclusions 277
Appendices 279
Appendix 1 pLJM1-EGFP plasmid purchased via AddGene (Cat. No. 19319). 280
Appendix 2 Lenti-CRISPR-V2 plasmid purchased via AddGene (Cat. No. 52961). 281
Appendix 3 pCW-Cas9 plasmid purchased via AddGene (Cat. No. 50661). 282
Appendix 4 psPax2 plasmid purchased via AddGene (Cat No. 12260) 283
Appendix 5 pMD2.G plasmid purchased via AddGene (Cat. No. 12259) 284
Appendix 6 LeGo-iG plasmid purchased via AddGene (Cat. No. 27358) 285
Appendix 7 Model flow cytometry plot indicating approximate gating for apoptosis (Appendix 7B) and cell cycle staging (Appendix 7C). 286
Appendix 8 Transcriptomic Alterations in AML-relevant pathways in NRAS over-expression models 287
Appendix 9 Alterations to Oxidative Phosphorylation. 296
Appendix 10. Alterations to cell NRAS trafficking. 298
Bibliography 299

List of Tables

Table 1.1. The French-American-British (FAB) AML classification system

Table 2.1. Components and purposes of key buffers used throughout this thesis

Table 2.2. Details and purposes of key kits used throughout this thesis

Table 2.3. Overview of parental cell lines used and relevant mutational statuses.

Table 2.4. Antibodies used in Western blotting.

Table 2.5. Plasmid backbones purchased via AddGene used throughout experiments detailed in this thesis.

Table 3.1 *NRAS* hotspot mutations genotyping primers.

Table 3.2. Ras isoform quantitative PCR primers.

Table 3.3. *NRAS* overlap mutation and pLJM1 cloning primers.

Table 3.4. Guide sequences targeting *NRAS.*

Table 3.5. *NRAS* knock-out screening primers.

Table 4.1. IC_{50} Values following 96 h Puromycin treatment in AML cell lines.

Table 4.2. HDR Template, guides and primers used for LeGo-iG Vector Cloning

Table 5.1. 48 h IC_{50} values (µM) of NRAS variant cell lines to AML-relevant small molecule therapeutics.

Table 5.2. Most altered cancer-associated gene expression in each over-expression cell line, compared to control cells.

Table 5.3. Primer sequences used to amplify common genes with modulated expression in at least two over-expression cell lines.

List of Figures

Figure 1.1. The haematopoietic system.

Figure 1.2. The heterogeneity of AML.

Figure 1.3. European Leukaemia Network (ELN) strategy for AML classification.

Figure 1.4. 5-year Overall Survival of AML patients with varying mutational backgrounds.

Figure 1.5. Leukaemogenesis.

Figure 1.6. Generalised schematic of the subclonal mutation-driven drug resistance phenotype.

Figure 1.7. 2D and 3D representation of Ras structure.

Figure 1.8. Ras activation cycle.

Figure 1.9. Key pathways controlled by Ras.

Figure 1.10. Post-translational modifications within Ras isoforms.

Figure 1.11. Key pharmacological agents targeting Ras-mediated pathways.

Figure 1.12. Distribution of point mutations occurring in KRAS, NRAS and HRAS across a multitude of cancers.

Figure 1.13. Distribution of NRAS mutants in AML.

Figure 1.14. Kaplan-Meier plot of AML patient overall survival.

Figure 1.15. Variant Allele Frequency (%) of NRAS-mutant patients with regards to treatment outcome.

Figure 2.1. Workflow of RNASeq analysis.

Figure 3.1 Genomic locations of primers used to genotype *NRAS* mutational hotspots.

Figure 3.2. *NRAS* Genotype in AML cell lines.

Figure 3.3. *KRAS* Genotype in AML cell lines.

Figure 3.4. *NRAS* isoform transcript abundance in parental and FLT3 inhibitor resistant cell lines.
Figure 3.5. Ras isoform protein expression in MOLM-13 and MV4-11 parental and FLT3-inhibitor resistant cell lines.
Figure 3.6. Signalling within FLT3-ITD+ AML cell lines, both parental and FLT3-inhibitor resistant (DR).
Figure 3.7. NRAS activation in FLT3-ITD+ AML cell lines, both parental and FLT3-inhibitor resistant (DR).
Figure 3.8. Sensitivity of FLT3-ITD+ cell lines towards numerous Ras pathway targeting agents and AML therapeutics.
Figure 3.9. Schematic of cloning steps required to generate NRAS wild-type and mutant over-expression plasmids.
Figure 3.10. Stepwise process of mutation generation from NRAS wild-type cDNA.
Figure 3.11. Sanger sequencing alignment of NRAS-mutated cDNA, cloned into the pLJM1 vector for over-expression in cell lines.
Figure 3.12. Proliferation rate of transient NRAS over-expressing cell lines
Figure 3.13. Signalling alterations in HEK293T cells when differing NRAS mutants are over-expressed.
Figure 3.14. Guide design and creation of delivery vector for generation of CRISPR-mediated *NRAS* knockout.
Figure 3.15. Sequence alignment of successfully cloned guides into the LentiCRISPR-V2 vector.
Figure 3.16. Validation of *NRAS* knock-out in transiently transfected HEK293T cells.
Figure 3.17. Proliferation curves following *NRAS* knock-out.

Figure 3.18. Key signalling dynamics altered by knockout of *NRAS* in HEK293T cells.
Figure 4.1. Transduction of EGFP-encoding lentivirus into a range of AML cell lines.
Figure 4.2. HEK293T cells transduced with inducible-Cas9-encoding lentivirus.
Figure 4.3. Sensitivity of MV4-11-DR cells to doxycycline.
Figure 4.4. Sensitivity of AML cell lines to puromycin.
Figure 4.5. MV4-11-DR cell viability following transduction with Cas9-encoding lentivirus and puromycin selection.
Figure 4.6. Confirmation of inducible Cas9-expression in a mixed pool of MV4-11-DR cells.
Figure 4.7. Titration of doxycycline to maximally induce Cas9 expression in a mixed pool of lentivirally transduced, puromycin-selected MV4-11-DR cells.
Figure 4.8. Subcloning of inducible Cas9 expressing MV4-11-DR cells.
Figure 4.9. Design of the CRISPR-Cas9 HDR template.
Figure 4.10. Workflow of HDR Template Cloning into LeGo-iG backbone.
Figure 4.11. Percentage GFP+ cells within the transduced MV4-11-DR inducible Cas9 population.
Figure 4.12. FACS plots following GFP-selection of control-transduced and HDR-transduced MV4-11-DR, inducible Cas9 cells.
Figure 4.13. Subcloning images at 7- and 14-days post-plating of LeGo-iG Ctrl and LeGo-iG-G5-HDR lentivirally transduced and GFP-sorted MV4-11-DR inducible Cas9 cells.
Figure 4.14. Basic PCR Screen of subcloned LeGo-iG-G5-HDR lentivirally transduced MV4-11-DR inducible Cas9 cells.

Figure 4.15. Quantitative PCR of the genomic *NRAS* DNA from a subset of the clones grown from the HDR-transduced, GFP+ selected MV4-11-DR inducible Cas9 cells.
Figure 4.16. Sequencing alignment of a subset of the clones grown from the HDR-transduced, GFP+ selected cells.
Figure 5.1. Generation and subcloning of NRAS wild-type and mutant over-expressing MOLM-13 cells.
Figure 5.2. Proliferative capacity of NRAS-mutant over-expressing cell lines.
Figure 5.3. Cell cycle analysis of MOLM-13 NRAS over-expressing cell lines.
Figure 5.4. Colony-forming potential of MOLM-13 NRAS-mutant over-expressing cell lines.
Figure 5.5. Sensitivity of MOLM-13 NRAS-over-expressing cell lines to relevant small molecule AML therapeutics.
Figure 5.6. FLT3 activation and expression in MOLM-13 NRAS-over-expressing cell lines, as determined by Western blotting.
Figure 5.7. Protein level alterations in MOLM-13-NRAS over-expressing cells.
Figure 5.8. Overall differential gene expression in MOLM-13 NRAS-over-expressing cell lines.
Figure 5.9. Distribution of up- and down-regulated genes in MOLM-13 NRAS over-expressing cell lines.
Figure 5.10. Dysregulated genes associated with AML in MOLM-13 NRAS-over-expressing cell lines.
Figure 5.11. Quantitative PCR validation of up- and downregulated genes identified by RNASeq.

Figure 5.12. Key cellular features and pathways most altered in NRAS-over-expressing cell lines, compared to parental MOLM-13 cells.
Figure 5.13. Analysis of the haematopoiesis and stemness associated pathways within MOLM-13-NRAS over-expressing cells.
Figure 5.14. KEGG Pathway Analysis of the Haematopoietic Cell Lineage in MOLM-13 NRAS-overexpressing cell lines.
Figure 5.15. Analysis of the haematopoietic stem cell markers within MOLM-13-NRAS over-expressing cells.
Figure 5.16. Gene expression level changes in the common HSC-associated signature, as determined by RNASeq data.
Figure 5.17. CD34 Expression in MOLM-13 NRAS-Over-expressing cell lines.
Figure 5.18. LSC17 Score Gene Expression in MOLM-13 NRAS-Over-expressing cell lines.

Abbreviations

ALL	Acute Lymphocytic Leukaemia
AML	Acute Myeloid Leukaemia
ARCH	Age-Related Clonal Haematopoiesis
ATRA	All Trans Retinoic Acid
BL1/3-A	Blue Laser 1/3-Area
BP	Base Pairs
cAMP	Cyclic AMP
CAR	Chimeric Antigen Receptor
CD	Cluster of Differentiation
CDK	Cyclin Dependent Kinase
CDS	Coding Domain Sequence
CHIP	Clonal Haematopoiesis of Indeterminate Potential
CHOP	Clonal Haematopoiesis of Oncogenic Potential
CIR	Cumulative Incidence of Relapse
CLL	Chronic Lymphocytic Leukaemia
CML	Chronic Myeloid Leukaemia
CR	Complete Remission
CRISPR	Clustered Regularly Interspaced Palindromic Repeats
CXCL	Chemokine (CXC) Motif Ligand
DAPI	4',6-Diamidino-2-Phenylindole, Dilactate
DHODH	Dihydroorotate dehydrogenase
DMEM	Dulbecco's Minimum Essential Media
DMSO	Dimethyl Sulfoxide

DNA	Deoxyribonucleic Acid
DSB	Double-Stranded Break
EDTA	Ethylenediaminetetraacetic acid
ELN	European Leukaemia Network
EMA	European Medicines Agency
ER	Endoplasmic Reticulum
ERK	Extracellular Regulated Kinase
FAB	French-American-British
FACS	Fluorescence Associated Cell Sorting
FBS	Foetal Bovine Serum
FDA	Food and Drug Administration
FITC	Fluorescein Isothiocyanate
FLT3	Fms-Like Receptor Tyrosine Kinase 3
FPKM	Fragments Per Kilobase of transcript per Million mapped reads
FSC-A	Forward Scatter (Area)
GFP	Green Fluorescent Protein
HDR	Homology Directed Repair
HPV	Human Papilloma Virus
HR	Hazard Ratio
HRAS	Harvey Rat-Associated Sarcoma
HRP	Horseradish Peroxidase
HSC	Haematopoietic stem cell
HSCT	Haematopoietic stem cell transplant
iPSC	Induced Pluripotent Stem Cell
IRES	Internal Ribosome Entry Site

ITD	Internal Tandem Duplication
KEGG	Kyoto Encyclopaedia of Genes and Genomes
KRAS	Kirsten Rat-Associated Sarcoma
LT-HSC	Long Term Haematopoietic Stem Cell
mAb	Monoclonal Antibody
MAPK	Mitogen Activated Protein Kinase
MDS	Myelodysplastic Syndrome
MEK	Mitogen Activated ERK Kinase
MPN	Myeloproliferative Neoplasm
mTOR	Mammalian Target of Rapamycin
NHEJ	Non-Homologous End Joining
NK Cells	Natural Killer Cells
NRAS	Neuroblastoma Rat-Associated Sarcoma
NSCLC	Non-Small Cell Lung Cancer
OS	Overall Survival
PCR	Polymerase Chain Reaction
PEI	Linear polyethyleneimine hydrochloride
PI	Propidium Iodide
PI3K	Phosphatidylinositol Kinase 3
PKC	Protein Kinase C
PTEN	Phosphatase and tensin homolog
qPCR	Quantitative Polymerase Chain Reaction
RARA/α	Retinoic Acid Receptor Alpha
RBD	Ras Binding Domain
RNA	Ribonucleic acid

RPMI-1640	Roswell Park Memorial Institute-1640
SII-P	Switch II Pocket
SCF	Stem cell factor
SDS	Sodium Dodecyl Sulfate
SEER Programme	Surveillance, Epidemiology, and End Results Programme
SOS	Son of Sevenless
SSC-A	Side Scatter (Area)
TAE	Tris-Acetate-EDTA
TALEN	Transcription Activator-Like Effector Nucleases
WGS	Whole Genome Sequencing
WHO	World Health Organisation
WT	Wild Type
ZFN	Zinc Finger Nucleases

Chapter 1

Introduction

1 Introduction

1.1 Haematopoiesis

The development and maintenance of the blood system is known as haematopoiesis. This occurs very early in embryonic development, and is maintained throughout an individual's lifetime. There are two key waves of haematopoiesis: primitive and definitive. Cell type development as well as gene expression are largely used to differentiate these two waves, as does the point in a lifetime. Typically, only the myeloid compartment arises in the primitive wave (which can then further differentiate into the erythroid lineage), with the definitive wave giving rise to both the lymphoid and myeloid lineages (Jagannathan-Bogdan & Zon, 2013). The two waves can be differentiated from each other by also considering gene expression: *RUNX1* expression is a key marker of definitive haematopoiesis, whereas *GATA2* expression typically signifies primitive (Bertrand & Traver, 2009; Jagannathan-Bogdan & Zon, 2013). The blood system originates from mesoderm tissue initially, with haemangioblasts forming as a result of the expression of genes including *GATA1.* These have very little pluripotency, and are considered pre-cursors for both endothelial cells and haematopoietic stem cells (HSCs). HSCs, by contrast, are considerably more pluripotent. These are considered as the basis of the haematopoietic system, since the myeloid and lymphoid lineages (and all cells within these, Figure 1.1) typically originate from HSCs. Expression of the transcription factor *PU.1* typically drives myeloid lineage differentiation, with factors such as *TRIM33* driving erythroid cell differentiation, from common myeloid progenitor cells (Jagannathan-Bogdan & Zon, 2013). This process is detailed in Figure 1.1.

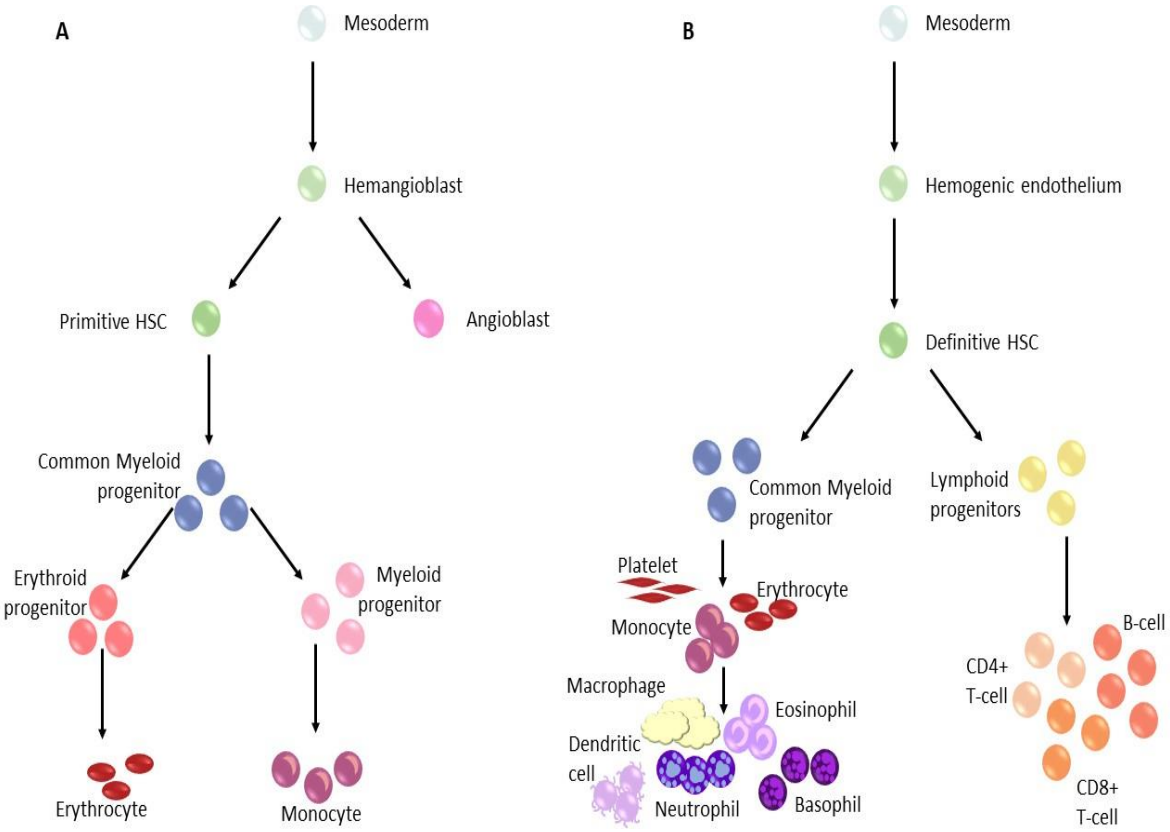

Figure 1.1. The haematopoietic system. A) The primitive haematopoietic system. The blood system originates from mesodermal cells, which develop into a (relatively) small pool of haemangioblasts and subsequently haematopoietic stem cells or angioblasts. Haematopoietic stem cells then have the capacity to further differentiate into myeloid progenitor cells, and eventually constitute the myeloid and erythroid compartments. **B) The definitive haematopoietic system.** Hemogenic endothelial cells are formed from mesodermal cells, with subsequent haematopoietic stem cells able to differentiate into the two key lineages of the haematopoietic system, the myeloid and lymphoid lineages. Further differentiation then occurs within these lineages, to constitute the conventional, diverse haematopoietic system. *Adapted from Jagannathan-Bogdan and Zon, 2013.*

1.1.1 Haematopoietic stem cells and the bone marrow niche

Haematopoietic stem cells have a unique expansion self-renewal capacity, regulated by three key factors: the bone marrow niche and the Notch and Wnt signalling pathways. The bone marrow is typically where the bulk of adult, mammalian haematopoiesis occurs, and is the most widely studied haematopoietic niche. This is

supported by key cytokines such as Chemokine (C-X-C motif) Ligands 4 and 12 (CXCL4, CXCL12), Stem Cell Factor (SCF) and pleiotropin (Griffin, Healy, Dahal, Floisand & Woolley, 2022). Nevertheless, cell type and cytokine abundances vary considerably throughout the bone marrow, and it has been proposed that this generates particular regions to favour and support development and maturation of individual haematopoietic components. For example, myeloid-biased HSCs typically cluster around the megakaryocyte-rich and sinusoidal regions of the bone marrow, whereas lymphoid-biased HSCs cluster in the arteriole regions (Pinho, Marchand, Yang, Wei, Nerlov & Frenette, 2018; Wu, Zhang & Lucas, 2021).

Over time, as the bone marrow niche ages, it becomes less able to support the development and maintenance of the 'standard' HSC (Matteini, Mulaw & Florian, 2021). Instead, whilst the overall HSC population may expand, the likelihood of lineage commitment is altered due to a complex rewiring of multiple stem-associated pathways (Florian et al., 2013). In this way, the myeloid lineage is generally favoured, thereby reducing the probability of a healthy, balanced immune system to continue to develop. This has been shown to be due to the exhaustion and ageing of the bone marrow niche itself, rather than the HSC capacity, since transplantation of HSCs from aged mice into younger mice (with a younger bone marrow niche) improves the function of the HSC. In contrast, re-transplantation of these improved HSCs back into aged mice causes a decrease in function (Guidi, Marka, Sakk, Zheng, Florian & Geiger, 2021; Kuribayashi et al., 2020). This favouring of the myeloid lineage also in part explains the higher incidence of myeloid leukaemias, rather than lymphocytic, amongst the elderly population. This will be further discussed in section 1.2.

The Notch signalling pathway plays a key role in regulating the self-renewal capacity of HSCs, and is typically associated with lymphoid lineage differentiation (Ge, Wang, Zhang, Li, Ye & Jin, 2022). In the haematopoietic context, Notch1 signalling is regulated through the DLL4 and Jagged1 ligands (Gama-Norton et al., 2015). Indeed, this signalling primarily occurs within the arteriolar regions, thereby providing further evidence to the role of the microenvironment in cell lineage fate determination and subsequent differentiation, as discussed above (Gama-Norton et al., 2015; Wu, Zhang & Lucas, 2021).

The Wnt signalling pathway is most involved in T cell differentiation of all differentiation pathways, however has some key roles in both HSC maintenance and myeloid development too (Luis, Ichii, Brugman, Kincade & Staal, 2012; Staal, Chhatta & Mikkers, 2016). The expression level and subsequent activity of β-catenin regulated through Wnt signalling appears to influence the stemness capacity of HSCs, with a sweet-spot apparent between an increase in stemness capacity and stemness arrest seeming apparent (Famili, Naber, Vloemans, de Haas, Tiemessen & Staal, 2015). This correlates with an increase in leukaemogenic capability and relapse risk when β-catenin levels are increased, a concept which is currently being investigated as a pharmacological target and will be further addressed in section 1.4.4 (Koury, Zhong & Hao, 2017).

1.1.2 Clonal haematopoiesis

Clonal haematopoiesis is the expansion of a population of haematopoietic cells which contain one or more somatic mutations (Bowman, Busque & Levine, 2018). This

concept is commonly considered in older individuals, as the size of the haematopoietic pool decreases. Whilst clonal haematopoiesis is not considered a disease in itself, it is largely associated as a pre-cursor for both haematological malignancies and cardiovascular disease, and has also been tentatively associated with a host of other diseases and disorders, including Alzheimer's disease, schizophrenia and diabetes (Bowman, Busque & Levine, 2018; Dumanski et al., 2016; Hirata et al., 2018; Jaiswal et al., 2014; Loftfield et al., 2018; Silver, Bick & Savona, 2021).

As previously discussed in section 1.1.1, haematopoiesis originated from the HSCs. These cells divide either in an asymmetrical fashion, resulting in one progenitor cell and one HSC, or in a symmetrical fashion, producing either two HSCs or two progenitor cells. Should the two progenitor cells be produced, the clonal potential of the cell is arrested, since the progenitor becomes more lineage committed and have less potential for further acquisition of mutations. Therefore, there becomes a pool of mutations within HSC compartment, some of which may confer a proliferative advantage. If this is the case, HSCs with this mutation will form a more dominant clone (Fuster, 2022), increasing the likelihood of lineage-committed progenitors arising from these proliferatively-advantageous-mutated HSCs, thereby increasing potential for abnormal haematopoiesis and oncogenic risk.

Clonal haematopoiesis can involve a range of mutations, including mosaicism and large-scale alterations of chromosomes, loss of heterozygosity and the acquisition of point mutations (single nucleotide variants) (Loftfield et al., 2018; Silver, Bick & Savona, 2021). Whilst loss of heterozygosity is most commonly seen in men, with the loss of the Y chromosome (occurring in approximately 40% of all men with clonal

haematopoiesis over the age of 70) (Silver, Bick & Savona, 2021; Thompson et al., 2019), the concept of clonal haematopoiesis was first discovered through a loss of heterozygosity in women. A 1996 study recognised a larger proportion of women over the age of 60 displaying an imbalance of X chromosome inactivation, than in those aged less than 60 (where almost no patients had such an imbalance) (Bowman, Busque & Levine, 2018; Busque et al., 1996; Silver, Bick & Savona, 2021). This loss of heterozygosity is typically, but not exclusively, associated with lymphoid lineage disorders (Niroula et al., 2021). This can result in changes in the expression of cell cycle-associated genes, DNA damage response genes and apoptotic genes, hence its association with an increased cancer susceptibility (Silver, Bick & Savona, 2021; Wright et al., 2017). Subsequent improvements in sequencing sensitivity has permitted better elucidation of the single nucleotide variant aspect of clonal haematopoiesis, with a contributing mutation now equating to that which has a variant allele frequency of ≥2% (Bowman, Busque & Levine, 2018). Clonal haematopoiesis in regards to single nucleotide variants is referred to as Clonal Haematopoiesis of Indeterminate Potential (CHIP). However, not all cases of CHIP will lead to cancer, and therefore the newer term Clonal Haematopoiesis of Oncogenic Potential (CHOP) has been coined to better identify individual subsets of clonal haematopoiesis (Valent et al., 2019).

The mutational signature of clonal haematopoiesis, and more-so CHOP, is similar to that found in myeloid malignancies including Acute Myeloid Leukaemia (AML), hence its consideration as a precursor for AML, myelodysplastic syndrome (MDS) and myeloproliferative neoplasms (MPNs), amongst others. However, a key feature of clonal haematopoiesis is the acquisition of these mutations over time. For example, *DNMT3A* and *JAK2* mutations have been shown to occur whilst the individual is aged

between 30 and 50, whilst other mutations such as *U2AF1* occur later, when the individual is in their 60s (Jaiswal & Ebert, 2019).

A person's increasing age typically predisposes them to acquisition of more mutations, which can eventually develop into a malignancy. This is often referred to as Age-Related Clonal Haematopoiesis (ARCH) (Jaiswal & Ebert, 2019; Jaiswal et al., 2014; Midic et al., 2020). ARCH does not purely drive leukaemia through the accrual of mutated genes to create the bulk of immature AML blast cells, it can also affect the development and capability of the immune system, including B and T cells (Shlush, 2018; Young, Challen, Birmann & Druley, 2016). This may cause a reduced level of immune surveillance and function with regards to the accumulation and detection of altered haematopoietic cells, which a 'younger' immune system may be able to eliminate.

1.2 Acute Myeloid Leukaemia (AML)

Acute Myeloid Leukaemia (AML) involves the clonal expansion of immature myeloid blasts, carrying certain mutations (Short, Rytting & Cortes, 2018). It is the most common type of acute adult leukaemia (Howlader, 2019; Shallis, Wang, Davidoff, Ma & Zeidan, 2019). The majority of diagnoses occur in those aged over 65, with over 30 cases per 100,000 people aged 75 and above in 2019 (Howlader, 2019). This is in part due to the fact that the diversity of the haematopoietic system decreases with advancing age. Though the Surveillance, Epidemiology, and End Results Program (SEER) database showed Chronic Lymphoid Leukaemia (CLL) is the most common form of leukaemia in the United States of America, AML accounts for most leukaemic deaths, with 2015 data showing only 29% patients surviving 5+ years post-diagnosis,

compared to 70%, 69% and 86% for CML, ALL and CLL, respectively (Howlader, 2019).

It has been shown that the entirety of the haematopoietic system can be traced to 20,000-200,000 individual HSCs in those under the age of 65, and yet, in older patients, the bulk of the haematopoietic system has been found to be derived from less than 20 individual HSC clones (Mitchell et al., 2022). This reduced diversity therefore makes it plausible that should one of these HSCs have a leukaemogenic mutation, it is likely that the resultant blasts would dominate the total blast population, giving rise to AML.

1.2.1 AML Mutational Signature

AML is a highly heterogenous disease, with many different, predominantly somatic, mutations causing the leukaemic phenotype. The most common mutations occur in the receptor tyrosine kinase Fms-like tyrosine kinase (*FLT3*), followed by the methyltransferase DNA Methyltransferase 3A (*DNMT3A*) and Nucleophosmin 1 (*NPM1*). These account for approximately 29%, 23% and 23%, respectively, and may be found in conjunction with each other. However, the mutational signature is highly heterogenous, with mutations in *IDH2*, *NRAS*, *TET2, RUNX1* also occurring in over 10% of patients (Cerami et al., 2012; Gao et al., 2013; The Cancer Genome Atlas, 2013; Tyner et al., 2018). A full breakdown of mutations occurring in >4% patients can be seen in figure 1.2, which equates to the top 20 most-mutated genes in AML. Mutations within these aforementioned genes are typically duplications, point mutations or the generation of fusion proteins, with *FLT3*, *NRAS* and *RUNX1* examples of each of these.

The stage of leukaemogenesis at which mutations occur differs, with some mutations considered 'landscaping', occurring early in clonal haematopoiesis, such as those in *DNMT3A* and *TET2.* However, others occur in the later stages of leukaemogenesis, and are considered the 'drivers' of leukaemic transformation to AML, including *FLT3* and *NRAS* (Döhner et al., 2022). In all however, it is the combination of these landscaping and driver mutations that give rise to the particular type of AML.

1.2.2 Classifying AML

Certain genetic and cytogenetic features can confer differing risk profiles, from 'Very High' risk, down to 'Very Low' risk. A monosomal karyotype or complex/unfavourable karyotype confer very high or high risk, respectively, with a 10-20% 4-year survival rate (Stone et al., 2017).

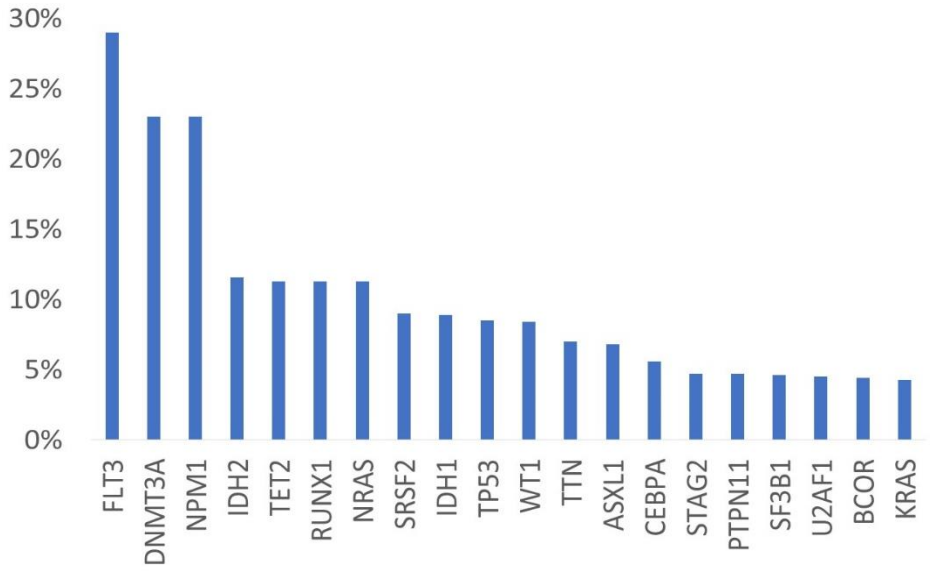

Figure 1.2. The heterogeneity of AML. The top 20 most mutated genes in AML, all of which occur in >4% patients. Data analysed from TCGA PanCancer Atlas, 2013, and Tyner et al., 2018 studies. Data was downloaded from cBioPortal, and graphed using Microsoft Excel.

AML can be classified in different ways. One, which has perhaps previously been the most well-recognised, though no longer typically used, is the French American and British (FAB) classification (Bennett et al., 1976). This categorises AML cases predominantly by morphology of AML blasts, and also the lineage along which they seem to be partially differentiated (Bennett et al., 1976; Schiffer CA, 2003). Such classification required a 30% blast percentage in the blood/bone marrow. Classifications range from M0-M7, which are summarised in Table 1.1.

To elaborate, the M1-M3 substituents of the FAB system predominantly show little evidence of maturation, however do start to show some level of granulocytic differentiation. M4 begins to show both granulocytic and monocytic differentiation. M5 is predominantly monocytic in nature, and M6 erythrocytic. M7 is the rarest subclassification, and has been considered as conferring the poorest prognosis (Schiffer CA, 2003; Stone et al., 2017).

Table 1.1. The French-American-British (FAB) AML classification system.

Category	Characteristics
FAB M0	Minimally differentiated AML
FAB M1	Myeloid Leukaemia without (myeloid) Maturation
FAB M2	Myeloid Leukaemia with (myeloid) Maturation
FAB M3	Acute Progranulocytic Leukaemia
FAB M4	Myelomonocytic Leukaemia
FAB M4EO	Myelomonocytic Leukaemia with Eosinophilia
FAB M5	Monocytic Leukaemia
FAB M6	Erythroleukaemia
FAB M7	Megakaryocytic Leukaemia

In contrast, the International Consensus Classification of AML, utilises a hierarchical system, with 'AML with recurrent genetic abnormalities' being the first subgroup within this classification. This is followed by 'Mutated *TP53* at VAF ≥ 10%,' then certain other mutated genes as group three. The fourth member of this hierarchy is based on complex karyotype, before the fifth is 'AML not otherwise specified'. In line with the new (2022) European Leukaemia Network (ELN) guidelines, this stratification is triggered by ≥10% myeloid blasts (or blast equivalent) in the bone marrow or blood. Should there be 10-19%, the disease should be classified as MDS/AML, and ≥20% is considered AML. This is true for all subgroups except for the AML-defining recurrent generic abnormalities – these cases are always only considered AML. Such classifications can however be further complicated by previous haematological

malignancies or therapy. Further details of this classification are given in Figure 1.3 (Döhner et al., 2022).

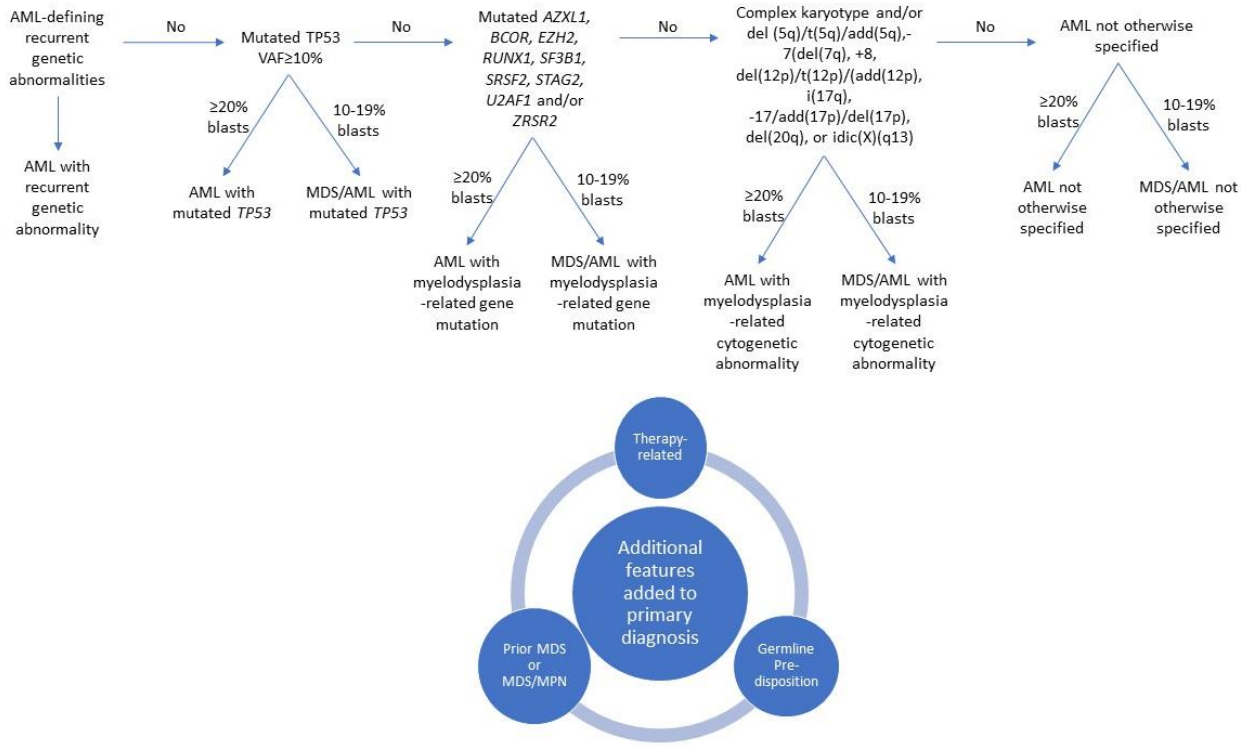

Figure 1.3. European Leukaemia Network (ELN) strategy for AML classification. Workflow shows pathway to diagnosis, with additional considerations also listed. Adapted from Dohner et al., 2022.

Based on these classifications, the ELN has stratified genetic analyses to be completed at diagnosis. This includes screening for genes to both diagnose and indicate actionable targets, more specifically *FLT3, IDH1, IDH2* and *NPM1*, which should all be done within the first three to five days following initial diagnosis. This would be accompanied by *CEBPA, DDX41, TP53, ASXL1, BCOR, EZH2, RUNX1, SF3B1, SRSF2, STAG2, U2AF1* and *ZRS2*, by the completion of the first treatment cycle. Genetic rearrangements (*PML::RARA, CBFB::MYH11, RUNX1::RUNX1T1, KMT2A* rearrangements, *BCR-ABL1* and others) and cytogenetics should also be screened for within approximately 5 days post-diagnosis. Other genes are also

recommended (but not mandated) for testing at the diagnostic stage, including *ANKRD26*, *BCORL1*, *BRAF*, *CBL*, *CSF3R*, *DNMT3A*, *ETV6*, *GATA2*, *JAK2*, *KIT*, *KRAS*, *NRAS*, *NF1*, *PHF6*, *PPM1D*, *PTPN11*, *RAD21*, *SETBP1*, *TET2* and *WT1* (Döhner et al., 2022). These genes are all either commonly associated with oncogenesis, such as *NRAS* and *KRAS*, or haematopoietic signalling and subsequent disorders, such as *GATA2* and *DNMT3A*.

Different mutational signatures are particularly associated with overall survival and progression-free survival. For example, it has been reported elsewhere that presence of the *FLT3*-ITD mutation confers considerably poorer prognosis than those with *IDH1* mutations alone, as shown in Figure 1.4 (Schlenk et al., 2014; The Cancer Genome Atlas, 2013; Tyner et al., 2018). Nevertheless, co-mutations are often critical in determining the prognosis of patients, as shown by Hou et al. (2015). Indeed, allelic burden can also impact prognosis and therapeutic response. Despite a high allelic burden conferring poor prognosis initially, patients with a higher FLT3-ITD allelic burden were found to be more responsive to allogeneic haematopoietic stem cell transplant than those with a lower burden (Schlenk et al., 2014).

1.2.3 The AML Niche

The tumour microenvironment is becoming increasingly studied and understood across a range of cancers, and AML is no different. It is important to understand the role of the supportive network for both bulk AML and the LSCs, in terms of both physical support and chemical support, from cytokines secreted within the niche. For example, it has been shown that the presence of mesenchymal stromal cells (MSCs) alongside AML cells can significantly increase the levels of various pro-survival

cytokines from primary AML cells, including CXCL5, CXCL8 and GM-CSF. This co-culture also significantly increased primary AML cell survival *ex vivo* by promotion of mTOR signalling, indicating their reliance on the niche (Brenner, Nepstad & Bruserud, 2017). Furthermore, these MSC-AML interactions also promote the Wnt/β-catenin pathway, which has already been described as being active in HSCs and LSCs (Koury, Zhong & Hao, 2017). These present just two examples of the supportive, co-operative nature of the AML niche, and perhaps disrupting the niche may present a therapeutic option for eradicating particularly the more dormant cells of the AML population.

For example, this could include the targeting of key cytokine receptors on leukaemic cells, such as the CXCR4/CXCL12 axis. Whilst this has proven successful in B cell malignancies, its utility in AML remains to be fully determined, with Phase I trials resulting in a 46% complete remission rate in patients given plerixafor (CXCR4 antagonist) alongside standard salvage chemotherapy (Uy et al., 2012). In AML mouse models, it has been shown that CXCL12 deletion enhances FLT3-ITD AML cells to chemotherapy, thereby suggesting a role for CXCL12, and indeed the niche itself, in decreasing drug sensitivity (Anderson et al., 2023).

1.2.4 Current Therapeutic Options for AML

Whilst approximately 65% of patients reach complete remission, overall long-term prognosis is poor, with a five-year survival rate of only 15% (Blackmon, Aldoss & Ball, 2022; Cancer Research UK, 2022). Indeed, relapse is common, although this varies considerably based on underlying genetic factors and treatment stratification.

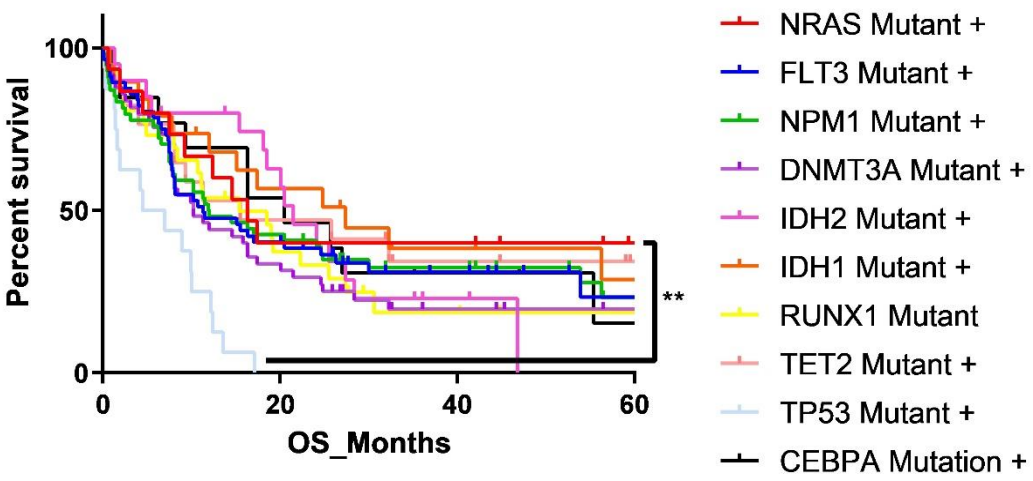

Figure 1.4. 5-year Overall Survival of AML patients with varying mutational backgrounds. Kaplan-Meier plot depicts the 10 most commonly mutated genes. Genes may be co-mutated in a subset of patients. Data analysed from the TCGA Pan Cancer Atlas (NEJM) 2013 dataset (The Cancer Genome Atlas, 2013), obtained through cBioPortal (Cerami et al., 2012; Gao et al., 2013), and plotted using GraphPad 6.0. Statistical significance was determined through the Log-Rank (Mantel-Cox) test, with only *TP53* mutations found to confer significantly poorer prognosis compared to *NRAS* mutations ($P<0.01$).

Typically, patients receive an anthracycline (commonly daunorubicin or doxorubicin), in conjunction with cytarabine. This is given initially in a 7+3 induction regimen, which is to say 7 days of cytarabine therapy, combined with the anthracycline on days 1-3 (Döhner, Weisdorf & Bloomfield, 2015). This would ideally then be followed by allogeneic haematopoietic stem cell transplant, which is considered to confer the best outcome. However, given the older age of many AML patients, transplantation is often unsuitable, due to harsh conditioning regimens and often numerous co-morbidities. Success of these generalised, highly cytotoxic chemotherapies can depend on the mutational profile of the disease, with *TP53* mutations causing a reduced overall survival outcome in some cases, compared to wild-type patients, for example (Döhner et al., 2018).

Alternative therapeutic regimens include the use of hypomethylating agents, such as azacytidine or decitabine. These are particularly useful in patients who are poor candidates for allogeneic haematopoietic stem cell transplant, such as elderly patients (Santini & Ossenkoppele, 2019). Such therapy is also used in some of the AML pre-cursor diseases, such as MDS. These are generally well-tolerated, presenting a positive option for patients, however therapy must be maintained for multiple cycles for a considerable, sustainable response. Such therapy has been compared to current standard-of-care cytarabine maintenance therapy, with improved prognostic effects seen in some AML patient subgroups, although this was dependent on the mutational signature of the disease (Döhner et al., 2018). This is perhaps unsurprising, since different mutations can lead to increased histone methylation, a form of pathogenesis in AML and indeed the target for these drugs. One such mutation is the *MLL*-rearranged leukaemias, as well as those harbouring mutations in *ASXL2*, *TET2* and *IDH1/2* (Prebet et al., 2016).

Targeting of anti-apoptotic proteins in AML has proven to be highly successful. This primarily involves the use of venetoclax, which is an inhibitor of the anti-apoptotic protein BCL-2. The effects of this can be further enhanced through combination therapy with the aforementioned hypomethylating agents, and has shown particularly positive results in eradicating the LSC. This ultimately inhibits oxidative phosphorylation as well as the pro-survival mechanism conferred by BCL-2, thereby eliciting cell death (Pollyea et al., 2018). This is particularly useful in elderly patients for whom generalised, highly cytotoxic chemotherapy is not well-tolerated (DiNardo et al., 2020a; DiNardo et al., 2018; DiNardo et al., 2020b). Indeed, venetoclax is now

FDA-approved in conjunction with azacytidine, decitabine or low-dose cytarabine for newly diagnosed AML patients over the age of 75 (Lai, Bhansali, Kuo, Mannis & Lin, 2023).

There has been some progress with therapies directly targeting AML drivers, including the highly myeloid-specific target FLT3 (CD135), which, as shown in Figure 1.2, is the most commonly mutated gene in AML. Mutations commonly involve a duplication of varying length, known as an internal tandem multiplication (ITD). Such inhibitors include gilteritinib, which is FDA and EMA approved, and quizartinib, which thus far is only approved in Japan. Indeed, the multi-kinase inhibitor midostaurin, which exhibits strong activity against FLT3, is also approved for therapeutic use in FLT3-ITD-mutated AML (Larson et al., 2021).

1.3 Drug Resistance

Resistance to therapies is an increasingly prevalent issue across all areas of disease, including cancer. This can occur soon after treatment has commenced, or after a longer time period (Santoni-Rugiu et al., 2019). There are two key classes of resistance: intrinsic and acquired. Intrinsic resistance occurs due to pre-existing factors, conferring reduced efficacy of the drug prescribed. This includes variations in protein expression levels (such as increased expression of the P-gp (MDR1) transporter), epigenetic modifications (including by long non-coding RNAs) and somatic mutations (Burrell, McGranahan, Bartek & Swanton, 2013; Marusyk, Almendro & Polyak, 2012). Moreover, changes conferring drug resistance can co-exist, resulting in a heterogenous resistant phenotype similar to that seen in the original disease itself (Gerlinger et al., 2012; Ramirez et al., 2016).

Acquired resistance arises predominantly through pre-existing and *de novo* mutations (Bhaduri et al., 2020; Russo et al., 2019). In recent times, the better-understood concept of clonal heterogeneity within cancer has provided greater insight into the causes of acquired resistance, suggesting chemoresistance and disease relapse occur as a result of minor subclonal populations. Given these likely contribute to the heterogenous nature of cancer, it is plausible that these also play a role in disease re-emergence and relapse (Bonnet & Dick, 1997; Gerlinger et al., 2012; Pattabiraman & Weinberg, 2014; Roy & Cowden Dahl, 2018; Seth et al., 2019). Within these minor clonal populations, resistant mutations may have existed during the initial stages of the disease, but remained dormant and undetectable (Pietrantonio et al., 2017; Russo et al., 2018). When the bulk of the cancer cells are eliminated by initial chemotherapy targeting rapidly dividing cells and potentially the overt mutations causing this phenotype, cells from a minor subclone have the space and potential to proliferate and become dominant in the tumour bulk (Jones et al., 2019; McMahon et al., 2019).

1.3.1 Cancer Stem Cells

This can be partially due to a second, related, resistance mechanism, known as cancer stem cells (CSCs). These exceedingly rare CSCs have unique properties compared to bulk tumour cells, including increased stemness capability and strong self-renewal capacity. These are considered intrinsically resistant to chemotherapy, with distinct immunophenotypic and molecular signatures (Bonnet & Dick, 1997). This includes increased expression of efflux transporter P-gp, and the ability to repair damaged DNA, which is manipulated as a common method of inducing cancer cell death (Dean, Fojo & Bates, 2005; Pattabiraman & Weinberg, 2014). This is supported by the

upregulation of many pathways, including the Wnt/β-catenin and Hedgehog signalling pathways. CSCs were first described in AML, but have since been applied to many other cancers including (but not limited to) breast cancer, colorectal cancer, myeloma and pancreatic adenocarcinoma (Bonnet & Dick, 1997; Koury, Zhong & Hao, 2017; Lapidot et al., 1994). These CSCs, and other minor clonal populations contribute to the well-established concept of disease heterogeneity, which can affect an individual's response to treatment and the occurrence of resistance (Burrell et al., 2013; Saygin, Matei, Majeti, Reizes & Lathia, 2019; Siravegna et al., 2015; Turajlic, Sottoriva, Graham & Swanton, 2019).

1.3.2 Leukaemic Stem Cells

Current understanding of AML relapse considers the leukaemic stem cell (LSC) as the foundation from which relapse occurs. These LSCs are derived from HSCs and exist as a genetically heterogeneous pool at a very low density (suggested as approximately 1 in 5000) within the pre-leukaemic state (Shlush et al., 2017) (Figure 1.5). LSCs differ considerably to bulk AML cells, with key properties of these LSCs include their self-renewal capacity, the expression of transcription factors common to HSCs, quiescence, and most importantly they are refractory to standard chemotherapy (Bahr, Correia & Trumpp, 2017; Reya, Morrison, Clarke & Weissman, 2001; Shlush et al., 2017). These functionally distinct LSCs appear to top the proposed hierarchy of the disease (Bonnet & Dick, 1997; Sutherland, Blair & Zapf, 1996). Their mutational profile, which differs to that of the dominant clone of leukaemic cells, is undetectable at diagnosis using regular diagnostic tests, due to the insufficient sensitivity of the most commonly available diagnostic tests. Transcriptional analysis of diagnosis and relapse samples has shown considerably different genetic signatures, further supporting the

idea of the development of relapse from LSCs (Shlush et al., 2017). Indeed, deeper analysis of paired diagnosis and relapse samples, along with patient-derived xenotransplantation experiments suggested a greater proportion of LSCs correlates with a higher rate of relapse and ultimately poorer prognosis (MacPherson & Dawson, 2017; Ng et al., 2016; Shlush et al., 2017).

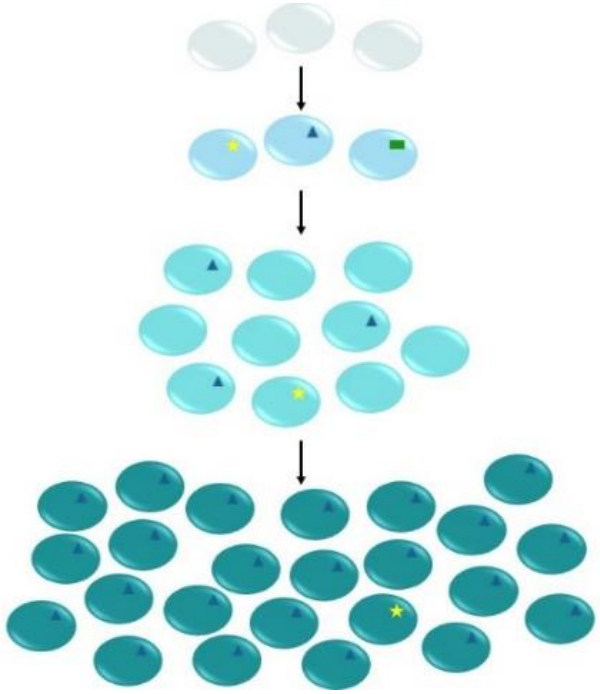

Figure 1.5. Leukaemogenesis. The leukaemic stem cell originates from a haematopoietic stem cell (white), but acquires certain mutations (star, triangle, rectangle), some of which may offer a proliferative advantage (pale blue). This ultimately inhibits differentiation at the blast cell stage (blue), forming a bulk population of immature blast cells which then proceed to dominate the haematopoietic system (green). Mutations arising within these cells can also confer a proliferative advantage, thus further enabling the overwhelming of normal haematopoiesis, giving rise to the leukaemic phenotype.

1.3.3 Drug-Resistant AML

As previously discussed, drug-resistance in cancer presents a huge biological challenge. In AML, the poor survival and indeed high relapse risk indicates a considerable incidence of drug resistance, potentially acting through the LSC

mechanism. LSCs are not typically affected by front-line chemotherapy, due to their maintenance in a quiescent state, rather than being an overly proliferatively-active cell, like the bulk population of leukaemic blasts. In the case of induction chemotherapy, this is most effective on rapidly dividing cells, given that cytarabine is a nucleoside analogue (Shlush et al., 2017). As previously discussed, drug-resistance occurring in this way would likely cause patient relapse, since a drug-resistant population derived from the LSC would take time to dominate the bulk leukaemic population, following the clearance of the original leukaemic burden initially.

As a result of severe toxicity associated with front-line, non-specific chemotherapeutics such as cytarabine, as well as a better disease understanding, targeted therapy in AML has been explored more widely in recent times. However, resistance to these therapies has still become evident. This again fits with the minor clonal populations concept. Such resistance has been seen in response to venetoclax, the Bcl-2 inhibitor (BH3 mimetic), and has been linked to the presence of *p53, FLT3* or Ras family mutations (Dhakal, Bates, Tomasson, Sutamtewagul, Dupuy & Bhatt, 2022).

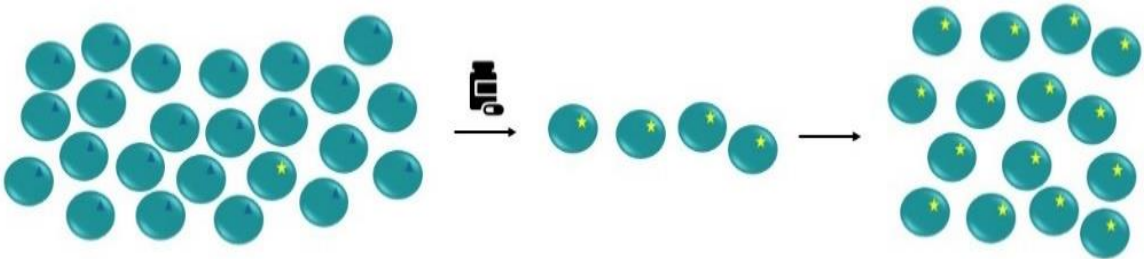

Figure 1.6. Generalised schematic of the subclonal mutation-driven drug resistance phenotype. One mutation (triangle) predominates the leukaemic clone, which can be almost eradicated using chemotherapy (such as targeted FLT3 inhibitors). However, mutations not targeted by this therapy persist, and are able to become the dominant clone.

Aberrant over-expression of key proteins is, as with all cancers, a common cause of AML drug resistance. This includes the over-expression of Multi-Drug Resistant Protein 4 (MRP4), also known as ABCC4. Endogenously high expression of this efflux pump in cell lines and mouse models was shown to decrease the cytotoxic effects of cytarabine in leukaemic cells of these causes increased drug efflux, thereby decreasing drug efficacy. Indeed, *in vitro* analysis revealed such insensitivity could be abrogated by inhibition/knockdown of this transporter. Nevertheless, this has been shown to be pharmacologically targetable using the ABCC4 inhibitor MK571, or the pan-kinase inhibitor sorafenib (Drenberg et al., 2016). Over-expression of these MRPs are correlated with resistance to many other nucleoside analogues in acute leukaemias, including 6-thioguanine (Guo et al., 2009).

In contrast, transport proteins may be under-expressed in a subset of patients, inhibiting drug influx. This can be the case in cytarabine-resistant patients, whereby the nucleoside transporter hENT1, encoded by the gene *SLC29A1,* is under-expressed, reducing cellular uptake of cytarabine. It has been shown that hENT1 expression is increased in cytarabine-sensitive patients, and down-regulated in cytarabine-resistant patients (Abraham et al., 2015; Hubeek et al., 2005).

Alternatively, over-activation of key proliferative pathways caused by somatic mutations plays a considerable role in drug resistance. This can occur for many reasons, including somatic mutations within key proliferative genes (e.g. Ras). As shown in Stahl et al. (2021), molecular characteristics frequently associated with better outcomes, as deemed by the ELN 2017 guidelines, in fact conveyed poorer venetoclax sensitivity in AML patients. This includes the presence of NRAS and KRAS mutations,

commonly associated with a favourable prognosis, however in the case of venetoclax gave a poorer overall survival outcome. As expected, this study also showed a considerable degree of clonal evolution, with the emergence of several pro-proliferative mutations in the relapsed/refractory patient samples not previously detected at diagnosis, such as FLT3 mutations (Stahl et al., 2021). Further examination of Ras contribution of AML drug resistance can be found in section 1.4.5.1.

Epigenetic modifications are becoming increasingly discussed in the AML drug-resistant landscape. Key mutations found in AML, such as *DNMT3A* mutations, affect cellular epigenetics, and thus are often treated using hypomethylating agents or other epigenetic modifiers, such as decitabine. It is therefore perhaps unexpected that such concepts can be hijacked in drug-resistance. For example, whilst decitabine resistance can occur in a similar way to cytarabine since it is also taken into the cell via the hENT1 transporter, its effects can also be manipulated and decreased epigenetically, by the microRNA miR29c (Karimi Kelaye et al., 2022; Yeh, Moles & Nicot, 2016). Briefly, microRNAs are capable of epigenetically-modifying protein expression of their target mRNAs, without affecting gene sequences directly (Yao, Chen & Zhou, 2019). Such miR-29c effect has also been witnessed in older AML patients, whereby increased expression reduced 5-azacytidine (another epigenetic modifier) efficacy, and thus reduced patient OS (Butrym, Rybka, Baczyńska, Poręba, Kuliczkowski & Mazur, 2016).

In a similar way to other cancers, there are a multitude of causes of AML drug-resistance, and it is often multi-faceted. Given the high heterogeneity of the disease

itself, it is unsurprising there is a strong heterogeneity of resistance, including to targeted therapy. However, it is the identification of the common mechanisms of resistance that can indicate potential solutions, or at least ameliorations, for drug-resistant AML.

1.4 The Ras Superfamily

1.4.1 The Structure of Ras

Ras proteins are a superfamily of small GTPases, with four key isoforms. These are HRAS, KRAS (of which there are two sub-isoforms, 4a and 4b), and NRAS. These isoforms share a high degree of sequence similarity, with 100% amino acid sequence fidelity in the first 85 amino acids of this 166-amino acid protein, followed by approximately 90% fidelity in the next 80. The final 20 amino acids have very little fidelity, and thus this region of the protein is known as the hypervariable region (HVR)

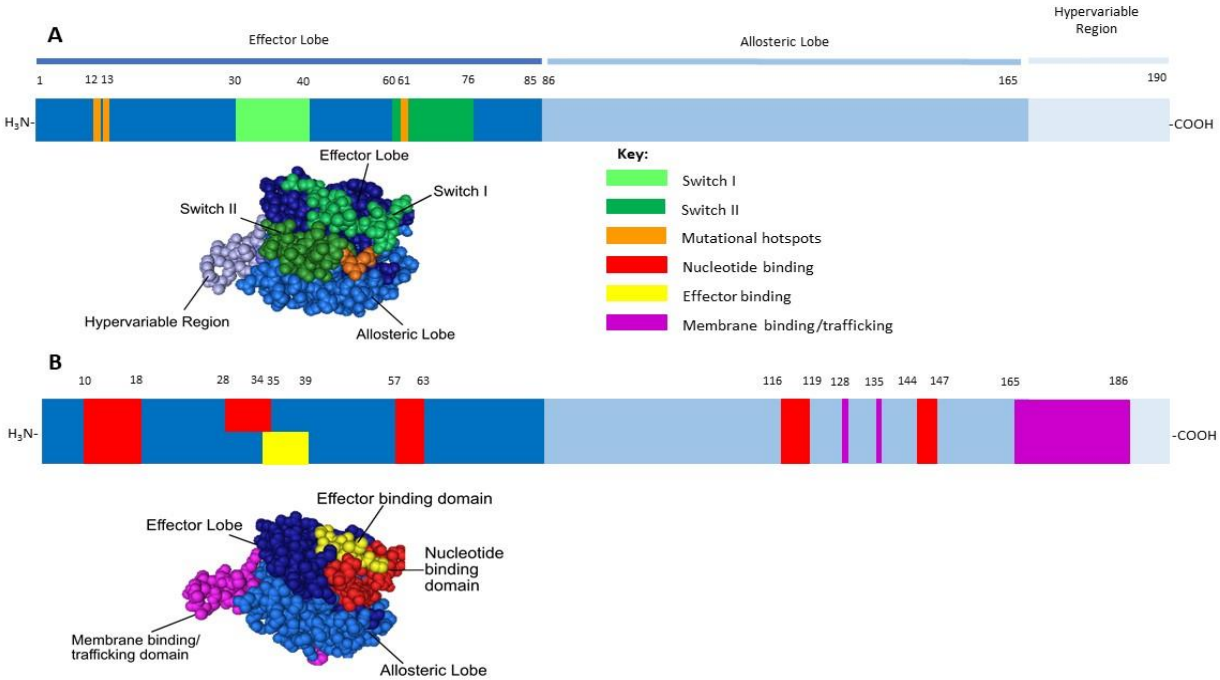

Figure 1.7. 2D and 3D representation of Ras structure. A) Key structural domains (switch regions and lobes), mutational hotspots G12, G13 and Q61 indicated. **B)** Physiological binding domains. Figure adapted from Healy, Prior and MacEwan (2022). 3D structures based on PDB 4DST.

(Figure 1.7). This segment permits trafficking from the Golgi body to the cell membrane, where it can be activated and thus carry out the bulk of its signalling. The HVR is where most post-translational modifications occur (which differ between the Ras isoforms). Such post-translational modifications are typically prenylations (typically farnesylation) or palmitoylations, with conditional phosphorylation also seen in some instances. The type of post-translational modification typically depends on the amino acid in question and indeed Ras isoform itself (Whyte et al., 1997). Ras can be post-translationally modified by almost all of the traditional mechanisms, including acetylation, ubiquitination, sumoylation and palmitoylation, amongst others (Dai, Xie, Chen & Choi, 2021). This is further detailed in section 1.4.2, and Figure 1.10.

Physiologically, Ras is inactive when it is GDP-bound, and active when GTP-bound. The switch from the GDP-bound state to the GTP-bound state is facilitated by Guanine Nucleotide Exchange Factors (GEFs), such as Son of Sevenless 1 and 2 (SOS1, SOS2). In contrast, GTPase Activating Proteins (GAPs), such as neurofibromin (NF), promote the conversion from the GTP-bound state to the inactive GDP bound state (Figure 1.8).

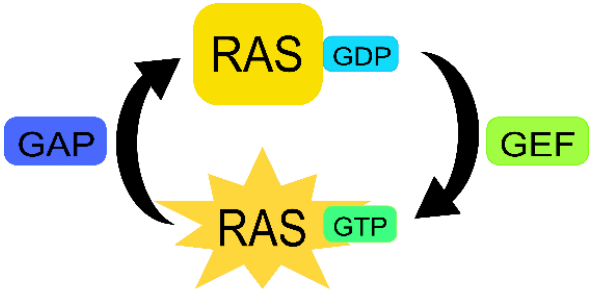

Figure 1.8. Ras activation cycle. Ras is activated when GTP bound, and inactive when GDP bound. Guanine nucleotide Exchange Factors (GEFs, such as SOS1/2) catalyse the switch for GDP for GTP, whilst GTPase Activating Proteins (GAPs) catalyse the inverse. Figure from Healy, Prior and MacEwan (2022).

When active, Ras mediates a range of intracellular signalling pathways, the most notable being the Mitogen-Activated Protein Kinase (MAPK) pathway, the PI3K/AKT pathway and the Ral pathway. These are ultimately responsible for cellular proliferation, differentiation and survival. Ras signalling has also been linked to other cellular properties, such as stemness, through the Wnt/β-Catenin pathway. Such pathways are shown in figure 1.9.

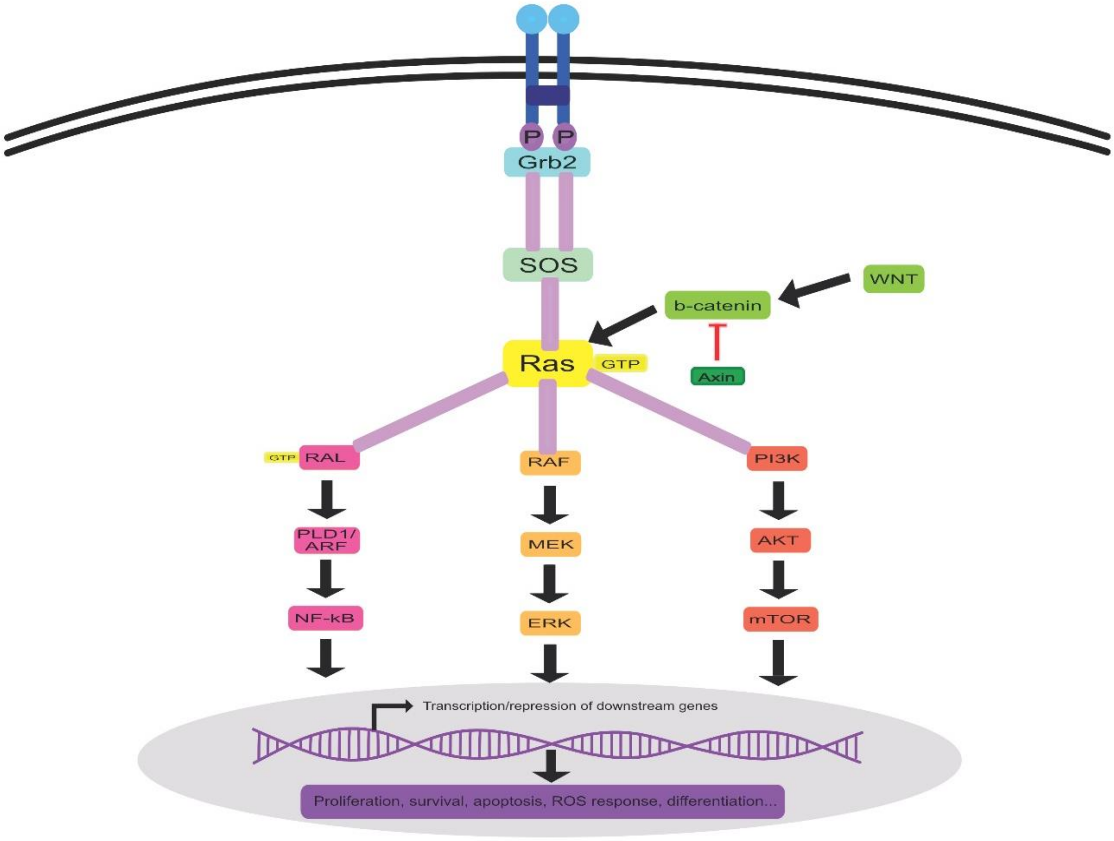

Figure 1.9. Key pathways controlled by Ras. Extracellular ligands bind receptor tyrosine kinases (e.g. FLT3, EGFR, blue) causing receptor dimerization and activation of downstream cascades, or alternatively G-Protein Coupled Receptors are stimulated by their own ligands. Subsequent membrane-bound complexes form, activating Ras. Non-canonical Ras activation pathways include through β-catenin activation (green). Downstream effector pathways include the Ral, MAPK and PI3K pathways, responsible for multiple phenotypic effects. In the case of oncogenic Ras, these downstream pathways may become constitutively activated irrespective of receptor stimulation. Figure adapted from Healy, Prior and MacEwan (2022).

1.4.2 Ras Trafficking

Post-translational modifications discussed in section 1.4.1 are essential in the trafficking of Ras to the cell membrane, where it forms complexes with adaptor and effector proteins to elicit its effects. Ras is synthesised within the cytosol, and relies on post-translational modifications (predominantly prenylation) to permit its trafficking to the cell membrane. This is through the addition of isoprenoid groups to the C-terminal CAAX motif by farnesyltransferase or geranylgeranyl transferase. This signals for the protein to move to the endoplasmic reticulum (ER) (Mor & Philips, 2006). Such trafficking has been targeted pharmacologically, which will be further discussed in section 1.4.3. These additional isoprenoid groups are then subsequently cleaved by the Ras Converting Enzyme (Rce1), and further modified by isoprenylcysteine carboxyl methyltransferase (ICMT) (Cox, Der & Philips, 2015). Subsequent modifications (including palmitoylation and, in the case of KRAS phosphorylation or calmodulin modifications) at the Golgi body ultimately results in the addition of a hydrophobic group, which permits membrane association (Campbell & Philips, 2021; Choy et al., 1999; Mor & Philips, 2006). In the case of NRAS and HRAS particularly, depalmitoylation decreases membrane affinity and causes dissociation of Ras from the membrane, ultimately leading to its re-internalisation at the ER and subsequent recycling (Mor & Philips, 2006; Rocks et al., 2005). Alternative post-translational modifications can also decrease Ras-mediated signalling by inhibiting its trafficking to the membrane, such as the sumoylation or ubiquitination (such as by Rabex-5) of Ras (Campbell & Philips, 2021; Dai, Xie, Chen & Choi, 2021). Ubiquitination is also highly controlled within the cell, with the deubiquitinase OTUB1

able to counteract the ubiquitin-mediated inhibition of Ras-membrane targeting (Campbell & Philips, 2021).

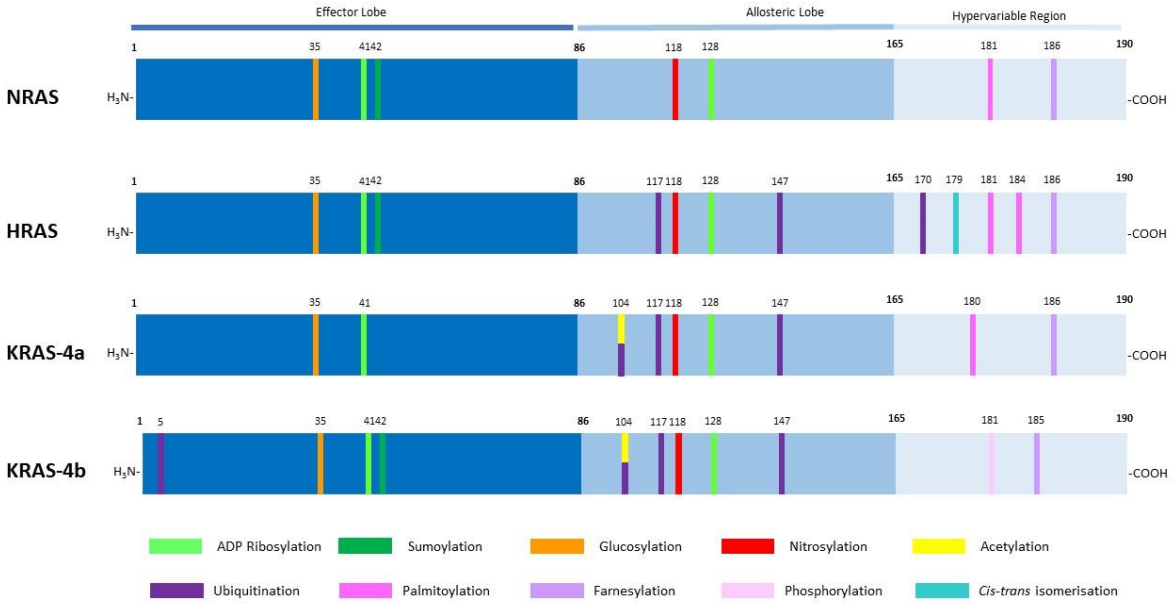

Figure 1.10. Post-translational modifications within Ras isoforms. Locations and types of PTMs differ between the four Ras isoforms, with only a subset conserved between isoforms.

1.4.3 Oncogenic Ras

However, point mutations in Ras can decrease affinity for GAPs, or increase GEF activity. Either way, oncogenic mutations render Ras constitutively active, typically causing increased proliferative signalling, one of the hallmarks of cancer. The most common mutations found across all four Ras isoforms are single nucleotide polymorphisms (SNPs), which occur at amino acids G12, G13 and Q61 of this protein, and are considered 'key mutational hotspots'. Various substitutions are made at these points and are detailed' in figure 1.7. KRAS isoforms are most commonly mutated in cancer, driving approximately 94% of Pancreatic Ductal Adenocarcinoma cases (Waters & Der, 2018). In contrast, HRAS is the most mutated isoform in head and neck squamous cell carcinoma (Prior, Hood & Hartley, 2020), and NRAS is most

frequently mutated in AML. In most Rasopathy settings, G12 and G13 mutants are considered to be most transforming, with the GTP-loaded state favoured, relative to the GDP (inactive) state, though the particular reasons for why certain mutants are more transforming are yet to be elucidated. However, this has somewhat helped to stratify drug development, as will be further discussed.

Whilst G12, G13 and Q61 are most frequently mutated across all cancers and cause clear oncogenic effects, other Ras mutants can be beneficial. For example, as a result of increased sequencing capability and sensitivity, the impact of A146 mutants are starting to be recognised more frequently (Miller & Miller, 2012). Indeed, other mutants have been shown to drive myeloid leukaemogenesis, including NRAS G60E (Tyner et al., 2009).The phenotypic effects of these mutations however differ considerably from the common hotspots, with a survival benefit seen for patients with these mutants (longer progression-free survival), compared to those with G12, G13 or Q61 variants. This is despite the mutant protein still favouring the active GTP-bound conformation, thus remaining active (Janakiraman et al., 2010; Miller & Miller, 2012). Whilst it remains to be elucidated why the effects are different, it has been previously shown that G12 and G13 mutants are more accessible by GEFs (therefore more likely to be activated) than wild-type Ras, whilst Q61 mutants have a decreased affinity for GAPs (Kolch, Berta & Rosta, 2023; Lu, Jang, Nussinov & Zhang, 2016).

1.4.4 Targeting Oncogenic Ras Therapeutically

Although Ras is a highly prevalent driver of cancer, therapeutic options for targeting Ras directly have been severely limited, and Ras was largely considered ‘undruggable’ until the last decade (Cox, Fesik, Kimmelman, Luo & Der, 2014; Moore, Rosenberg, McCormick & Malek, 2020). Ras is particularly difficult to target directly given its

exceptionally high affinity for GTP and GDP, thus limiting potential for competitive inhibition of Ras activation. This is coupled with what was perceived as a distinct lack of alternative binding sites for small molecule inhibitors, given its smooth surface and small size.

As a result of this, many therapeutics against Ras-mediated cancers target downstream of oncogenic Ras, such as trametinib, which targets MEK. This compound binds MEK, preventing its phosphorylation by Raf, and thus subsequent activation of downstream elements, such as ERK. Currently used in patients with BRAF-mutated cancers, trametinib is currently in trials for inclusion into Ras-mutated cancers, including Ras-mutant myeloid malignancies (Borthakur et al., 2016). However, given the diverse nature of Ras signalling and its ability to activate a host of other pathways, it is unsurprising that resistance to these drugs often occur. Means of abrogating this include the addition of AKT pathway inhibitors with dabrafenib (Raf inhibitor), however pre-clinical *in vivo* work showed no improvement on relapse rates (Lassen et al., 2014), and 25% of patients in Phase I clinical trials prescribed this regimen exhibited Grade III-IV toxicity. Thus, whilst such combination therapies may be theoretically useful, there remains a considerable task ahead to successfully target Ras-mutant cancer in this way.

In the early 2000s, small molecule inhibitors such as lonafarnib and tipifarnib, which targeted the post-translational modifications of Ras, such as farnesylation, showed promise for a time. However, increased clinical data showed no overall benefit to patients prescribed these drugs, and so manufacture ceased and they were withdrawn from the market (Borthakur et al., 2006; Burnett et al., 2012; Harousseau et al., 2009;

Van Cutsem et al., 2004). Nevertheless, this strategy is currently under review, with these compounds showing promise in some HRAS-mutated cancers (Gilardi et al., 2020; Lee et al., 2020).

Ras is intrinsic in physiological cell signalling, and so non-cancer-targeted arrest of its pathways undoubtedly puts patients at greater risk of on-target toxicity. Therefore, there is a compelling argument for targeting mutant-Ras itself, something which has shown promise in the last ten years. The Shokat group (amongst others) have paved the way for a cancer-specific Ras inhibitor, through targeting of specific Ras mutations (Ostrem, Peters, Sos, Wells & Shokat, 2013). This work began with the design of a KRAS G12C inhibitor, which was considered the most appropriate target given the prevalence of KRAS mutations in cancer. Indeed, the G12C mutation was found to be most targetable given the potential for covalent binding mediated by the cysteine residue, and the presence of a newly discovered allosteric binding site, only present when Ras is in its active conformation (which is the favoured conformation of Ras G12C). After careful target validation and compound optimisation (Janes et al., 2018; Li, Balmain & Counter, 2018), AMG510 (Sotorasib) was FDA-approved for KRAS-G12C-mutant lung cancer in 2021, the first of its kind to do so (Canon et al., 2019; Govindan, 2019; Romero, 2020). Such work has paved the way for other G12C inhibitors, such as MRTX849 (Adagrasib), which recently received accelerated FDA-approval. These drugs will be game-changing for KRAS-G12C-mutant patients, for

whom therapeutic options, and particularly targeted options, have been non-existent for so long.

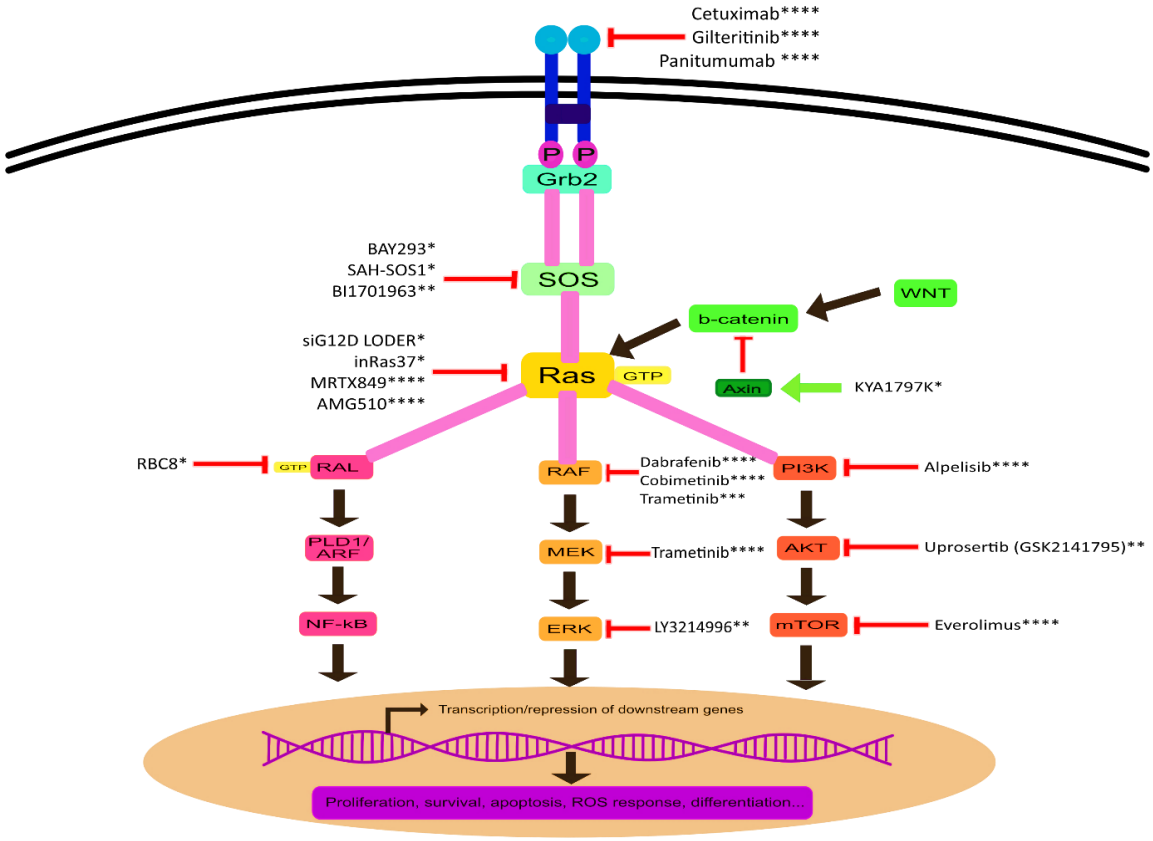

Figure 1.11. Key pharmacological agents targeting Ras-mediated pathways. Examples of pharmacological agents used to target Ras are depicted, with the level of approval denoted using asterixis. *pre-clinical studies, **phase I clinical trials, ***phase II clinical trials, ****FDA approved use. Figure adapted from Healy, Prior and MacEwan (2022).

Nevertheless, whilst these compounds are extremely important and represent huge advances in the field of Ras therapeutics, there remains a considerable need to target the other Ras isoforms and mutations. As shown in figure 1.12, G12C mutations only comprise 3.5% of all Ras mutations across cancer, and whilst KRAS is most frequently mutated (83% patients), many patients do still suffer from the effects of NRAS and HRAS mutations (The ICGC/TCGA Pan-Cancer Analysis of Whole Genomes Consortium, 2020). Therefore, there is a new focus in the field of Ras biology for

targeting these other mutations. Whilst structural differences between the various mutated Ras isoforms limit the use of a ‘one drug fits all mutations’ approach, lessons can be learned from the successful generation of G12C inhibitors.

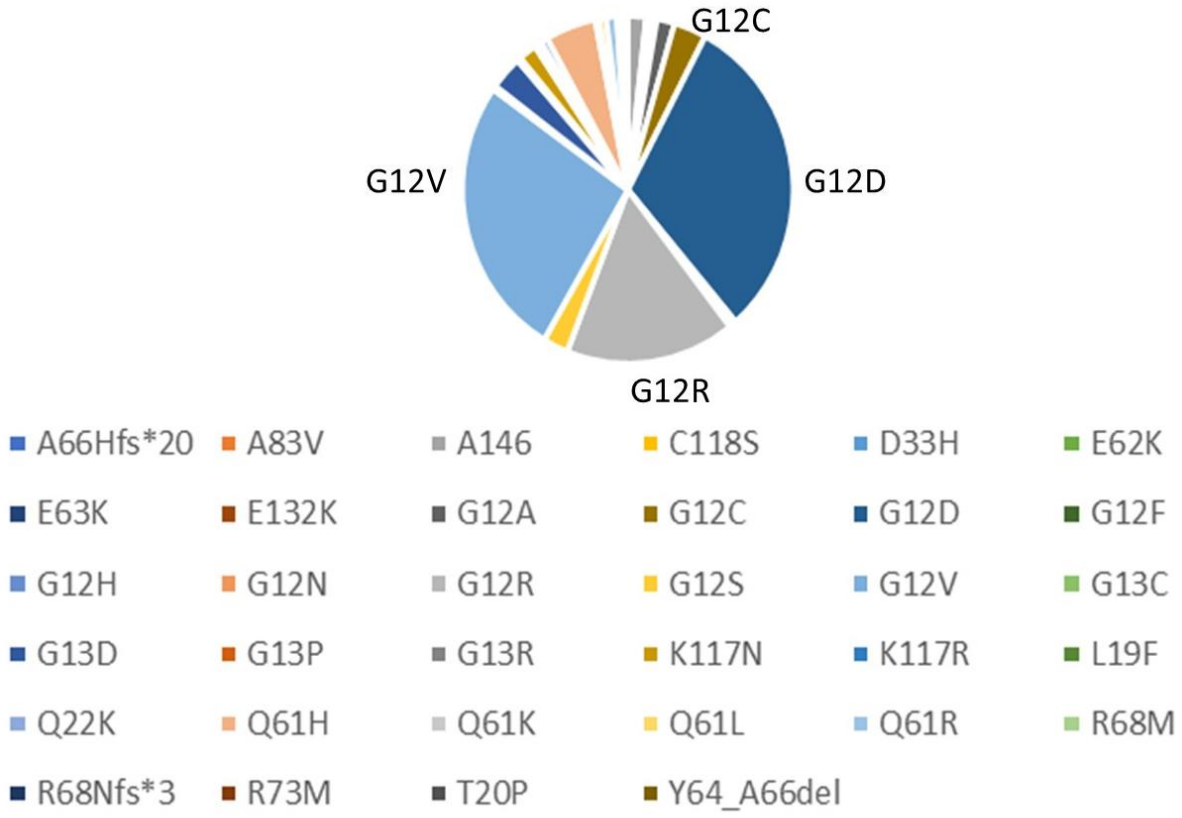

Figure 1.12. Distribution of point mutations occurring in KRAS, NRAS and HRAS across a multitude of cancers. The three mutations most commonly found in cancer are highlighted, alongside G12C for reference. Data from the (The ICGC/TCGA Pan-Cancer Analysis of Whole Genomes Consortium, 2020) downloaded from cBioPortal (Cerami et al., 2012; Gao et al., 2013), and analysed using Microsoft Excel.

Further recent publications by the Shokat and Suga groups have used several structural biology and modelling mechanisms to design a KRAS G12D-specific compound, in a similar way to the G12C compounds previously developed, though without the reliance on covalent interaction possible due to the cysteine mutant. A complex cyclic peptide (termed KD2) was identified as having strong specificity for the KRAS-G12D-mutated Switch II pocket, relative to wild-type KRAS. Moreover, KD2 had

a greater affinity for GTP-loaded KRAS, thus further enhancing its potential utility, given that G12D-mutated KRAS is considered to favour the GTP-loaded state. Blockade of this pocket subsequently inhibited the Ras-Raf interaction, indicating its potential for cessation of aberrant signal transduction (Zhang et al., 2020).

Use of peptides has been examined as a means of targeting other Ras isoforms and mutations, such as KYA1697K, and others. This investigational peptide compound targets Axin, thereby inhibiting β-catenin and subsequent Ras signalling. This could therefore prove useful in a Ras-mutated AML context, given the implication of the Wnt/β-catenin pathway in cancer stemness, as previously discussed (Koury, Zhong & Hao, 2017).

Since oncogenic Ras mutations typically cause Ras to alter its sensitivity for GEFs and GAPs, certain compounds have been designed to inhibit the Ras-SOS interaction, to prevent (or at least limit) Ras' over-activation. This includes the currently pre-clinical compound BAY293, the first of its kind. This showed promise in pre-clinical work, using compound library screening, structural modelling and cell line methods of G12C mutant KRAS (Hillig et al., 2019).

Other small molecule inhibitors are also in development to block Ras effectors from binding to Ras, preventing their subsequent activation. This includes the pan-Ras antibody inRas37, which has shown good *in vitro* and *in vivo* clinical activity. Although cell surface permeability this antibody, like all antibody-based therapies, is challenging, once the antibody has been following binding to the integrins αVβ3 and αVβ5, it is cleaved due to the change in endosomal pH relative to the extracellular pH,

permitting binding to the RAF binding domain on Ras (RBD). It has been reported that inRas37 has higher affinity for binding the RBD on mutant Ras relative to wild-type, thereby presenting the potential for reduced on-target toxicity in other (healthy) cells, as is seen with some of the other means of Ras pathway inhibition. It is important to note that only KRAS G12D and G13D have been examined so far, with positive results seen (Shin et al., 2020). Nevertheless, given the differing activities of varying mutants and differences in structure as a result of different mutants, there is potential for this increased affinity to only apply to certain mutants. As a result, this would require further stratification in patients, rather than being suitable for all Ras-mutant patients.

1.4.5 Ras in AML

It has been acknowledged since the 1980s that Ras mutations can drive leukaemogenesis, particularly myeloid leukaemia and other myeloproliferative disorders (Bartram, 1988). NRAS is another frequent driver of AML (albeit less common than the aforementioned three main mutations), accounting for approximately 11% cases (Bailey et al., 2018; Cerami et al., 2012; Gao et al., 2013; Tyner et al., 2018). Indeed, AML is the second-most common cancer (behind melanoma) to be driven by NRAS mutations, as recorded by the TCGA pan-cancer study (The Cancer Genome Atlas, 2013; The ICGC/TCGA Pan-Cancer Analysis of Whole Genomes Consortium, 2020). NRAS is the most commonly mutated Ras isoform in AML, in contrast to the majority of other cancers, where KRAS is most often mutated. The overall mutational burden of NRAS, and indeed its individual mutations, is indicated in figure 1.13. As per the COSMIC database, NRAS G12A, G12D, G12R, G13C, G13D, G13R, G13V, Q61H and Q61P mutations are most commonly found in haematopoietic and lymphoid cancerous tissue, approximately 3-10 times more than

in the second-most common tissue where these mutations occur, typically the skin or the large intestine (Tate et al., 2019).

In *de novo* AML, NRAS mutations are typically considered to confer a favourable prognosis, with no significant difference seen in five-year overall patient survival seen in the TCGA dataset, between those patients with wild-type or mutated NRAS (Figure 1.14) (Cerami et al., 2012; Gao et al., 2013; The Cancer Genome Atlas, 2013).

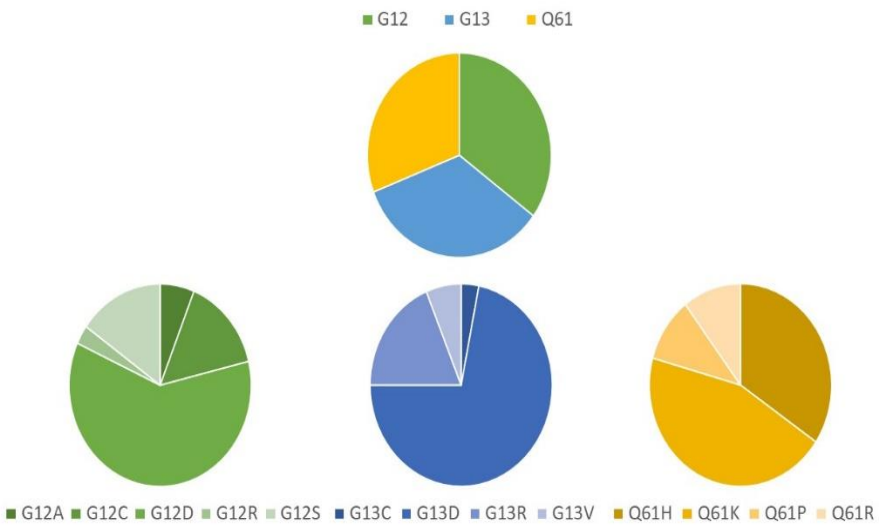

Figure 1.13. Distribution of NRAS mutants in AML. Whilst G12, G13 and Q61 mutants are reasonably evenly distributed across NRAS-mutated AML, G12D, G13D and Q61K are the most common of each hotspot mutation. Data analysed from the TCGA Pan Cancer Atlas (NEJM) 2013 dataset (The Cancer Genome Atlas, 2013), obtained through cBioPortal (Cerami et al., 2012; Gao et al., 2013), and plotted using Microsoft Excel .

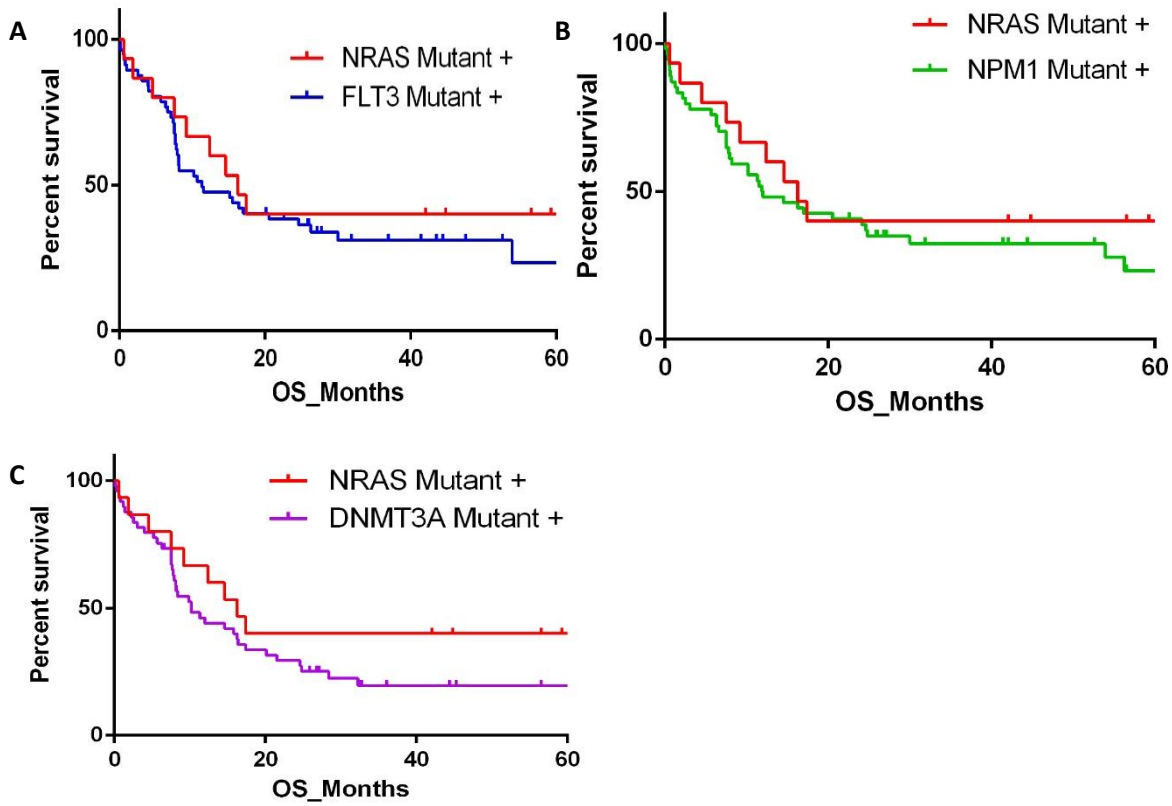

Figure 1.14. Kaplan-Meier plot of AML patient overall survival. **A)** FLT3 vs. NRAS-mutated patients. **B)** NPM1 vs. NRAS-mutated patients. **C)** DNMT3A vs. NRAS-mutated patients. These genes were chosen since they are the three most commonly mutated in AML, and are associated with more favourable (NPM1) or less favourable (FLT3) outcomes. Data analysed from the TCGA Pan Cancer Atlas (NEJM) 2013 dataset (The Cancer Genome Atlas, 2013), obtained through cBioPortal, and plotted using GraphPad 6.0 (Cerami et al., 2012; Gao et al., 2013). Statistical significance was determined through the Log-Rank (Mantel-Cox) test, however there was not deemed to be a statistically significant difference in patient 5-year OS.

1.4.5.1 Ras in AML Drug Resistance

Nevertheless, NRAS is particularly implicated in drug resistance in AML, with recent literature showing emergence of NRAS-mutated clones as a resistance mechanism to the FLT3 inhibitors crenolanib and gilteritinib (McMahon et al., 2019; Perl et al., 2019). Targeted next-generation and single-cell DNA sequencing of patient blood and/or

bone marrow samples at diagnosis and post-gilteritinib relapse identification revealed the emergence of various Ras/MAPK pathway mutations, the most common of which were NRAS mutations. Indeed, further *in vitro* analysis of NRAS and FLT3 mutants indicated a role for NRAS mutants conferring a resistant phenotype (McMahon et al., 2019).

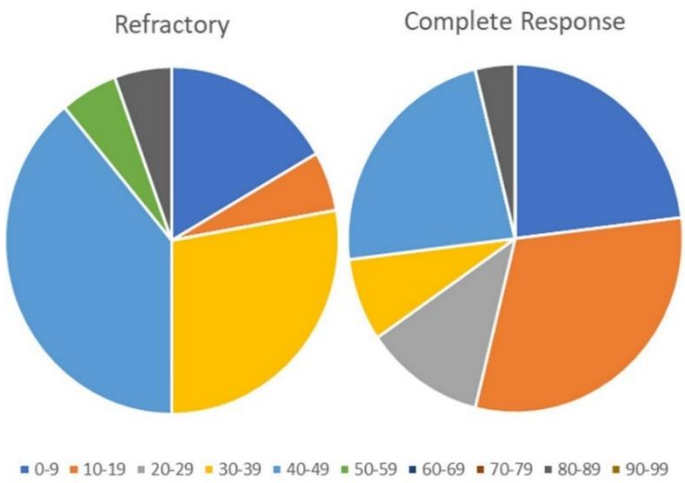

Figure 1.15. Variant Allele Frequency (%) of NRAS-mutant patients with regards to treatment outcome. A greater proportion of chemotherapy-refractory patients have a higher NRAS VAF than NRAS-mutant patients who go into complete remission following induction therapy. Data analysed from the TCGA Pan Cancer Atlas (NEJM) 2013 dataset, obtained through cBioPortal, and plotted using Microsoft Excel (Cao et al. 2012, Gorrini and Harris, 2013).

Such resistance has also been seen to both conventional therapy (e.g. allogeneic haematopoietic stem cell transplant), as well as novel, investigational therapies, including ivodsidenib (IDH1 inhibitor), and entospletinib, the SYK inhibitor (Choe et al., 2020; de Witte et al., 2017; Loftus et al., 2021; McMahon et al., 2019; Zhang et al., 2019). The TCGA and OHSU datasets also revealed a tendency for those patients

with higher NRAS variant allele frequencies to be refractory to induction chemotherapy (The Cancer Genome Atlas, 2013; Tyner et al., 2018). Though the dataset for NRAS-mutated patients is small, 50% of those who had an NRAS-mutant VAF >40% were refractory to induction chemotherapy, compared to 27% in the complete response (CR) group, at the same cut-off (Figure 1.15).

1.5 Gene Editing

Manipulation of disease-implicated genes is vital in assessing the therapeutic potential of activating or inhibiting such genes. This would be traditionally considered using small molecule inhibitors or other pharmacological agents in patients, although more recently the administration of gene manipulating techniques themselves to patients has been explored and successfully used. Gene editing broadly comprises of double-stranded breaks (DSBs) being generated in DNA at a desired location, and then this break being repaired using either Non-Homologous End Joining (NHEJ), typically creating small insertions/deletions (indels), or by Homology-Directed Repair (HDR), which creates specific mutations based on a carefully-designed repair template. Because of the differences between these methods, NHEJ is commonly used to 'knock-out' a gene, by interrupting the coding sequence. HDR, on the other hand, can be used to correct or generate particular mutations, down to a single nucleotide level.

There are four typical mechanisms of gene manipulation, comprising mega-nucleases, Zinc-Finger Nucleases (ZFNs), Transcription Activator-Like Effector Nucleases (TALENs), and Clustered Regularly Interspaced Palindromic Repeats (CRISPR). Whilst mega-nucleases presented the first opportunity for such genetic editing, it is CRISPR which has now been adopted as the most common means of gene editing,

particularly in regard to therapeutic applications. Nevertheless, each of these techniques presents its own benefits and drawbacks, which will be described below.

1.5.1 Mega-nucleases

Mega-nucleases are a class of endonucleases which create double-stranded breaks at large recognition sites. These recognition sites are between 12 and 40 base pairs in length, which presents an issue for oncologic mutation correction. These could be engineered for specific oncogenic-associated mutations, such as translocated genes. Endogenous mega-nucleases would not be an option therapeutically since they would only recognise 'normal', and not oncogenic, gene sequences. Furthermore, since key oncogenic mutations can be single nucleotide variants, the risk of off-target editing in healthy cells is considerable, since one base difference in forty bases may not be recognised by, and therefore prevent binding of, the mega-nuclease. Not only does this present an off-target risk, but it also results in a low efficiency of the desired gene editing, which has been recorded as 1-20% in human cells (Epinat et al., 2003). Indeed, the use of mega-nucleases have now been largely superseded by subsequent techniques, which will be further discussed.

1.5.2 Zinc Finger Nucleases (ZFNs)

ZFNs are fusion proteins, where chains of 30 amino acids, stabilised by interaction with zinc, are fused to the cleavage domain of the enzyme *FokI*. The 30 amino acid zinc-finger protein (ZFP) must contain 2 cysteines and 2 histidines, known as the Cys_2His_2ZF motif. A ZFP binds DNA at a 3-4 base pair recognition sequence, however the specificity of this can be increased by fusing up to three ZFPs with the FokI cleavage domain, creating a 9-base pair recognition sequence. However, in practice,

the ZFN is most effective at inverted sequences, thereby further increasing the recognition sequence to 18bp, as well as perhaps limiting its superior efficacy to duplicated sites only. Therapeutically, use of ZFNs is limited, owing to targeting difficulties. Despite the fusion of up to three ZFPs to the cleavage domain creating increased specificity, there remains potential for only one of these three ZFPs to recognise and bind DNA at once. With its recognition site of 3-4bp, this presents a high likelihood of off-target effects) (Carroll, 2011). Overall, whilst the targeting concept is better, there remained too many issues and this technology was largely superseded by TALENs and CRISPR.

1.5.3 Transcription Activator-Like Effector Nucleases (TALENs)

TALENs are multi-domain proteins with the capability of localising to the nucleus, binding DNA and activating transcription of a particular target gene. Their creation utilised the *FokI* endonuclease concept, combined with the three domains responsible for the aforementioned localisation, binding and activating properties. The DNA binding domain can be artificially modified so that the monomers at positions 12 and 13 of this 30-amino acid domain can specifically bind any desired base. TALENs are used in pairs, with one binding the sense strand, and the other binding roughly 12-25 base pairs either side on the anti-sense strand. This then directs the endonuclease to cut in this region, creating the double-stranded break (Nemudryi, Valetdinova, Medvedev & Zakian, 2014).

1.5.4 Clustered Regularly Interspaced Palindromic Repeats (CRISPR)

CRISPR-Cas9 was subsequently developed, using similar principles but instead involved a guide RNA sequence, rather than the small proteins as described for ZFNs

and TALENs. The Cas9 endonuclease was isolated from *S. pyogenes* bacteria, hence its recognition as *sp*Cas9 (Ran, Hsu, Wright, Agarwala, Scott & Zhang, 2013). This is the most common form of Cas9 used for CRISPR, and will be focussed upon throughout this thesis. Subsequent research has utilised other forms of Cas9, such as that from *S. aureus*, which will be further discussed in Chapter 4. *sp*Cas9 creates double-stranded breaks in the DNA, and can do this at specified sites using a 20 base pair RNA guide sequence. These RNA guides must be designed 3 base pairs from a Protospacer Adjacent Motif (PAM) site, which enables the Cas9 to cleave the DNA. For *sp*Cas9, the PAM site follows the structure NGG, where N is any nucleotide, and G encodes Guanine (Chandrasegaran, 2017). This guide RNA sequence must be supplied in conjunction with associated non-coding, short repeating RNA sequences. This whole complex can also be referred to as CRISPR-RNA (crRNA). The tracrRNA sequence, encoding the scaffold for the Cas9 nuclease, must also be introduced into the cell, often in the same delivery vector as the crRNA, and the coding domain sequence for Cas9 (Ran, Hsu, Wright, Agarwala, Scott & Zhang, 2013).

The means by which both CRISPR and TALENs carry out their effects are similar, as are some of the limitations of the techniques. The advantage to CRISPR compared to TALENs is the smaller size (and therefore simpler delivery) of the element directing the site of DNA cleavage. Nevertheless, efficient delivery of these components remains challenging, owing to the size of endonucleases and a lack of ability to easily cross the cell membrane. However, both present the risk of a high-level of off-target effects, whereby the endonuclease is directed to undesired parts of the genome. This can be mitigated by optimising guide design, and indeed using multiple guide sequences around the area to be cleaved. To aid with this, regions with high

proportions of repeated sequences and strong homology with other genomic regions should be particularly avoided when designing targeting sequences.

1.5.5 Therapeutic Gene Editing

Nevertheless, such techniques have been optimised not only for in vitro investigations, but also for use in therapy. Such gene editing has been used across multiple diseases, including ophthalmic diseases and haematological malignancies. This includes the potential use of ZFNs and TALENs as a means of engineering HIV-resistant subpopulations of immune cells, as well as the *ex-vivo* deactivation of pro-leukaemic immune-related genes in some childhood leukaemia.

CRISPR-Cas9 has always presented the opportunity to edit cells directly, ushering in a new era of gene therapy. Indeed, the game-changing nature of CRISPR-Cas9 was recognised by the 2020 Nobel Prize Committee, with the Prize for Chemistry awarded to Jennifer Doudna and Emmanuelle Charpentier, the pioneers of CRISPR-Cas9 research (Westermann, Neubauer & Köttgen, 2021).

Clinical applications of CRISPR are becoming more widely explored and understood now. This includes its success in a small-scale trial solid tumour trial, as well as in the treatment of β-thalassemia (Ledford, 2020; Ledford, 2022). Such therapy has also been successful for patients with ocular disease (Choi et al., 2023).

Recently, the use of CRISPR-base editing has gained prominence, with its successful therapeutic use reported in a young T-ALL patient in December 2022. CRISPR base-editing is a derivative of the aforementioned CRISPR-Cas9 technique, however uses

a smaller version of Cas9, Cas9 nickase, to create the specific singular base changes. The advantage to its small size is the overcoming of the low-efficiency of component delivery, as discussed above. However, with base-editing, only certain bases can be changed to others, with C-T base editors developed first, and subsequently A-G (Rees & Liu, 2018).

This technique was used to remove the lymphoid/T-cell markers CD7 and CD52 from the patient's T cell population *ex vivo*, and reintroduce a CD7 Chimeric Antigen Receptor (CAR), with these edited T cells then re-introduced into the patient. This CD7 CAR would then recognise and destroy the leukaemic cells, which remained CD7+. Such therapy was successful, with the patient in remission following treatment with this therapy and a second bone marrow transplant (Chiesa et al., 2023).

1.6 Thesis Hypothesis and Aims

Whilst there is an overwhelming general consensus that Ras mutations confer a proliferative advantage to cells, it remains to be fully elucidated the extent to which each individual mutation controls this phenotype. Given the vast number of different mutations that occur in the three key Ras isoforms, I hypothesise that these mutants will confer different phenotypes, particularly with regards to drug resistance in leukaemia. As shown above, mutations at the three key NRAS mutational hotspots occur almost equally across AML patients, however one mutant within each position tends to dominate. This should be further explored, to better understand the role of each mutation, and the reasons for the favouring of one over another in this highly heterogenous disease. Through a more comprehensive understanding of this, drug pipelines and treatment regimens may have the potential to be better stratified for AML, which, as discussed, is currently a disease with poor prognosis as a result of

sub-optimal therapies. Given that NRAS mutational status is now suggested to be screened for following diagnosis as part of the ELN 2022 guidelines, a better understanding of the impacts of these individual mutants should be obtained.

The key aims for this thesis are to interrogate to what extent differing NRAS mutations are implicated in AML pathogenesis, with a particular focus on their individual roles in drug resistance. This will particularly focus on their role in resistance to promising novel therapeutics, as well as traditional, front-line therapies, as a contribution to the ever-growing literature surrounding the potential for patient treatment stratification, to ultimately improve outcomes. These will be outlined in the following chapters:

- Characterisation of Ras in Acute Myeloid Leukaemia Cell Lines
- Use of CRISPR-Cas9 Gene Editing to Revert Drug-Resistance Induced NRAS Mutants
- Effects of NRAS Overexpression in Acute Myeloid Leukaemia

Chapter 2

Materials and Methods

2 Materials and Methods

The following chapter details the reagents used and protocols followed to carry out the work in this thesis. Occasionally, protocols were adapted from those listed here, and have been detailed in the relevant sections.

2.1 Buffers

Table 2.1. Components and purposes of key buffers used throughout this thesis

Buffer	Recipe	Purpose
50X Tris-Acetate-EDTA	2M Tris Base 1M Glacial Acetic Acid 0.05 M EDTA (pH 8.0)	Agarose Gel Preparation
10X Tris-Buffered-Saline-Tween	200 mM Tris Base 1.5 M NaCl 1% (v/v) Tween-20 pH 7.6	Western Blot membrane washing, antibody/blocking buffer dilution
10X Tris-Glycine-SDS (Electrode Buffer)	250 mM Tris Base 1.92 M Glycine 1% SDS pH 8.6	SDS-PAGE Protein separation
10X Tris-Glycine (Transfer Buffer)	250 mM Tris Base 1.92 M Glycine Diluted to 1X with methanol (20% final v/v) and water	Transfer of protein from SDS-PAGE Gel to nitrocellulose membrane
SDS Lysis Buffer	50 mM Tris-HCl 10% Glycerol	Whole cell lysis buffer for protein extraction

	5 mM EDTA 1% SDS pH 6.8	
5X Laemelli Buffer	200 mM Tris-HCl 20% Glycerol 10% SDS 10% β-Mercaptoethanol Bromophenol Blue pH 6.8	Protein loading dye for use in Western blotting.
Resolving gel buffer	375 mM Tris-HCl 0.1% SDS 10-12% Poly-acrylamide pH 8.8	Component of SDS-PAGE Protein separation gel
Stacking gel buffer	500 mM Tris-HCl 0.4% SDS 5% Poly-acrylamide pH 6.8	Component of SDS-PAGE Protein separation gel
5X Annexin V Binding Buffer	50 mM HEPES-NaOH, 700 mM NaCl, 12.5 mM $CaCl_2$ pH 7.4	Flow cytometry-mediated analysis of apoptosis

2.2 Purchased Reagents and Kits

Table 2.2. Details and purposes of key kits used throughout this thesis

Kit	Manufacturer	Cat. No.	Purpose
Active Ras Detection Kit	CST	8821	Determination of GTP-bound Ras in relevant cell lines
Agarose, Ultrapure	Invitrogen	16500500	RNA/DNA Separation
BCA Protein Assay	Thermo Fisher	23225	Protein concentration quantification
Bovine Serum Albumin (BSA)	Sigma	A7906	Blocking buffer/ antibody dilution
Carbenicillin Disodium Salt	Thermo Fisher Scientific	10177012	Antibiotic selection marker for bacterial colony growth
Complete Mini, EDTA-free Protease I Protease Inhibitor Tablets	Roche	11836170001	Inhibition of protease activity in protein lysates
Deoxynucleotide (dNTP) Solution Mix	New England Biosciences	N0447S	PCR
Dulbecco's Modified Eagle Medium (DMEM) with high glucose, Glutamax supplement	Invitrogen	31966047	Cell culture media (for HEK293T and HS5)

Foetal Bovine Serum (FBS)	Invitrogen	10437028	Media supplement for cell culture
GeneRuler 100bp DNA Ladder	Invitrogen	SM0241	DNA length reference
GeneRuler 1kb DNA Ladder	Invitrogen	SM0311	DNA length reference
LB (Luria Bertani) Agar	Invitrogen	22700025	Generation of bacterial growth agar plates
LB (Luria Bertani) Broth	Sigma	L3397	Generation of bacterial growth media
Linear Polyethyleneimine Hydrochloride (Mn 20,000)	Sigma	764965	Plasmid transfection reagent
Methylcellulose (4000 cp)	Sigma Aldrich	M0512	Used in semi-solid media in cell culture
Mix & Go! *E.coli* Transformation Kit and Buffer Set	Zymogen	T3001	Growth of competent *E.coli* for use in transformation
OneTaq Quick-Load 2X Master Mix with Standard Buffer	New England Biosciences	M0486S	PCR
OptiMem-I	Invitrogen	11058021	Plasmid transfection media

Penicillin/Streptomycin	Invitrogen	15140122	Media supplement for cell culture (reduction in contamination risk)
Phosstop Phosphatase Inhibitors	Roche	4906837001	Inhibition of phosphatase activity in protein lysates
Pierce™ ECL Western Blotting Substrate	Thermo Fisher	32106	Enhanced chemiluminescence used for HRP-linked protein detection
Polybrene	Sigma	TR-1003-G	Lentiviral Transduction
Q5 High-Fidelity DNA Polymerase	New England Biosciences	M0491S	PCR
QIAprep Spin Miniprep Kit (250)	Qiagen	27106	Plasmid extraction from bacterial culture
QuantiTect Rev. Transcription Kit (50)	Qiagen	205311	Conversion of RNA to cDNA
RNeasy Plus Mini Kit (50) QIAprep Spin	Qiagen	74134	RNA Isolation
RPMI 1640 Medium (RPMI 1640) with Glutamax supplement	Invitrogen	61870044	Cell culture media (for all cell lines unless stated otherwise)
SYBR Green Jumpstart Taq Readymix	Sigma	S4438	Quantitative PCR

T4 DNA Ligase	New England Biosciences	M0202S	Molecular Cloning
Trypsin 0.25% EDTA	Invitrogen	25200072	Detachment of adherent cells from flask base
Ultrapure water	Invitrogen	10977035	DNA/RNA elution
Westar Supernova	Cynagen	Reference XLS3,0100	Super-Enhanced chemiluminescence used for HRP-linked protein detection
Wizard® SV Gel and PCR Clean-Up System	Promega	A9282	DNA extraction from PCR/Agarose gel
Wizard® SV Genomic DNA Purification System	Promega	A2360	Genomic DNA isolation from cell lines

2.3 Cell lines

THP-1, MV4-11, U937, OCI-AML-3, HeLa and HEK293T cell lines were obtained from American Type Culture Collection (ATCC). AML cell line MOLM-13 was obtained from Leibniz Institute DSMZ-German Collection of Microorganisms and Cell Cultures. HS5 cells were a gift from Dr. Kathy Till. Key genomic features of each cell line are detailed in Table 2.3, with Ras status validated in Figure 3.2 by Sanger sequencing for AML cell lines.

Table 2. 3. Overview of parental cell lines used and relevant mutational statuses.

Blank boxes are due to the mutational status not being reported in the Cancer Cell Line Encyclopaedia, Cellosaurus™, or by the distributor of the cell line (ATCC, DSMZ). Ras status is further characterised in Figures 3.1-3.3.

Cell Line	Derived From	Ras status	Other relevant mutations
HeLa	Cervical cancer		
HEK293T	Kidney		
HS5	Breast cancer	HRAS G12D heterozygous	
OCI-AML-3	AML	NRAS Q61L homozygous	NPM1 W288Cfs*12(dup) heterozygous, DNMT3A D882C heterozygous
HL60	APML	NRAS Q61L heterozygous	Homozygous TP53 deletion, CDKN2A D80*(Ter)
MOLM-13	AML	Wild-type	MLL-AF9 fusion, Heterozygous FLT3-ITD
MV4-11	AML	Wild-type	KMT2A-AFF1 fusion, Homozygous FLT3-ITD
THP-1	AML	NRAS G12D heterozygous	CSNK2A1-DDX39B fusion, MLL-AF9 fusion, TP53 D174fs*3(del) heterozygous
U937	AML		CALM-AF10 fusion, PTEN G129fs*51(ins) hemizygous, PTPN11 G60R heterozygous, TP53 V173Wfs*59 homozygous. WT1 R301*(Ter)

2.4 Antibodies

Table 2.4. Antibodies used in Western blotting. 'P-' denotes antibodies detecting phosphorylated proteins only. Where appropriate, phosphorylation sites are denoted in brackets. All exhibit anti-human reactivity.

Protein	Source	Dilution	Conjugate	Application	Cat. No (Supplier)
NRAS	Mouse	1:200, milk	N/A	Western blotting (WB)	sc-31 (Santa Cruz)
KRAS	Mouse	1:1000, TBST	N/A	WB	(LSBio)
HRAS	Rabbit	1:1000, TBST	N/A	WB	Cell Signalling Technologies (CST)
Ras	Rabbit	1:1000, milk	N/A	WB	ab52939 (AbCam)
NRAS G12D	Rabbit	1:1000, milk	N/A	WB	14429 (CST)
p-ERK (Thr 202/Tyr 204)	Mouse	1:500, BSA	N/A	WB	sc-136521 (Santa Cruz)
p-AKT (Ser 473)	Rabbit	1:1000, BSA	N/A	WB	4060 (CST)
p42/44 MAPK (ERK 1/2)	Rabbit	1:1000, milk	N/A	WB	4695, CST

AKT (pan)	Rabbit	1:1000, milk	N/A	WB	4691, CST
Cas9	Mouse	1:2000, milk	N/A	WB	14697 (CST)
B-RAF	Mouse	1:1000, TBST	N/A	WB	sc-5284 (SantaCruz)
P-PI3K (p85)	Rabbit	1:1000, TBST	N/A	WB	60225-1-Ig (ProteinTech)
P-STAT5 (Tyr 694)	Rabbit	1:1000, TBST	N/A	WB	4322 (CST)
STAT5	Rabbit	1:1000, TBST	N/A	WB	25656 (CST)
Vinculin	Mouse	1:2000, TBST	N/A	WB	13901 (CST)
GAPDH	Rabbit	1:1000, TBST	N/A	WB	60004-1-Ig (ProteinTech)
Anti-Mouse IgG,	Horse	1:3000, milk or BSA	HRP	WB	7076 (CST)
Anti-Rabbit IgG	Goat	1:3000, milk or BSA	HRP	WB	7074 (CST)
CD33	Mouse IgG1, κ	1:100 perm. buffer	APC 647	Fluroescence microscopy	366605 (Biolegend)
4',6-Diamidino-2-Phenylindole, Dilactate (DAPI)	N/A	1:3600 perm. buffer	405	Fluroescence microscopy	422801 (Biolegend)

Calreticulin	Rabbit	1:100 perm. buffer	555	Fluroescence microscopy	52286 (CST)
NRAS	Rabbit	1:100 perm. buffer	CoraLite 647	Fluroescence microscopy	10724-1-AP
CD34	Mouse IgG1, κ	1:100 flow staining buffer	FITC 488	Flow cytometry	343503 (Biolegend)

2.5 Plasmids

Plasmids were either purchased through AddGene, or modified in-house. Purchased plasmids are listed in Table 2.5 and included in the appendices, with modified versions of these plasmids detailed in chapters 3 and 4 as appropriate.

Table 2.5. Plasmid backbones purchased via AddGene used throughout experiments detailed in this thesis.

Name	Purpose	Selection Marker	Lab	AddGene Ref.
psPAX2	Lentivirus generation (packaging)	Ampicillin	Didier Trono	12260
pMD2.G	Lentivirus generation (VSVG envelope)	Ampicillin	Didier Trono	12259
pLJM1-EGFP	Lentiviral vector backbone and transfection control	Ampicillin, Puromycin, EGFP	David Sabatini	19319

LentiCRISPR-V2	Lentiviral backbone – CRISPR guide delivery	Ampicillin, Puromycin	Feng Zhang	52961
LeGo-iG	Lentiviral backbone – CRISPR guide and HDR template delivery	Ampicillin, EGFP	Boris Fehse	27358
pCW-Cas9	Lentiviral compatible, tetracycline-inducible Cas9 delivery	Ampicillin, puromycin	David Sabatini, Eric Lander	50661

2.6 Cell Culture

All AML cell lines, as well as the HeLa cell line were routinely cultured in Roswell Park Memorial Institute (RPMI) 1640 medium, supplemented with 10% Foetal Bovine Serum (FBS) and 100 Units per ml Penicillin/Streptomycin. HEK293T and HS5 cells were cultured in Dulbecco's Modified Eagle Medium (DMEM) supplemented with 10% FBS and 100 Units per ml Penicillin/Streptomycin. All cells were grown at 37ºC containing 5% CO_2. All media and supplements listed here were purchased from Invitrogen, UK.

Cells were routinely passaged every 2-3 days. Suspension cells were either diluted with additional growth media or split in a 1:5 ratio, to a final seeding density of 300,000 cells per ml. Adherent HEK293T and HeLa cells were cultured up to 60-70% confluency, before being detached using 1X Trypsin-Ethylenediaminetetraacetic Acid

(EDTA) (Invitrogen, UK), centrifuged (300 x g, 4 min) and diluted to a concentration of 30,000 cells per ml. Adherent HS5 cells were cultured up to 80% confluency and then detached using 0.25% Trypsin-EDTA, centrifuged (300 x g, 4 min) and split 1:10 into fresh growth media, to a final concentration of 200,000 cells per ml.

2.7 Cryopreservation of cells

When not required in culture, approximately 5 million cells were centrifuged for 5 min at 300 x g, before the supernatant was removed and the pellet resuspended in 1ml freezing media. Freezing media comprised of 50% FBS, 40% normal culture media and 10% FBS. This was stored in cryovials and frozen gradually using a 'Mr Frosty™' (Fisher Scientific, UK), whereby vials are surrounded by isopropanol to permit cooling at approximately 1°C per minute. This container was stored at -80°C, until cells were frozen, and then each vial was transferred to liquid nitrogen for long-term storage.

2.8 Preparation of Competent *E. coli* Cells

One-Shot STBL3 or DH5α Competent *E. coli* were purchased from ThermoFisher (Cat. No. C737303 and EC0111, respectively). Competent *E. coli* were grown at 30°C whilst agitated overnight in 50 ml Super Optimal Broth (SOB) media. Competent *E. coli* were concentrated from this culture using the Zymogen 'Mix and Go' *E. coli* transformation kit, as per the manufacturer's protocols. Working stocks were stored in 100 µl aliquots for single-use only to avoid repetitive freeze-thawing and potential subsequent bacterial degradation.

2.9 Ligation

Following plasmid digestion with appropriate restriction enzymes, 5ng of digested plasmid was mixed with the DNA to be inserted, which had been modified (through digestion, oligonucleotide design or PCR) to have compatible enzyme restriction sites. Different concentrations of DNA inserts were tested, accounting for the size difference between the insert and vector backbone (digested plasmid). This was combined with T4 DNA ligase (1 µl) and the corresponding T4 10X Ligase buffer and water, to a final volume of 20 µl. The ligation occurred in either 1 h at room temperature, or 4°C overnight. Following ligation, the plasmids were then transformed using *E.coli.*

2.10 Transformation and Purification of Plasmids

5 ng of plasmid was added to 25 µl competent *E.coli* cells and incubated on ice for 30 min. The bacteria were heat shocked at 42ºC for 1 min before being returned to ice for 2 min. 350 µl SOC media was added to the bacteria and incubated, shaking at 37ºC for 45 min. 100-200 µl of bacterial suspension was then spread on a Luria-Bertani (LB) Broth-Agar plate containing the antibiotic corresponding to the antibiotic resistance gene within the plasmid and incubated overnight at 37ºC (16-18 h). For almost all plasmids used in this thesis, Carbenicillin (Thermo Fisher) was added to the LB broth and agar, up to a final concentration of 50 µg/ml. Where applicable, successful ligation of the plasmid was screened for using colony PCR, using primers specific to the inserted DNA. This was done by a small scraping of a selection of colonies into a 15 µl OneTaq PCR (section 2.12), the product of which was screened on an agarose gel. Positive colonies were then picked into LB broth the following day and were incubated, shaking at 37ºC overnight. Plasmid DNA extraction was then carried out using the Qiagen Miniprep Kit, according to manufacturer's instructions. Briefly, bacteria were

pelleted, lysed and the subsequent supernatant passed through a spin column. The plasmid DNA contained within the supernatant was bound to the membrane, washed and eluted in Ultrapure water, ultimately purifying the desired plasmid DNA. The final concentration of the extracted plasmid DNA was measured using a NanoDrop 2000 Spectrophotometer (ThermoFisher Scientific).

2.11 Restriction Digest

1 µg of the plasmid of interest was incubated at 37°C for 1 hour, with the appropriate enzyme(s) to create the desired digestion product, along with 10X Cutsmart buffer (NEB, UK), and water, to normalise the volumes between each sample to 20 µl. For certain enzymes, they were then heat inactivated at either 65°C or 95°C for five minutes. Successful digestion was then confirmed by agarose gel electrophoresis (Section 2.13) of an aliquot of the final reaction (5 µl digestion product plus 1 µl 6X DNA loading dye (NEB)). For digestions being taken forward for ligation, the appropriate fragment was then gel extracted, using the gel extraction method detailed in section 2.14.

2.12 Polymerase Chain Reaction

DNA was amplified using the OneTaq Quick-Load 2x Master Mix for most of the PCRs completed. Typical reactions had a total volume of 15 µl, made up of 7.5 µl OneTaq Quick-load 2X Master Mix, 1.5 µl 10 µM primers (forward and reverse), 300 ng (1 µl) DNA, 5 µl Nuclease-free water. Initial DNA denaturation occurred at 95ºC for 2 min, followed by 35 cycles of 30 s of DNA denaturing (95ºC), 30 s of primer annealing (58ºC) and 30 s of DNA extension (72ºC). The final extension step was carried out at

72ºC for 10 min, before the DNA was incubated at 4ºC until required. Experiment-specific deviations from this generic protocol are indicated in chapters 3-5.

In certain cases, Q5 polymerase (NEB, UK) was selected instead, because of its higher fidelity in terms of DNA replication compared to OneTaq, given the 'error checking' mechanism it employs. This included the generation of the HDR template. Q5 polymerase (1 µl) was combined with 10 µl Q5 reaction buffer, 500 ng template DNA, 5 µl of 10 µM primers (forward and reverse), as well as 1 µl dNTPs. This reaction mixture was made up to 50 µl, and run in a thermocycler using a similar protocol to that listed above, for the OneTaq PCR reaction. The annealing temperatures were generally increased by 1-2°C compared to the OneTaq PCR, given differences in the polymerase. The final product was generally separated by electrophoresis and visualised under ultraviolet light.

2.13 Agarose Gel Electrophoresis

DNA fragments were separated using a 0.8-1.5% (w/v) agarose gel. The gel was prepared through dissolution of agarose powder in 1X Tris-Acetate-EDTA buffer by microwaving. 4 µl SybrSAFE dye was added and the gel was poured into a casting tray. Once set, the gel was loaded into a Mupid-One electrophoresis system and run at 100 V for 25 min and visualised using a ChemiDoc system (BioRad, UK). DNA fragment size was compared to a reference ladder, selected based on expected product size. GeneRuler 100bp Plus Ladder was used when to visualise PCR products, whereas GeneRuler 1kb Ladder was used when visualising plasmids and associated fragments.

2.14 Gel Extraction/PCR Clean-up

DNA regions of interest were excised from an 0.8% agarose gel under ultraviolet light, with the DNA purified using the Promega (Hampshire, UK) Wizard SV Gel Extraction/PCR Clean-up Kit (Cat. No. A9281), according to manufacturer's protocol. Briefly, gel fragments were digested in 200 µl Membrane Binding Buffer at 55°C for 10-15 min, and then purified by passing through a DNA binding filter column, with buffers (binding and wash) filtered through by centrifugation. Finally, DNA was eluted into 55 µl UltraPure water and the concentration was measured using a NanoDrop. For sequencing regions of interest, 50 ng of DNA cleaned in this way was sent, along with the forward primer from the PCR reaction, to be Sanger sequenced (Source Biosciences, Cambridge, UK).

2.15 Transient Transfection

One day prior to transfection, 300,000 HEK293T or HeLa cells were plated in 2 ml antibiotic-free DMEM containing 10% FBS (6 well plate), or 3 million HEK293T or HeLa were plated in 10 ml antibiotic-free media containing 10% FBS (10 cm dish). 1 µg plasmid DNA per 300,000 cells was combined with Opti-MEM (10% final culture volume; Invitrogen, UK)), and Polyethylenimine hydrochloride (PEI, used at 3x DNA mass; Sigma, UK), vortexed, and incubated for 20 min at room temperature. This DNA mix was then pipetted drop-wise onto the cells, and incubated in normal growth conditions for 72 h. Following this, cells were collected following trypsinisation, and used in future experiments (such as DNA extraction, protein extraction or re-plating for growth assays).

2.16 CRISPR-Cas9 Gene Editing – *NRAS* Gene Knock-out

20 base pair oligonucleotide guide sequences were designed specific to the regions of interest. In the case of *NRAS* knock-out cell line generation, guides were designed in between *NRAS* exon 1 and *NRAS* exon 2, as well as in the intron between *NRAS* exons 2 and 3. This was to eliminate the ATG (Methionine) start codon of *NRAS,* located in *NRAS* exon 2. A schematic of this is present in Chapter 3 (Figure 3.14). A BsmBI-compatible restriction site was also added to each of the guide sequences, to permit cloning into the lentiviral-compatible vector. These sequences were purchased as single strand oligonucleotides from Integrated DNA Technologies (IDT, Leuven, Belgium). The single strand oligonucleotides were then annealed and phosphorylated, and cloned into the LentiCRISPR V2 vector (Table 2.5, Appendix 2), which had previously been digested with the enzyme BsmBI to generate compatible overhangs. The restriction digestion protocol is further discussed in section 2.11. Since the LentiCRISPR V2 plasmid contains the guide RNA scaffold, as well as constitutively-expressed Cas9 (from the bacterial strain *S. pyogenes,* thus known as spCas9 under control of the CMV promoter. Each plasmid therefore contained one guide.

For CRISPR-Cas9 gene editing to occur with an increased likelihood of success, two guide sequences were used per transfection. 1 µg of each plasmid was transfected into 300,000 HEK293T or HeLa growing in antibiotic-free media alongside 3 µg PEI and 200 µl Optimem. As a vector control, the original LentiCRISPR V2 plasmid was also transfected into a separate well of cells. Transfection was carried out according to the transient transfection protocol detailed in section 2.15.

2.17 CRISPR-Cas9 Gene Editing – *NRAS* G12D Mutation Reversal

In the case of the NRAS G12D mutation correction within the MV4-11-DR cell lines, the guide sequence was designed within exon 2, spanning the region to be mutated. This was purchased as single stranded 20 bp oligonucleotides, annealed and phosphorylated as detailed above. These oligonucleotides also had BsmBI compatible restriction sites on the ends, and they were subsequently cloned into the LentiCRISPR V2 plasmid detailed above. A region of this plasmid, also encompassing the guide RNA scaffold and the BmtI restriction site at the 3' end, was then PCR amplified, with an XbaI restriction site added at the 5' end in the PCR primer design. Following purification, this resulted in a product capable of being cloned into the EGFP-containing, lentiviral-compatible LeGo-iG plasmid.

The HDR template was designed so that it spanned 305 bp around NRAS exon 2. There were also silent mutations designed into the HDR template, to reduce the incidence of guide binding following a successful edit, so that the 'corrected' DNA following HDR remained undamaged by subsequent guide binding and Cas9 cutting. This is detailed further in Figure 4.9 (section 4.3.2). The guide sequence and HDR template were cloned into the LeGo-iG vector already containing the guide and scaffold sequences, as detailed above. The HDR template was positioned downstream of the SFFV promoter, and upstream of the IRES-promoted *EGFP* gene, enabling successful transduction of the 'CRISPR machinery' to be detected by fluorescence. This occurred through restriction digest using a Sbf1-compatible restriction site at the 5' end, and the NotI-compatible restriction site at the 3' end of the HDR template, since the destination plasmid (LeGo-iG + guide + scaffold) had been digested accordingly. This plasmid was then transfected into HEK293T to make lentivirus (section 2.15), and then transduced into the MV4-11-DR cell line (following

the protocols detailed in section 2.19. The schematic for this cloning can be found in figure 4.10.

2.18 Generation and Concentration of Lentivirus

Lentivirus expressing the genes of interest to be expressed in AML cell lines was generated using the third-generation lentiviral system. This involves the separation of the viral envelope gene VSVG, packaging genes *HIV gag-1* and *HIV pol*, and the gene/sequence of interest across three different plasmids (pMD2.G and psPax2, respectively, along with any Lentiviral-compatible vector for the gene of interest), which also incorporate other elements of the Human Immunodeficiency Virus (HIV) necessary to generate a virus capable of transducing mammalian cell lines. These plasmids were purchased from the Didier Trono lab, via Addgene (USA). These plasmids were then combined in a co-transfection to generate the desired virus, using HEK293T cellular machinery. HEK293T were used given their previous transformation (relative to HEK293) to have a greater transfection uptake capacity, thereby rendering them more amenable to a greater level of lentiviral production. This is due to the presence of the SV40 viral T antigen which was stably introduced to these cells (Tan, Chin, Lim & Ng, 2021).

Four million HEK293T cells were seeded in 10 ml RPMI-1640 media supplemented with 10% FBS, one day prior to transfection. Cells were transfected with 4.5 µg of plasmid containing the gene of interest, 2.3 µg of the psPax2 viral packaging plasmid, and 1.1 µg of the pMD2.G viral envelope plasmid, using 24 µg PEI and 1ml OptiMem (Invitrogen, Paisley, UK). 3 days after transfection, the media now containing lentivirus was collected and aliquoted, either for long-term storage (-80°C) or for direct

transduction onto the cell line of interest. Concentration of lentivirus was attempted in different manners, either using ultracentrifugation or Polyethyleneglycol-40 (PEG-40). Where ultracentrifugation was used, 10 ml virus-rich media was collected, and centrifuged at 100,000 x g for 2 h, and then resuspended in 100 µl sterile PBS, resulting in 100-fold concentration. Where PEG-40 was used, 10 ml virus-rich media was collected, and 2.5 ml PEG-40 was added (20% v/v final concentration). This was incubated, agitated, overnight, at 4°C. The suspension was then centrifuged at 1500 x g for 45 min at 4°C, before the supernatant was discarded, and the subsequent pellet resuspended in 100 µl sterile PBS, again resulting in 100-fold concentrated lentivirus, which could then be used to transduce cells.

2.19 Lentiviral Transduction

500,000 cells of the cell line of interest were plated in 2 ml at least 4 hours prior to transduction, in RPMI-1640 media supplemented with 10% FBS. The virus was titrated onto the cell line of interest, using 100-1000 µl dose range (non-concentrated virus), or 5-50 µl 100-fold concentrated virus. Polybrene was also added to a final concentration of 8 µg/ml, to assist with viral uptake. Cells were immediately centrifuged at 450 x g for 1 h at 37°C, then moved to the incubator. The total culture volume was doubled after 16 h, thereby diluting the polybrene to 4 µg/ml, to reduce the risk of cell toxicity. Virus-containing media was removed from the cells after 72 h, at which point selection was started, or FACS was performed, as required.

2.20 Selection of Transduced Cells

For cells transduced with plasmids containing a puromycin selection marker, 100,000 transduced cells were treated with 0.1 µg/ml puromycin. This concentration had been

optimised, as described in section 4.3.1.1. Cells were counted at 48, 72 and 96 h, and cell death was compared to non-transduced cells also treated with puromycin. After 96 h, remaining cells were then resuspended in 1ml fresh RPMI-1640 media supplemented with 10% FBS and 100 Units per ml Penicillin/Streptomycin. Cells were gradually expanded over a period of 2-3 weeks, before protein was extracted and overexpression of the protein of interest was assessed by Western immunoblotting.

2.21 Sorting of GFP+ Transduced Cells

Cell sorting was carried out with the kind assistance of Dr Sandra Pereira Cachinho, of the University of Liverpool's Flow Cytometry and Cell Sorting Facility. 48 h following removal of puromycin, to allow cells some recovery time. GFP+ cells were then sorted using the FACS Canto II system, at a speed of one million cells per hour. Gating of GFP+ cells is indicated in Figure 4.12. GFP+ cells were then immediately plated for subcloning.

2.22 Subcloning of Transduced cell lines

HS5 cells were trypsinised, pelleted and resuspended in fresh RPMI-1640 medium supplemented with 20% FBS and 100U/ml Penicillin/Streptomycin, at a concentration of $1x10^6$ cells per ml. Following irradiation at 150 Gy (3 Gy/min, 50 min), 100 µl of cells were plated in a 96 well plate at a concentration of $2x10^5$ cells per ml. The plate was then incubated at 37ºC at 5% CO_2 overnight to allow cells to adhere.

The cell line (generated through lentiviral transduction) to be subcloned was serially diluted in RPMI-1640 with 20% FBS and 100U/ml Penicillin/Streptomycin to a final concentration of 2 cells per ml. 100 µl of this suspension were added on top of the

irradiated HS5 cells, to achieve a theoretical concentration of 0.2 cells per well. 6 days later, a further 100 µl media was added to each well. Wells were checked frequently for development of clonal populations using a light microscope, or GFP fluorescence if appropriate. 11 days post plating, wells with monoclonal populations were re-plated into a 96 well plate without the HS5 stromal cell feeder layer, and cells continued to proliferate. These cells were gradually expanded, with full size culture typically established after 3-4 weeks. Protein or DNA was then extracted as required and the necessary validation tests performed to test lentiviral transduction efficacy.

2.23 Western Immunoblotting

Following protein quantification using the ThermoFisher (USA) BCA Assay kit, protein was mixed with 5x Laemelli Buffer and diluted with dH_2O, to obtain a final concentration of 1 µg/µl. 25 µg protein was loaded into 12% poly-acrylamide gels, the exception being 8% if probing for Cas9 expression, given its 160kDa size. Gels were run at 135V for approximately 90 min (until the protein had been fully separated), and then transferred to a nitrocellulose membrane at 100 V for 75 min. Membranes were blocked for 1 h in 4% milk or BSA (phospho-proteins only) diluted in TBST, and incubated (agitated) with primary antibody overnight, at 4°C (Table 2.4). Membranes were washed the following day in TBST for 5 min, 3 times. HRP-linked secondary antibody was added for 1 h, before membranes were washed again for 5 min, 3 times in TBST. Enhanced chemiluminescence was added on to the membrane for 1 min before imaging using a ChemiDoc system (BioRad, UK). Protein bands appearing on the blot were validated against the PageRuler Plus Protein Ladder (ThermoFisher, UK).

2.24 Ras Activity Assay

This was performed using the Active Ras Detection Kit, from Cell Signaling Technologies (Leiden, The Netherlands). Briefly, cells were lysed using the Triton-X-based lysis buffer, with protein subsequently quantified using the BCA assay (ThermoFisher, UK). 1 µg of protein from each cell line of interest was then loaded into spin columns containing a glutathione resin and the GST-Raf1-RBD, rendering it possible for GTP-bound (active) Ras to bind to the glutathione resin via the GST-linked binding protein. After incubating in an agitated fashion for 1 h at 4°C, the excess (unbound) protein was removed by centrifugation, and the GTP-bound (active) protein was eluted using an SDS-based reducing sample buffer. The quantity of GTP-bound Ras was then determined using Western blotting, probing the nitrocellulose membrane with a primary (pan) Ras antibody (section 2.23).

2.25 Cytotoxicity Assays

300,000 cells were plated in 1 ml RPMI-1640 media supplemented with 10% FBS and 100U/ml Penicillin/Streptomycin, at least 4 h prior to drug treatment. Drugs were added in a log-fold manner between 0.01-10 µM, and cell death was typically assessed using Annexin V-FITC/Propidium Iodide staining every 24 h (up to 72 h post-treatment), using Fluorescence Activated Cell Sorting (FACS), using the Attune NxT flow cytometer (Invitrogen, Paisley, UK). Annexin-V-FITC+ cells are considered to be going through apoptosis. This is due to the ‘flip’ of the phosphatidylserine from the intracellular side of the cell membrane, to the extracellular side of the cell membrane, thereby permitting Annexin V binding, causing cells to fluoresce with FITC. Propidium iodide binds cytosolic DNA, which is typically found as cells are dying by necrosis,

since they lose their structural integrity. Therefore, propidium iodide can be used as a marker for necrosis. Gating of cell populations for this protocol is detailed in Appendix 7. Following data acquisition, the IC_{50} value was determined using non-linear regression in GraphPad Prism V8.0, with significance between cell lines determined using unpaired (independent) t-tests, conducted in the same programme.

2.26 Colony Forming Assays

100 cells were plated in 1 ml 2.1% methylcellulose (4000 cp) (Sigma, Gillingham, UK) diluted in RPMI-1640 media (10% FBS) in technical triplicate and incubated for 7 days. Colonies were counted after 7 days using a light microscope, x20 magnification. This was repeated for biological replicates (N=3). Statistical significance was determined using unpaired (independent) t-tests in GraphPad Prism V8.0.

2.27 Cell Proliferation Assay – Trypan Blue

Trypan blue is cell impermeable, and therefore only able to stain cells should there be a loss of membrane integrity, and indeed cell death. In this way, when cells are studied under a light microscope, live cells will appear white and dead cells appearing blue. 100,000 cells were plated in 1ml RPMI-1640 media (in triplicate), supplemented with 10% FBS. 50 µl of culture was removed every 24 h (up to 96 h) and stained in a 1:1 ratio with 0.4% Trypan Blue. Cell number was counted manually using a haemocytometer and scaled up to cells per ml. Both technical (4) and biological (3) replicates were carried out for this assay.

2.28 Cell Proliferation Assay – Carboxyfluorescein Succinimidyl Ester (CFSE)

CFSE dye diffuses into cells and is catalysed by esterases causing the formation of fluorescent molecules. These binds proteins, and are retained within the cell. However, the manner of binding means the dye (and more importantly its fluorescent properties) are not passed from parent to daughter cells. As such, the more rounds of mitotic cell division a cell undergoes, the fewer cells (proportionally) that will contain the dye. This confers a decreased signal when analysing the cells by fluorescence-associated cell sorting (FACS). 1.5 million cells were stained in 1ml CFSE-PBS (1:2000 dilution) by incubating at 37°C for 30 min, before excess dye was diluted in excess media and then removed by centrifugation. Subsequently, stained cells were resuspended in 3 ml RPMI-1640 (10% FBS). Proliferation was measured by flow cytometry, through monitoring progressive decrease in percentage of stained cells every 24 h, up to 96 h, using the BL1-A channel on the Attune NxT flow cytometer. Data was subsequently downloaded into FCSalyzer to show visual comparisons between data sets.

2.29 Cell Cycle Analysis – 7-Aminoactinomycin D (7AAD) Staining

7AAD binds DNA through intercalation in G-C rich regions of the double helix. Therefore, the greater the amount of DNA present, the more intense the signal. Such signal can be detected by fluorescence-associated cell sorting (FACS), as used here. Cells were initially serum starved for 18 h by growth in RPMI-1640 without the addition of FBS, to somewhat synchronise cell cycles between cell lines. 300,000 cells were plated in 2 ml RPMI-1640 media (in triplicate), supplemented with 10% FBS. 100 µl of culture was removed every 24 h (up to 96 h), washed twice in PBS and resuspended

in 70% ethanol, whilst being gently vortexed. Cells were fixed in this ethanol for up to 1 week post-harvest, and then stained with 7AAD (1:40 dilution, as per the manufacturer's protocol). Staining (and therefore relative DNA quantity) was measured using the BL1-A channel on the Attune NxT flow cytometer. Data was subsequently downloaded into FCSalyzer and analysed using GraphPad 8.0. Independent t-tests were used to test for statistical significance once N=3 was achieved. Gating of each phase is exemplified in Appendix 7.

2.30 Quantitative PCR

RNA was extracted from 10 million cells of the cell line of interest, using the Qiagen RNeasy Plus Mini Kit (Cat. No. 74134) and eluted in 55 µl RNAse-free water, with concentration confirmed by NanoDrop. This was converted to cDNA in 1 µg reactions, using the QuantiTect Rev. Transcription Kit (Cat. No. 205311). Quantitative PCR was then performed using 20 ng cDNA, and the SYBR® Green Jumpstart™ Taq Readymix™ kit (Sigma Aldrich, Gillingham, UK). QPCR primers were designed specific to the N-terminal region (exon 2). Reactions were performed in triplicate, both in terms of biological and technical replicates, using an Aria MX3005P machine. Data was analysed using the ΔΔCt method, being compared to the GAPDH housekeeping control. A list of primers used in each experiment can be found within the relevant results sections, in Chapters 3-5.

2.31 Immunofluorescence

This work was carried out with the kind assistance of James Griffin, and the facilities available in the Centre for Cell Imaging at the University of Liverpool. A black 96 well Phenoplate (Perkin Elmer, Pontyclun, UK) was coated with 100 µl 50 µg/ml Poly-D-

Lysine (Invitrogen, Paisley, UK), which was left to adhere at room temperature for 1 hr. The remaining solution was then removed by pipetting, and the well washed three times using distilled water, before storage at 4°C until use.

Elsewhere, 100,000 cells per protein to be imaged for each cell line of interest were collected, washed using 1X PBS (centrifuged at 300 x g, 4 min) and were fixed at room temperature for 20 minutes in 200 µl 4% paraformaldehyde/PBS fixation buffer, before being removed from this buffer by centrifugation (500 x g, 5 min). Cells were then permeabilised by resuspension in 1X permeabilisation buffer (diluted from 10X stock in PBS) (Invitrogen, Paisley, UK). Cells were removed immediately from this buffer by centrifugation (500 x g, 5 min). Fluorescent antibodies were diluted to the concentrations given in Table 2.4 in 1X permeabilisation buffer. Cells were stained using 100 µl diluted antibody and incubated in the dark at room temperature for 30 min. This stain was diluted by adding 1 ml 1X permeabilisation buffer and cells were removed from this buffer/dye mix by centrifugation (500 x g, 5 min). Cells were resuspended in 200 µl PBS, and added to the pre-coated Phenoplate. Cells adhered to the Poly-D-lysine coated surface, before being imaged using the Elyra 7 fluorescent microscope.

2.32 Cell Surface Staining

Antibodies were prepared in flow staining buffer (1% FBS/PBS), at a 1:100 dilution. 200,000 cells of the cell line of interest were pelleted by centrifugation at 300 x g (4 min), washed once in PBS, and resuspended in 50 µl flow staining buffer with antibody. Cells were incubated in the dark at room temperature for 30 min, before being pelleted by centrifugation. This pellet was then resuspended in 200 µl flow staining buffer and

the sample was analysed by flow cytometry, collecting 10,000 events using the relevant lasers on the Attune NxT flow cytometer. All stains were compared to an unstained sample treated the same bar the addition of antibody, to indicate the percentage increase in receptor expression.

2.33 RNA Extraction and Quality Check

10 million cells were harvested and washed twice in PBS. Using the Qiagen RNA Extraction kit, cells were lysed and genomic DNA degraded using gDNA wipeout columns, ultimately resulting in the Isolation of RNA. All centrifuge steps were performed at 4°C, and all bench work was performed on ice, to preserve RNA quality. Concentration was determined using a NanoDrop™ (ThermoScientific, Altrincham, UK), with good quality RNA determined by the A260/280 and A260/230 ratios both being ≥ 2.00. RNA quality was also validated using a 1.5% Agarose/1% bleach gel, whereby the agarose was dissolved in 1X TAE buffer, by microwaving for approximately 2 min. 1% bleach and 4 µl SYBRSafe were added prior to gel casting. Samples were dyed using 6X DNA loading dye (NEB, Wiltshire, UK), and loaded into the gel, alongside the GeneRuler 1kb ladder. Good quality was determined should the upper band (representing 28S RNA) be thicker than or equivalent to the lower band (representing 18S RNA).

2.34 Genomic DNA Extraction

2 million cells were collected, pelleted by centrifugation at 300 x G (4 min), and washed twice in PBS. Genomic DNA was extracted using the Wizard SV Genomic DNA Extraction kit (Promega). Briefly, this involved cell lysis with the included SV lysis

buffer, and then spun through a DNA binding column. The resulting DNA was then purified by four washes of the membrane using the Column Wash solution included in the kit, and finally eluted in 55 µl Ultrapure water. This elution was carried out using 30 µl Ultrapure water initially, which was added to the column before the column was incubated at 42°C for 2 min, and centrifuged at 21000 x g for 5 min. This process was repeated with 25 µl Ultrapure water. Quality and concentration of each DNA sample was validated using a NanoDrop™ (ThermoScientific, Altrincham, UK).

2.35 Transcriptomic Analysis by RNASeq

2.35.1 Quality Control and Gene Expression Quantification

This was performed by Novogene Ltd., Cambridge, UK, using R. 2-4 µg of high quality RNA (as deemed by A260/230 and A260/280 values ≥2) was sent for sequencing and analysed. Quality Control was also carried out by Novogene, consisting of the base calling error rate (qPhred score, in the case of the Illumina sequencing platform), validation of the GC content distribution and data filtering to remove low quality (N>10% or Qscore where 50% of bases are <5) or adapter-containing reads. The RNA sequence was obtained using the Illumina platform. Alignments of the RNA sequences of the cell lines in question to the reference sequence were carried out using the HISAT2 platform, and mapped to the *Homo sapiens* hg38 reference genome. Data was normalised using the Fragments Per Kilobase of transcript per Million mapped reads (FPKM) counts method, to quantify and subsequently analyse gene expression levels, with both sequencing depth and gene length accounted for (Mortazavi, Williams, McCue, Schaeffer & Wold, 2008). Expression analysis was measured using the edgeR software (Robinson, McCarthy & Smyth, 2010), with the p value calculated using the Negative Binomial Distribution model.

2.35.2 Differential Expression and Functional Analysis

Analysis of differential gene expression and structural analysis was carried out and used to inform functional analysis. Significance of this was determined using the p-adjusted (padj) of <0.05, since there was a high number of genes analysed, thus presenting a risk of a high degree of false positives. Therefore, the padj value can be calibrated to control for this.

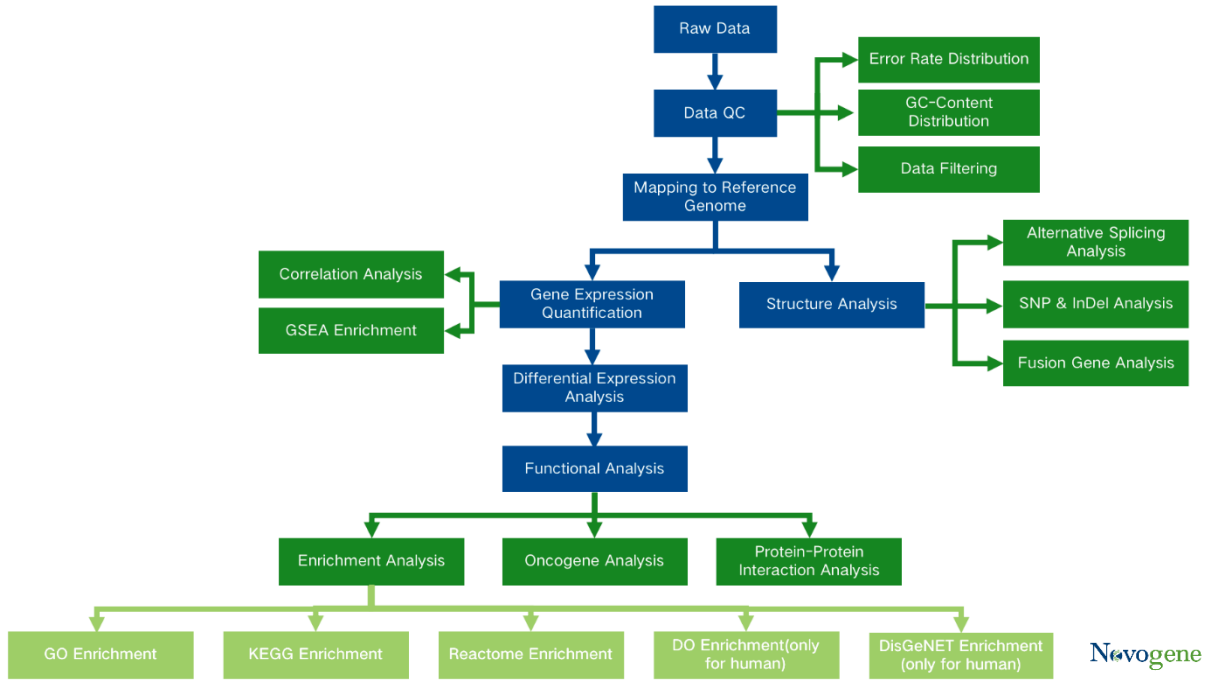

Figure 2.1. Workflow of RNASeq analysis. Pathways followed by Novogene to obtain a wide breadth of analysis regarding sequences and resultant pathway and cellular alterations. *QC = Quality control; GSEA = Gene Set Enrichment Analysis; SNP = Single Nucleotide Polymorphism; InDel = Insertion/Deletion; GO = Gene Ontology; DO = Disease Ontology; DisGeNET = Gene-Disease Association online interrogation platform.*

Functional analysis, based on the differential gene expression, included Kyoto Encyclopedia of Genes and Genomes (KEGG) pathway analysis and Gene Ontology Enrichment, amongst others. These were carried out using the clusterProfiler software

(Yu, Wang, Han & He, 2012). All quantification and analyses discussed here and illustrated below (Figure 2.1) were carried out by Novogene. Specific targets, as detailed in chapter 5, were interrogated using the FPKM-normalised gene enrichment analysis files provided by Novogene (Section 2.35.1).

2.36 Statistical Analysis

Statistical analysis was typically carried out in GraphPad V8.0, once biological replicates of N≥3 had been achieved. Unpaired (independent) t-tests were selected for this, comparing only two cell lines at a time. This was chosen given the lack of dependency on one variable to another (comparison between one cell line and another only). This test also assumes equal distribution. Where more than two variables were to be compared, the One-Way ANOVA test was carried out on the whole experiment carried out, with subsequent t-tests indicating significance between different groups.

Chapter 3

Characterisation of NRAS in Acute Myeloid Leukaemia Cell Lines

3 Characterisation of NRAS in Cell Lines

3.1 Introduction

NRAS mutations at the G12, G13 and Q61 hotspots are often considered activating, since they typically favour the GTP-bound (active) conformation, irrespective of the intrinsic GEF and GAP activity within the cell. This is believed to be either through a stabilisation in the GTP-bound state (and thereby a decreased intrinsic GTPase activity as would be expected), or a decreased for GAPs, such as NF1 (Burd et al., 2014; Gillies, Pargett, Silva, Teragawa, McCormick & Albeck, 2020). However, the precise mechanism by which each mutant confers this preference for the GTP-bound state remains to be elucidated.

The majority of disease studies surrounding Ras mutants have been carried out in pancreatic or lung cancer, where KRAS is the most commonly mutated isoform (Prior, Hood & Hartley, 2020; Prior, Lewis & Mattos, 2012). Even for NRAS-specific disease studies, it is predominantly melanoma that is studied, where, like in AML, NRAS is the most commonly mutated Ras isoform (Burd et al., 2014). Nevertheless, as previously discussed in the introductory chapter (section 1.4), there is a strong implication for NRAS-driven pathogenesis in AML, which will be further characterised in this chapter. As shown in figure 1.12, numerous different amino acids within NRAS are mutated across cancer. Whilst G12, G13 and Q61 are particularly favoured, in keeping with their recognition as mutational hotspots, the base substitutions and resultant changes in amino acid differ considerably (Figure 1.13). The reasons for the differing mutations yet to be elucidated, though given the development of mutant-specific inhibitors, it is

an upcoming and important field of research. Work carried out here will focus on the three key mutational hotspots, for more direct comparison between these AML cell lines and the available literature.

3.2 Aims and Hypothesis

Based upon current literature and the considerable heterogeneity seen in patients, I hypothesise that there will be a considerable phenotypic effect seen in the presence of NRAS mutations within a leukaemic cell. This will be coupled with a pro-survival effect in response to drugs targeting up-stream of Ras, such as FLT3 inhibitors.

This chapter aims to characterise innate Ras-mediated effects in both parental and drug-resistant AML cell lines. This will be at the genomic and phenotypic levels, with particular focus on the three key mutational hotspots and the common Ras-mediated MAPK and PI3K-AKT pathways. This will largely be done through molecular methods and cellular assays, including genotyping by Sanger Sequencing, Western blotting and drug sensitivity analysis. It is hypothesised that presence of NRAS mutations will increase the activity of these pathways, and could confer drug resistance.

The second aim of this chapter is to generate tools required to investigate individual mutant over-expression in parental AML cell lines characterised in the first half of this chapter. This will be performed using a host of molecular methods to create an NRAS-wild-type expression vector, and subsequently introduce key NRAS hotspot mutations into this using overlap PCR. The efficiency and utility of these vectors will be initially tested in an easily-transfectable model (HEK293T), and an easily-transfectable cancer context (HeLa), before being stably expressed in AML cell lines using lentiviral transduction (which will be detailed in Chapter 5).

3.3 Results

3.3.1 NRAS Genotype in AML cell lines

A wide panel of AML cell lines was initially studied, each of these with their own key genotypic features, representing the widely heterogenous nature of the AML. Key genotypic features, as detailed by online databases and the commercial biobanks from which the cells were obtained are listed in the Materials and Methods chapter (Table 2.3). However, given the significance of the Ras hotspot mutations throughout this project, exons 2 and 3 of *NRAS* were Sanger sequenced to validate the genotypes and decide with which cell lines to proceed with. Previously-generated FLT3-inhibitor resistant forms of the MOLM-13 and MV4-11 cell lines were also genotyped. These will be hereafter referred to as MOLM-13-DR and MV4-11-DR. These cell lines had been generated within our lab by Dr Vanessa Marensi previously to the commencement of this project, through prolonged exposure to the FLT3-ITD-specific inhibitor quizartinib, and so their generation will not be further discussed here (Marensi et al., manuscript in preparation). Validation of this resistance will, however, be further proven and discussed, in section 3.6.

Genomic DNA was extracted from all AML cell lines of interest, and regions containing the NRAS mutational hotspots (exons 2 and 3) were amplified using PCR. Primers were designed in the intergenic and intronic regions to permit full amplification of each exon (Figure 3.1). Table 3.1 summarises the PCR conditions for each primer set.

Table 3.1. *NRAS* hotspot mutations genotyping primers

Primer	Sequence	T_M (°C)
***NRAS* Exon 2 Forward**	CCG GTG TTT TTG CGT TCT C	62.7
***NRAS* Exon 2 Reverse**	ATA CAA TCA GAC AGT CTC GC	61.2
***NRAS* Exon 3 Forward**	GAG GGA CAA ACC AGA TAG GCA G	68.4
***NRAS* Exon 3 Reverse**	CCC TAG TGT GGT AAC CTC ATT TCC C	71.8
***KRAS* Exon 2 Forward**	CTT GTG GTA GTT GGA GCT GG	65.3
***KRAS* Exon 2 Reverse**	CAC AGC CAG GAG TCT TTT CTT C	66.3
***KRAS* Exon 3 Forward**	GAG GCC ATT TGT CCG TCA TCT TTG	69.9
***KRAS* Exon 3 Reverse**	GGT TTC AAT CCC AGC ACC AC	65.3

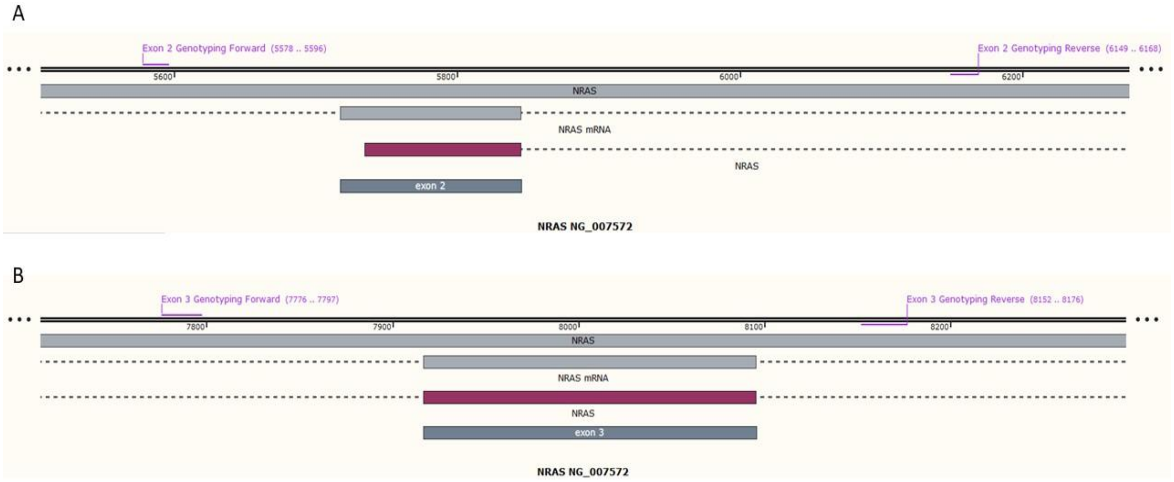

Figure 3.1. Genomic locations of primers used to genotype *NRAS* mutational hotspots. A) Primers spanning exon 2 (mutational hotspots G12 and G13). **B)** Primers spanning exon 3 (mutational hotspot Q61). KRAS genotyping primers were designed in a similar manner.

As expected, Sanger sequencing revealed a wide range of Ras genotypes throughout the eight cell lines tested (Figure 3.2). Mutations in each exon were exclusive; no cell line had both exon 2 and exon 3 mutations. Whilst the results of this sequencing showed that the mutations were the same as is published in the literature (Table 2.3)

in terms of the substitutions that had occurred, the zygosity of the mutations appeared different. For example, the NRAS G12D in THP-1 is reported to be heterozygous, though our results showed it to be homozygous. This is likely due to a lack of sequencing sensitivity, since the sequencing shown in Figure 3.2 was carried out using simple Sanger sequencing. However, since the mutational site and substitution, rather than the zygosity, were the main features for this work, deeper sequencing was not performed in this case.

Most notable was the genotype for the FLT3-inhibitor resistant cell lines. These acquired NRAS mutations relative to their parent cell line, however individual mutation differed between each of the cell lines. MOLM-13-DR became homozygous for the NRAS Q61L, and MV4-11-DR became NRAS G12D-heterozygous. For reference, both of these cell lines were NRAS wild-type before being made drug-resistant. This is in-keeping with publicly available data, which suggests FLT3-inhibitor patients acquire either of these mutations (McMahon et al., 2019). This Sanger sequencing data of *NRAS* exon 3 also shows that the oncogenic features associated with NRAS in this case are restricted to the mutational hotspots, since there are no G60E mutations, which have previously been associated with leukaemogenesis (Tyner et al., 2009; Tyner et al., 2018).

Following the discovery of these mutations and selection of the MOLM-13 and MV4-11 parental and drug-resistant cell lines as the model for this thesis, exons 2 and 3 of *KRAS*, which is more rarely mutated in AML, within these cell lines were also examined using the same Sanger sequencing method. Primer sequences for this can be found in Table 3.1. As expected, none of the cell lines co-expressed mutations both NRAS

and KRAS (Figure 3.3). This is supported by publicly available patient data, both from TCGA and other publications. Therefore, this further affirmed the validity of studying NRAS-mutants in a FLT3-inhibitor-resistant context, using the model previously generated in our lab.

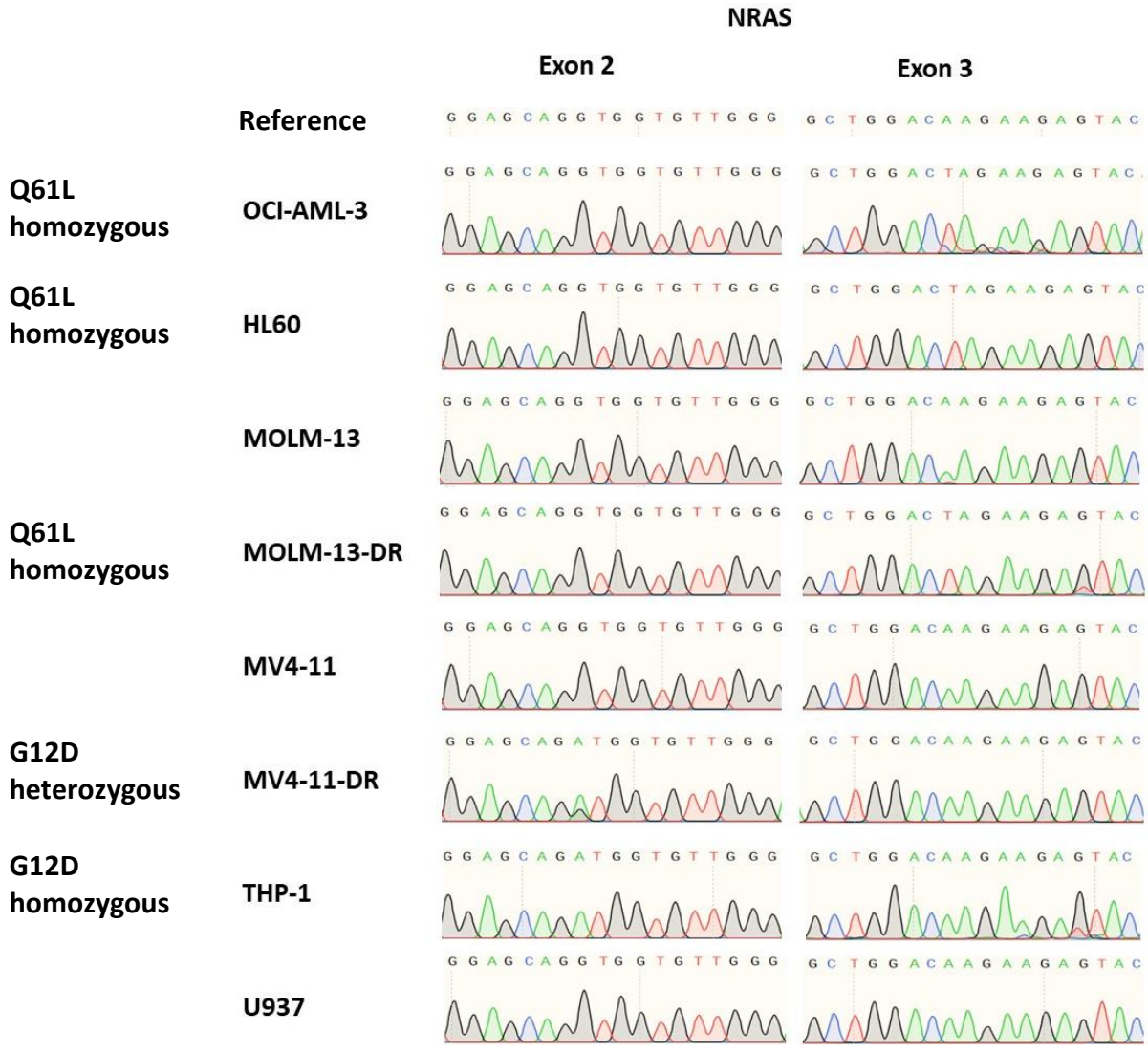

Figure 3.2. *NRAS* Genotype in AML cell lines. The genomic region of interest (exon 2 and exon 3) was amplified and Sanger sequenced, to assess *NRAS* genotype. Amino acid changes (relative to the NCBI GRCh38.p14 reference sequence, shown above) shown in bold on the left of the chromatograms. Double peaks within the same base in a chromatogram illustrate a heterozygous mutation, as is evident in the MV4-11-DR cells, which are heterozygous for the G12D mutation.

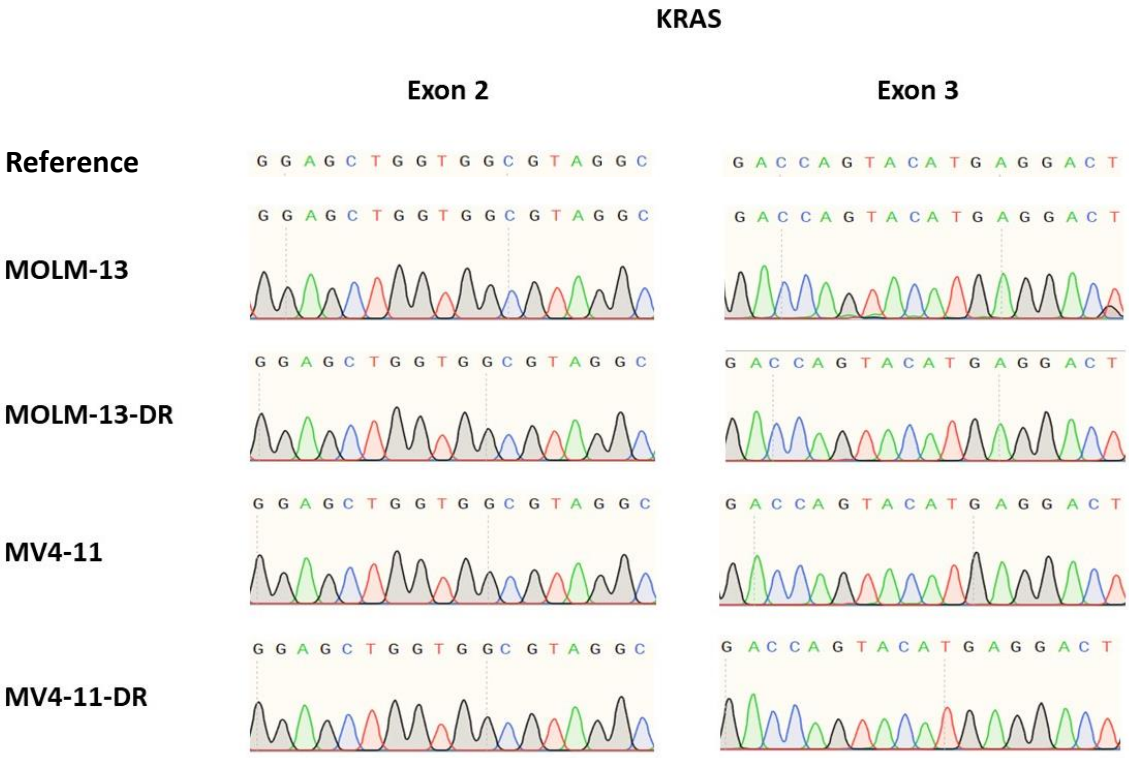

Figure 3.3. *KRAS* Genotype in AML cell lines. The genomic region of interest (exon 2 and exon 3) was amplified and Sanger sequenced, to assess *KRAS* genotype. NCBI GRCh38.p14 reference sequence indicated above the sequencing data. No mutations detected compared to the reference sequence at these mutational hotspots.

3.3.2 Ras transcript abundance in AML Cell Lines

Previous studies concerning NRAS-mediated drug resistance have shown NRAS transcript levels to be increased following the development of tyrosine kinase inhibitor resistance (Ninomiya et al., 2018). This has not yet been widely explored in AML, therefore NRAS transcript abundance was measured using Real-Time PCR (RT-PCR) in our FLT3 inhibitor resistant cell lines. NRAS was focussed upon here due to the emergence of mutations within the drug-resistant lines, and therefore it would be interesting to investigate whether these mutations correlated with alterations to transcript level.

Primers were designed specific to the NRAS isoform, to avoid any cross-amplification of other Ras isoforms that are not the focus of this study, which could have occurred as a result of high sequence similarity (Table 3.2). Data was normalised using the housekeeping gene *GAPDH*. Abundance in drug resistant (DR) cells was compared to the parental cells, and shown in Figure 3.4. *NRAS* transcript abundance was significantly elevated in both MOLM-13-DR and MV4-11-DR cells compared to the parental cells. As a result of the genomic differences between *NRAS* seen in the parental and drug-resistant MOLM-13 and MV4-11 cell lines, these were taken forward for further study.

Table 3.2. Ras isoform quantitative PCR primers

Primer	Sequence (5'-3')	T_M (°C)
qPCR NRAS Forward	GCA GGT GGT GTT GGG AAA AGC	67.7
qPCR NRAS Reverse	GCC AGT TCG TGG GCT TGT TTT G	68.4
qPCR GAPDH Forward	CCA CTT TGT CAA GCT CAT TTC C	64.3
qPCR GAPDH Reverse	TCT CTT CCT CTT GTG CTC TTG	64.0

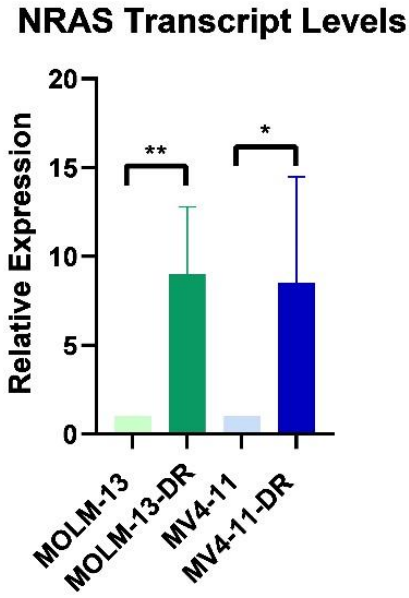

Figure 3.4. *NRAS* isoform transcript abundance in parental and FLT3-inhibitor-resistant cell lines. Transcript abundance quantified by qPCR, relative to *GAPDH* housekeeping gene using the ΔΔCt method of analysis. Data represent N=3 +/- SEM, biological repeats. * denotes *P*<0.05, * denotes *P*<0.01. Control levels normalised to 1, indicating fold-change for DR cells.

3.3.3 Ras-Mediated Signalling in AML Cell Lines

Relative Ras expression levels of each cell line was determined via Western blotting, as shown in Figure 3.5. In the FLT3-inhibitor resistant cell lines which had a mutated *NRAS* genotype, NRAS expression was increased relative to the parental, wild type NRAS cell lines. This also correlated with an increase in KRAS and indeed total (pan) Ras in the resistant cell lines, implicating Ras as a mediator of drug resistance. HRAS, however, was unaffected, and indeed only expressed at a much lower level compared to the other isoforms.

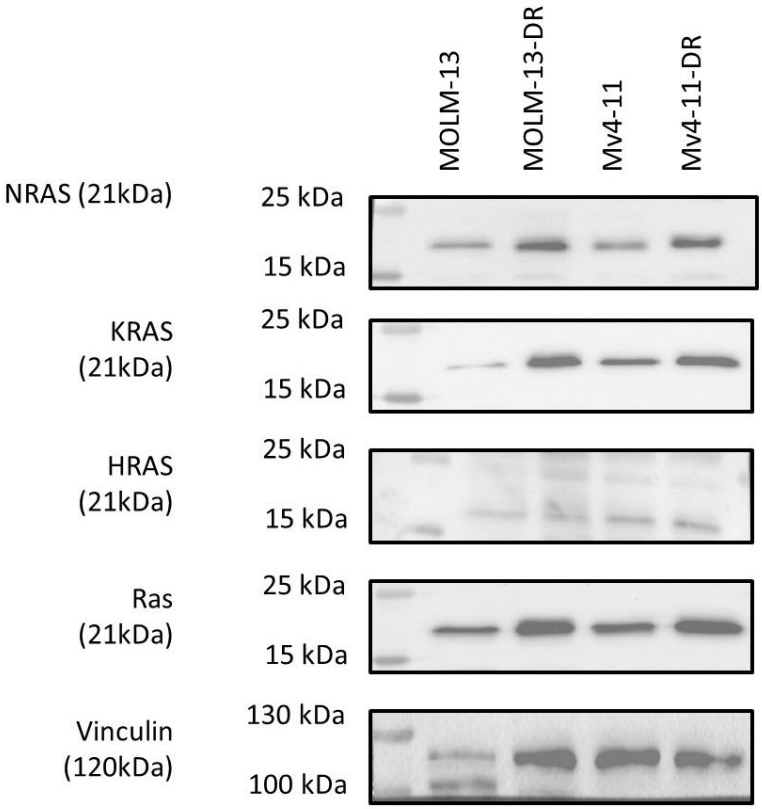

Figure 3.5. Ras isoform protein expression in MOLM-13 and MV4-11 parental and FLT3-inhibitor resistant cell lines. Protein levels determined by Western blotting and compared to Vinculin as a loading control.

Figure 3.6 details signalling changes within Ras-dependent pathways, including the PI3K/AKT and MAPK pathways. In the drug-resistant cells, BRAF expression levels were considerably increased, relative to the parental cells. This correlates with a somewhat increased ERK activation signal, indicating a role for the MAPK pathway in the maintenance of the drug-resistant phenotype. Whilst AKT activation increased in the MOLM-13-DR cell line, it decreased in the MV4-11-DR cell line, both relative to their parental controls. STAT5 signalling, known to be involved in AML signalling although not Ras dependent, was difficult to detect by Western blot, though there appeared to be a decrease in STAT5 activation in the resistant cells. PTEN levels were also somewhat increased in the drug-resistant cells.

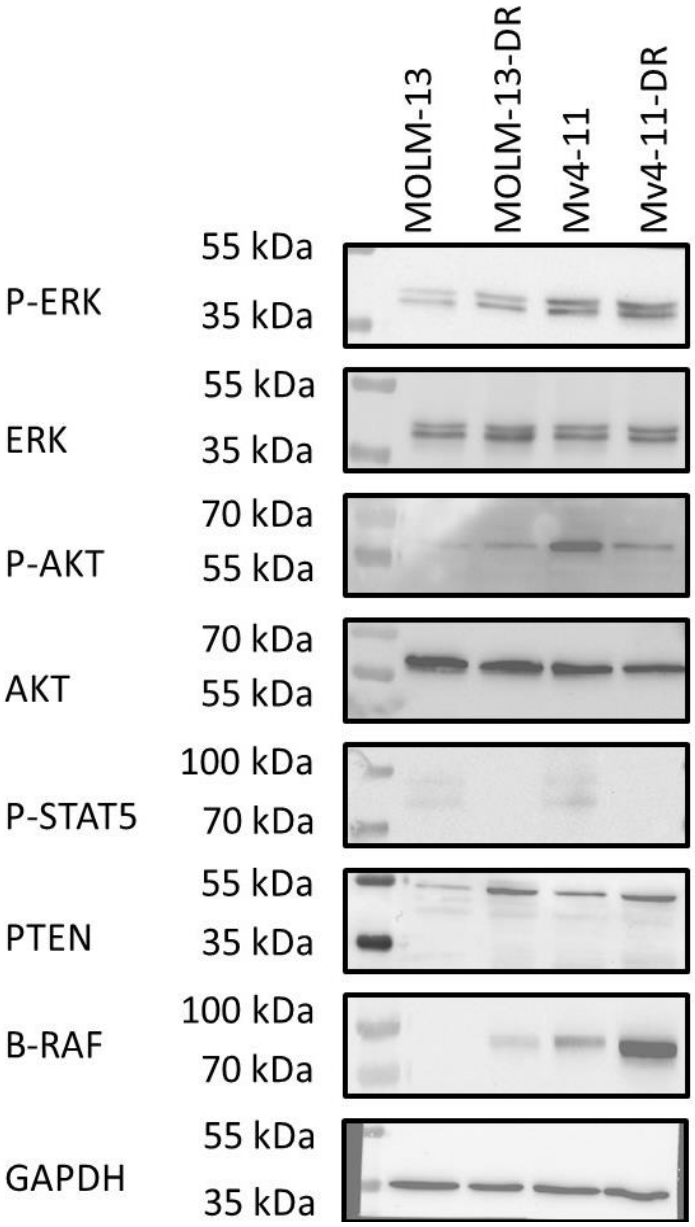

Figure 3.6. Signalling within the FLT3-ITD+ AML cell lines, both parental and FLT3-inhibitor resistant (DR). Proteins within key pathways relevant to AML were analysed by Western blotting to determine intrinsic signalling differences between FLT3-ITD heterozygous (MOLM-13) and FLT3-ITD homozygous (MV4-11), in relation to their drug-resistant counterparts. Key pathways studied include the MAPK pathway, PI3K/AKT pathway, and the STAT5 signalling pathway. Relative Ras isoform expression was also analysed in this way (Figure 3.5). GAPDH was used as a loading control.

Ras activity was measured using a GTP-binding assay. Briefly, this assay involved incubation of protein isolated from the MOLM-13 and MV4-11 parental and drug-resistant cells with agarose beads conjugated to the Raf1 Ras binding domain. This resulted in isolation and pull down of only GTP-bound NRAS, which was then separated by SDS-PAGE and analysed by Western blot. To ensure equal protein loading between samples, an initial 1 mg protein of each sample was loaded into the columns for the pull-down assay, following quantification using the BCA assay (R^2=0.995). As is evident from Figure 3.7, there was an increased level of NRAS activation in the drug-resistant cells, compared to their parental counterparts.

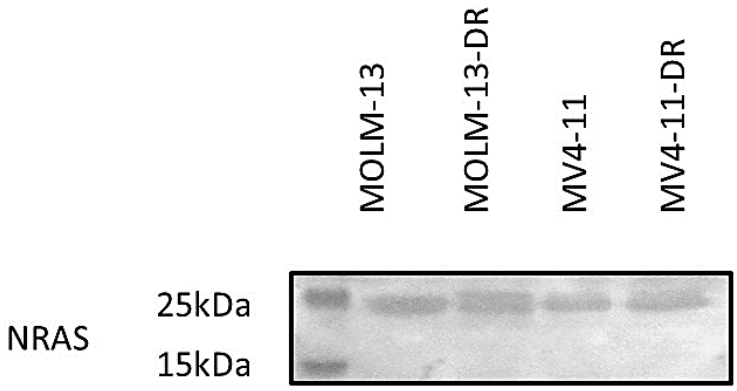

Figure 3.7. NRAS activation in FLT3-ITD+ AML cell lines, both parental and FLT3-inhibitor resistant (DR). Protein was isolated from cell lines, quantified and 1 mg of such was bound to the Raf1-Ras binding domain. This was then separated using SDS-PAGE and analysed by Western blotting.

3.3.4 Pharmacological Inhibition of Ras-mediated signalling in wild-type and drug-resistant cell lines

Response to multiple drugs targeting different elements of the Ras pathway was tested in the parental and drug-resistant cell lines, as well as response to the front-line therapy for AML, cytarabine. Although these drug-resistant cells were generated

through prolonged exposure to FLT3 inhibitors (Marensi et al., manuscript in preparation), they also showed a considerable level of resistance to cytarabine. This suggests a severely limited therapeutic landscape for a subset of patients, those also exhibiting such a strong resistance phenotype. This has already been suggested in a selection of patients, although remains unconfirmed (Döhner, Weisdorf & Bloomfield, 2015). It is therefore essential to decipher key targets within these resistant lines to ideally lead to treatment stratification, as well as identifying the optimal therapeutics to target these highly resistant cases. As a result, in line with the aforementioned sequencing data revealing the emergence of NRAS mutations in these resistant cells, various elements of Ras-mediated pathways were targeted pharmacologically.

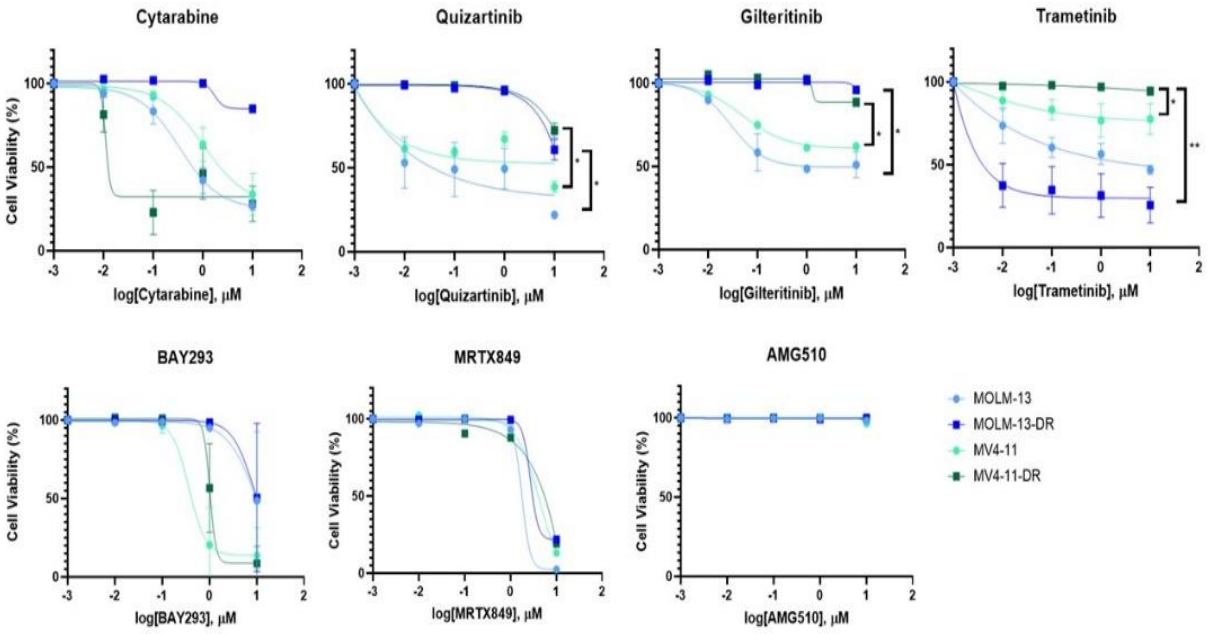

Figure 3.8. Sensitivity of FLT3-ITD+ cell lines towards numerous Ras pathway targeting agents and AML therapeutics. Cell viability was determined 48h post-treatment with 0-10 µM of drug in a logarithmic dosing fashion. N=3 +/-SEM, with the exception of AMG510 and MRTX849, which is N=1 +/-SD. Significant differences were initially analysed by ANOVA, with individual comparisons subsequently carried out using Unpaired t-tests. * denotes *P*<0.05, ** denotes *P*<0.01.Non-logistic regression shown by curves.

As previously shown in Figure 1.11, the compounds tested here cover a range of elements within both the AML and Ras therapeutic landscape. Cytarabine is a nucleoside analogue, part of the front-line therapy that the vast majority of AML patients will receive, in conjunction with an anthracycline (commonly daunorubicin). Gilteritinib is a pan receptor tyrosine kinase (RTK) inhibitor that has been recently approved as a third-line therapy for FLT3-ITD positive patients upon disease relapse. Quizartinib is a FLT3-ITD-specific inhibitor that is currently approved in Japan for patient use, and is in Phase III clinical trials in Europe and the USA, awaiting approval by the EMA and FDA, respectively. Trametinib is a MEK inhibitor, approved for use in a range of cancers, such as BRAF V600E-mutated melanoma and BRAF V600E-mutated NSCLC, as well as other BRAF V600E-mutated solid tumours. More detail on these drugs will be provided in Chapter 6. BAY293 is a pre-clinical compound, designed to inhibit the interaction between KRAS and SOS1. AMG510 and MRTX849 have recently been approved as direct targeting KRAS G12C inhibitors for use in lung cancer, and are the first of their kind.

Figure 3.8 illustrates the significant difference between sensitivity to the FLT3 inhibitors Quizartinib and Gilteritinib, as was the goal when these cells were generated in our lab. Whilst there appears to be a decrease in cytarabine sensitivity in the MOLM-13-DR cell line relative to the parental control, this was not deemed to be significant, despite the fact the IC_{50} was >10 µM at 48h. Interestingly, the MOLM-13 cell line (both parental and resistant) were sensitive to trametinib and remained so in the resistant cell line, perhaps to an even greater degree (non-significant). In contrast, the MV4-11 cell line was not as sensitive to the drug, and this became statistically significantly more resistant in the MV4-11-DR cells.

All cells showed a particularly low sensitivity to BAY293, the Ras-SOS interaction inhibitor. This was most prominent in the MV411-DR cell line, though there was no significant difference between any of the cell lines.

MRTX849 also conferred a high IC_{50}, and there was no significant difference between any cell line. All cell lines were also completely insensitive to AMG510, with no toxicity seen in any of the four tested at any dose.

3.3.5 Over-expression of NRAS Mutants *in vitro*

3.3.5.1 Construct Generation

To assess the phenotypic significance of different mutations in NRAS, selected NRAS mutations were over-expressed in HEK293T and HeLa cells. NRAS wild-type cDNA was amplified from MOLM-13 cells and cloned into the pLJM1 backbone, using AgeI and EcoRI restriction enzymes (Table 3.3). This was subsequently mutated using overlap PCR, to generate the NRAS mutants G12C, G12D and Q61K, all of which are common in AML and other cancers, with Ras G12C mutations representing a novel drug target, and G12D also under investigation. A model workflow for the generation of these wild-type and mutants (Figure 3.9) are shown below, with NRAS-G12D used as an example and agarose gels shown as validation of these steps (Figure 3.10). A similar process was followed for G12C and Q61K mutants, again using site-directed mutagenesis to create each mutation. Sanger sequencing was used to confirm successful mutagenesis (Figure 3.11).

Table 3.3. NRAS overlap mutation and pLJM1 cloning primers

Primer	Sequence (5’ - 3’)	Tm (°C)
NRAS cDNA Forward + AgeI	GCT ACC GGT ATG ACT GAG TAC AAA CTG GTG	62.0
NRAS cDNA Reverse +EcoRI	GCT GAA TTC TTA CAT CAC CAC ACA TGG CAA TC	65.8
NRAS G12C Overlap Forward	GTT GGA GCA TGT GGT GTT GG	65.3
NRAS G12C Overlap Reverse	CCA ACA CCA CAT GCT CCA AC	65.3
NRAS G12D Overlap Forward	GTT GGA GCA GAT GGT GTT GG	65.3
NRAS G12D Overlap Reverse	CCA ACA CCA TCT GCT CCA AC	65.3
NRAS Q61K Overlap Forward	ACA GCT GGA AAA GAA GAG TAC	62.0
NRAS Q61K Overlap Reverse	GTA CTC TTC TTT TCC AGC TGT	62.0

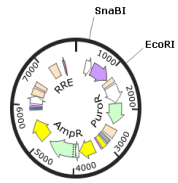

pLJM1-NRAS-G12D
7903 bases

INSERT FRAGMENT
Replace
SnaBI (265) – EcoRI (1104)
Insert
SnaBI (28) – EcoRI (867)

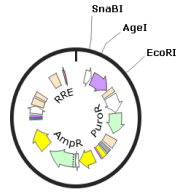

pLJM1-NRAS-WT
7903 bases

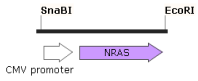

NRAS_G12D_CMV_SnaBI_EcoRI
878 bases

INSERT FRAGMENT
Replace
AgeI (525) – EcoRI (1284)
Insert
AgeI (4) – EcoRI (583)

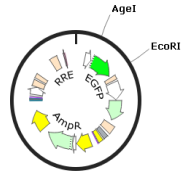

pLJM1-EGFP
8083 bases

NRAS cDNA+ Restriction Sites
588 bases

OVERLAP EXTENSION PCR
Overlap and amplify
1 .. 337
Overlap and amplify
1 .. 561

Fragment 1
337 bases

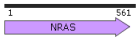

Fragment 2
561 bases

PCR
Amplify 1 .. 337 using:
pLJM1-NRAS_SnaBI_F
NRAS_G12D_Overlap_R

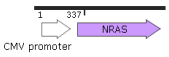

NRAS_CMV_SnaBI+EcoRI_PCR
878 bases

PCR
Amplify 318 .. 878 using:
NRAS_G12D_Overlap_For
pLJM1-NRAS_EcoRI_Rev

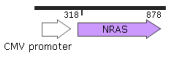

NRAS_CMV_SnaBI+EcoRI_PCR
878 bases

PCR
Amplify 238 .. 1115 using:
pLJM1-NRAS_SnaBI_F
pLJM1-NRAS_EcoRI_Rev

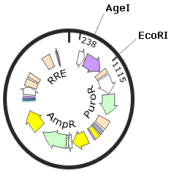

pLJM1-NRAS-WT
7903 bases

PCR
Amplify 238 .. 1115 using:
pLJM1-NRAS_SnaBI_F
pLJM1-NRAS_EcoRI_Rev

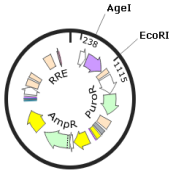

pLJM1-NRAS-WT
7903 bases

INSERT FRAGMENT
Replace
AgeI (525) – EcoRI (1284)
Insert
AgeI (4) – EcoRI (583)

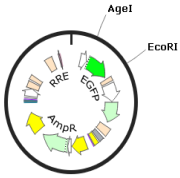

pLJM1-EGFP
8083 bases

NRAS cDNA+ Restriction Sites
588 bases

Figure 3.9. Schematic of cloning steps required to generate NRAS wild-type and mutant over-expression plasmids. Briefly, RNA was extracted from MOLM-13 cells and the NRAS coding region was amplified by PCR with restriction sites complimentary for the replacement of the *EGFP* gene within the original pLJM1 backbone. Where necessary, this cDNA was subject to several overlap PCRs, to create the mutant NRAS, to create the required vectors.

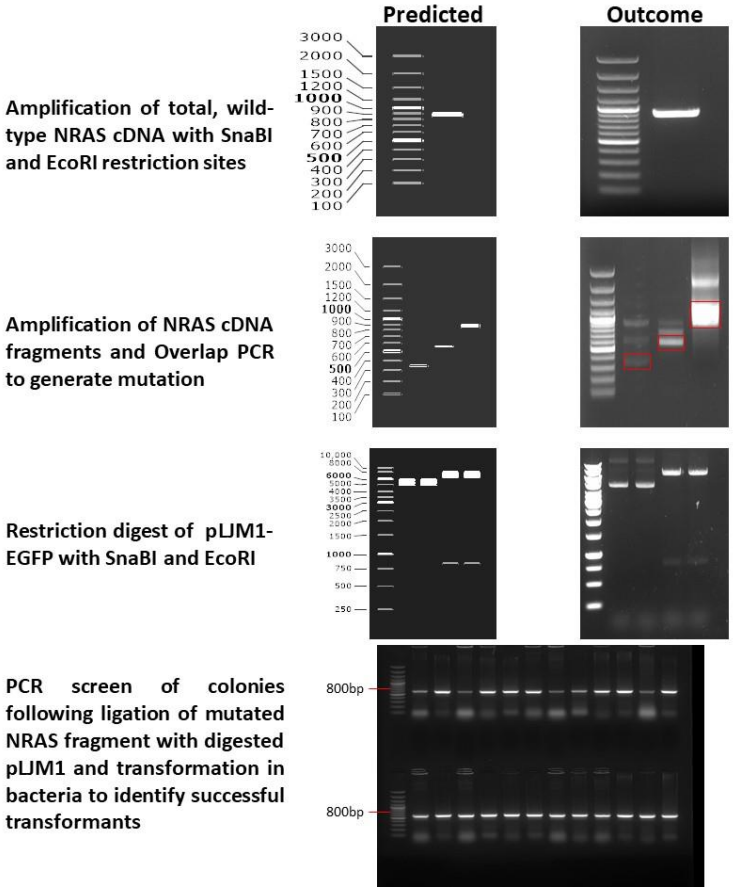

Figure 3.10. Stepwise process of mutation generation from NRAS wild-type cDNA. Using the schematic from Figure 3.9, NRAS G12C, G12D and Q61K mutant cDNA was generated by overlap PCR with sequence-specific primers, and cloned into the pLJM1 vector, which was digested with SnaBI and EcoRI. Predicted images included here were generated using Snapgene.

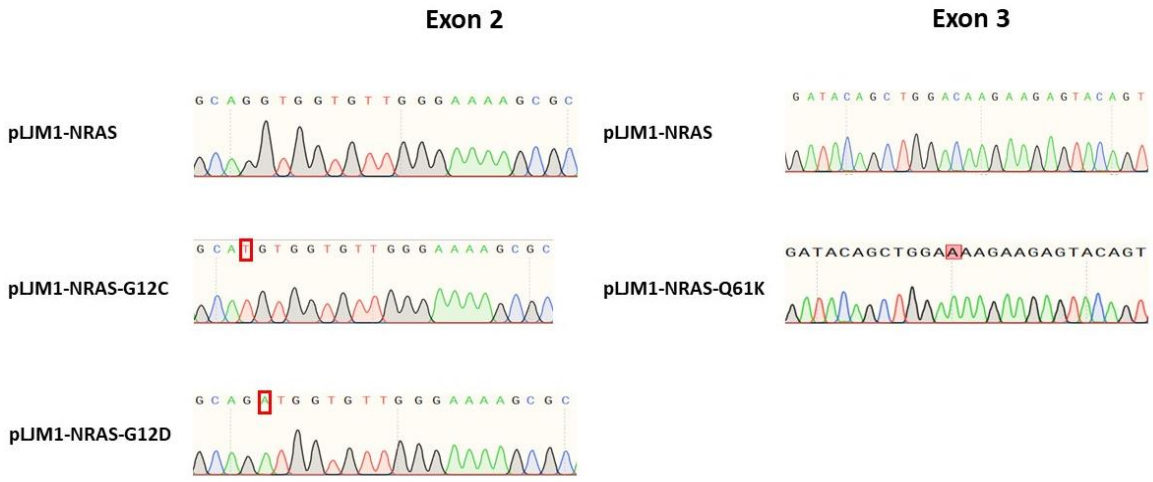

Figure 3.11. Sanger sequencing alignment of NRAS-mutated cDNA, cloned into the pLJM1 vector for over-expression in cell lines. Successful cloning and mutagenesis was verified by Sanger sequencing (Source Biosciences, UK).

3.3.5.2 Phenotypic Effects of NRAS Mutant Over-expression in Healthy and Cancerous Contexts

These vectors were then used to transfect HEK293T and HeLa, to analyse the effects of individual NRAS mutations in a physiological (HEK293T) and cancerous (HeLa) state. Cell proliferation was quantified in the transfected HeLa cells, over the course of 96 h (Figure 3.12). In HeLa cells, over-expression of NRAS (wild-type or mutated) conferred a proliferative advantage, relative to the control (pLJM1-EGFP-transfected) cells. In line with the literature regarding the transformative nature of Ras mutants, NRAS-G12C conferred the greatest proliferative advantage, with there being no significant differences between NRAS-wild-type and NRAS-Q61K transfected cells. Nevertheless, all NRAS-transfected HeLa showed a statistically significant proliferative advantage compared to the control. However, this was not the case for the HEK293T, where the growth rate appeared similar between all conditions (Figure 3.12A).

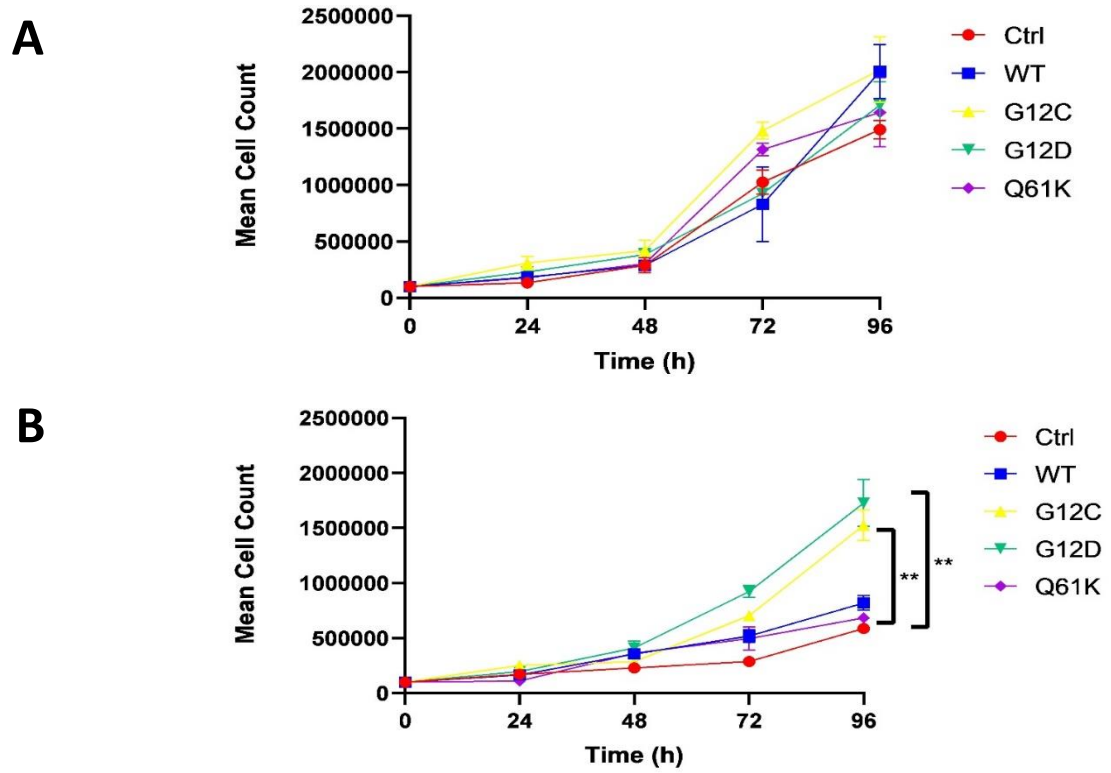

Figure 3.12. Proliferation rate of transient NRAS over-expressing cell lines. A) HEK293T. **B)** HeLa. These cells were generated using the previously described pLJM1 plasmids, to over-express NRAS WT, G12C, G12D or Q61K. Cell counts were measured by counting following staining with trypan blue, every 24 h up to 96 h post-plating. Data represents mean +/- SEM, N=3, biological repeats. Statistical tests were carried out using GraphPad Prism 8.0.1. Data analysed by two-way ANOVA and subsequently multiple t-tests between each time point, comparing over-expression to the control. ** denotes *P<0.01.* No significant difference was found between growth rate in the HEK293T.

3.3.5.3. Signalling Alterations of NRAS Mutant Over-expression in Healthy and Cancerous Contexts

Western blotting was carried out on these transfected HEK293T and HeLa cells to detect any alterations in signalling dynamics arising from the presence of these mutants.

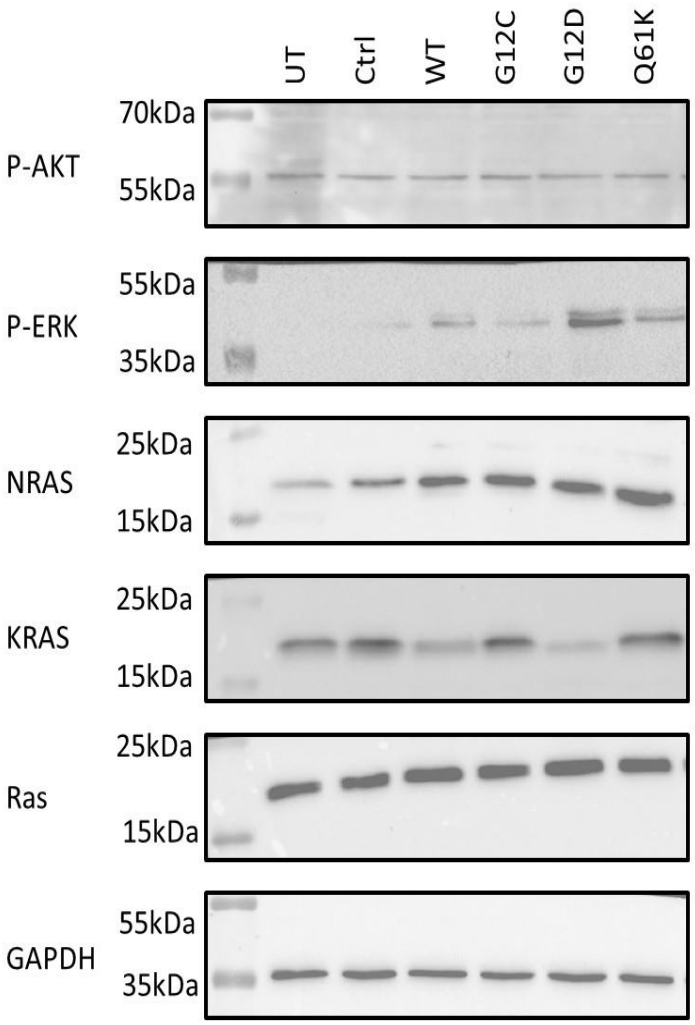

Figure 3.13. Signalling alterations in HEK293T cells when differing NRAS mutants are over-expressed. HEK293T cells were transiently transfected with a pLJM1-backbone plasmid, encoding NRAS WT, G12C, G12D, Q61K or EGFP as a control. Cells were transfected for 72 h, before cells were collected, protein extracted and analysed through Western blotting. UT refers to untransfected HEK293T cells. Ctrl refers to cells transfected with the pLJM1-EGFP (control) plasmid.

These Western blots primarily confirmed function of the over-expression plasmids, since there was an increase in NRAS expression in all four cell lines transfected with NRAS-encoding plasmids (panel three of Figure 3.13). ERK and AKT activation were also assessed here. ERK activation was seen to be increased in all four NRAS over-expressing conditions relative to the EGFP and untransfected samples, with the greatest activation seen in the NRAS G12D over-expressing cells. AKT pathway activation was not affected by over-expression of NRAS wild-type or any of the variants, though it was already activated to a higher degree in HEK293T cells than ERK. There was some fluctuation in KRAS levels, as well as a total increase in Ras protein content in the transfected cells.

Following successful validation of these plasmids through sequencing (Figure 3.11) and Western blotting (Figure 3.13), lentivirus encoding over-expression of NRAS G12C, G12D and Q61K, as well as wild-type NRAS would be generated using these vectors to induce such expression in MOLM-13 cells. Such cell lines would then be compared back to the parental and drug-resistant MOLM-13 cells. This is detailed in chapter 5.

3.3.6 CRISPR-Cas9-mediated Knock-out of *NRAS* in a Healthy and Cancerous Context

3.3.6.1 Component Generation

Using CRISPR-Cas9, *NRAS* was knocked out in HEK293T cells. This was performed using two guides, one designed in the intergenic region prior to exon 2 which encodes the start codon of *NRAS*, and the other in the intron between exons 2 and 3 (Table 3.4

and Figure 3.14). These guides were designed to be compatible with *S. pyogenes* Cas9 (*Sp*Cas9), and designed in reference to the GRCh37/hg19 and 1000 Genomes SNP databases, using the online CRISPOR.org database (Concordet & Haeussler, 2018). The optimal guides were chosen based on the minimum number of off-target effects, and the highest efficiency possible, according to the Doench 2016 score (Doench et al., 2016). The guide sequences are shown in Table 3.4, alongside predicted efficiency scores and off-targets for 0-4 mismatches. The Moreno-Mateos et al. (2015) score is also provided for completeness, however this is less important in this case since the score is more accurate when considering guide delivery requiring *in vitro* T7 RNA polymerase-mediated transcription, which was not the mechanism utilised here (Concordet & Haeussler, 2018). Instead, the guides were delivered in a lentiviral plasmid also containing Cas9 (Figure 3.14 and Appendix 2).

A

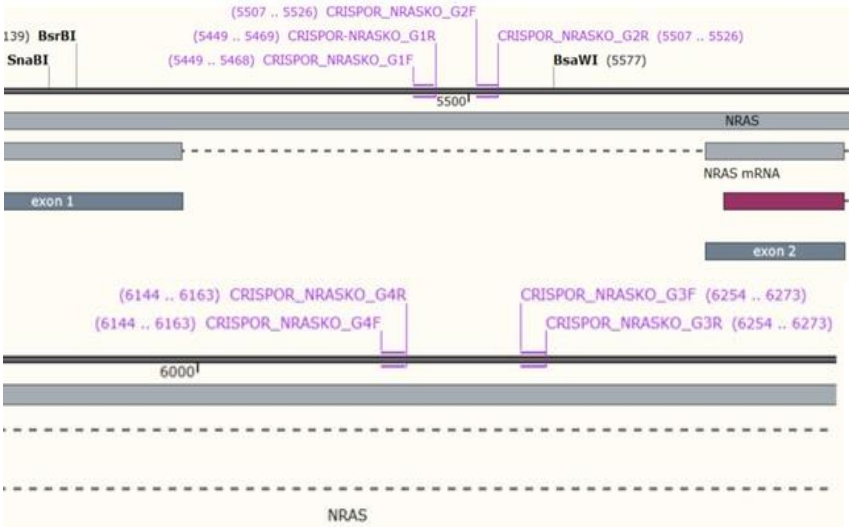

B

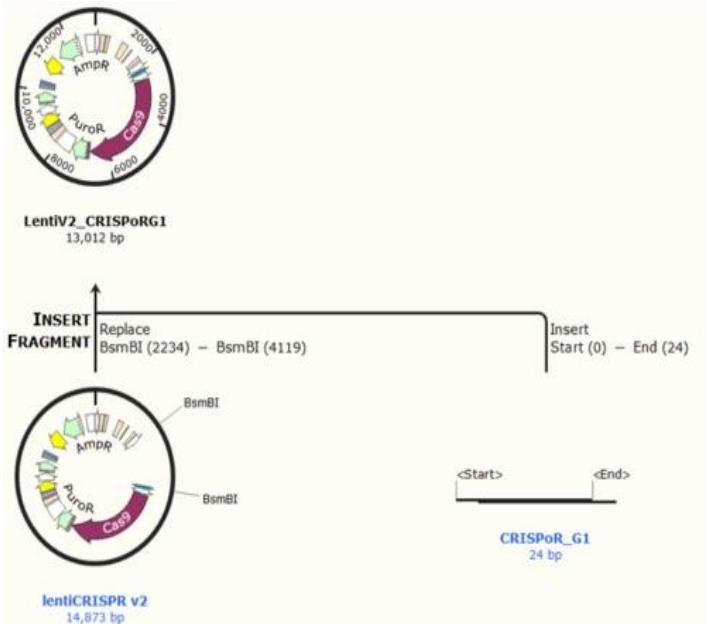

Figure 3.14. Guide design and creation of delivery vector for generation of CRISPR-mediated *NRAS* knockout. A) Location of guide RNA sequences targeting *NRAS*. Guides would ideally be delivered in pairs (1+3, 1+4, 2+3 or 2+4), thereby increasing the likelihood of a successful Cas9-mediated cut and subsequent knock-out of gene function. **B)** Schematic of annealed and phosphorylated guide cloned into LentiCRISPR-V2, which also encodes constitutively active Cas9.

Table 3.4. Guide sequences targeting *NRAS*. Efficiency of Cas9 direction and subsequent double-stranded cutting was calculated by the CRISPOR Tool, in respect to the algorithms published by Concordet and Haeussler (2018); Doench et al. (2016). Number of off-targets represents number of alternative binding sites throughout the genome when 0-4 base pair mismatches are permitted for binding.

Guide	Sequence (5' - 3')	Efficiency score		No. off-targets
		Doench 2016	Moreno-Mateos 2015	
G1	CCT TCG GGG AGT AAT AGG AA	58	49	72
G2	GGA CTG TTG AAA AAT AGC TA	59	13	144
G3	TTC TTG CTA CTC CAA TCA TC	42	11	138
G4	ATC AGA CAG TCT CGC TAC TA	44	41	37

These single-stranded oligonucleotide guide sequences were initially used as PCR primers (Guide 1 and 2 acting as the forward primer, and 3 and 4 acting as the reverse primers), to validate their specificity for the DNA of the cell lines they would ultimately be delivered to. Two out of the four possible pairs (1+4 and 2+4) resulted in detectable PCR products using agarose gel electrophoresis, and therefore would be used in future transfections.

To deliver these guides into the cell line of interest, complimentary single-stranded oligonucelotides (containing BsmBI-compatible restriction site overhangs) were annealed (creating double-stranded DNA suitable for cloning), phosphorylated using T4 PNK, and cloned into the LentiCRISPR-V2 plasmid, which had been digested with BsmBI. This plasmid was chosen since it is also a lentiviral-compatible plasmid already containing Cas9, therefore permitting subsequent stable editing of the AML cell lines, once the optimum guide pair had been identified. Colonies were first screened by PCR using a primer in the U6 promoter, and the reverse, single-stranded oligonucleotide. To further ensure accurate cloning, plasmids were sequenced, with the results shown in Figure 3.15.

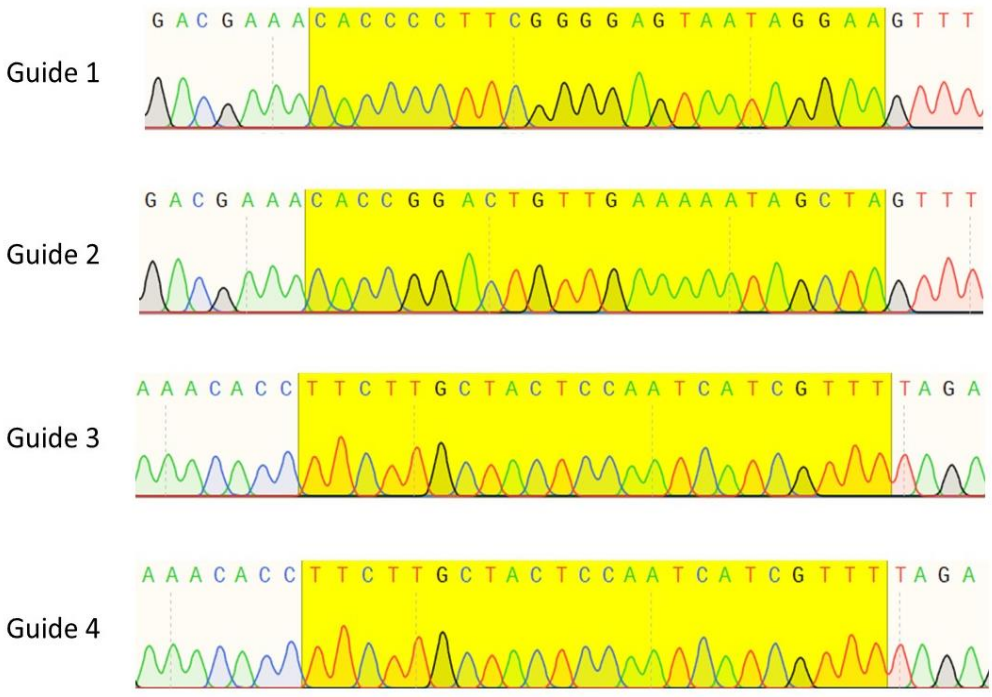

Figure 3.15. Sequence alignment of successfully cloned guides into the LentiCRISPR-V2 vector. Guide sequences are highlighted in yellow, alongside compatible BsmBI restriction sites that had been previously generated in LentiCRISPR-V2 to permit cloning.

3.3.6.2 Confirmation of Gene Editing

These guides were delivered to the HEK293T cells using transient transfection initially, to determine the optimum guide pair to take forwards experimentally. Successful editing was validated in numerous ways: basic PCR of the edited region followed by agarose gel electrophoresis and Sanger sequencing of resulting cut fragments, as well as by Western blotting. Only two guide pairs were identified by PCR (using primers detailed in Table 3.5) as being specific for the NRAS sequence (1+4 and 2+4). The agarose gel in Figure 3.16A suggests an inefficiency of Guide 3 at directing a cut, since there were no specific products of a smaller size generated in PCR and shown on the gel. Figure 3.16 below illustrates the genetic alterations caused by the Cas9-mediated editing, and it can be seen that there was a deleted region (shown in red) of the edited cells between the two guides delivered. This is illustrated in Figure 3.16B, with the large red band of dashes occurring in the gene-edited cells sequence, indicating bases were missing compared to the control-transfected cells. Of the two guide combinations initially tested, the best results (most efficient knock-out as seen by Western blotting) coming from pair 2+4 (Figure 3.18).

Table 3.5 *NRAS* knock-out screening primers

Primer	Sequence	T_M (°C)
NRAS KO Genotyping F	GGG CTG TGG AAT GTT CAG GC	67.3
NRAS KO Genotyping R	ATA CAA TCA GAC AGT CTC GC	61.2

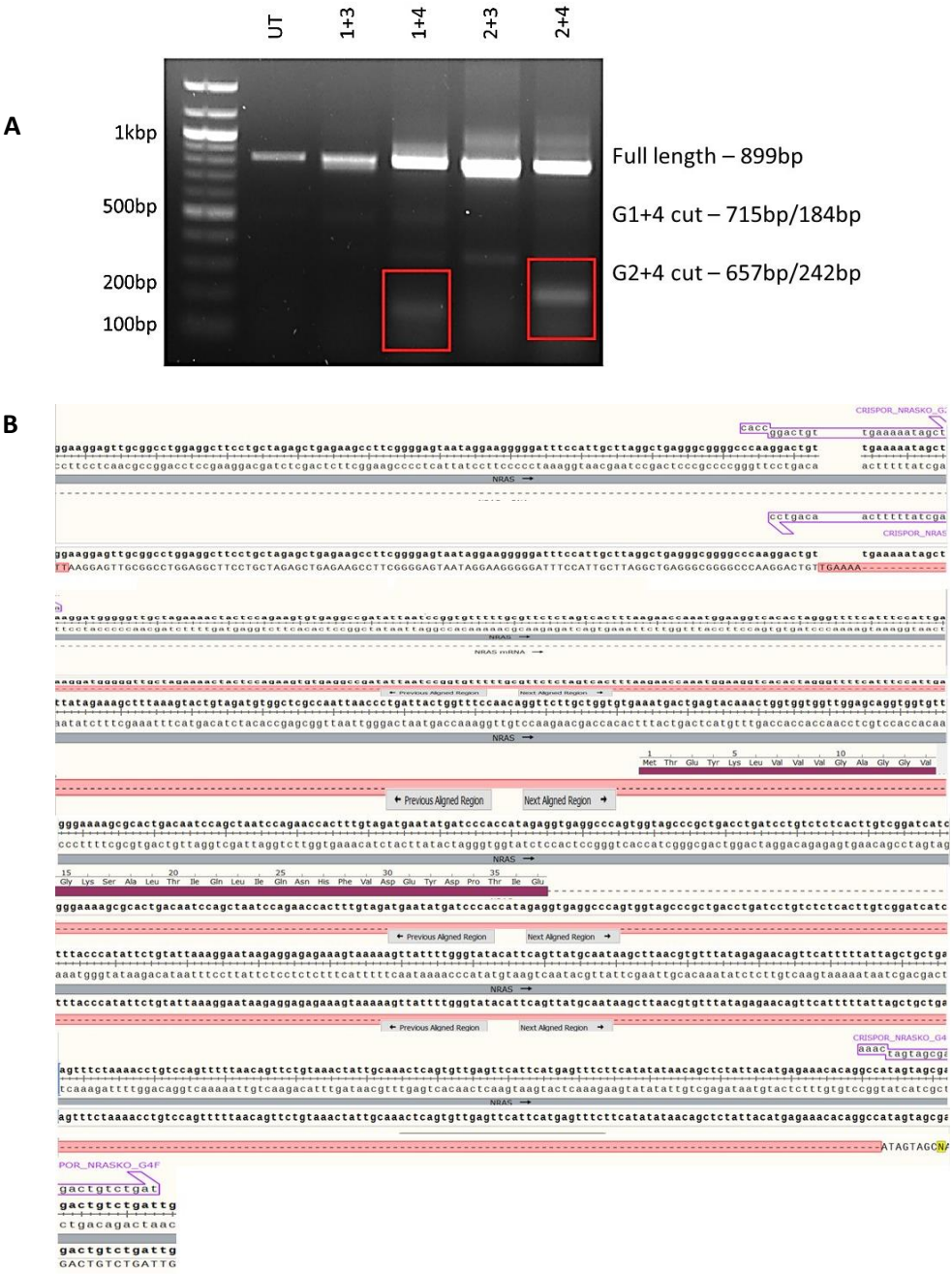

Figure 3.16. Validation of *NRAS* knock-out in transiently transfected HEK293T cells. A) DNA was isolated from cells transiently transfected with plasmids made in Figure 3.15, the region of interest amplified by PCR, electrophoresed and visualised with RedSafe gel staining. **B)** Purification and Sanger sequencing result of upper bands seen in **A**. Dashes highlighted in red bars indicate missing bases, which occur immediately after the cut site from the Cas9, as directed by the guide (indicated in purple). Dark pink indicates the coding region of *NRAS* Exon 2.

3.3.6.3. Phenotypic Effects of CRISPR-Cas9-Mediated NRAS Knock-Out

Given NRAS' role in controlling proliferation generally, the growth rate of the HEK293T cells following *NRAS* knock-out was also measured. This illustrated a significant inhibition of proliferation at 72h ($P<0.05$) and 96h ($P<0.01$), relative to the control-transfected cells. This is detailed in Figure 3.17, with a 2.2-fold difference in cell count between the two cell lines after 96 h. In contrast, *NRAS* knock-out in HeLa conferred a significant proliferative advantage relative to the control-transfected cells, again with

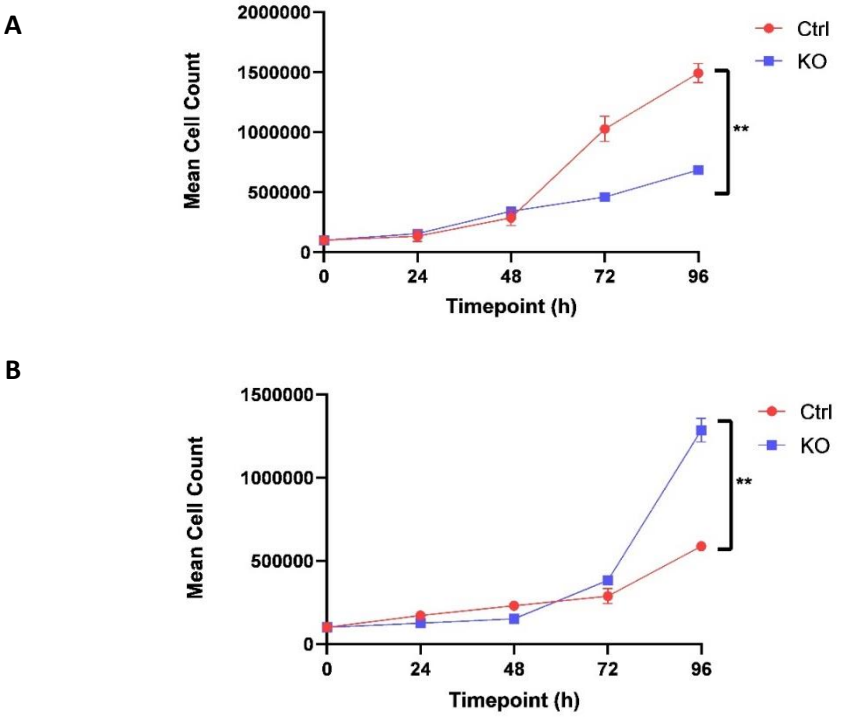

Figure 3.17. Proliferation curves following *NRAS* knock-out. A) HEK293T and **B) HeLa** cells were transfected for 72 h with plasmids encoding the CRISPR components (guides 2 and 4, Cas9, scaffold), or the original Lenti-V2 (Ctrl). Following confirmation of successful transfection by Western blotting (Figure 3.18), 100,000 cells were plated in technical triplicates, one well per time point measured. Cells were trypsinised at the appropriate time points and counted using trypan blue staining and a haemocytometer. Data represents mean +/- SEM, N=3 biological repeats. Statistical tests were carried out using GraphPad Prism 8.0.1. Data analysed by two-way ANOVA and subsequently multiple t-tests between each time point, comparing over-expression to the control transfected cells. ** denotes *P<0.01.*

a 2.2-fold difference in cell count between the two cell lines. Whilst this was unexpected, this could suggest that cancer cells have a greater ability to re-wire pathways within a short time-frame to overcome genetic manipulation. A further analysis of the altered signalling dynamics within these cells may explain this, since it has also been shown that different NRAS mutants are able to dysregulate pathway signalling, and over-expression of NRAS wild-type or mutant contributes differently to the proliferative capacity of the cell.

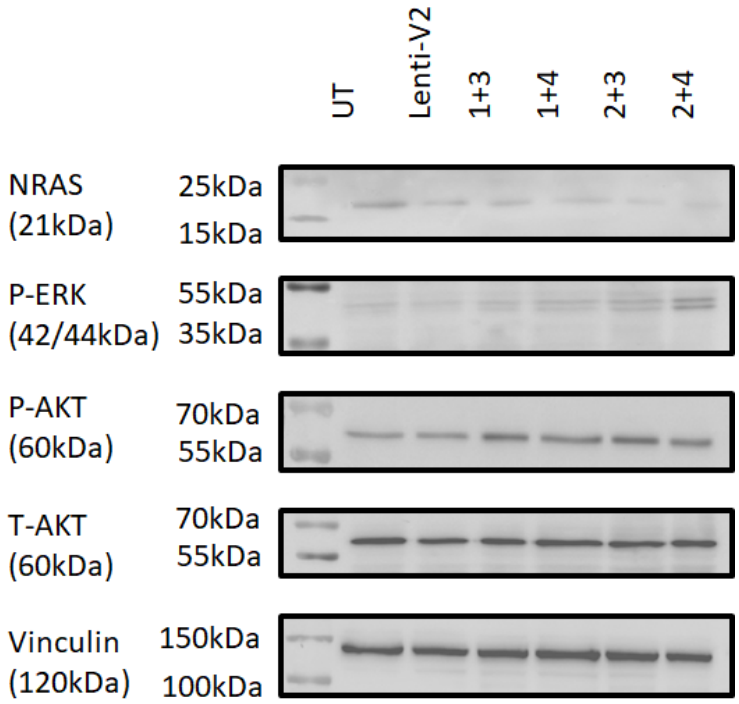

Figure 3.18. Key signalling dynamics altered by knockout of *NRAS* in HEK293T cells. Cells were transfected for 72 h with plasmids encoding the CRISPR components (guides, Cas9, scaffold), or the original Lenti-V2 (backbone) before harvesting, lysing and separating using SDS-PAGE and analysed by Western blotting. Four guide pairs were initially tested (1+3, 1+4, 2+3 and 2+4), with the best results (largest degree of knockout) seen with guide pair 2+4.

As indicated above in Figure 3.18, Ras-dependent proliferative signalling pathways were also measured in the transfected HEK293T. Whilst cells that had been

transfected with this pair showed little change in AKT activation, there was an increase in ERK activation compared to untreated cells, which was surprising. This may indicate a redundancy mechanism for Ras inhibition, which may have implications of its own. It has already been suggested that ERK can be involved in positive feedback mechanisms in the presence of Ras inhibition, which may explain such results here.

3.4 Discussion

The work carried out here served three key purposes: to develop a better understanding of Ras mutant biology, as well as to establish the generic implication of Ras in AML. The final part of this chapter combined these two areas and explained the creation of tools which would be used in the AML cell lines of interest to combine these areas and develop a better understanding of Ras-mutant AML, the results of which are detailed in chapter 5.

It has been shown here that, in line with published datasets and global understanding, AML is a highly heterogenous disease faithfully recapitulated across the original panel of cell lines studied (Papaemmanuil et al., 2016). The mutational spectrum of NRAS followed the same pattern of heterogeneity, with various mutations detected across the panel studied. However, it was most interesting to reveal that there were NRAS mutations arising within the two FLT3-inhibitor resistant cell lines. Given this is a well-categorised leukaemic driver, and has been associated in patients with drug resistance, this formed the basis of future studies (Choe et al., 2020; de Witte et al., 2017; Döhner et al., 2022; Loftus et al., 2021; McMahon et al., 2019; Zhang et al., 2019). Chapter 4 will discuss the reversal of the G12D mutation occurring in the MV4-11-DR using CRISPR-Cas9 gene editing. This is to assess the impacts that this NRAS

mutation has on the drug-resistance of the cells, as well as on the overall genotype and phenotype.

The increased expression of KRAS at a protein level in our FLT3 inhibitor resistant cell lines was somewhat unexpected here (Figure 3.5), since it is generally accepted that one isoform predominates over the other in terms of expression, with mutations often proving mutually exclusive (Hood, Sahraoui, Jenkins & Prior, 2023; Nagakubo, Hirotsu, Amemiya, Oyama, Mochizuki & Omata, 2019). Nevertheless, the relationship between these isoforms is less well-understood in leukaemia compared to solid tumours, and therefore could be an option for future investigation. There may be some level of co-operation between the isoforms in a drug-resistant context, to prevent the inhibition of proliferative signalling by FLT3 inhibitors. Interestingly, upon NRAS over-expression in the HEK293T cells (Figure 3.13), KRAS expression appeared to decrease in the presence of certain over-expression lines (NRAS WT and NRAS G12D), which could suggest that there may be different reliance on other Ras isoforms depending on genotype. This in turn would suggest the need to target different mutants differently, since this is just one indication of different pathway re-wiring.

The development of tools to carry out these studies was imperative, and in themselves revealed differences between the effects of different NRAS mutants and different cellular contexts. This supported the concept of co-operation between different genes and pathways, which will be explored to more detail in an AML-specific manner in Chapters 5 and 6. Already in this chapter it has been determined that perhaps, in an AML context, the MAPK pathway is more relevant to drug-resistance than the PI3K-AKT pathway, although this remains to be fully elucidated. It was interesting to see the

differences between the Ras-mediated signalling pathways in a healthy (non-cancer) context of the HEK293T, where ERK expression and signalling was almost non-existent in the parental cells, compared to the MOLM-13 and MV4-11 cell lines. In contrast, the AKT pathway was more strongly activated compared to the MAPK pathway (ERK) expression in HEK293T. The opposite was true in the MOLM-13 and MV4-11 AML cell lines. This further indicated the need for the study of NRAS in an AML-relevant context, since there is somewhat more of a gap in the literature regarding the importance of NRAS in AML, compared to other cancers such as lung adenocarcinoma. Indeed, the considerable variation of NRAS mutations adds further complexity to the overall role of NRAS – it is possible that different mutations cause different genotypes and phenotypes. This is evident with the differences in ERK signalling with the over-expression of NRAS mutants in HEK293T cells: whilst ERK activation increased with all mutants over-expressed, some mutants (such as NRAS G12D) appeared to cause a greater upregulation of ERK activation than others (such as G12C). This will be interesting to probe further into during chapter 5, with focus on signalling changes within a leukaemic context.

Interestingly, there was an increase in ERK pathway activation when *NRAS* was knocked-out using CRISPR-Cas9 in HEK293T cells. Given that ERK is typically inactive in the HEK293T cells, this could represent some form of pathway re-wiring to mitigate for the *NRAS* knock-out. Unexpected ERK activation has been seen following KRAS inhibition in pancreatic cancer, which was believed to contribute to dysregulation of the cell cycle and result in a pro-proliferative phenotype (Diehl et al., 2021). In the future, it would be interesting to see whether similar pro-proliferative redundancy pathways were also implicated following *NRAS* knock-out. Given the

increase in ERK signalling in both an NRAS-mutant over-expressing context within the HEK293T, as well as in the *NRAS* knock-out HEK293T cells, it would be interesting to further probe whether there is a similarity in the mechanism underpinning the ERK upregulation, such as the cell cycle control pathways proposed by Diehl et al. (2021).

To conclude, the emergence of NRAS mutations in FLT3-inhibitor resistant cell lines correlate with changes in NRAS expression levels as well as in downstream proliferative signalling pathways. Over-expression of different NRAS mutants in a transient manner in a non-cancer context confer upregulation of different signalling pathways, with some mutants able to activate pathways (e.g. ERK) not typically active in the control cells. Increased signalling within these pathways however was not associated with an increased proliferative capacity of these cells, although *NRAS* knockout resulted in a decreased proliferative potential. The data presented here ultimately indicates a reliance of HEK293T cells on NRAS-PI3K-AKT pathway signalling, with ERK pathway activation potentially able to rescue cells (but not their full proliferative potential) when *NRAS* is knocked out. However, their proliferative capacity seems unable to be enhanced by the over-expression of NRAS mutants, somewhat suggesting the PI3K-AKT pathway is already acting at maximal capacity and is not liable to oncogenic transformation using these NRAS mutations only. However the same was not seen in the cancerous context. Instead, in HeLa, *NRAS* knock-out resulted in a significantly increased proliferative potential. In future, it will be interesting to probe this further in a wider cancer panel, to fully assess the signalling changes implicated and understand the different potentials for targeting NRAS and its associated pathways across a range of cancers.

Chapter 4

Using CRISPR-Cas9 to Revert Drug-Induced NRAS Mutations

4 Using CRISPR-Cas9 to Revert Drug-Induced Mutations

4.1 Introduction

The field of gene editing has advanced considerably over the last 20 years, with genetic manipulation for biological investigation and treatment now becoming increasingly possible. This began with cutting DNA using nucleases including Zinc Finger Nucleases and TALENs, however the specificity and efficiency of each of these was limited (Carroll, 2011). ZFNs are small proteins of around 28-30 amino acids, containing 2 Cysteines and 2 Histidines (Cys_2His_2), and arranged in two β-sheets and one α-helix. Within this protein, there are two key domains: the recognition (binding) domain and the cleavage domain. Whilst the *Fok1* cleavage domain is specific for creating double-stranded breaks in the DNA, the recognition domain directs such cleavage, since the cleavage domain itself has no sequence specificity (Carroll, 2011).

TALENs can be considered a derivative of ZFNs, and act by turning on transcription of specified genes, also utilising the *Fok1* endonuclease system (Nemudryi, Valetdinova, Medvedev & Zakian, 2014). Such technology has a range of applications, both pre-clinically in the study of over and under-activated genes in a disease context, as well as *in vivo* gene editing (Li, Yang, Hong, Huang, Wu & Zhao, 2020).

The discovery and development of CRISPR-Cas9 gene editing was revolutionary in the advancement of this field, pioneered by the Nobel Prize-winning Jennifer Doudna and Emmanuelle Charpentier (Ledford & Callaway, 2020). In a similar way to ZFNs and TALENs, double-stranded breaks in DNA are created, with these breaks

potentially repaired in either a homologous or non-homologous way, depending on the presence of a repair template. However, whereas the ZFN system requires the inclusion of the recognition domain within the protein to direct the site of the cut, CRISPR-Cas9 DNA breaks are directed using guide RNAs (Chandrasegaran, 2017; Ran, Hsu, Wright, Agarwala, Scott & Zhang, 2013). This can be provided to the cell at either the same time as the Cas9, or indeed at a later point: cutting will only occur at that site when the guide is present. Indeed, once the Cas9 is expressed within the cell, it confers the potential for many different, permanent edits (Ran, Hsu, Wright, Agarwala, Scott & Zhang, 2013). Hence, this provides the option of generating multiple gene knockouts within a cell in a more simplistic way (since only one 20 base pair double stranded nucleotide, i.e. the guide, would be required to generate further knockouts), the efficacy of which would only be affected by the tiring and directed disruption of cellular machinery. Alternative versions of Cas9, and indeed other Cas proteins such as Cas12a, have been isolated and generated to further provide flexibility and adaptation of CRISPR-mediated editing (Schubert et al., 2021).

All three of these gene editing methods have progressed to clinical trials, as reviewed by (Li, Yang, Hong, Huang, Wu & Zhao, 2020). These trials spanned a range of diseases, including Human Immunodeficiency Virus (HIV), as well as leukaemias, metastatic solid tumours and other haematopoietic disorders. The commonality between the vast majority of these trials was the editing of haematopoietic cells, primarily to invoke or alter an immune response. This includes the generation of CAR-T cells, whose specificities are modulated to directly target disease-inducing cells. Alternatively, immune-related genes which are aberrantly upregulated in disease, such as the anti-inflammatory PD-1 in lung cancer, can also be targeted by CRISPR

and other editing methods to silence their effects and re-awaken the immune system to the presence of cancer cells, eliciting their cell killing effects (Han, Liu & Li, 2020; Li, Yang, Hong, Huang, Wu & Zhao, 2020; Lu et al., 2020).

4.2 Aims and Hypothesis:

It has previously been established that NRAS mutations emerge in drug-resistant patients (McMahon et al., 2019). However, given the spectrum of mutations co-occurring within these patients, the particular effect of these NRAS mutations within this drug-resistant mutational profile, remains to be fully elucidated, especially in response to a range of AML-targeting therapies.

I hypothesise that the emergence of this G12D (c.35G>A) heterozygous mutation will have induced some level of resistance. However, reversion of this mutation will not fully restore sensitivity to all drugs if corrected using CRISPR-Cas9 gene editing, based on the literature (Aikawa et al., 2020; McMahon et al., 2019). Despite cell lines originating from one patient source and being immortalised, it is likely there remains some level of clonal heterogeneity. Since NRAS G12D mutations emerged within this population, it is likely there are other mutations which have also emerged in the development of FLT3-inhibitor resistance, that contribute, alongside NRAS, to the drug-resistant phenotype. It is possible that not all cells within the population have developed an NRAS G12D heterozygous mutation, yet Sanger sequencing from Figure 3.2 reveals this to be the dominant genotype (rather than NRAS wild-type). In addition, steps will be taken to ensure that the final cell population studied can be identified as having been reverted back to the wild-type NRAS, from a mutated form. Comparisons will be drawn between the CRISPR-Cas9-mutated cell lines, non-

CRISPR-Cas9-mutated but lentivirally transduced (control) cell line, and the original, parental MV4-11 stock, and the MV4-11-DR cells derived from these. This will permit validation of altered gene expression and signalling due to NRAS G12D, excluding other factors.

Moreover, this clonally diverse pool also presents the possibility of multiple mutations emerging in one cell, and there being a level of co-operation between these mutations conferring resistance. Based on this understanding, I hypothesise that it is therefore unlikely that reversal of this NRAS G12D mutation will fully re-sensitise the cells to all drugs, since there could well be other co-mutations which contribute to the resistant phenotype towards some drugs more than others. However, I hypothesise that transcriptome analysis, which will be carried out following the acquisition of RNASeq data in Chapter 5, will indicate co-mutations occurring in the control, resistant and reverted samples, which can be further interrogated.

Based on previous literature discussed here, it is likely there will be a strong phenotype associated with the reversal of this mutation. Given Ras' essential nature in a myriad of cellular processes, as well as its consideration as a leukaemic driver mutation in its own right (Döhner et al., 2022) it is likely that its constitutive activation contributes strongly to a drug-resistant phenotype, alongside other mutations.

To test this hypothesis, I aim to use CRISPR-Cas9 to revert the G12D mutation (encoded by c.35G>A) in the MV4-11-DR cells back to wild-type. This will involve the establishment of a doxycycline-inducible Cas9 system within these MV4-11-DR cells, followed by delivery of a guide RNA sequences, by a second lentiviral transduction.

Positively-transduced cells will be sorted after each round of transduction, either by antibiotic selection or fluorescence.

I aim to validate progress at each step, using flow cytometry to test transduction efficiency, as well as PCR and Sanger sequencing to identify a population of successfully edited cells. The subsequent transcriptional and genotypic effects of the mutation reversal in these new cells will be analysed in Chapter 5.

The purpose of using CRISPR-Cas9 to do this, rather than purely just using the over-expression models previously discussed and generated in Chapter 3, is to stably revert the mutation at the gene level, thereby wholly eliminating this as a potential cause of resistance, in an otherwise genetically identical background. Thus, should there be any re-sensitisation to the FLT3 inhibitors or other drugs that the MV4-11-DR cells had previously been proven to be resistant to, it would suggest a dependence on the emergence of this particular NRAS G12D (c.35 G>A) mutation. The two types of models will, in theory, support each other in identifying the true resistance-mediated changes within the cell, potentially identifying actionable targets to be pharmacologically inhibited or activated in conjunction with standard or novel chemotherapy.

4.3 Results:

4.3.1 Generation of Cas9-expressing cell lines

4.3.1.1 Optimisation of a lentiviral transduction protocol in haematopoietic cell lines:

The cell lines of interest MOLM-13, MOLM-13-DR, MV4-11 and MV4-11-DR were to be transduced with lentivirus encoding Cas9. Lentivirus was used as a means of introduction of the Cas9 gene into the genome to permit stable integration of the gene. This virus was generated using the pCW-Cas9 plasmid (Addgene #50661, Appendix 3), which regulates Cas9 expression through a tetracycline-inducible promoter. Doxycycline is most commonly used for this induction. Inducible Cas9 expression was preferred in this case to reduce unintended incidences of double-stranded breaks and subsequent genome damage. Thus, transcription and subsequent expression of Cas9 introduced using lentivirus only occurs in the presence of doxycycline.

To generate the inducible-Cas9 encoding lentivirus, HEK293T cells were transiently transfected with the three plasmids encoding the viral packaging, viral envelope and Cas9 proteins (psPax2, pMD2.G and pCW-Cas9, respectively) (Appendices 3-5). Three days post-transfection, media was collected and either concentrated using ultracentrifugation (100,000 x g, 2 h) or polyethylene glycol (PEG-40) (25% v/v) or added straight to the cell line of interest. This procedure was initially tested by making EGFP-encoding lentivirus (using the pSMAL-GFP vector), rather than the non-fluorescent pCW-Cas9 vector, and transducing six AML cell lines. Percentage transduction was calculated through FACS. Figure 4.1 represents cells directly transduced with non-concentrated virus. In all cases, percentage transduction was greater than 50%.

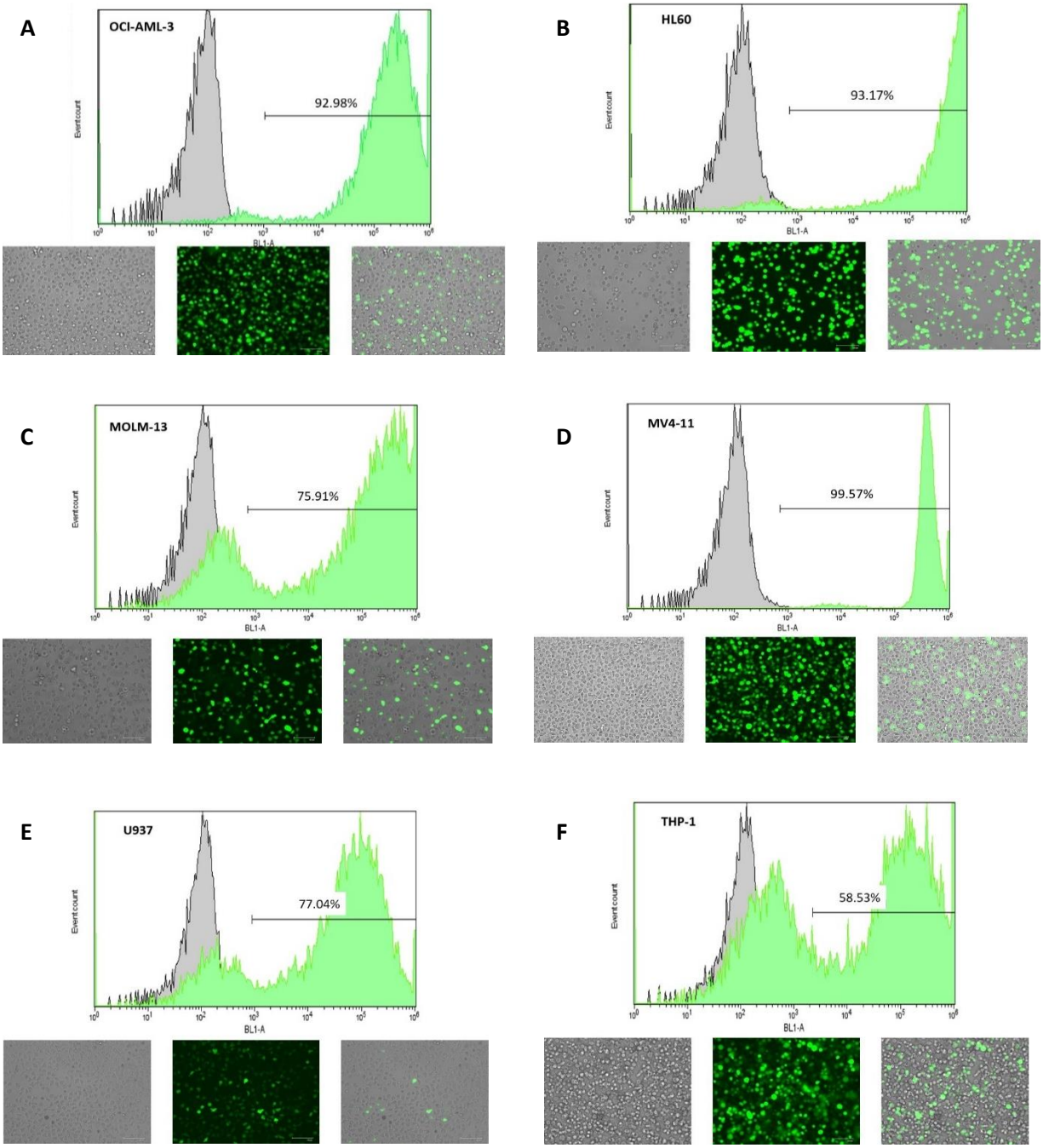

Figure 4.1. Transduction of EGFP-encoding lentivirus into a range of AML cell lines. This was used as a marker of transduction efficiency initially whilst developing lentiviral protocols. Lentivirus generated using pSMAL-EGFP plasmid. Fluorescence microscopy images are shown of the transduced cell lines, 72 h post-transduction, using white and green lights, and then the merged images. Images were taken using an EVOS FLoiD Imaging System (Life Technnologies). FACS plots of transduced cells, with the proportion of GFP-positive cells denoted by the horizontal marker. **A)** OCI-AML-3 **B)** HL60 **C)** MOLM-13 **D)** MV4-11 **E)** U937 **F)** THP-1.

The Cas9-encoding lentivirus that was generated at the same time and in the same manner as this GFP control lentivirus was validated in HEK293T cells. This was predominantly to confirm the potential of creating lentivirus in this way with this plasmid, and to confirm that the Cas9 expression was indeed inducible, as was desired. Inducible Cas9 was to be used in this instance to reduce the incidence of subsequent, off-target editing following initial delivery of the guide RNAs, as will be explained further, with a Western blot of transduced HEK293T shown in Figure 4.2. In Figure 4.2A, 20 µl of ultracentrifuge concentrated Cas9-encoding lentivirus was used to transduce the HEK293T for 72 h, before cells were treated with 0-8 µg/ml doxycycline. As indicated, the Cas9 expression was only present in the presence of doxycycline, however the extent to which it was expressed was similar irrespective of the dose of doxycycline administered. Nevertheless, Cas9 expression remained low, so a further transduction was carried out in previously-untreated HEK293T, using 50 µl concentrated virus (Figure 4.2B). In this case however, one dose of doxycycline was picked to induce the Cas9, with varying amounts of puromycin added for the selection of Cas9-transduced cells. Cas9 expression was not detectable in these cells before they had undergone selection, indicating a poorer efficiency of the lentivirus generated, or indeed a poorer efficiency of the promoter under which Cas9 transcription is controlled, compared to the EGFP. As a means of ameliorating this, concentrated virus was used rather than the non-concentrated virus due to the need for considerable Cas9 expression, which is shown in Figure 4.2 (non-concentrated virus supernatant not shown). Further detail on the difference between the promoters is provided on this in section 6.14.5.

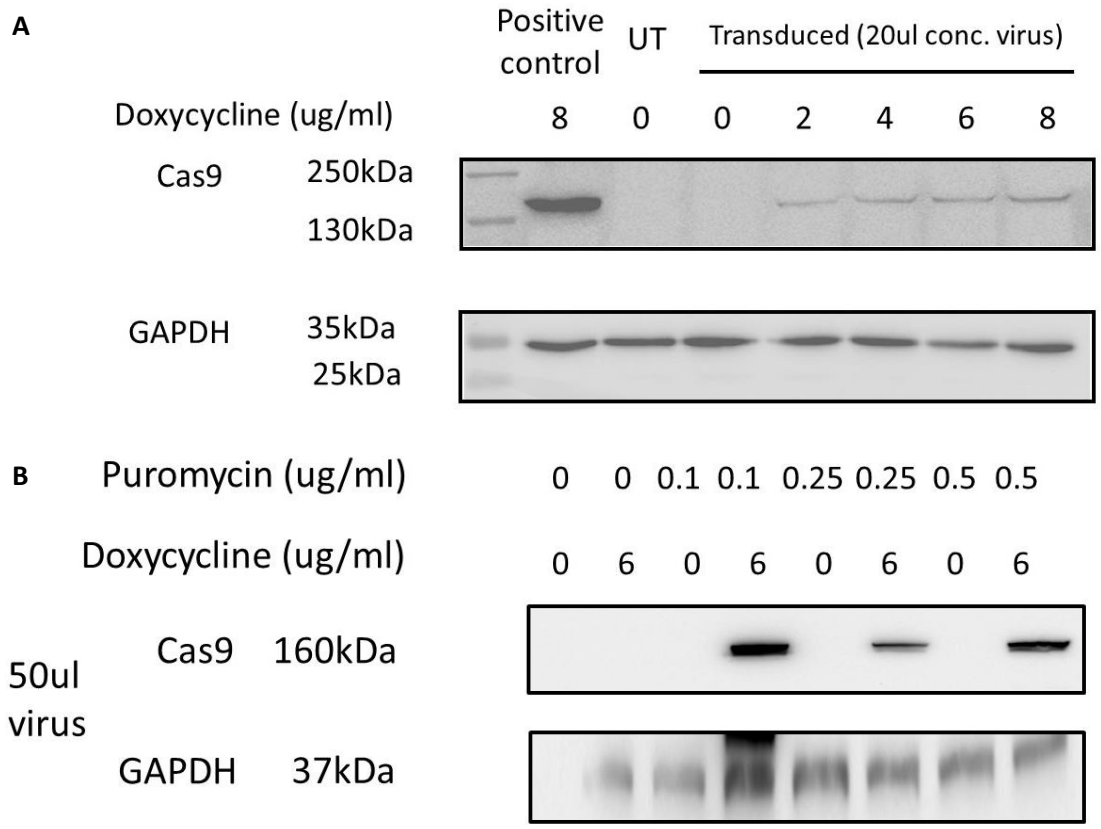

Figure 4.2. HEK293T cells transduced with inducible-Cas9-encoding lentivirus. Cells were transduced with ultracentrifuge-concentrated (100-fold) lentivirus for 72 h, positively selected with puromycin for 96 h, and then half were induced with doxycycline for 24 h prior to lysing for Western blotting. **A)** Titration of doxycycline dose to obtain optimal Cas9 expression. **B)** Titration of puromycin in Cas9-transduced HEK293T to optimise Cas9 expression despite the low transduction efficiency seen in A.

Given that doxycycline has previously been shown to be toxic to AML cell lines (Song, Fares, Maguire, Sidén & Potácová, 2014), the cytotoxic nature of doxycycline was assessed in the MV4-11-DR cells, over 24 and 96h (Figure 4.3). These timepoints were selected since cells would typically only be subject to doxycycline for 24 h before harvest for protein isolation, when validating the Cas9 expression, or cells may be exposed for 96 h, when the Cas9 is induced and guide RNAs transduced into the cell to carry out the CRISPR-Cas9-mediated gene editing. As illustrated in figure 4.3, there

was no concerning cytotoxic effect seen in the MV4-11-DR cells at either of the two time-points analysed, with >95% cell survival in both cases.

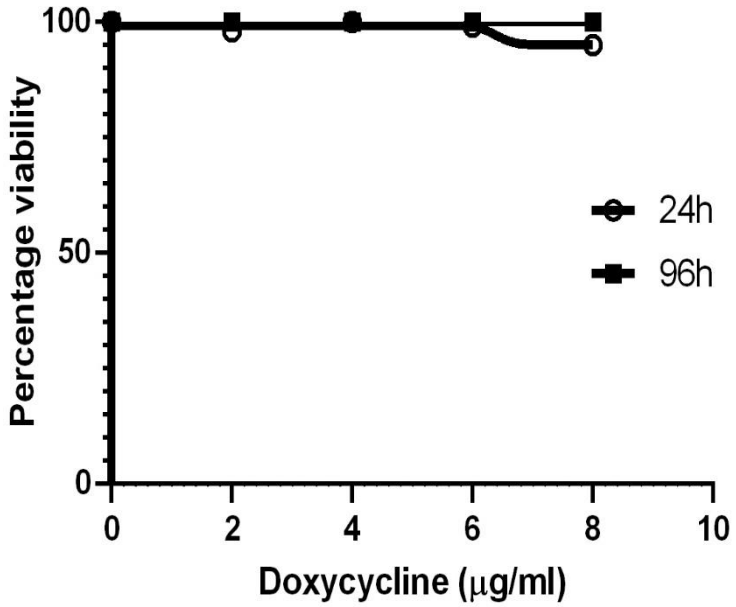

Figure 4.3. Sensitivity of MV4-11-DR cells to doxycycline. 24 and 96 h cell viability is shown as a proportion of vehicle (DMSO) treated cells (N=1). Data plotted using GraphPad Prism V6.

However, transduction efficiency when using the pCW-Cas9 plasmid in the MV4-11-DR cells was even poorer, likely due to the increased size of the Cas9 containing plasmid relative to the pSMAL-GFP previously tried in the AML lines, and also the difference in promoter. CMV promoters have been shown to have relatively poor transcription ability in haematopoietic cells (and not in HEK293T cells), with other promoters, such as SFFV (as is present in the pSMAL-GFP vector), preferred instead (Almarza et al., 2007; Winiarska et al., 2017). In this case however, given the desire for an inducible Cas9, the promoter used was the Tet (Tetracycline)-ON promoter. To account for this lower transcription efficiency, as well as the poorer transduction efficiency associated with haematopoietic cells relative to HEK293T cells, selection

was performed to improve the proportion of cells able to express the Cas9 (under doxycycline treatment, as previously discussed). The response of non-transduced cells to puromycin was initially examined, to better understand the sensitivity of various cell lines to 0-10 µg/ml puromycin. Each cell line tested was found to respond to puromycin in a similar manner, as detailed in figure 4.4, whereby the IC_{50} was similar across all cell lines. IC_{50} values are denoted in Table 4.1.

Table 4.1. IC_{50} Values following 96 h Puromycin treatment in AML cell lines.

Cell Line	96 h IC_{50} (µg/ml)
U937	0.09
OCI-AML-3	0.01
MOLM-13	0.02
MV4-11	0.02
MOLM-13-DR	0.09
MV4-11-DR	0.08

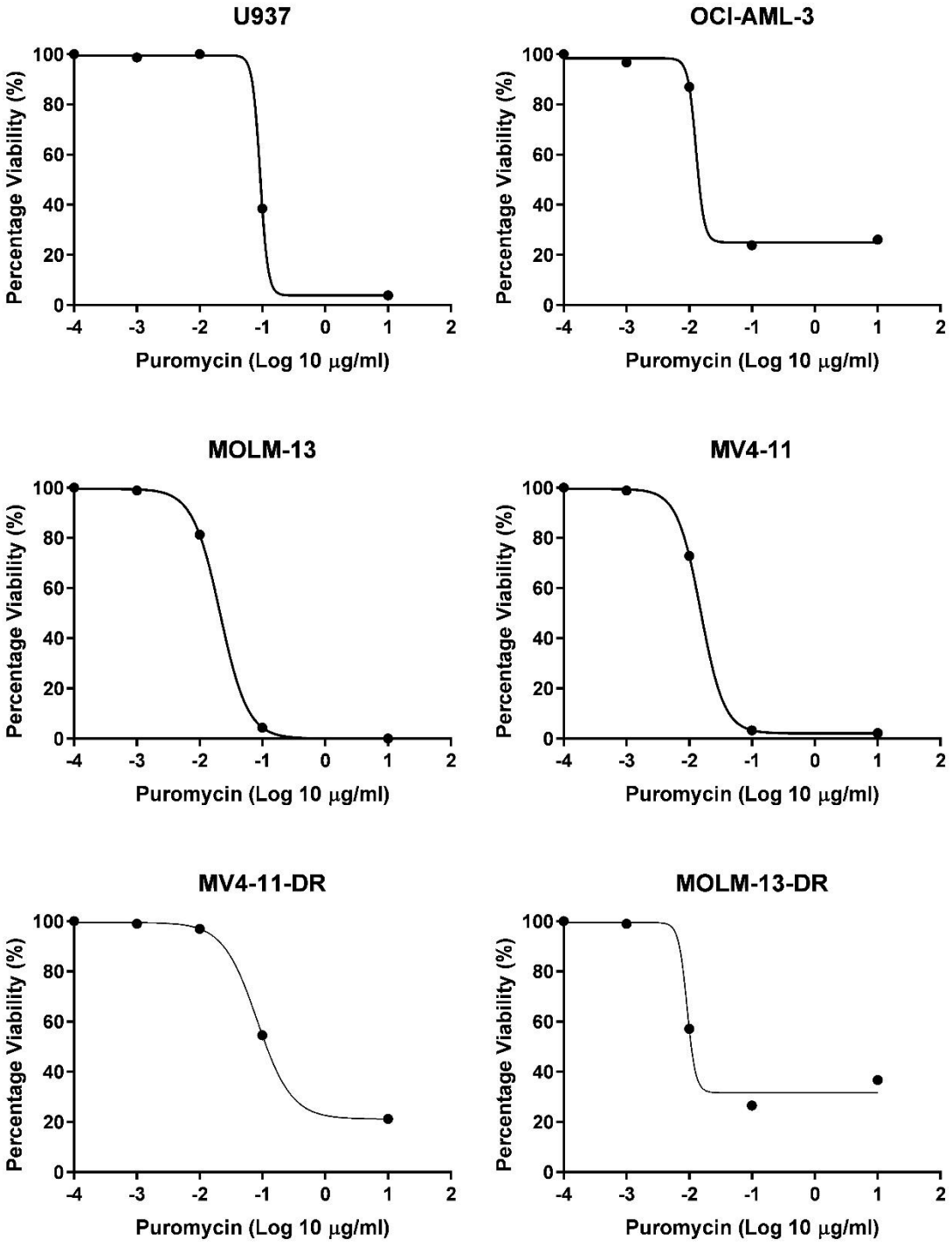

Figure 4.4. Sensitivity of AML cell lines to puromycin. 96 h cell viability is shown as a proportion of vehicle (DMSO) treated cells (N=1-2). Data plotted using GraphPad Prism V6.

4.3.1.2 Transduction of AML cell lines

MV4-11-DR cells were transduced with 5 µl or 20 µl concentrated Cas9-encoding lentivirus, or 50 or 200 µl non-concentrated virus. Based on data from Figure 4.4 and previous work in our lab with these cell lines, cells were initially treated with 0-0.5 µg/ml puromycin for 96 h, with cell counts taken after 48, 72 and 96 h. Treatment with 0.25 or 0.5 µg/ml appeared to be exceptionally cytotoxic to both the transduced cells as the non-transduced cells (regardless of the manner of lentiviral transduction) within 24 h (data not shown). This is likely due to a low percentage initial lentiviral transduction efficiency, and so the accumulation of apoptotic factors in the presence of puromycin likely caused too much stress on the successfully-transduced cells, resulting in cell death. Therefore, any future selection (including on the MOLM-13, MOLM-13-DR and MV4-11 cell lines) was carried out with 0.1 µg/ml puromycin. Absolute cell counts are shown in Figure 4.5, comparing proliferation between each cell line with and without 0.1 µg/ml puromycin. In this instance, only the cells treated with 200 µl non-concentrated virus showed any growth in the presence of puromycin (Figure 4.5), and so these were removed from puromycin after 96 h and then gradually expanded for use in future experiments.

4.3.1.3 Validation of Inducible Cas9 expression

Following the establishment of a full culture of puromycin-selected, Cas9 lentivirus transduced MV4-11-DR cells, cells were treated with 6 µg/ml doxycycline and Cas9 expression was tested by Western blotting. This concentration was chosen initially, since it had been validated as being possible to induce Cas9 in HEK293Ts (Figure 4.2A), yet was not too high to cause cell toxicity (Figure 4.3). As is evident in Figure 4.6, the Western blot also provided validation of the inducible system, since Cas9 was only expressed in the presence of the doxycycline.

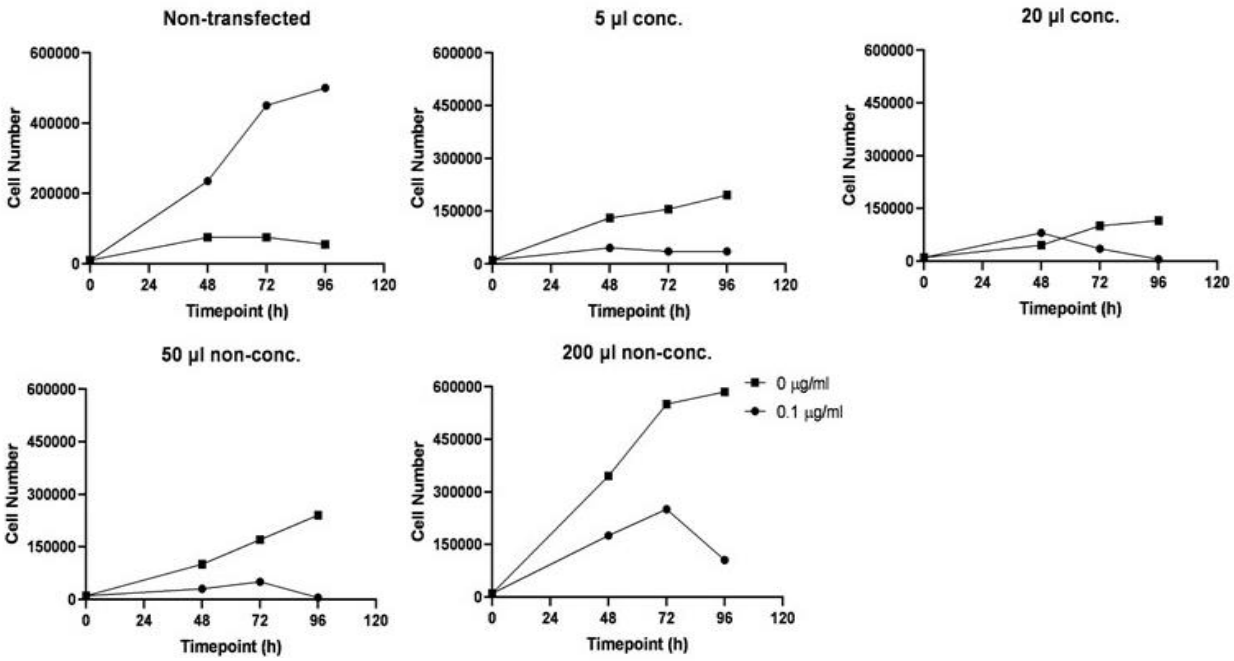

Figure 4.5. MV4-11-DR cell viability following transduction with Cas9-encoding lentivirus and puromycin selection. Cells underwent different transduction protocols, using either concentrated (conc.) or non-concentrated lentivirus. Cells were treated with 0.1 µg/ml puromycin and compared to an untreated inducible Cas9-encoding lentivirus control. Puromycin was toxic and slowed growth in most transduction conditions, with the 200 µl non-concentrated lentivirus showing the best signs of survival, as is most evident at 72 h. Cells counted using a haemocytometer following trypan blue staining, with data collated using GraphPad Prism V6.

4.3.1.4 Optimisation of Doxycycline-Mediated Induction

Following initial validation, optimal doxycycline concentration for Cas9 induction was identified. Doxycycline was titrated on to MV4-11-DR-iCas9 cells, with doses ranging from 0-8 µg/ml. Lysates were collected 24 h post-doxycycline treatment, and Cas9 expression was assessed via western blotting. As shown in figure 4.7, maximum Cas9 expression following transduction with this batch of lentivirus was achieved at the highest concentration tested (8 µg/ml). Figure 4.3 had already validated that there would be no adverse effects on cell survival following treatment with this concentration of doxycycline, with 96% survival at this concentration. Furthermore, to ensure no adverse effects from the doxycycline-induced Cas9 induction on Ras-relevant pathways, p-ERK levels were also analysed by Western blotting, with no difference seen between the uninduced and the induced cells (Figure 4.6). As a result, this concentration was used in future experiments.

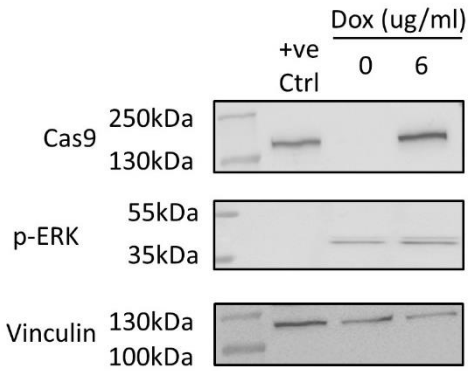

Figure 4.6. Confirmation of inducible Cas9-expression in a mixed pool of MV4-11-DR cells. Following transduction of MV4-11-DR cells with 200 µl inducible-Cas9-encoding lentivirus for 72 h, selection with 0.1 µg/ml puromycin for 96 h and 24 h induction with doxycycline, Cas9 expression was confirmed by Western blotting. Maintenance of Ras-mediated signalling in the presence of doxycycline within the lentivirally transduced MV4-11-DR cells was briefly validated using p-ERK. HEK293T transiently transfected to express Cas9 not under doxycycline control was used as the positive control.

4.3.1.5 Establishing a pure population of inducible Cas9-expressing cells

Following selection with puromycin, MV4-11-DR-iCas9 cells were subcloned using the HS5 feeder layer method, with full culture established after approximately 4 weeks. This involved dilution of puromycin-selected cell suspension of MV4-11-DR inducible-Cas9 expressing cells to a theoretical concentration of 0.25 cells/well. These were plated in 96 well plates containing 20,000 irradiated HS5 stromal cells and gradually expanded up to full culture over approximately 4 weeks (Section 2.11). Alternatively, cells were resuspended in 2.1% methylcellulose, grown to form colonies of approximately 70-100 cells, and then expanded in a similar manner to the stromal cell-grown subclones. Once full-sized culture was established and using 8 µg/ml doxycycline treatment, Cas9 was induced in these cells, and lysates were collected 24 h later. Identification of Cas9-positive clones was identified by Western blotting. As shown in figure 4.8, clone 7F6 appeared to have the greatest Cas9 expression, and so this clone was used for future HDR-virus transductions.

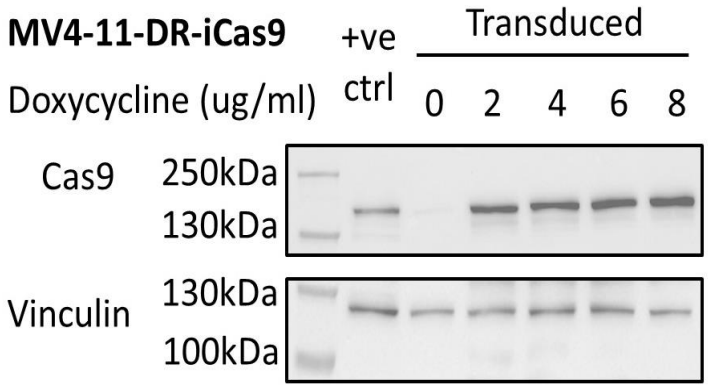

Figure 4.7. Titration of doxycycline to maximally induce Cas9 expression in a mixed pool of lentivirally transduced, puromycin-selected MV4-11-DR cells. A mixed pool of Cas9-expressing cells were treated with 0-8 µg/ml doxycycline for 24h prior to collection and lysis, with Cas9 expression analysed through Western blotting. HEK293T transiently transfected to express Cas9 not under doxycycline control was used as the positive control.

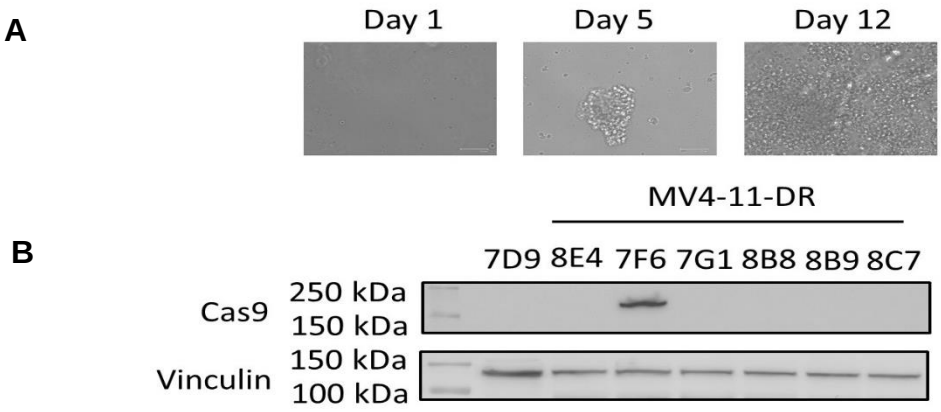

Figure 4.8. Subcloning of inducible Cas9-expressing MV4-11-DR cells. A) Light microscope images of subclones of cells growing as a colony from one original cell. Full-sized culture was established after approximately three weeks of gentle expansion, from 96 well plate (pictured here). Images were taken using an EVOS FLoiD Imaging System (Life Technnologies). **B)** Western blotting of various clones obtained following subcloning, with positive clones (e.g. 7F6) identified following Cas9 induction with 0.1 µg/ml doxycycline.

4.3.2 CRISPR-Mediated Editing of NRAS G12D

4.3.2.1 Generation of CRISPR Component Vectors

Following identification of a Cas9-expressing population, a 20-nucleotide guide sequence was used to direct the Cas9 to cut at the desired location. This was designed to span the region containing the desired mutation (NRAS D12), i.e. bases 24-44 of *NRAS* exon 2. BsmBI-compatible overhangs were added to both the 5' and 3' ends of the guide, and this was then cloned into LentiCRISPR_V2 (Addgene no. 52961), which had been digested with BsmBI (Table 4.2). This permitted the cloning of the guide in between the U6 promoter and the sgRNA scaffold, thus creating a cassette of all necessary components to direct the Cas9 to the desired cut site. This entire cassette was then PCR-amplified with NheI and EcoRI-compatible ends added and ligated into the LeGo-iG plasmid (Addgene no. 27358), which had been digested accordingly. This

plasmid was chosen as the backbone for the delivery of the guide and HDR template, since the HDR template could be cloned in downstream of an SFFV promoter, and prior to an EGFP tag, under the control of an IRES element, maintaining expression controlled by the upstream SFFV promoter. Therefore, cells which would be transduced (and thereby have the potential to have been edited) would fluoresce green.

To generate the HDR template, genomic DNA was extracted from MV4-11 cells, and PCR amplified, with SbfI and NotI restriction sites added the 5' and 3' ends of the amplicon, respectively. This was then subjected to overlap PCR, wherein several mutations were created around the guide region (figure 4.9). The vast majority of these were silent mutations, with the exception of the G>A mutation at base 141 on the HDR template amplicon, which encoded the desired D>G amino acid substitution at *NRAS* codon 12 (c.35G>A). The remaining silent mutations were designed to reduce the risk of any future editing in this region, since the sequence would be too different for the guide to subsequently bind. Furthermore, the presence of these mutations provided a screening option for positive clones to be identified, since a primer could be designed specific to the mutations within this sequence, and thus would not bind to any non-edited cells. This was then ligated into the LeGo-iG plasmid containing the guide, which had also been digested with SbfI and NotI. This is summarised in the schematic of figure 4.10, with primers detailed in Table 4.2.

Table 4.2. HDR Template, guides and primers used for LeGo-iG Vector Cloning

Name	Sequence	T_m (°C)
HDR Template	CTA GGG TTT TCA TTT CCA TTG ATT ATA GAA AGC TTT AAA GTA CTG TAG ATG TGG CTC GCC AAT TAA CCC TGA TTA CTG GTT TCC AAC AGG TTC TTG CTG GTG TGA AAT GAC TGA GTA CAA ACT GGT GGT CGT TGG TGC AGG TGG TGT CGG GAA GAG CGC ACT GAC AAT CCA GCT AAT CCA GAA CCA CTT TGT AGA TGA ATA TGA TCC CAC CAT AGA GGT GAG GCC CAG TGG TAG CCC GCT GAC CTG ATC CTG TCT CTC ACT TGT CGG ATC ATC TTTA CCC ATA TTC TGT ATT AAA GGA AT	N/A
HDR Template Amplification Forward + SbfI	GAA TTC CTG CAG GCT AGG GTT TTC ATT TCC ATT GAT TAT AG	66.5
HDR Template Amplification Reverse + NotI	GTA GCG GCC GCA TTC CTT TAA TAC AGA ATA TGG GTA AAG	65.3
HDR Mutant Template F	CTG AGT ACA AAC TGG TGG TCG TTG GTG CAG GTG GTG TCG GGA AGA GCG CAC TGA CAA TCC	85.6*
HDR Mutant Template R	GGA TTG TCA GTG CGC TGT TCC CGA CAC CAC CTG CAC CAA CGA CCA CCA GTT TGT ACT CAG	85.6*

NRAS D12G Guide 5 Forward + BsmBI	CAC CTG GTT GGA GCA GAT GGT GTT	N/A
NRAS D12G Guide 5 Reverse + BsmBI	AAA CAA CAC CAT CTG CTC CAA CCA	N/A
gRNA Scaffold Forward + XbaI	GCT CTA GAC AGG GAC AGC AGA GAT CCA GTT TG	71.5
gRNA Scaffold Reverse	GCA CCG GAG CCA ATT CCC AC	69.4

* denotes exceptionally high T_m due to primer length (necessary due to mutagenesis) – 65°C used as the annealing temperature (acceptable for two homology arms of the primer) in PCR in these cases, to render it compatible with external primer.

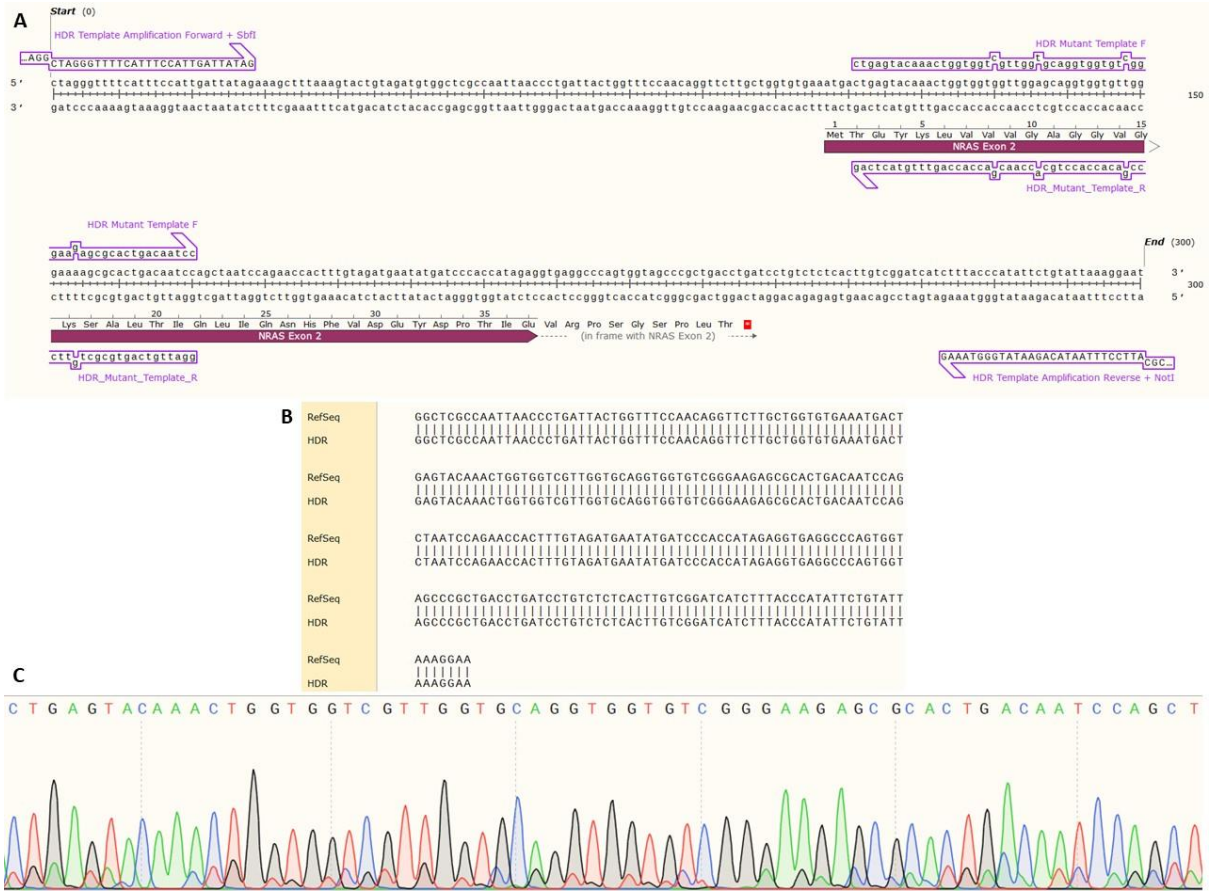

Figure 4.9. Design of the CRISPR-Cas9 HDR template. A) Primer location within/around NRAS Exon 2 sequence (maroon) of MV4-11-DR cells, with primers used to generate point mutations (denoted by superscript/subscript) highlighted in purple. **B)** Alignment of predicted sequence to Sanger sequencing result pf amplified HDR template. **C)** Overlap region Sanger sequencing quality highlighted.

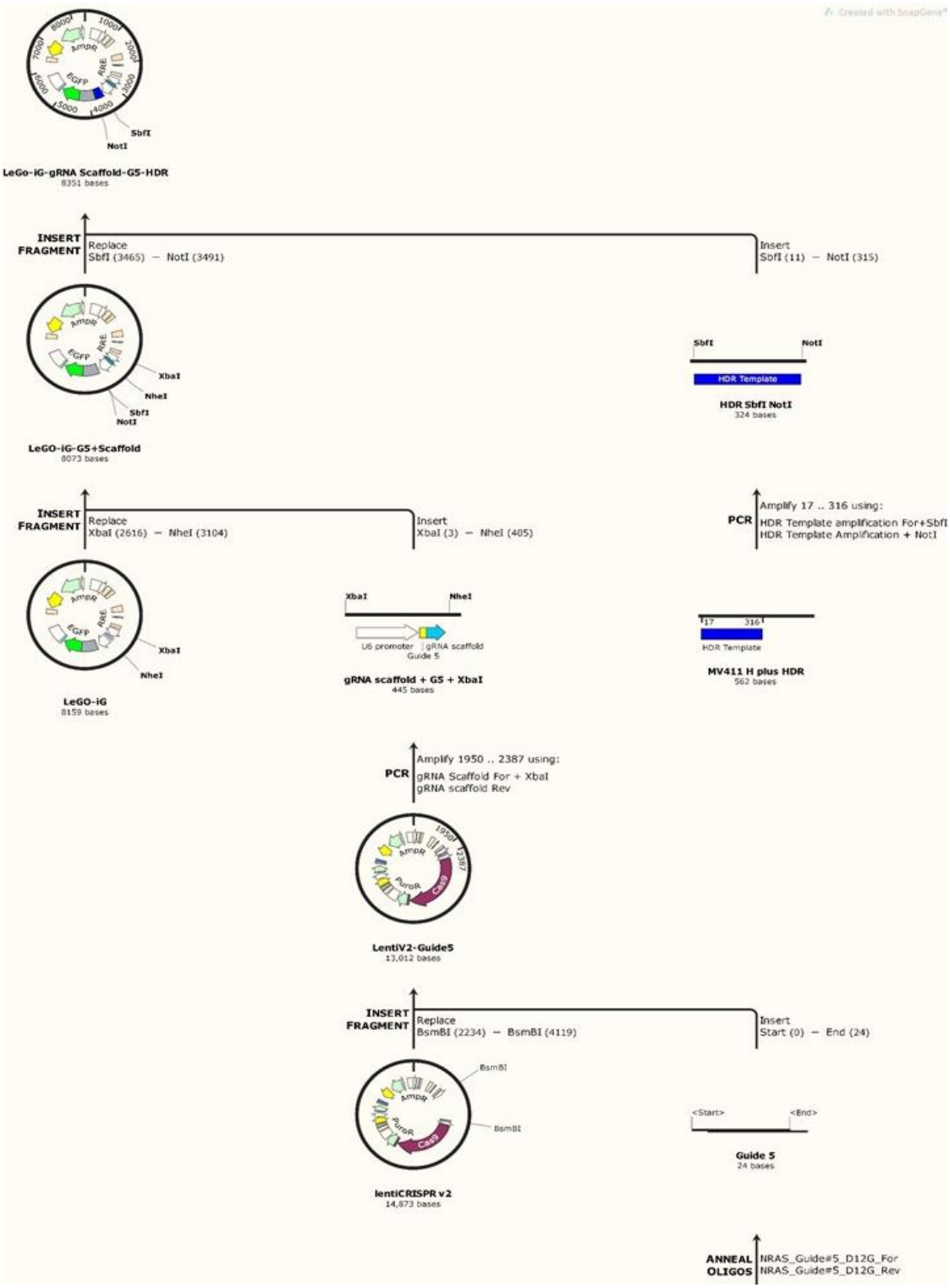

Figure 4.10. Workflow of HDR Template Cloning into LeGo-iG backbone. Following several rounds of cloning, the plasmid was successfully created to include the three key elements required for the way in which this CRISPR experiment had been designed: the guide RNA sequence, the homology-directed repair template and the *EGFP* gene used for selection.

4.3.2.2 Transduction of CRISPR Components into MV4-11-DR

Lentivirus encoding the HDR template and guide was generated in the same way as the inducible Cas9 virus had been generated, and was added in various ratios to the MV4-11-DR-iCas9 7F6 clone as described above. These ratios ranged from 1:1 to 1:10 of viral media volume: culture volume. As detailed in figure 4.11, transduction efficiency was low, however was high enough that a small population of GFP+ cells could be obtained to then be subcloned, to identify an edited population. However, due to initial difficulties with transduction this process was somewhat optimised. The optimum protocol for this viral transduction appeared to be with a spinoculation step, during which the cells were spun at 450 x g for 1 h at 37°C after transduction with differing amounts of lentivirus (Figure 4.11)

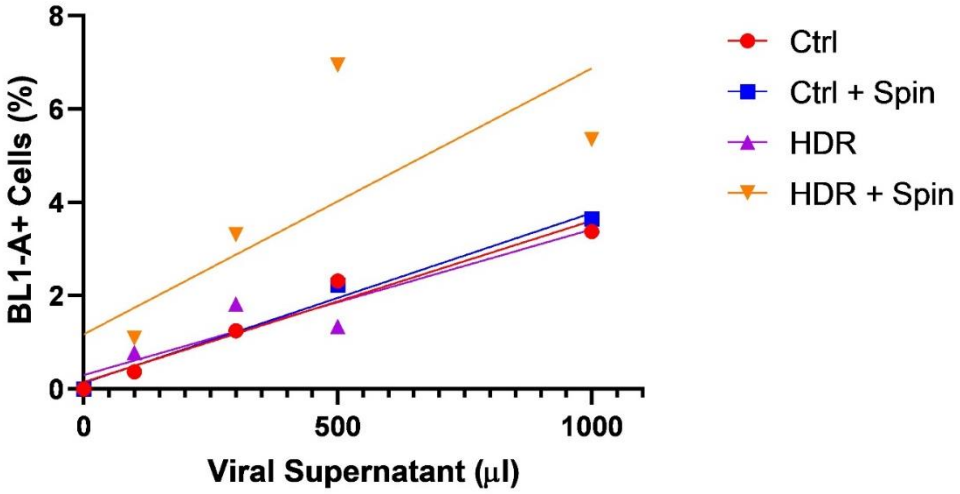

Figure 4.11. Percentage GFP+ cells within the transduced MV4-11-DR inducible Cas9 population. GFP (determined by BL1-A positivity following flow cytometry) was encoded in the same vector as the HDR template and guide RNA, thereby increasing the likelihood of successfully edited cells being identified. Percentage transduction remained low, however was highest when cells were treated with 500 µl lentivirus (yellow), and spinoculated. Ctrl refers to LeGo-iG only, HDR is LeGo-iG-G5-HDR. Linear regression lines also shown, performed using GraphPad 8.0.

4.3.2.3 Sorting of Transduced Cells

GFP-positive cells were selected for using the FACS Canto II System. Cells were sorted at a flow rate of one million cells per hour, and GFP+ cells were retained. As shown in figure 4.12, 5.9% of the HDR template-transduced cells, and 3.8% of the

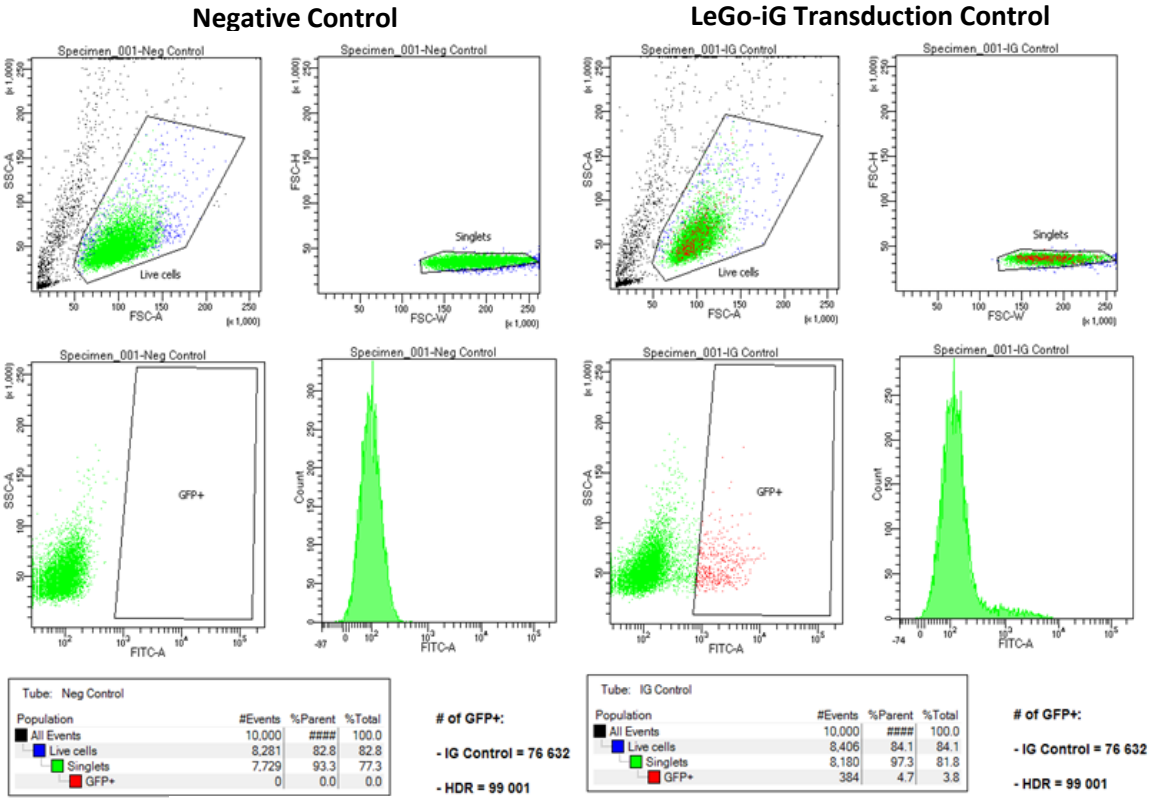

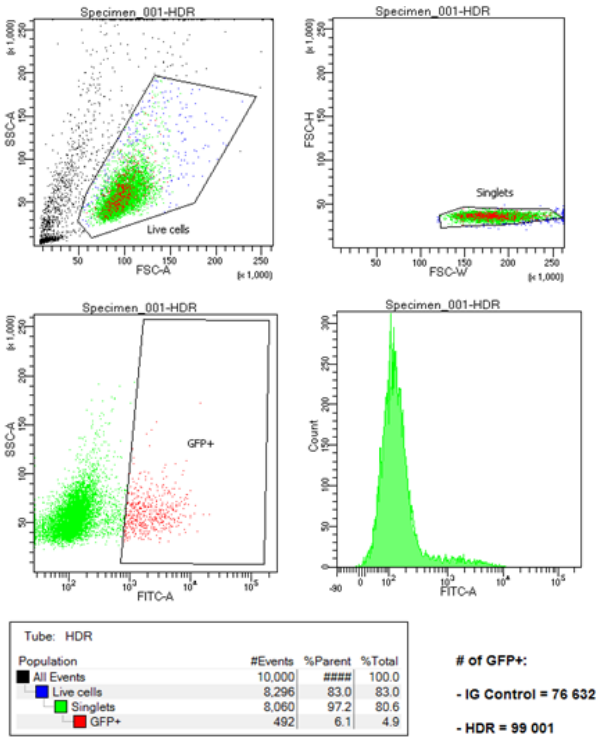

Figure 4.12. FACS plots following GFP-selection of control-transduced and HDR-transduced MV4-11-DR, inducible Cas9 cells. Transduction efficiency was low, as indicated by the low percentage of GFP-positive cells, however approximately 100,000 cells were selected in all cases, which were then taken forward to future work.

Control-transduced cells were GFP positive. These were subcloned, using the HS5 feeder layer method or methylcellulose.

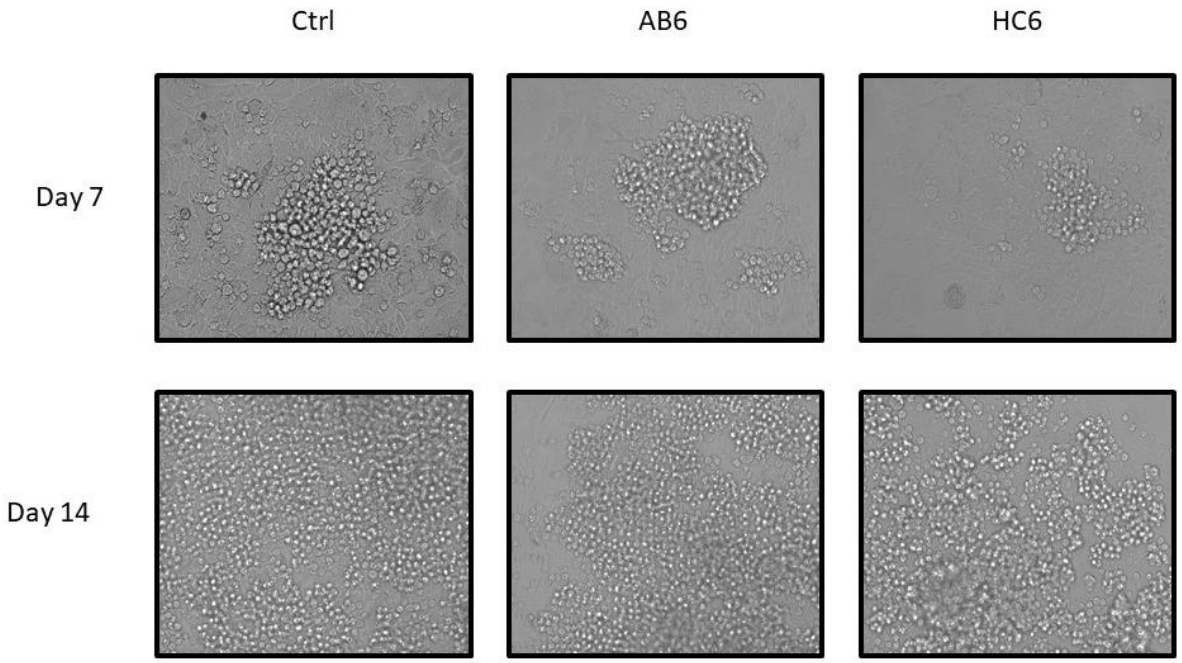

Figure 4.13. Subcloning images at 7- and 14-days post-plating of LeGo-iG Ctrl and LeGo-iG-G5-HDR lentivirally transduced and GFP-sorted MV4-11-DR inducible Cas9 cells. Cells were grown on top of an irradiated HS5 feeder layer for up to 3 weeks before re-plating without the feeder layer once the colony had reached approximately 70% confluency. Images included here are after 7 and 14 days. Images were taken using an EVOS FLoiD Imaging System (Life Technologies).

4.3.2.4 Identification of Mutated Cells by PCR

Full-sized culture of subcloned cells was established within approximately 4 weeks, with clones gradually expanded from a 96-well, to 48-well, to 24-well and finally to a 12-well plate, once they reached approximately 60-70% confluency. From here, genomic DNA was extracted using the Promega SV DNA extraction kit. A region of the HDR template (incorporating the desired mutations) was amplified by PCR, using either a forward or reverse primer designed to include the mutations included within the HDR template, plus either the forward or reverse HDR template amplification

primer, as detailed in figure 4.14. However, despite a series of mutations having been created within the HDR template with the aim of aiding screening for successful editing by PCR, a PCR product was also obtained in the control-transduced cell lines. This indicates the specificity of the PCR was insufficient to successfully detect the mutations as desired.

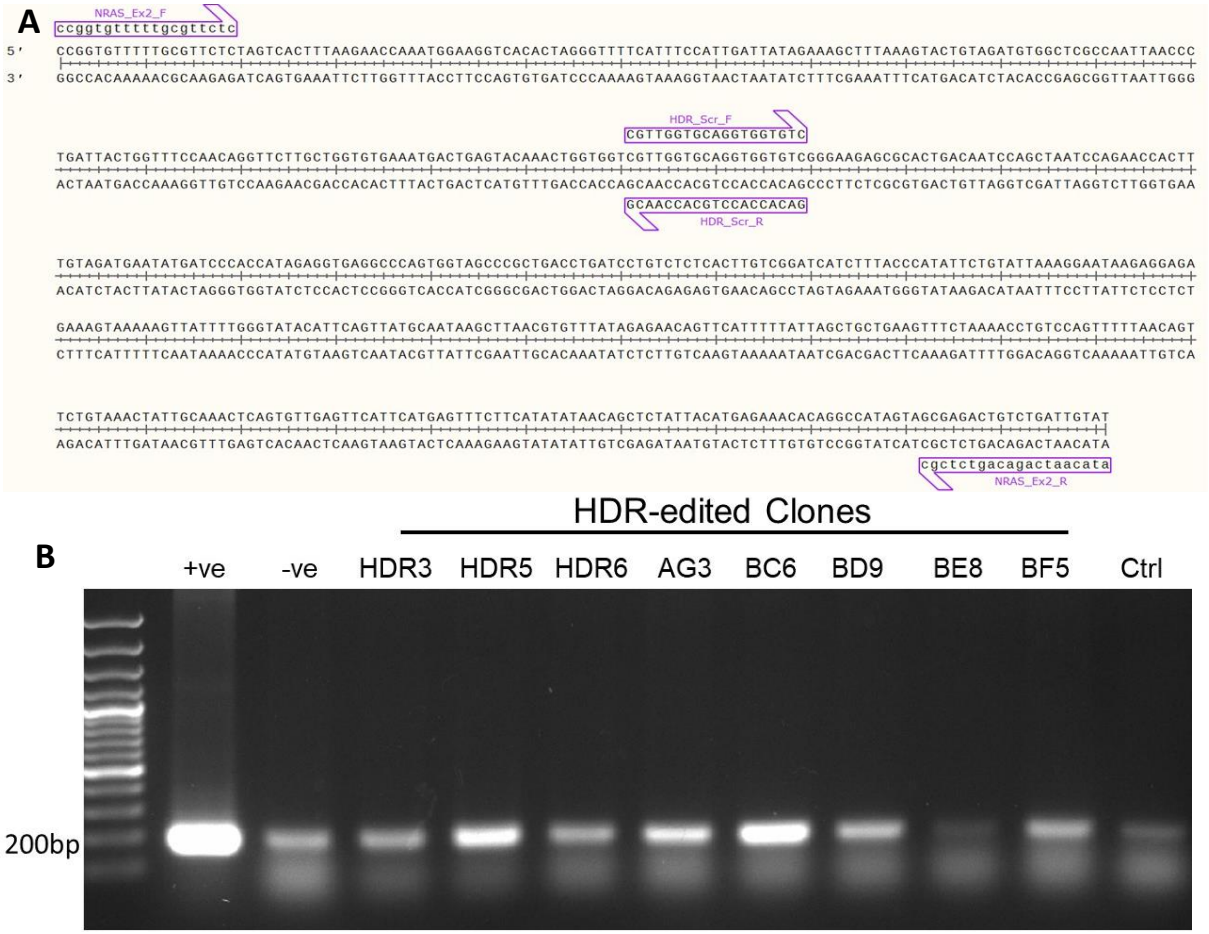

Figure 4.14. Basic PCR Screen of subcloned LeGo-iG-G5-HDR lentivirally transduced MV4-11-DR inducible Cas9 cells. A) Primers designed specific to HDR template, alongside primers within the intergenic (NRAS_Ex2_F) and intronic (NRAS_Ex2_R) regions. **B)** Agarose gel visualisation of product resulting from PCR of LeGo-iG-G5-HDR lentivirally transduced MV4-11-DR cells. PCR shown here was conducted using NRAS_Ex2_F and HDR_Scr_R primers, illustrated in part A.

4.3.2.5 Identification of Mutated Cells by qPCR

As an alternative, quantitative PCR was carried out on the genomic DNA extracted from these cells, with the anticipation that there would be greater binding affinity of the primers designed to be mutation specific to edited cells, than the wild type. It would therefore be expected that the Cq value for edited cells would be lower than that of the non-edited cells, with ultimately ΔΔCq values appearing higher in the edited cells than the controls, when normalised to the housekeeping gene (*GAPDH*) levels. This was the case for a subset of clones tested by qPCR, as shown by Figure 4.15. These clones were then sent for Sanger sequencing.

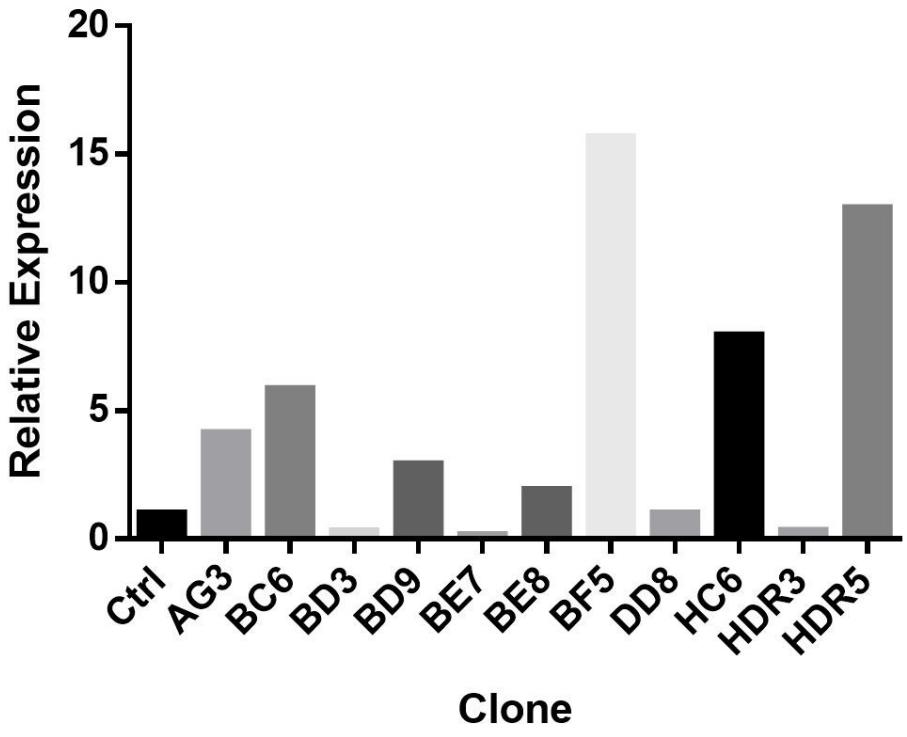

Figure 4.15. Quantitative PCR of the genomic *NRAS* DNA from a subset of the clones grown from the HDR-transduced, GFP+ selected MV4-11-DR inducible Cas9 cells. Those with relative expression greater than the control (normalised to 1) were Sanger Sequenced (Section 4.3.2.6). Data normalised using the ΔΔCq method and visualised using GraphPad V8.0.

4.3.2.6 Sequencing of Transduced Clones

Unfortunately, despite the measures taken to improve and optimise editing, the low efficiency of transduction and CRISPR-Cas9 HDR-mediated editing resulted in no clones found to be edited in the manner desired, so the G12D mutation occurring in the MV4-11-DR cells was not reversed (as exemplified in Figure 4.16), with >100 clones that were ultimately Sanger sequenced yielding negative results. It is important to note that the inclusion of several silent mutations helped to analyse whether the desired editing had occurred, particularly since the attempted mutation was heterozygous, so sequencing was occasionally read at G12, rather than D12 (as in clone BD9, Figure 4.15). However, it was clear that the editing had not been completed in the desired way due to the lack of the other silent mutations within the sequence. Nevertheless, it is believed that the guide used here was suitably effective at creating the double-stranded break, since some of the clones appeared to be knock-outs, when the sequence was analysed, as shown by Figure 4.16). This is exemplified by clone CE8, in there was no sequence read after the position at which the guide cut. This implies the issue was the efficiency of the HDR-mediated repair, rather than the cut itself.

Figure 4.16 Sequencing alignment of a subset of the clones grown from the HDR-transduced, GFP+ selected cells. RefSeq refers to the original MV4-11-DR sequence of the cells to be edited. Mutated refers to the sequence desired following inclusion of the HDR template. The bottom four rows illustrate the sequence of four clones: AD6, AD8, BD9 and CE8. Green lettering refers to Adenine matches between the original MV4-11-DR reference sequence and the sequence in question, blue to Cytosine matches, yellow to Guanine matches, and pink to Thymine matches. White lettering refers to a base mismatch between the sequence in question and the MV4-11-DR reference sequence. Dashes refer to missing bases. *NRAS* codon 12 is highlighted by the red box, and guide 5 positioning is indicated by the blue arrow.

4.4 Discussion

This chapter aimed to generate a gene edited AML model, reverting a drug-induced NRAS oncogenic mutation using CRISPR-Cas9. Several elements of the processes followed were successfully carried out within this chapter, despite the final edited product not being achieved. Although several options have been attempted here, particularly with regards to detection of edited clones and lentiviral delivery mechanisms, providing the means of repeating this process perhaps with alternative genes or at different sites. Given that these drug-resistant cells are likely to have obtained a wealth of mutations throughout their resistance acquisition, it is useful to have developed the inducible Cas9 model to further probe the effects of other resistance-associated genes. This could range from further single gene or sites investigations such as those described here, to larger CRISPR screens to examine a wide panel (Sun et al., 2019)

Indeed, establishment of the transduction and subcloning protocols for AML/suspension cells were particularly useful. The use of subcloning enabled a greater degree of certainty as to the true genotype of the cell, ensuring that, had this been successful, any genotypic or phenotypic changes seen were as a result of the reversion of the NRAS mutation. As a result of their development here, these have been taken forwards for work in Chapter 5.

The main issue appeared to be with the editing process itself, likely due to the inability of the cells to follow the HDR mechanism. This could be further improved by optimisation of the repair template itself or the mechanism it is delivered by. It could be that improved efficiency of HDR may be possible through cell cycle regulation, and therefore present an option for future improvements of this work (Czeiszperger, Wang & Chung, 2020; Ferrari et al., 2021; Gutschner, Haemmerle, Genovese, Draetta & Chin, 2016). Nevertheless, this would need to be carefully controlled, so as to avoid introduction of cellular stresses which could impact already precarious and tightly regulated signalling, with cell viability often decreasing after transduction. Potential improvements that could be made to this process to increase success will be further analysed in Chapter 6. Ultimately, although the final endpoint of generating the NRAS drug-resistant reversion model was not achieved, the models created in chapter 3 can still be used to assess the involvement of NRAS in FLT3-inhibitor resistance, which will be depicted in chapter 5.

Chapter 5

Effects of NRAS Overexpression in Acute Myeloid Leukaemia

5 Effects of NRAS Overexpression in Acute Myeloid Leukaemia

5.1 Introduction:

The presence of various NRAS mutants has already been proven in our array of AML cell lines, yet the phenotypic effects of these individual mutants still remains to be elucidated. The tools created in Chapter 3 present the opportunity to investigate these in greater detail, to analyse any differential impact between the mutants, in a FLT3-ITD+ context. Therefore, there could be directly compared in a genetically identical background.

It is important to study the impact of these mutants from both a genotypic (transcriptomic) and phenotypic angle, to best validate the differences between them. This will help to identify key interactors that could be manipulated in the future, as well as better understand the differences in patient outcome arising from differing drug sensitivities. Given that treatment can now be stratified based on KRAS mutant genotype in some cancers given the FDA-approval of AMG510 (Sotorasib) and MRTX849 (Adagrasib), it is plausible that there may, in the future, be the potential for NRAS mutant directed therapy, as drug development pipelines become even further refined. However, there is also the possibility that just by mutant genotype screening, patients could be more appropriately treated, since it is likely there will be differences between the phenotypic effects of all of these mutants. For example, pathways up-regulated by particular NRAS mutants could be inhibited by directly targeting these pathways with already available inhibitors, and therefore AML pathogenesis be

reduced. Such effects have been seen *in vitro* with simvastatin, the cholesterol lowering drug (Jang, Lee, Jang, Jung & Park, 2019).

5.2 Aims and Hypothesis:

Whilst it has been shown previously (McMahon et al., 2019) that the general presence of *NRAS* mutants can confer resistance to a range of therapeutics used in AML, analysis of individual NRAS mutations in a leukaemic context remains to be fully explored. In this way, this chapter aims to provide a new perspective on changes incurred by one mutant over another.

Given the current literature and the emergence of different NRAS mutations within our own FLT3-inhibitor resistant cell lines, I hypothesise that there will be a phenotypic difference in the leukaemogenic and drug-resistant potential of the MOLM-13 cell line over-expressing various NRAS mutants. Since G12 mutants are classically believed to be 'more transforming', it is likely that they contribute to a greater leukaemogenic potential, however the impacts of each mutant on a drug-resistant phenotype remains to be elucidated. This will also likely be drug-dependent, whether the drug is on-target for the Ras pathway, or off-target. Ras-mediated pathway-targeting drugs may not have a selective preference for particular Ras mutations, since their usual mechanism and resulting effects would be subverted by the presence of over-active Ras. On the other hand, off-target drugs (e.g. cytarabine) may show more of a selection preference for the more leukaemogenic mutants, likely G12. This would be because their mechanism of action would not be inhibited specifically, and therefore would require a strong leukaemic driver mutation to overcome its effects. Indeed, it may be that there is no resistance potential conferred to the over-expression of NRAS, since the drugs'

considerable potency may enable it to overcome the accumulation of several mutations and a variety of leukaemic backgrounds.

Following the generation of NRAS over-expressing AML cell lines using tools detailed in Chapter 3, the genotypic and phenotypic effects of NRAS (wild-type and mutant) over-expression will be assessed, and compared to the parental and drug-resistant data previously obtained and discussed in Chapter 3. This will include analysis of functional effects including leukaemogenic potential, as well as proliferative capacity and drug sensitivity. Genotypic effects will be assessed through RNASeq, with the most upregulated and downregulated genes further analysed by qPCR and Western blotting amongst other techniques, when possible.

5.3. Results

5.3.1 Generation of NRAS over-expressing cell lines

As detailed in chapter 3 (section 3.3.5.1), lentiviral plasmids were generated to over-express NRAS wild-type, G12C, G12D and Q61K. Following a co-transfection of these plasmids with psPax2 and pMD2.G (Appendices 4 and 5), four NRAS-encoding lentiviruses, as well as a control, were generated. These were used to transduce the MOLM-13 parental cell line, to assess the differences between these mutants in a genetically identical background. The same transduction protocol was used as had been somewhat successful for other transductions (section 4.3.1.2): addition of 200 µl of non-concentrated lentivirus and 8 µg/ml polybrene to 500,000 cells, followed by spinoculation for one h at 37 °C. Polybrene was diluted to 4 µg/ml after 6 h by doubling the media volume in the well. Viral media was changed after 72 h. Cells were then selected using 0.1 µg/ml puromycin for 96 h, before being subcloned and gradually

expanded using the stromal cell feeder layer method, as described in section 4.3.1.5. Figure 5.1 represents the different levels of over-expression seen at different points in the process of generating these cells.

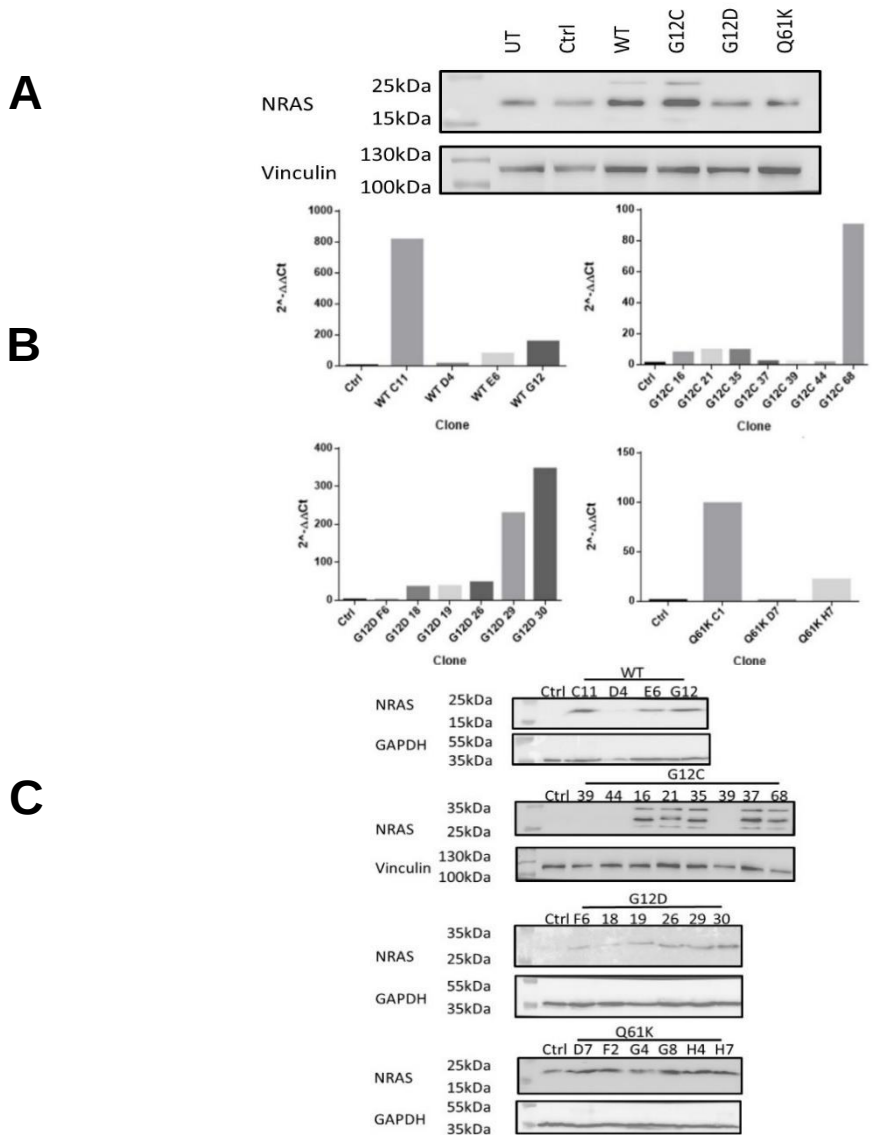

Figure 5.1. Generation and subcloning of NRAS wild-type and mutant over-expressing MOLM-13 cells. Ctrl refers to non-transduced cells, throughout figures A-C. **A)** Over-expression of NRAS variants seen following lentiviral transduction and puromycin selection. Lysate taken from polyclonal population (prior to subcloning). **B)** qPCR results of MOLM-13 subclones over-expressing NRAS wild-type, G12C, G12D or Q61K. **C)** NRAS protein levels in different over-expressing subclones. The NRAS Q61K blot was imaged using stronger enhanced chemiluminescent reagents due to poorer blot quality. UT refers to untreated MOLM-13 cells. Ctrl in this case refers to MOLM-13 cells transduced with a lentivirus made with the same pLJM1 backbone as the NRAS plasmids.

Cell subclones were selected to ensure the entire population being studied were over-expressing NRAS, and had been successfully transduced and selected. It was apparent from the Western blot of the polyclonal pools (Figure 5.1A) and the subsequent analysis (Figure 5.1B/C) that there was not a fully over-expressing population generated purely from the transduction and selection, hence the requirement for subcloning. This lack of full over-expression following transduction and selection was to be expected, given the MOLM-13 cell line's aversion to transduction, as previously discussed. NRAS over-expression within the subclones was validated at a transcript and protein level, using both qPCR and Western blotting, respectively (Figure 5.1B/C). All bands appear stronger in the NRAS Q61K transduced blot compared to those above since a stronger ECL reagent was used due to original poor blot and temperamental antibody quality. Nevertheless, certain clones appeared to more strongly express NRAS compared to the control transduced cell line, which paired with the data shown in Figure 5.1B. Eventually, WT G12, G12C 68, G12D 29 and Q61K H7 were all taken forwards for genotypic and phenotypic evaluation, based on a range of factors including level of over-expression at the RNA and protein level and overall cell health and survival.

5.3.2 Proliferative Potential

Following generation of these cell lines, their phenotype was characterised in several ways. Alterations to proliferative potential was first assessed. Leukaemogenic potential, and in particular drug-resistant leukaemia, relies on an increased proliferative capacity of the blast cells, one of the key hallmarks of cancer (Hanahan, 2022; Hanahan & Weinberg, 2011). To assess any alterations in this potential in the

NRAS mutant cell lines generated in this thesis, proliferation assays were carried out over the course of 96 h (Figure 5.2). Trypan blue staining was used to initially determine any proliferative changes, with overexpression of the NRAS mutants G12C, G12D and Q61K conferring increased proliferation compared to the parental and NRAS WT over-expressing cells. There was a significant difference between the mutant over-expressing cell lines compared to the WT over-expressing and control cell lines at 96 h, with $P<0.0001$ in all cases. However, there was no significant difference in proliferative capacity between mutants themselves. This data somewhat correlated with the G12 mutant-only increase in proliferative potential of HeLa cells, as previously described in Figure 3.12. Such data was then supported by CFSE staining of the MOLM-13 NRAS over-expressing cell lines, and in this assay was also compared to the MOLM-13-DR cells too. The principle of this assay involves a decrease in the proportion of stained cells with increased cell proliferation, since the stain is not passed to daughter cells following mitosis. As shown in Figure 5.2B, this also showed an increase in proliferation in the mutant over-expressing cells, compared to the parental and NRAS wild-type over-expressing cells.

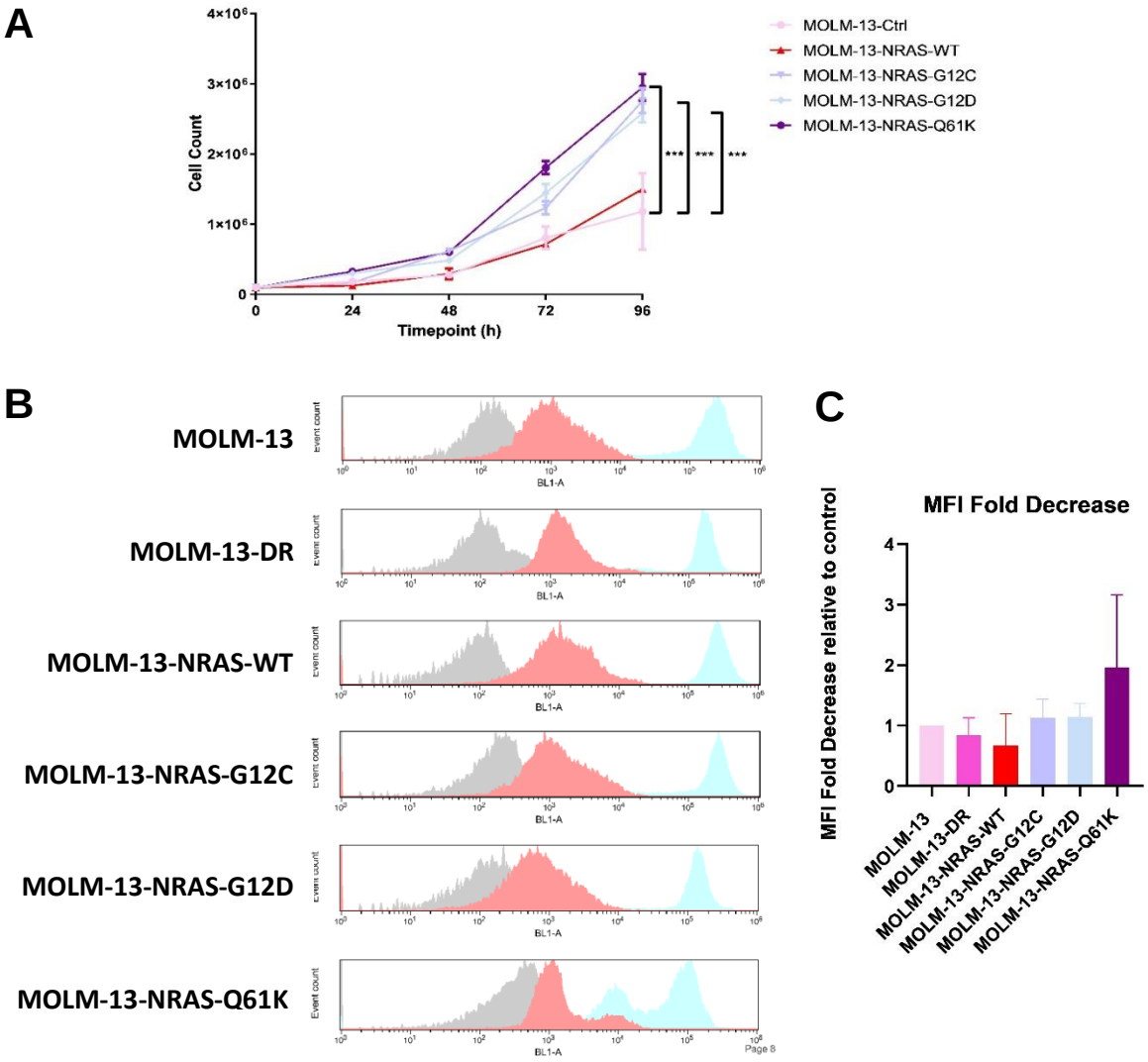

Figure 5.2. Proliferative capacity of NRAS-mutant over-expressing cell lines. A) Measured by Trypan Blue staining and manual counting with a haemocytometer. Data represent *N* = 3 +/- SEM (biological replicates). *** denotes *P*<0.001. Statistically significant data also seen between all mutants and NRAS wild-type, however not shown here for legibility. **B)** Measured by CFSE staining, detected by flow cytometry. Grey indicates unstained cells, blue indicated CFSE-stained cells at 0 h, red indicates stained cells at 96 h. **C)** Relative fold decrease of median fluorescence intensity (MFI) after 96 h treatment with CFSE, compared to the MOLM-13 parental cell line. Statistical significance was assessed using One Way ANOVA and unpaired independent t-tests between individual groups, with no significance found.

5.3.3 Cell cycle analysis

Given there is a difference in proliferative potential as determined by cell number over 96 h, it was hypothesised that this would reflect differences in cell cycle. Cell cycle analysis was performed on the NRAS-mutant over-expressing MOLM-13 cell line, using 7AAD staining. A model of gating for each of the cell cycle phases is shown in Appendix 8. Cells were initially serum-starved for 18 h (grown in RPMI-1640 without FBS) prior to analysis, with the aim of bringing all of the cells to the same point in the cycle, thereby rendering the subsequent changes more comparable. This was largely achieved, though the MOLM-13-NRAS-WT over-expressing cells appeared to have an increased level of cells in G2/M phase compared to the other cell lines, following serum starvation. Variations in the time spent in each phase of the cell cycle was seen to be mutation dependent, though all mutants conferred a different cell cycle pattern to the MOLM-13-DR cell line. Indeed, certain mutants appeared to cause a faster progression through the cell cycle than others, as shown in Figure 5.3. It appears, however, that the G1 levels almost always remain higher than the control cell line in the cells over-expressing NRAS G12C and G12D. This implies a maintenance in proliferative phase. In contrast, the cells over-expressing NRAS WT appeared to show the lowest proliferative capacity, since there were minimal levels of cells in G1 phase, and indeed very little fluctuation in the percentage of cells in each phase. This implies a decrease in the rate of cell cycle, conferring ultimately a lower proliferative capacity.

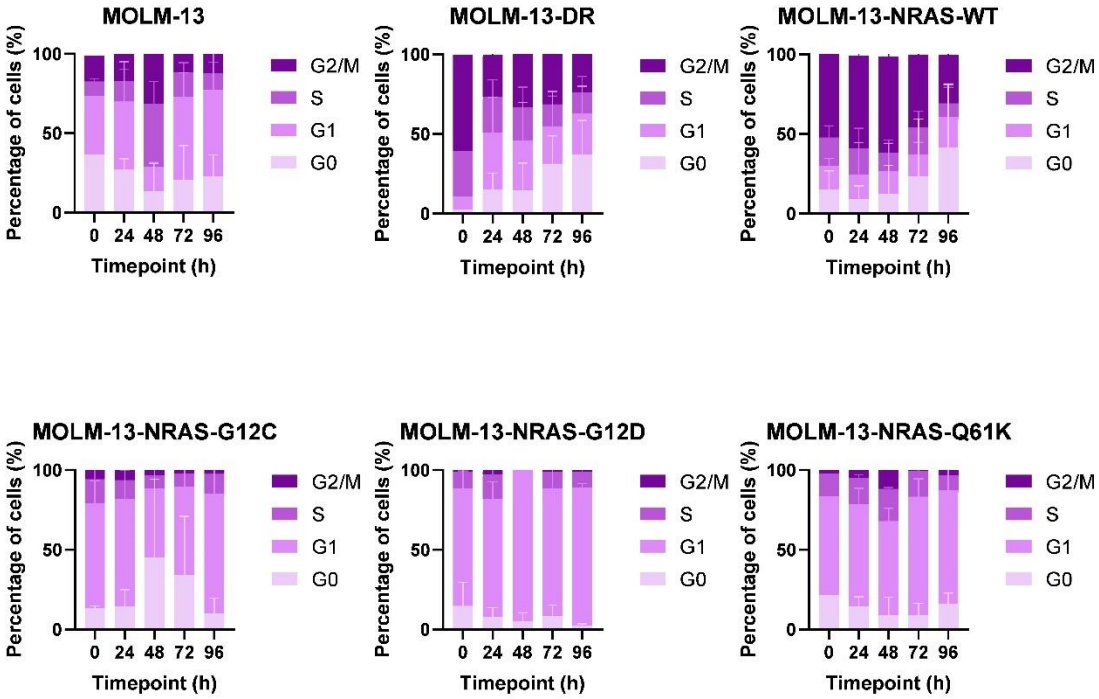

Figure 5.3. Cell cycle analysis of MOLM-13 NRAS over-expressing cell lines. Determination of cell cycle by quantification of 7AAD staining. Cells were serum starved for 18 h, prior to the 0 h timepoint being assessed by flow cytometry. Following this, cells were harvested and stained with 7AAD, before DNA content was quantified as a marker of cell cycle. N≥3 +/- SEM.

5.3.4 Colony Forming Potential

Colony forming potential is a key marker of a cell's clonal expansion capability, as well as stemness capability. Having already illustrated the increased proliferative potential of the MOLM-13 NRAS mutant over-expression cells compared to the MOLM-13 transfection control, the colony forming assay was carried out to assess whether this also correlated with increased stemness and expansion capacity. Given that one of the key functions of drug-resistant leukaemia is its potential to emerge following targeting and elimination of the bulk AML population, the colony forming potential of these over-expressing cell lines was studied. The colony forming assay, using

methylcellulose, is a means of measuring leukaemogenic potential. As shown by Figure 5.4, there was a significant increase in colony forming potential of the NRAS-mutant over-expressing cell lines, as well as those over-expressing NRAS wild-type, relative to the control MOLM-13 cell line. In comparing the differences between the mutants, NRAS-G12C over-expressing MOLM-13 cells conferred a significantly greater proliferative capacity than the NRAS-WT over-expressing cells. This suggests there is a greater leukaemogenic potential in the G12C mutant over-expressing cell lines, further supporting the increased proliferative capacity findings detailed in section 5.2.

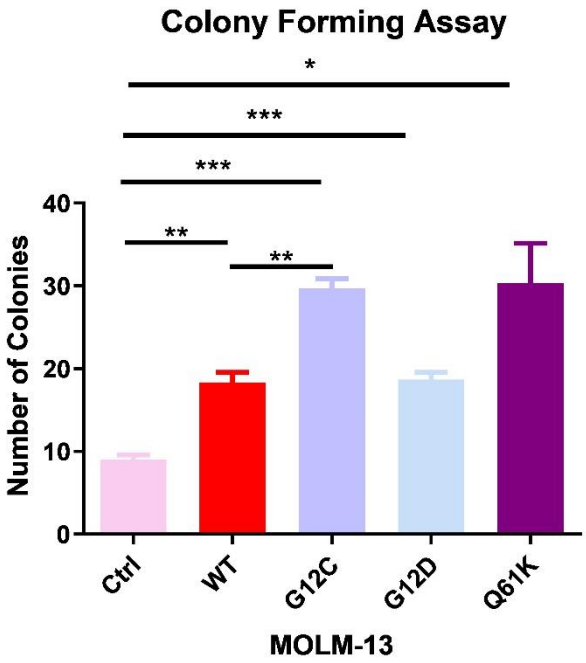

Figure 5.4. Colony-forming potential of MOLM-13 NRAS-mutant over-expressing cell lines. Measured by counting number of colonies after 10 days plating in 2.1% methylcellulose/RPMI-1640 media. *N* = 3 +/- SEM, biological replicates. * denotes *P*<0.05, ** denotes *P*<0.01, *** denotes *P*<0.001.

5.3.5 Drug Sensitivity

Given the considerable quantity of literature describing the emergence of NRAS mutants in drug-resistance, sensitivity of the NRAS over-expressing MOLM-13 cell lines to numerous compounds was assessed. Cells were treated with the compound of interest for 48 h, with cell viability determined by Annexin V-FITC and Propidium Iodide staining. These detect markers for apoptosis (externalised, membrane-bound phosphatidylserine) and necrosis (cytoplasmic DNA fragments), respectively. The compounds used here were selected due to their current or potential use in AML, or their ability to inhibit an element of the Ras-mediated proliferation and survival pathways, as has been discussed previously (Section 1.4.3 and Figure 3.8). Data were analysed using Non-Linear Regression to generate IC_{50} values, and each cell line was compared using One-Way ANOVA and subsequently unpaired t-tests. Data was plotted and statistical tests were carried out using GraphPad Prism V6. IC_{50} values are reported in Table 5.1 within the bounds of the drug concentrations tested. As is shown in Figure 5.5 and Table 5.1, there is a considerable difference in drug sensitivity between the different mutants.

Figure 5.5A indicates each of the MOLM-13 NRAS over-expressing cell lines are responsive to the front-line AML therapeutic cytarabine. There is some level of drug resistance present in the MOLM-13-DR cell line, as evidenced by a five-fold increase in the IC_{50} value, compared to cell line. Indeed, there looks to be a decrease in cytarabine sensitivity within the MOLM-13-NRAS-G12D over-expressing cell line. Nevertheless, there is no statistically significant differences between the response to cytarabine in any of the cell lines tested.

Sensitivity towards FLT3 inhibitors differed between the different NRAS over-expression cell lines. Figure 5.5B affirms the quizartinib resistance of the MOLM-13-DR cell line, as was previously reported in Figure 3.8 and Marensi et al. (manuscript in progress). However, Figure 5.5B also indicates a significant level of resistance in the MOLM-13-NRAS-Q61K cell line towards quizartinib, compared to the MOLM-13 control cell line. Whilst the NRAS wild-type over-expressing cells also appeared less sensitive to quizartinib, this was not deemed to be significant. The IC_{50} values of the control, wild-type and G12 mutant over-expressing cell lines were all lower than the concentrations tested. Analysis of Figure 5.5C indicates there is no statistically significant resistance conferred by NRAS towards the FLT3-inhibitor gilteritinib. This is in spite of a considerably increased IC_{50} value of the NRAS wild-type over-expressing cells (>100 fold), compared to the control cell line. Interestingly, further analysis of the NRAS over-expressing cell lines with the poorer response to FLT3 inhibitors revealed a decrease both in FLT3 activation and overall FLT3 protein expression, which may explain the decrease in drug efficacy here (no/considerably reduced on-target binding, therefore no on-target effect). This is highlighted in Figure 5.6. A decrease in *FLT3* transcript level was also seen in the MOLM-13-NRAS-WT and MOLM-13-NRAS-Q61K cell line as determined by transcriptomic sequencing, further supporting this data (Section 5.6 and Appendix 8.2 and 8.5). This was not seen at a transcriptomic level for MOLM-13-NRAS-G12C or -G12D, which correlates with a maintained sensitivity to FLT3 inhibitors in these cell lines.

Trametinib, as shown in Figure 5.5D, is a MEK inhibitor, therefore acting downstream of oncogenic NRAS. The data presented in Figure 5.5D indicates NRAS Q61K mutations can confer a level of resistance to trametinib. It would appear that while G12

mutants do not confer a significant level of resistance compared to the control over-expression of NRAS wild-type and Q61K does significantly increase the trametinib resistance potential of the cells.

The sensitivity towards various direct Ras targeting agents were tested against the mutant cell lines. The control and drug resistant cell lines are included in Figure 5.5E-G for reference. All of these agents (BAY293, MRTX849 and AM510) were designed against KRAS. In the case of BAY293, it appears that the NRAS mutant over-expression can outcompete the intrinsic KRAS expression, which is suppressed in the MOLM-13 control cell line, and somewhat in the MOLM-13-DR cell line too. However, over 70% of cells treated with 10 µM BAY293 remained alive after 48 h.

As previously discussed in Chapter 3, MRTX849 directly targets KRAS G12C, acting through binding at KRAS-specific residues. The data shown in Figure 5.5F supports the previously published data that this drug is not effective in other Ras mutant (or wild-type, as determined by the MOLM-13 control cell line) cancer cell lines. In contrast, AMG510 appears to be less isoform-specific. There is a statistically significant increase in the sensitivity of the NRAS G12C over-expressing cell line compared to any of the other cell lines, indicating that this drug is able to act against other Ras isoforms, provided that there is a G12C mutation to permit the covalent binding of the drug.

Table 5.1. 48 h IC_{50} values (μM) of NRAS variant cell lines to AML-relevant small molecule therapeutics. N/A refers to not assessed. UD refers to undetermined, with the dose interval used.

Drug	MOLM-13	MOLM-13-DR	MOLM-13-NRAS-WT	MOLM-13-NRAS-G12C	MOLM-13-NRAS-G12D	MOLM-13-NRAS-Q61K
Cytarabine	0.34	1.5	0.57	0.35	0.69	0.73
Quizartinib	<0.01	UD	<0.01	<0.01	<0.01	>10
Gilteritinib	0.023	>10	9.2	<0.01	0.76	UD
Trametinib	<0.01	<0.01	UD	<0.01	<0.01	UD
BAY293	2.5	>10	N/A	<0.01	>10	UD
MRTX849	1.9	6.6	N/A	2.2	0.9	>10
AMG510	>10	<0.01	N/A	<0.01	<0.01	>10

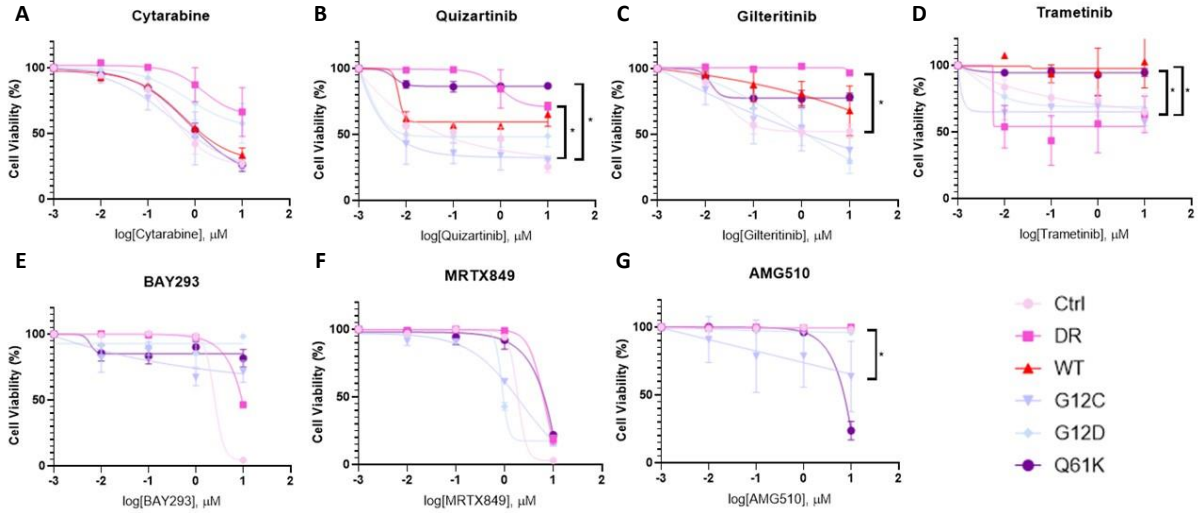

Figure 5.5. Sensitivity of MOLM-13 NRAS-over-expressing cell lines to relevant small molecule AML therapeutics. A) Front-line AML therapeutic cytarabine. **B)** FLT3-inhibitor quizartinib, currently in Phase III clinical trials for FDA/EMA approval. **C**) FDA/EMA-Approved FLT3-inhibitor gilteritinib. **D)** FDA/EMA-approved MEK inhibitor Trametinib. **E)** Ras-SOS1 interaction inhibitor chemical probe BAY293. **F)** MRTX849, FDA/EMA-approved KRAS G12C inhibitor. **G)** AMG510, FDA/EMA KRAS G12C inhibitor. As described in the legend, pale pink represents MOLM-13 (parental cells, non-transduced), dark pink represents MOLM-13-DR, red represents MOLM-13-NRAS-WT, lilac represents MOLM-13-NRAS-G12C, pale blue represents MOLM-13-NRAS-G12D and purple represents MOLM-13-NRAS-Q61K. Data represent N=3 biological replicates +/- SEM. * indicates *P*<0.05 following an unpaired t-test. Statistical analysis carried out using GraphPad Prism V6, with non-linear regression curves shown here.

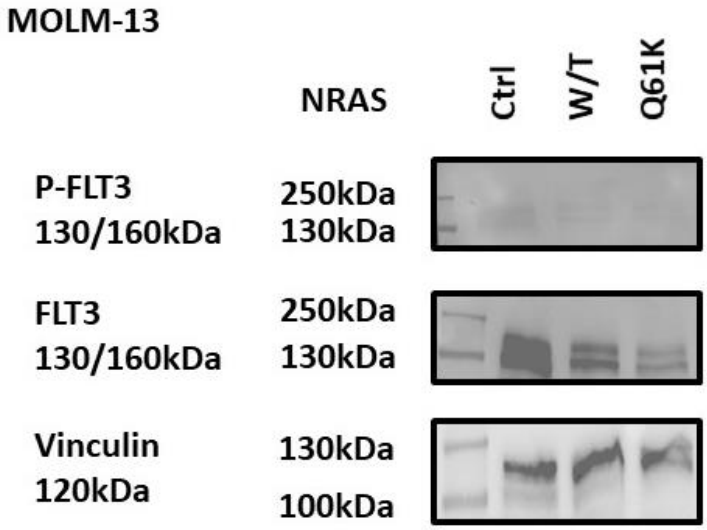

Figure 5.6. FLT3 activation and expression in MOLM-13 NRAS-over-expressing cell lines, as determined by Western blotting. Cell lines (W/T and Q61K) shown here are those in which FLT3 expression is shown to be manipulated, as per the transcriptomic data. These also confer different sensitivities to FLT3 inhibitors. Ctrl refers to cells non-transduced cells.

5.3.6 Signalling Alterations

Alterations to key signalling pathways within the NRAS over-expressing cell lines were detected by Western blotting, as well as analysed by transcriptomic sequencing, as will be described in section 5.3.6 and Appendix 8. Western blotting mostly supported the transcriptomic data, with regards to the upregulation of genes involved in the MAPK pathway (Figure 5.7). An increase in active ERK was seen in most of the NRAS over-expressing cell lines, though surprisingly not in the MOLM-13-NRAS-G12D cell line. This contradicts the HEK293T data, which suggested an increase in ERK activation when NRAS G12D is over-expressed. This therefore suggests that the effects of NRAS mutants are disease context dependent, particularly with regards to the different mutants. AKT activation levels remained low, and were seemingly unaffected by NRAS wild-type or mutant over-expression. This correlates with the

unchanged AKT levels in the transfected HEK293T cells. Indeed, Figure 5.7 also indicates a down-regulation of HRAS in the MOLM-13-NRAS-Q61K cell line, as was evident in the same cell line in the transcriptomic data. This also correlated with a decrease in KRAS in the same cell line. This was not, however, replicated in the G12C and G12D over-expression lines, with increased levels of HRAS and KRAS seen here. Overall Ras levels appeared to decrease, perhaps ultimately indicating that in this over-expression model, exogenous NRAS is able to outcompete the transcription and translation of other Ras isoforms, and indeed compensate for a reduction in the total Ras content, perhaps including other rarer isoforms not probed here. This would coincide with the decrease in *MRAS* levels seen in the MOLM-13-NRAS-Q61K transcriptomic data (Appendix 8). This is particularly evident in the mutant over-expressing cell lines. Interestingly, a similar pattern in total Ras levels was followed in the MOLM-13-DR cell line.

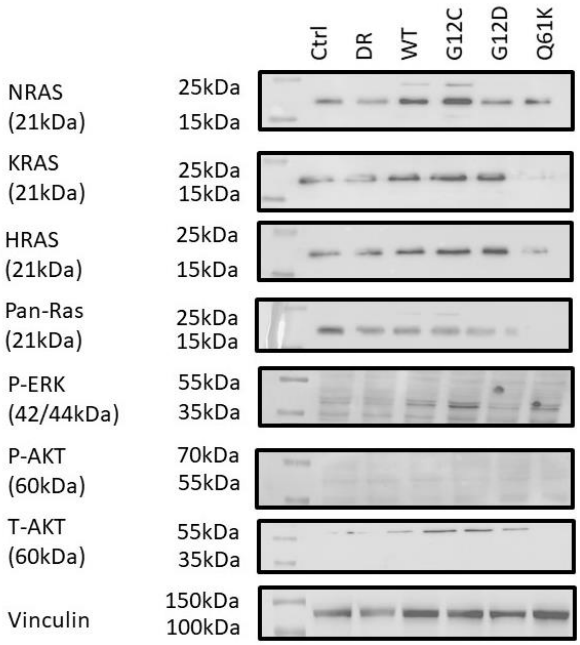

Figure 5.7. Protein level alterations in MOLM-13-NRAS over-expressing cells. Alterations in PI3K-AKT and MAPK pathway signalling in all over-expression cell lines, as well as key Ras isoform expression. Levels determined by Western blotting, with vinculin used as a loading control. Ctrl refers to cells non-transduced cells.

Changes to these signalling pathways, as well as the JAK-STAT pathway which is also implicated in AML, were assessed to a greater detail using transcriptomic sequencing and interrogated by KEGG pathway analysis (Section 5.6 and Appendix 8). This is detailed further in Appendix 8. To elucidate these alterations to a greater degree, the genes were stratified by up- and downregulation in each of the cell lines, with similarities shown using Venn diagrams (Appendix Figures 8.4-8.6). Briefly, as expected, from this data show distinct differences in the gene families that are altered between different NRAS-overexpressing cell lines, particularly within the MAPK and PI3K-AKT pathways. Over 150 genes in total were altered in both of these pathways between cell lines. This was expected, since both of these pathways are Ras-mediated. There was less of a difference seen between each cell line with respect to the JAK-STAT pathway, as expected since this is not a Ras-mediated pathway.

5.3.6 Detecting Transcriptomic Alterations

5.3.6.1 Quality Control of RNASeq Samples

To determine the impacts of NRAS over-expression at a gene level, the transcriptome was profiled using RNASeq, determined by the Illumina array chip. Prior to sequencing, sample quality was validated by separating 16S and 28S RNA using a denaturing (bleach) agarose gel, as well as validation of the Absorbance (A) 260/280 and A260/230 ratios being >2.0 for each sample sent. At least 42 million reads were carried out per sample by Novogene (Cambridge, UK). As a brief overview, gene expression was estimated using the Fragments Per Kilobase of transcript sequence per Millions base pairs sequenced (FPKM) method, which considers sequencing depth and gene length when counting the numbers of fragments read for the region of the genome corresponding to that gene. Analysis conducted by Novogene was performed

in R, with the Pearson's Correlation Coefficient used to determine significance. An adjusted *p* value was also provided, with the smaller the value representing a greater degree of significance in the differential expression of genes between the groups in question. This data has been taken forwards for analysis, either by Novogene or myself. For reference, figures produced by Novogene are referenced as such, indicated by inclusion of their logo.

5.3.7.2 Identification of Global Transcriptomic Profile Alterations

Transcriptomic analysis revealed considerable differences in the gene expression between the various cell lines tested. As can been seen in Figure 5.8, there were 8199 genes commonly expressed in all five cell lines tested, presumably critical to the survival and maintenance of the parental MOLM-13 cell line. It could be argued that of these 8199 genes however though, 7,363 were somewhat manipulated by NRAS over-expression itself, whether wild-type or mutated, since there were 836 genes with a unique expression signature in the MOLM-13 parental cell line only, as denoted by figure 5.6A. Over-expression of NRAS wild-type however changed the expression landscape considerably, with 1841 genes uniquely expressed in this cell line, compared to the other over-expression cell lines, as shown in the Venn diagram in figure 5.6B. It is apparent however that there is strong similarity in expressed genes between all of the NRAS forms which were over-expressed, as >8300 genes were found to be commonly expressed. Indeed, there was a strong similarity in gene expression between the NRAS G12C and G12D over-expressing cells, with over 1000 genes commonly expressed here. The greatest lack of similarity however was seen between two cell lines was between the NRAS WT and G12C, with only 87 commonly expressed genes. Indeed, there were <200 commonly expressed genes between all

of the mutants (but not the control cells), indicating that there may be a mutational site-specific difference in gene regulation. This concept has not been widely explored in the literature, in the context of AML. The gene regulation signatures differed considerably between cell lines, shown not only by the extent of gene up- and downregulation (as demonstrated in the volcano plots in Figure 5.9), but also with regards to the genes involved in AML pathogenesis, as well as other pathways. This will be further explored and validated throughout the remainder of this chapter.

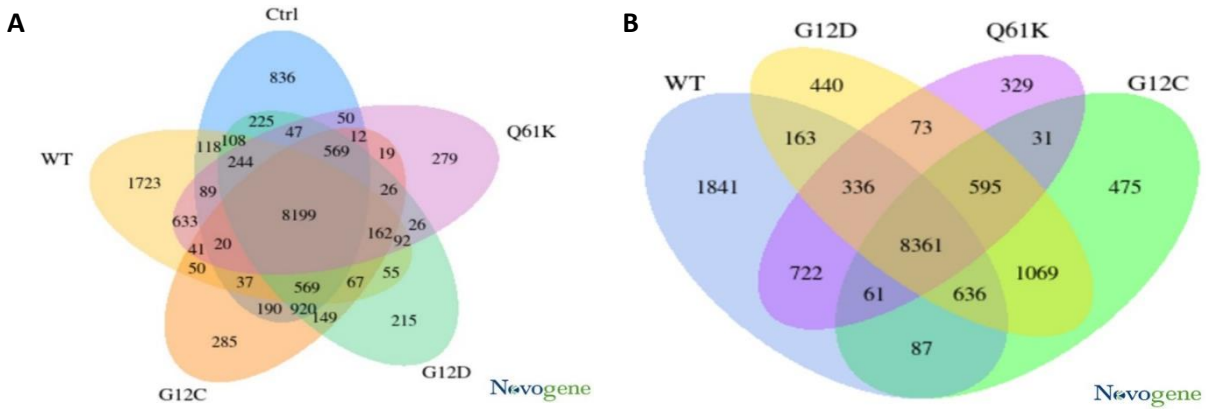

Figure 5.8. Overall differential gene expression in MOLM-13 NRAS-over-expressing cell lines. Numbers represent commonly expressed genes in each group identified, with those expressed in one group only also identified. **A)** All genes compared with the MOLM-13 parental cells. **B)** Expansion of Figure A highlighting commonalities and differences between cells over-expressing the three different NRAS mutants investigated, compared to the wild-type NRAS over-expressing cells.

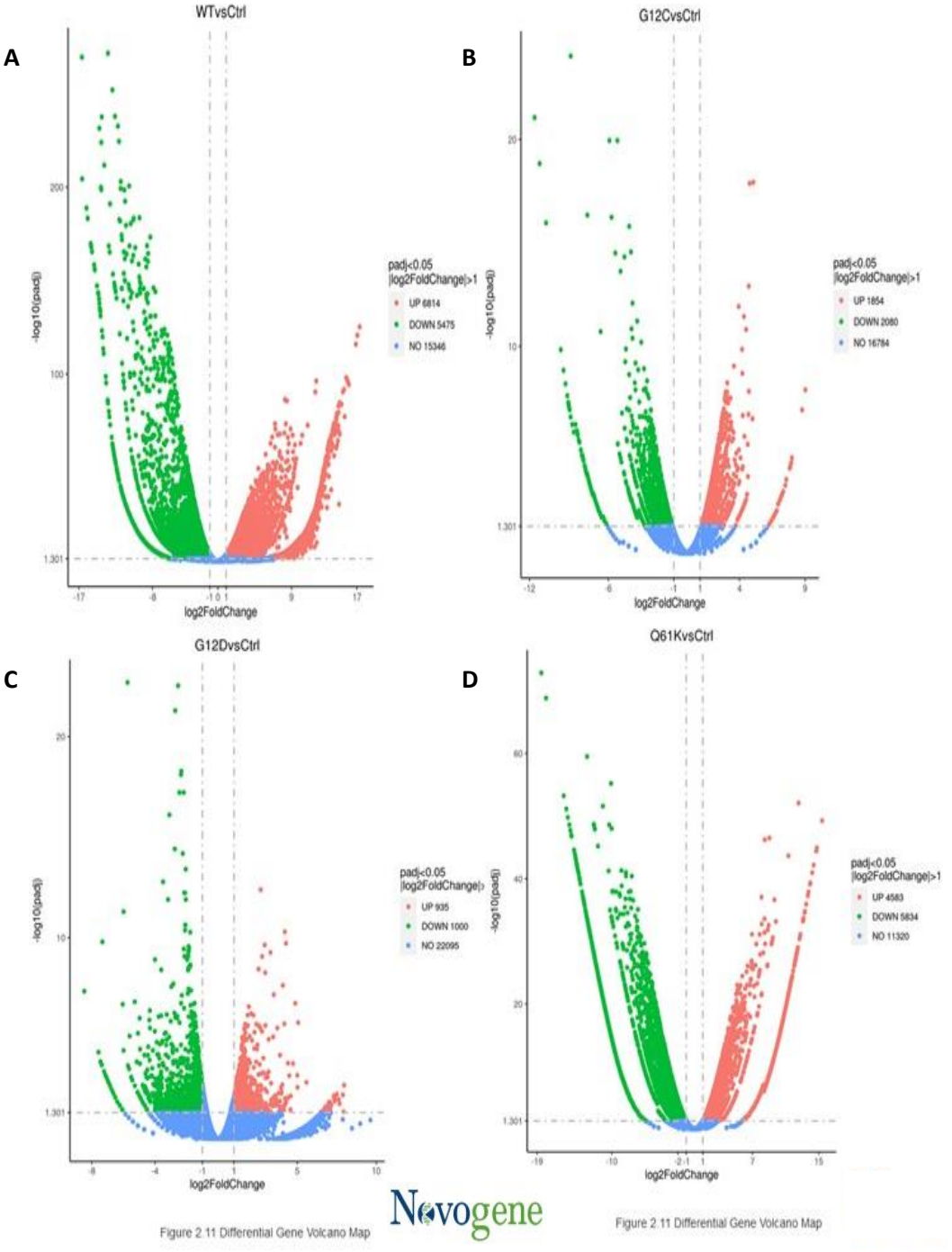

Figure 5.9. Distribution of up- and down-regulated genes in MOLM-13 NRAS over-expressing cell lines. Green indicates down-regulated genes, with red indicating up-regulated genes. Blue represents genes whose expression did not significantly change between the groups analysed. Data compared to MOLM-13 control cells.

5.3.6.3 Identification of AML Transcriptomic Profile Alterations

Transcriptomic profiles differ between diseases, and so gene alterations can be stratified by disease. Given the multi-faceted, heterogenous nature of AML, it is interesting to analyse the differences in leukaemogenic driver gene expression caused by over-expression of the different mutant over-expressing lines. In depth analysis of the transcriptomic data achieved by RNASeq illustrates the differences that these mutants can confer with regards to AML pathogenesis, and key signalling pathways regulating this. For example, over-expression of NRAS Q61K caused the upregulation of 21 genes which are identified as AML-associated by KEGG pathway analysis (Figure 5.10). This was coupled with the down-regulation of 17 genes. The NRAS G12C and G12D over-expressing MOLM-13 showed a more similar transcriptomic profile to the control cells with respect to the KEGG-determined AML profile, since only seven genes were upregulated in the G12C over-expressing cells, and six in the G12D over-expressing cells. This is coupled with six and three genes downregulated, respectively. With regards to over-expressing wild-type NRAS, there are several AML-related genes uniquely over-expressed, some of which are down-regulated in the mutant over-expressing cell lines, such as *KIT* and *TCF7L2*. In contrast, while *DUSP6* is downregulated in the NRAS wild-type over-expressing cell line, it is upregulated in each of the NRAS mutant over-expressing lines, relative to the controls.

Interestingly, *CEBPA* is the only gene which is upregulated in the MOLM-13-NRAS-G12D over-expressing cell line, and *RARA* is the only gene which is upregulated in the MOLM-13-NRAS-G12C over-expressing cell line. Indeed, these genes are downregulated in the NRAS wild-type over-expressing cell line. This implies, perhaps, a reliance on presence of these mutants with an increased expression of these well-

described leukaemogenic driver mutations to confer the leukaemic phenotype. This is in support of the literature, which will be further discussed in section 6.1. In contrast, while the *MYC* transcript level is increased only in the MOLM-13-NRAS-Q61K over-expressing cell line, it is only down-regulated in the MOLM-13-NRAS-G12C over-expressing line.

5.3.6.4 Identification of Most Altered Genes

Aside from the gene alterations within the 67 gene signature corresponding to the KEGG pathway AML profile, the most up and downregulated genes were also studied. It is important to elucidate these alternative genes, as a means of potentially elucidating actionable drug targets in the future. This ultimately may confer potential for treatment stratification, based on *NRAS* genotype. Table 5.2 indicates the top ten up- and downregulated genes in each MOLM-13-NRAS over-expressing cell line, compared to the control. Those related to cancer were selected here, as a means of identifying the most actionable targets.

A

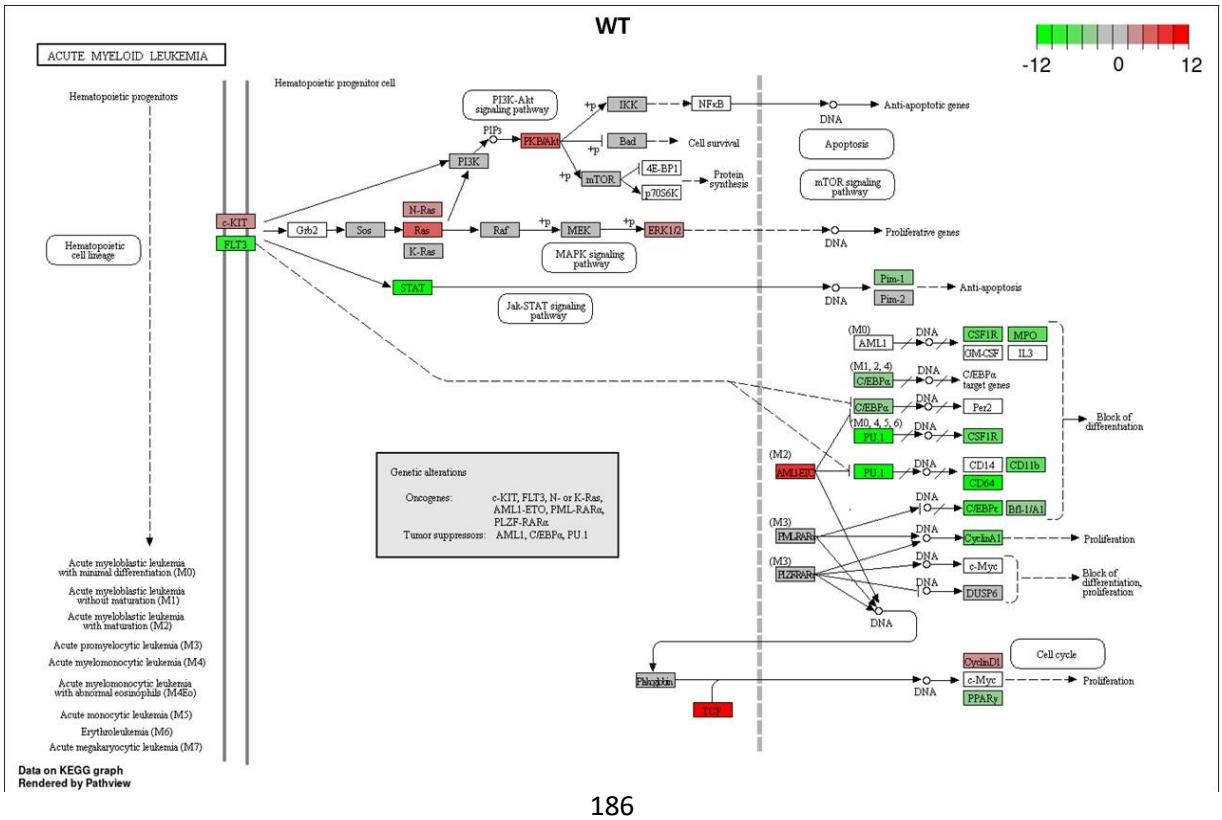

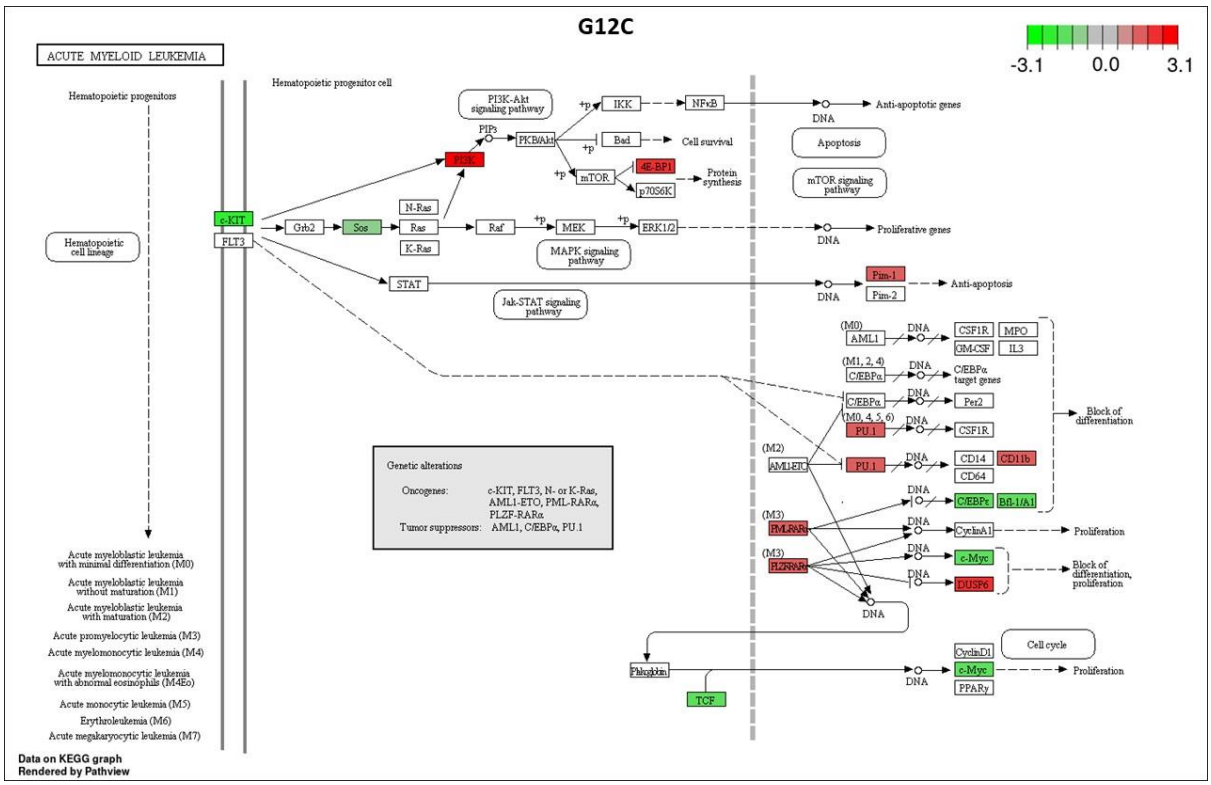
G12C
-3.1
0.0
3.1
ACUTE MYELOID LEUKEMIA
Hematopoietic progenitors
Hematopoietic progenitor cell
Hematopoietic cell lineage
c-KIT
FLT3
Grb2
Sos
Ras
N-Ras
K-Ras
Raf
MEK
ERK1/2
MAPK signaling pathway
PI3K-Akt signaling pathway
PI3K
PIPs
PKB/Akt
IKK
NFκB
Bad
Cell survival
mTOR
4E-BP1
p70S6K
Protein synthesis
Apoptosis
mTOR signaling pathway
Anti-apoptotic genes
Proliferative genes
STAT
Jak-STAT signaling pathway
Pim-1
Pim-2
Anti-apoptosis
DNA
(M0)
AML1
CSF1R
MPO
GM-CSF
IL3
(M1, 2, 4)
C/EBPα
C/EBPα target genes
Pu.1
Per2
(M0, 4, 5, 6)
(M2)
AML1-ETO
CD14
CD11b
CD64
C/EBPε
Bgl-1/A1
(M3)
PML-RARα
CyclinA1
Proliferation
PLZF-RARα
c-Myc
DUSP6
Block of differentiation
Block of differentiation, proliferation
Genetic alterations
Oncogenes: c-KIT, FLT3, N- or K-Ras, AML1-ETO, PML-RARα, PLZF-RARα
Tumor suppressors: AML1, C/EBPα, Pu.1
Acute myeloblastic leukemia with minimal differentiation (M0)
Acute myeloblastic leukemia without maturation (M1)
Acute myeloblastic leukemia with maturation (M2)
Acute promyelocytic leukemia (M3)
Acute myelomonocytic leukemia (M4)
Acute myelomonocytic leukemia with abnormal eosinophils (M4Eo)
Acute monocytic leukemia (M5)
Erythroleukemia (M6)
Acute megakaryocytic leukemia (M7)
Data on KEGG graph
Rendered by Pathview
β-catenin
TCF
CyclinD1
Cell cycle
PPARγ

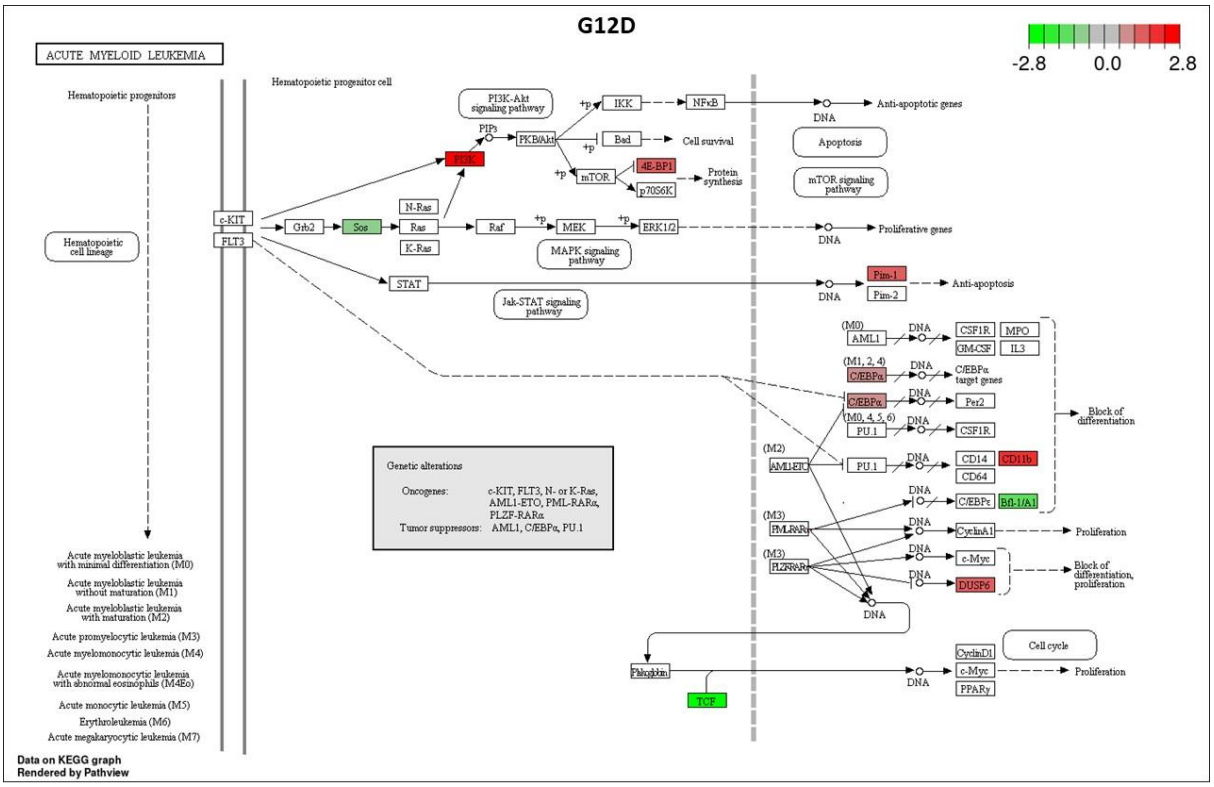
G12D
-2.8
0.0
2.8
ACUTE MYELOID LEUKEMIA
Hematopoietic progenitors
Hematopoietic progenitor cell
Hematopoietic cell lineage
c-KIT
FLT3
Grb2
Sos
Ras
N-Ras
K-Ras
Raf
MEK
ERK1/2
MAPK signaling pathway
PI3K-Akt signaling pathway
PI3K
PIPs
PKB/Akt
IKK
NFκB
Bad
Cell survival
mTOR
4E-BP1
p70S6K
Protein synthesis
Apoptosis
mTOR signaling pathway
Anti-apoptotic genes
Proliferative genes
STAT
Jak-STAT signaling pathway
Pim-1
Pim-2
Anti-apoptosis
DNA
(M0)
AML1
CSF1R
MPO
GM-CSF
IL3
(M1, 2, 4)
C/EBPα
C/EBPα target genes
Pu.1
Per2
(M0, 4, 5, 6)
(M2)
AML1-ETO
CD14
CD11b
CD64
C/EBPε
Bgl-1/A1
(M3)
PML-RARα
CyclinA1
Proliferation
PLZF-RARα
c-Myc
DUSP6
Block of differentiation
Block of differentiation, proliferation
Genetic alterations
Oncogenes: c-KIT, FLT3, N- or K-Ras, AML1-ETO, PML-RARα, PLZF-RARα
Tumor suppressors: AML1, C/EBPα, Pu.1
Acute myeloblastic leukemia with minimal differentiation (M0)
Acute myeloblastic leukemia without maturation (M1)
Acute myeloblastic leukemia with maturation (M2)
Acute promyelocytic leukemia (M3)
Acute myelomonocytic leukemia (M4)
Acute myelomonocytic leukemia with abnormal eosinophils (M4Eo)
Acute monocytic leukemia (M5)
Erythroleukemia (M6)
Acute megakaryocytic leukemia (M7)
Data on KEGG graph
Rendered by Pathview
β-catenin
TCF
CyclinD1
Cell cycle
PPARγ

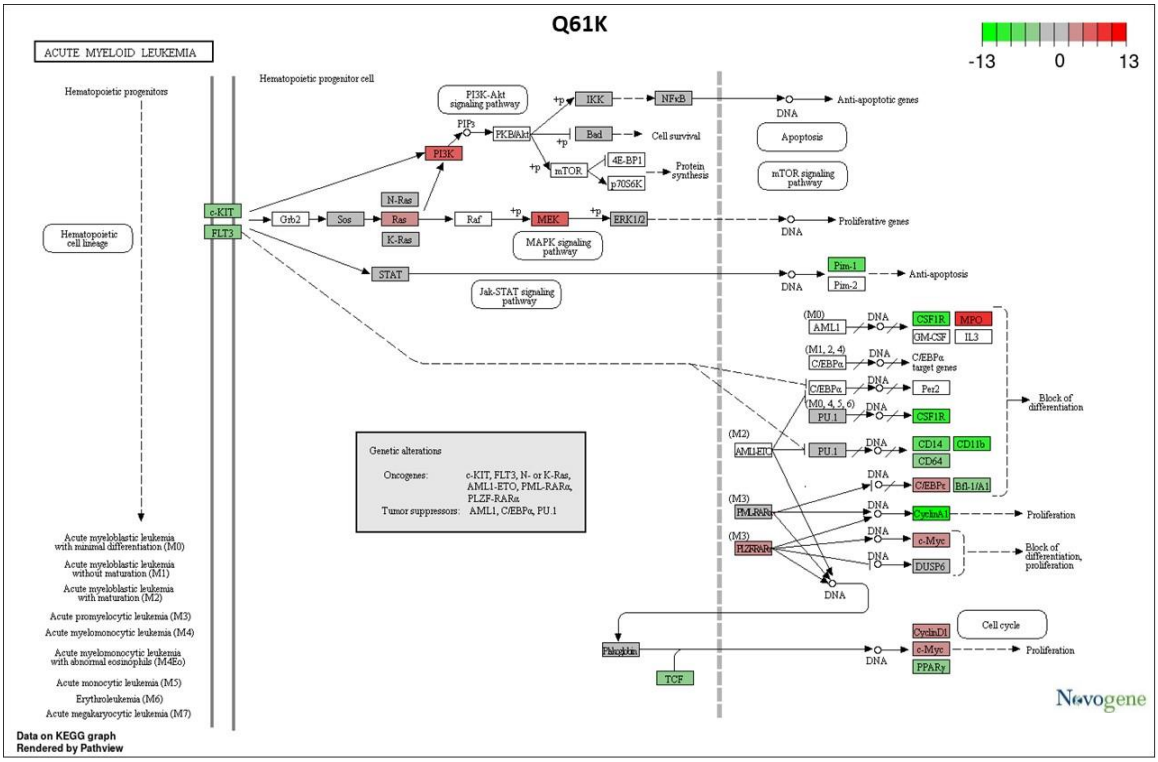

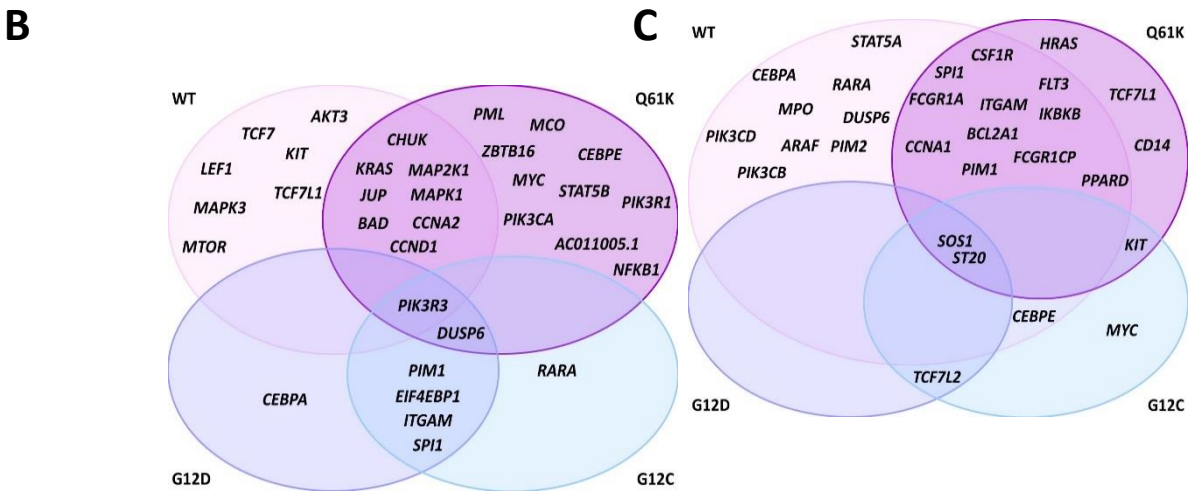

Figure 5.10. Dysregulated genes associated with AML in MOLM-13 NRAS-over-expressing cell lines. AML-associated genes determined by KEGG pathway analysis. **A)** Global overview of AML-related pathways with changes occurring in each cell line. **B)** Upregulated genes in each cell line, showing cross-over between each cell line. **C)** Downregulated genes in each cell line, showing cross-over between each cell line.

As can be seen in Table 5.2, there are certain commonly up-regulated and down-regulated genes between each of the groups studied. These are: *BCL9, CD74,*

TNFRSF14, CRLF2, FCGR2B, HMGA2, HOXD13, FLT4 and CDKN2A. As per the PANTHER Classification System searched using the Gene Ontology Resource database, all of these genes are involved in the regulation of production of molecular mediators of immune response, and the regulation of metabolic processes. 8 of these 9 genes are involved in the regulation of cell population proliferation (*FLT4, CRLF2, HMGA2, CD74, HOXD13, FCGR2B, CDKN2A* and *TNFRS14*). Many are involved in the signal transduction and cell communication (all but *HOXD13*). This is highly as expected, given that NRAS and its mutants are well-understood to be tumorigenic drivers, and critically involved in cell proliferation. This data also supports the phenotype shown in Figure 5.2. Indeed, 5 of these 9 commonly over-expressed genes (*CRLF2, CD74, FCGR2B, CDKN2A* and *TNFSRF14*) are all involved in the regulation of (B) cell activation, which is plausible for maintaining a malignant haematopoietic cell phenotype. Interestingly however, *CD74, FCGR2B* and *CDKN2A* are considered

negative regulators of haematopoiesis. The haematopoietic signature will be further assessed in section 5.3.6.6.

Table 5.2. Most altered cancer-associated gene expression in each over-expression cell line, compared to control cells. Top 10 genes of each group shown here, both up (↑) and down (↓) regulated.

WT↑	*WT↓*	*G12C↑*	*G12C↓*	*G12D↑*	*G12D↓*	*Q61K↑*	*Q61K↓*
CDKN2A	*P2RY8*	*CDKN2A*	*MUTYH*	*BCL9*	*FGFR4*	*HMGA2*	*HOXA9*
HEY1	*CSF3R*	*HEY1*	*ASPSCR1*	*ROS1*	*SEPTIN5*	*HOXD13*	*HLA-A*
FLT4	*FCGR2B*	*FLT4*	*SDHAF2*	*CIITA*	*TNFRSF14*	*FLT4*	*FCGR2B*
HOXD13	*FANCF*	*HOXD13*	*MRTFA*	*JAZF1*	*CRLF2*	*CDKN2A*	*CD74*
HMGA2	*PTPRC*	*HMGA2*	*ERCC2*	*MYCL*	*TCF7L2*	*BCL9*	*AFF3*
PBX1	*LYL1*	*PBX1*	*MYD88*	*CD74*	*ALDH2*	*PAX5*	*GPC3*
MAF	*TNFRSF14*	*MAF*	*FBXW7*	*IL21R*	*ATP2B3*	*HOXD11*	*ARHGEF12*
SMO	*CD74*	*SMO*	*CDKN2C*	*U2AF1*	*NTRK3*	*NFIB*	*ZNF521*
LIFR	*MLH1*	*LIFR*	*GOPC*	*IL7R*	*TSHR*	*LHFPL6*	*JAK3*
MET	*FLT3*	*MET*	*FSTL3*	*HIST1H4I*	*NR4A3*	*LRIG3*	*CRLF2*

A selection of genes occurring in two or more columns of Table 5.2 were used to validate the transcriptomic data in our laboratory, using qPCR. Primers were designed accordingly, and are listed in Table 5.3. These genes were seen to be most beneficial in validating the data since they would produce the most obvious changes by qPCR, which is a less sensitive technique than the original RNA sequencing. Other validation methods will also be explored in later stages of this chapter. As can be determined

from Figure 5.11, a similar pattern of significant gene up- and downregulation was seen by qPCR and RNASeq, as expected.

Table 5.3. Primer sequences used to amplify common genes with modulated expression in at least two over-expression cell lines.

Primer Name	Sequence (5'-3')	T_M (°C)
BCL9_qPCR_F	GGG AAA GGA CCC ACT TCC AC	67.3
BCL9_qPCR_R	CTT GCA GTC ACA AAC GGG AC	65.3
CD74_qPCR_F	TTG GAG CAA AAG CCC ACT GA	63.2
CD74_qPCR_R	GAG TGG CAG ATA GTT GCC GT	65.3
FLT4_qPCR_F	GAC TGT GGC TCT GCC TGG	65.5
FLT4_qPCR_R	GGT GTC GAT GAC GTG TGA CT	65.3
CDKN2A_qPCR_F	GGG TCG GGT AGA GGA GGT G	68.9
CDKN2A_qPCR_R	GCT GCC CAT CAT CAT GAC CT	65.3
qPCR_GAPDH_F	CCA CTT TGT CAA GCT CAT TTC C	64.3
qPCR_GAPDH_R	TCT CTT CCT CTT GTG CTC TTG	64.0

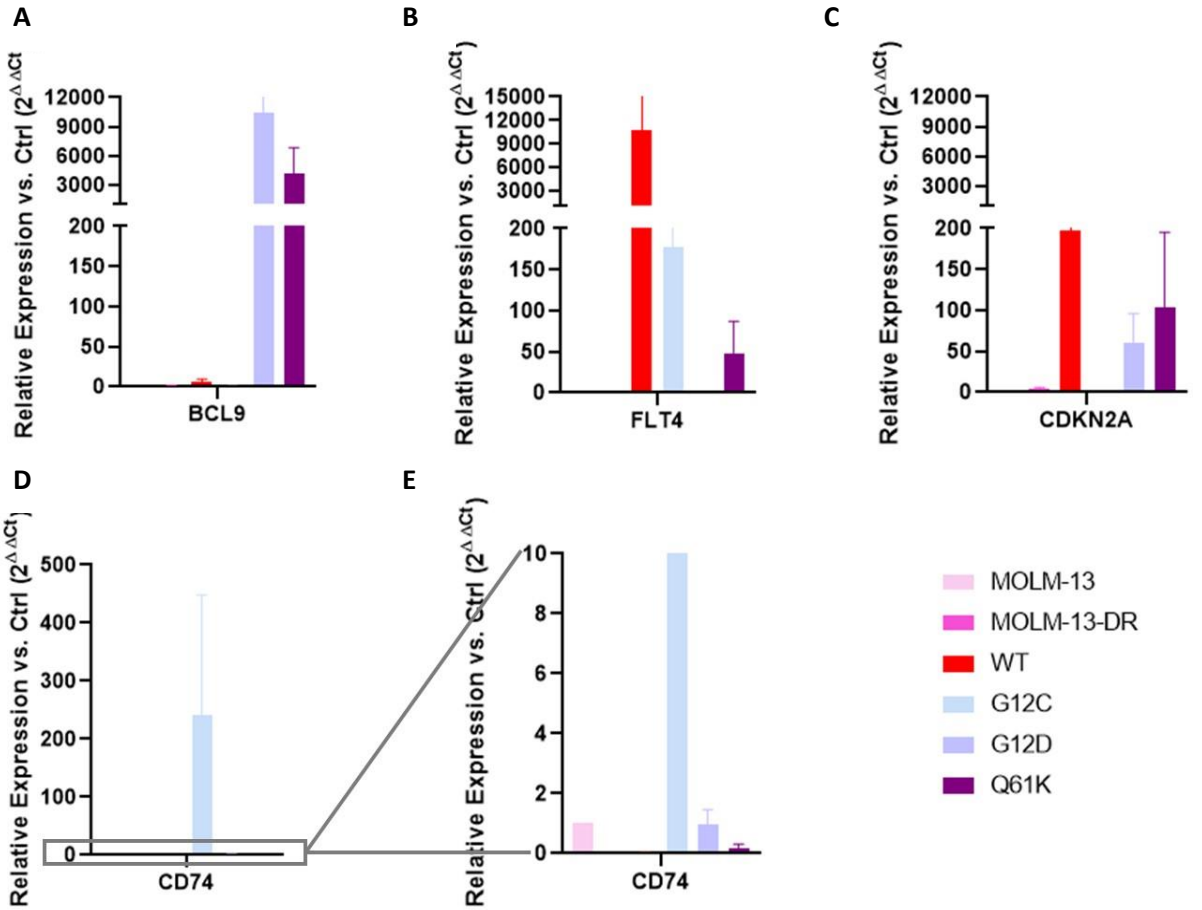

Figure 5.11. Quantitative PCR validation of up- and downregulated genes identified by RNASeq. **A)** *BCL9* **B)** *FLT4* **C)** *CDKNA2* **D)** *CD74* **E)** Expanded version of lowest values of *CD74* cDNA levels, identifying the under-expression of *CD74* in MOLM-13-NRAS-Q61K, relative to MOLM-13 control. Genes were validated were MOLM-13 WT, G12C, G12D and Q61K over-expressing cell lines, relative to MOLM-13 control, which was normalised to 1, following analysis using the ΔΔCt method. *GAPDH* was used as a housekeeping gene control. MOLM-13-DR expression levels also shown here where scale-appropriate for comparison. Data represents N=3 biological replicates (different subclones of over-expressing cell lines) +/- SEM.

5.3.6.5 Identification of Altered Pathways by Transcriptomics

Broadly speaking, there is a considerable variety in the genes which are up- and down-regulated between the different over-expressing groups examined. This correlates with the variation in biological processes, cellular components and molecular functions

described in Figure 5.12, and further supports the hypothesis that different mutants give rise to differences in leukaemic signalling and perhaps drug sensitivity.

Differences in the regulation of biological processes, cellular component generation and molecular function were analysed through Gene Ontology Mapping, with the top 10 most-affected of these classifications illustrated in Figure 5.10. It is evident that the different mutants all confer differing regulation of different processes, with a considerable variation of altered processes between each over-expressing line, when compared to the control.

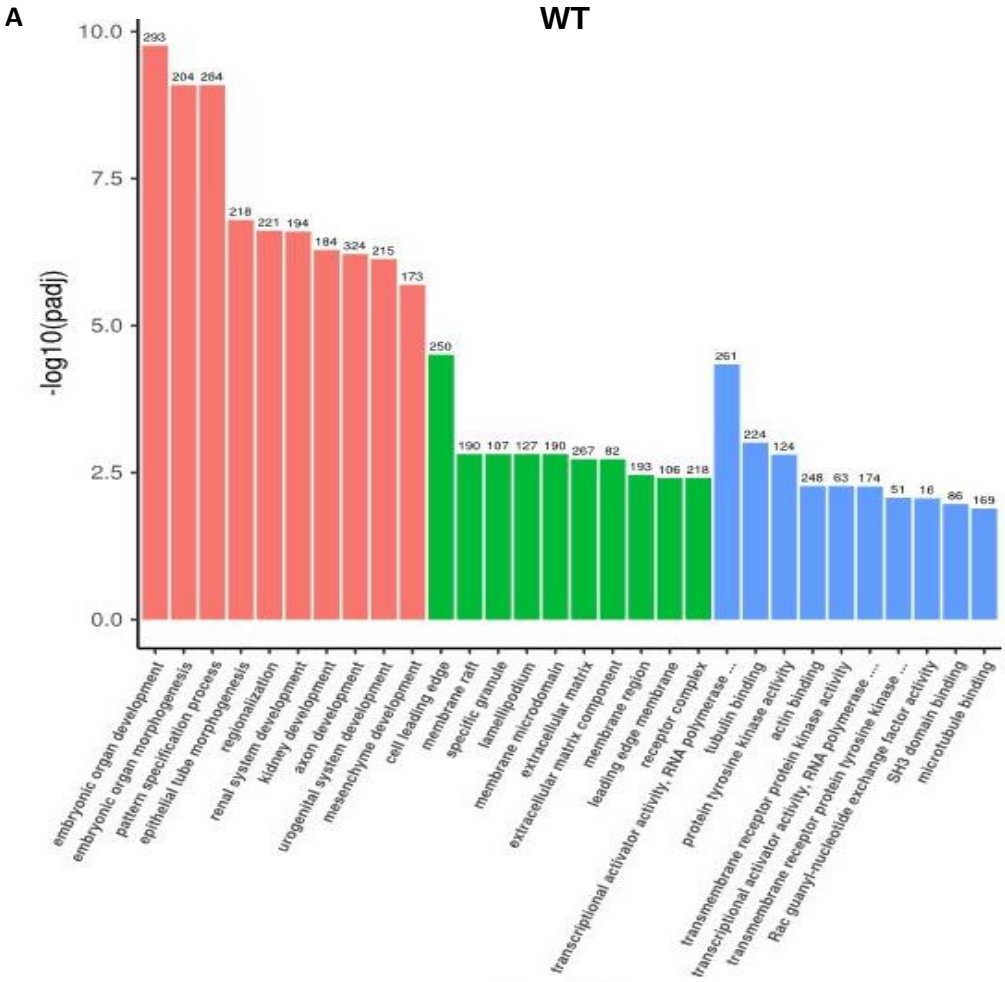

B

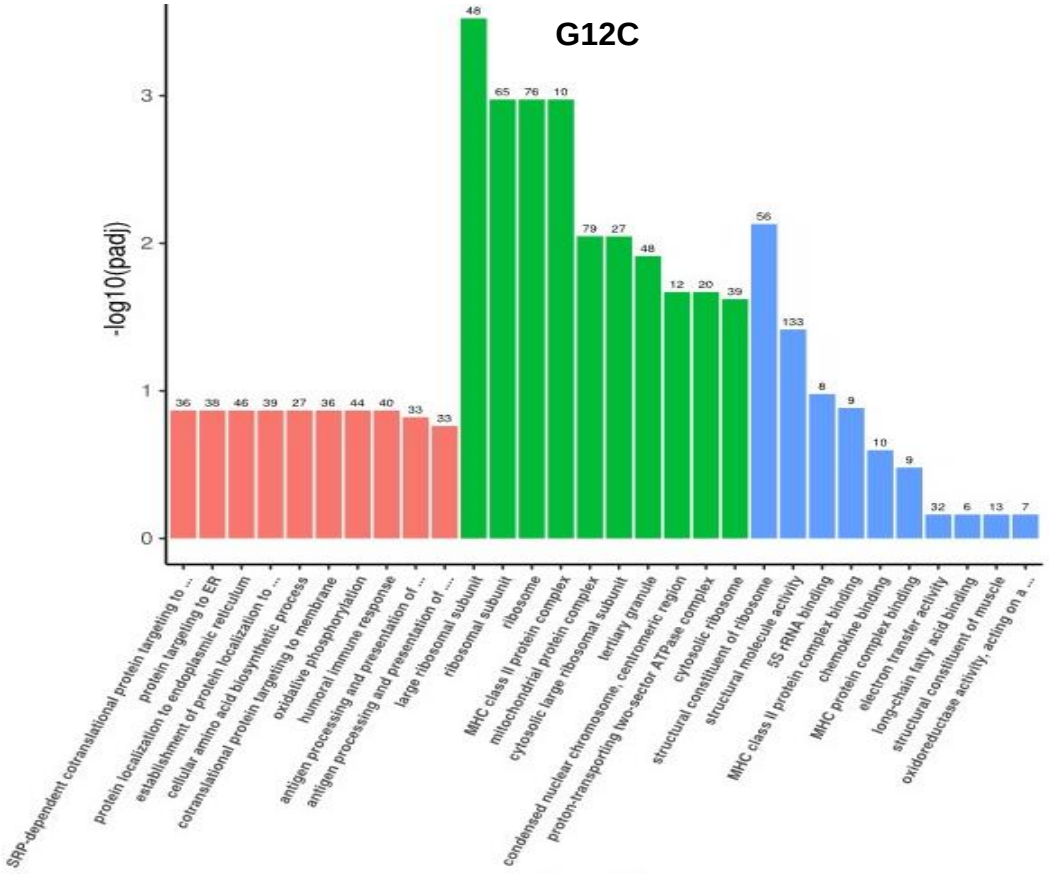
G12C
-log10(padj)
0
1
2
3
36 38 46 39 27 36 44 40 33 33 48 65 76 10 79 27 48 12 20 39 56 133 8 9 10 9 32 6 13 7
SRP-dependent cotranslational protein targeting to ...
protein targeting to ER
protein localization to endoplasmic reticulum
establishment of protein localization to ...
cellular amino acid biosynthetic process
cotranslational protein targeting to membrane
oxidative phosphorylation
humoral immune response
antigen processing and presentation of ...
antigen processing and presentation of ...
large ribosomal subunit
ribosomal subunit
ribosome
MHC class II protein complex
mitochondrial protein complex
cytosolic large ribosomal subunit
tertiary granule
condensed nuclear chromosome, centromeric region
proton-transporting two-sector ATPase complex
cytosolic ribosome
structural constituent of ribosome
structural molecule activity
5S rRNA binding
MHC class II protein complex binding
chemokine binding
MHC protein complex binding
electron transfer activity
long-chain fatty acid binding
structural constituent of muscle
oxidoreductase activity, acting on a ...

C

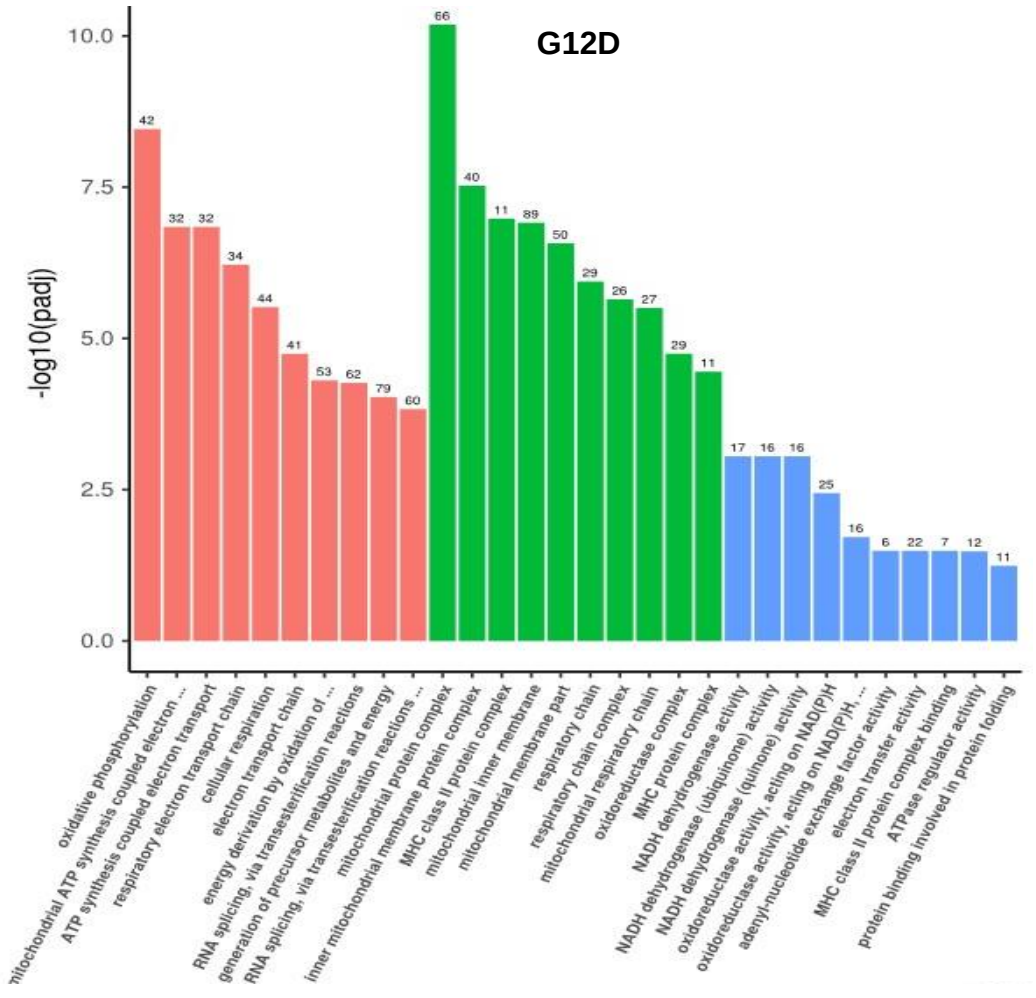
G12D
-log10(padj)
0.0
2.5
5.0
7.5
10.0
42 32 32 34 44 41 53 62 79 60 66 40 11 89 50 29 26 27 29 11 17 16 16 25 16 6 22 7 12 11
oxidative phosphorylation
mitochondrial ATP synthesis coupled electron ...
ATP synthesis coupled electron transport
respiratory electron transport chain
cellular respiration
electron transport chain
energy derivation by oxidation of ...
RNA splicing, via transesterification reactions
generation of precursor metabolites and energy
RNA splicing, via transesterification reactions ...
inner mitochondrial membrane protein complex
mitochondrial membrane protein complex
MHC class II protein complex
mitochondrial protein complex
mitochondrial inner membrane
mitochondrial membrane part
respiratory chain
respiratory chain complex
mitochondrial respiratory chain
oxidoreductase complex
MHC protein complex
NADH dehydrogenase activity
NADH dehydrogenase (ubiquinone) activity
NADH dehydrogenase (quinone) activity
oxidoreductase activity, acting on NAD(P)H
oxidoreductase activity, acting on NAD(P)H, ...
adenyl-nucleotide exchange factor activity
electron transfer activity
MHC class II protein complex binding
ATPase regulator activity
protein binding involved in protein folding

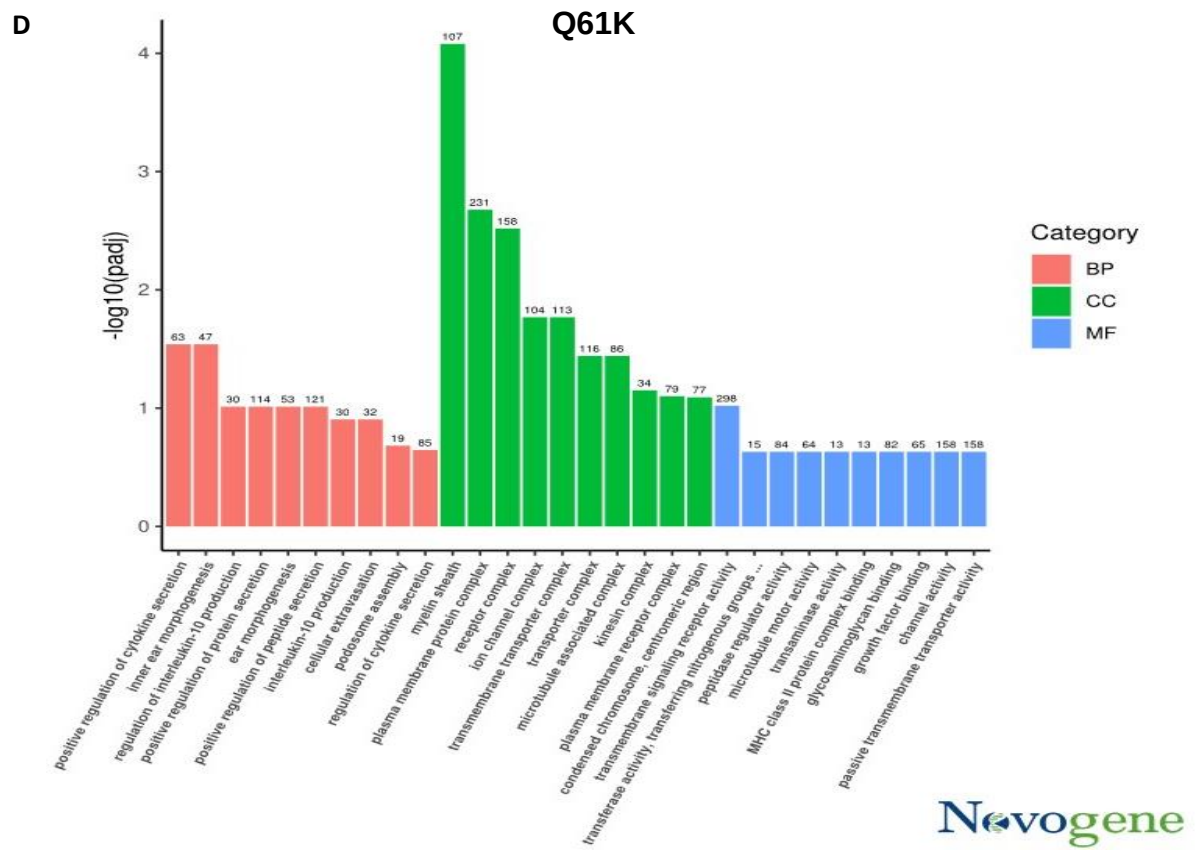

Figure 5.12. Key cellular features and pathways most altered in NRAS-over-expressing cell lines, compared to parental MOLM-13 cells. Top 10 altered pathways (as determined by p(adj) value) listed for each group here. **A)** NRAS-WT **B)** NRAS-G12C **C)** NRAS-G12D **D)** NRAS Q61K. Red bars denote differences in biological processes (BP), green bars denote alterations in cellular component production (CC), and blue bars represent differences in molecular functions (MF).

Figure 5.12A, comparing MOLM-13-NRAS WT to parental MOLM-13 cells, clearly illustrates the necessity of NRAS in development, with both embryogenesis and an array of organ-specific development processes being most altered within these cells. Localisation also seems to be implicated with this over-expression, which is perhaps unsurprising given the importance for specific Ras localisation within the cell to permit sufficient signalling (as discussed in section 1.4.2).

Figure 5.12B shows a different picture for the implication of NRAS G12C over-expression, compared to what was seen with NRAS wild-type over-expression. Rather than impacting development, it seems NRAS G12C is far more implicated with a host of intracellular localisation processes, which, again, is critical in the oncogenic Ras signalling associated with this G12C mutant. However, it remains to be elucidated yet which proteins are mis-localised, which may be explored as pharmacological targets in conjunction with the novel Ras-G12C inhibitors. It is essential that Ras is trafficked to the cell membrane to elicit its effects. This feature has already been explored pharmacologically, using farnesyltransferase inhibitors, albeit unsuccessfully. Ras localisation was somewhat explored in Appendix 10.

In contrast, NRAS-G12D over-expression shows a markedly different biological processes signature, with a strong involvement in cellular respiration, such as through the regulation of oxidative phosphorylation. Aside from cellular respiration-related biological processes, this transcriptomic analysis has also revealed increased expression of genes encoding cellular components of the mitochondria, its respiratory chain and the oxidoreductase complex (Appendix 10). It is well known that the pro-survival nature of cancer cells, including AML, relies on the detoxification of oxidative phosphorylation by-products, such as through the anti-oxidant NRF2/Keap1 axis (Rushworth, Zaitseva, Murray, Shah, Bowles & MacEwan, 2012). It may be that the NRAS G12D-mutant signature contributes to or relies on this dysregulation of oxidative phosphorylation.

Finally, as shown in Figure 5.12D, over-expression of NRAS Q61K seems to affect the secretome of the cell, with alterations in the secretion of cytokines and peptides some

of the most affected biological processes. This is coupled with alterations in the expression of receptor and transporter complexes, both at the plasma membrane (e.g. receptors and ion channels), as well as intracellularly, such as microtubule organisation. This could be associated with the fact that Q61K is known to be less 'transforming' (perhaps considered less oncogenic), however the alterations in receptors may explain the drug-resistance patterns seen in the MOLM-13-NRAS-Q61K over-expressing cells, since drug influx or efflux could be negatively manipulated in this way.

Overall, figure 5.12 strongly suggests a considerable difference in the effects of the different NRAS mutants on cell signalling, and perhaps function. This in turn in part explains the differences in cell phenotype, both in terms of their intrinsic phenotypes, and the differing drug sensitivity witnessed too. In the remainder of this chapter, the haematopoietic signature will be discussed. However, transcriptomic data based on alternative key pathways relating to AML can also be found in Appendix 8.

5.3.6.6 NRAS-mediated Haematopoietic Alterations

As demonstrated in Table 5.2, *FLT3* is downregulated in NRAS-WT over-expressing cells. As detailed in section 1.1, it is known that FLT3 is essential in haematopoiesis, for differentiation into a myeloid phenotype. Given that there is a down-regulation of FLT3 in the NRAS-WT over-expressing MOLM-13, as well as an upregulation of genes encoding development (*SMO, FLT4, HMGA2, PBX1, CDKN2A, HEY1* and *MAF)*, it could be that NRAS-WT over-expression forces cells to revert back to a more undifferentiated, stem-like state. This correlates with a significant increase in *CD34* and *ITGA3* expression also seen in this transcriptomic analysis. CD34 is a well

characterised marker of the HSC, with ITGA3 also considered a marker of the Long-Term Haematopoietic Stem Cell (LT-HSC) (Rix, Maduro, Bridge & Grey, 2022; Tomellini et al., 2019). Interestingly, this significant increase in *CD34* and *ITGA3* expression was only seen when NRAS wild-type was over-expressed, not any of the three mutants examined here.

It is therefore apparent that NRAS could be involved with haematopoietic cell development and the regulation of haematopoiesis. A global analysis of the 139 genes outlined in the KEGG pathway analysis as being associated with haematopoiesis illustrates a markedly different signature between the NRAS-WT over-expressing MOLM-13, compared to the MOLM-13 control cell line, and the mutant over-expressing line. Nevertheless, the MOLM-13-NRAS-Q61K over-expressing cells did also show some level of this altered signature, as is shown by the heatmap in Figure 5.13A. This is accompanied by changes in the 95 gene signature associated with signalling in pluripotent stem cells (as determined by the KEGG pathway), also detailed in Figure 5.13B. Here, the stemness-associated genes are considerably up-regulated in the NRAS-WT over-expressing cells, compared to all other cell lines analysed in this manner. This could suggest perhaps that NRAS-WT over-expression enforces a more pluripotent stem cell state, with an inhibition of typical haematopoiesis along the myeloid lineage.

The elements of these pathways that were altered were analysed in greater detail using KEGG pathway analysis. Figure 5.14 indicates there is a far more altered

haematopoietic signature in the NRAS wild-type over-expressing line when compared to the G12C, G12D or Q61K over-expressing cells.

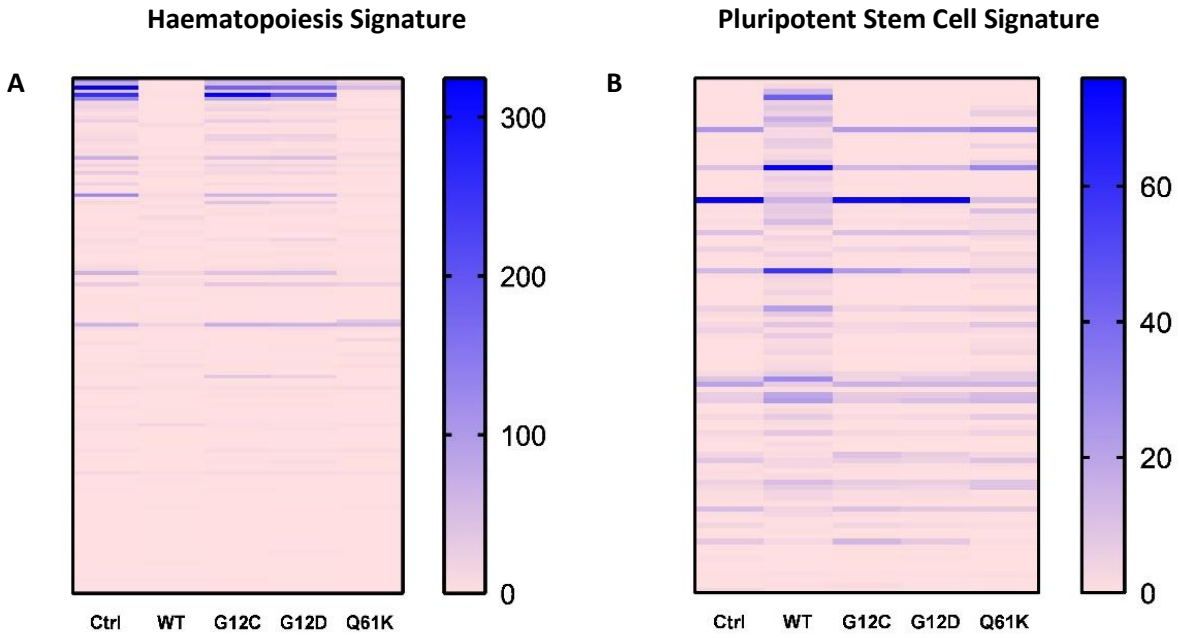

Figure 5.13. Analysis of the haematopoiesis and stemness associated pathways within MOLM-13-NRAS over-expressing cells. A) Genes associated by KEGG pathway analysis with haematopoiesis. **B)** Genes associated by KEGG pathway analysis with pluripotent stem cells. Heat maps constructed using mean FPKM values, in GraphPad Prism 8.0. Genes are arranged by the highest level of association with the particular pathway in question to the lowest.

Four out of six genes implicated in the HSC are modulated in the MOLM-13-NRAS-WT cell line: three upregulated, and one (*CD135*, also referred to as *FLT3*) downregulated. As evident in the lower part of Figure 5.12A, there is a downregulation of several myeloid lineage-associated genes, including *CD11b, CD123* and *CD35.* These elements support the suggestion of the reversal to and subsequent maintenance of MOLM-13-NRAS-WT in a stemness state.

However, the mapping does also indicate a decrease in several lymphoid-associated markers, in the MOLM-13-NRAS-Q61K cells. Whilst the MOLM-13-NRAS-Q61K cells

do also downregulate several myeloid lineage markers in a similar fashion to the MOLM-13-NRAS-WT cells, there is almost equal downregulation of lymphoid lineage markers, as well as a lack of alteration in HSC markers. This presents a different phenotype again, perhaps suggesting no particular overall effect on cell type and its driving of differential phenotypes, yet a larger impact on individual biological processes (as discussed in Section 5.3.6.5).

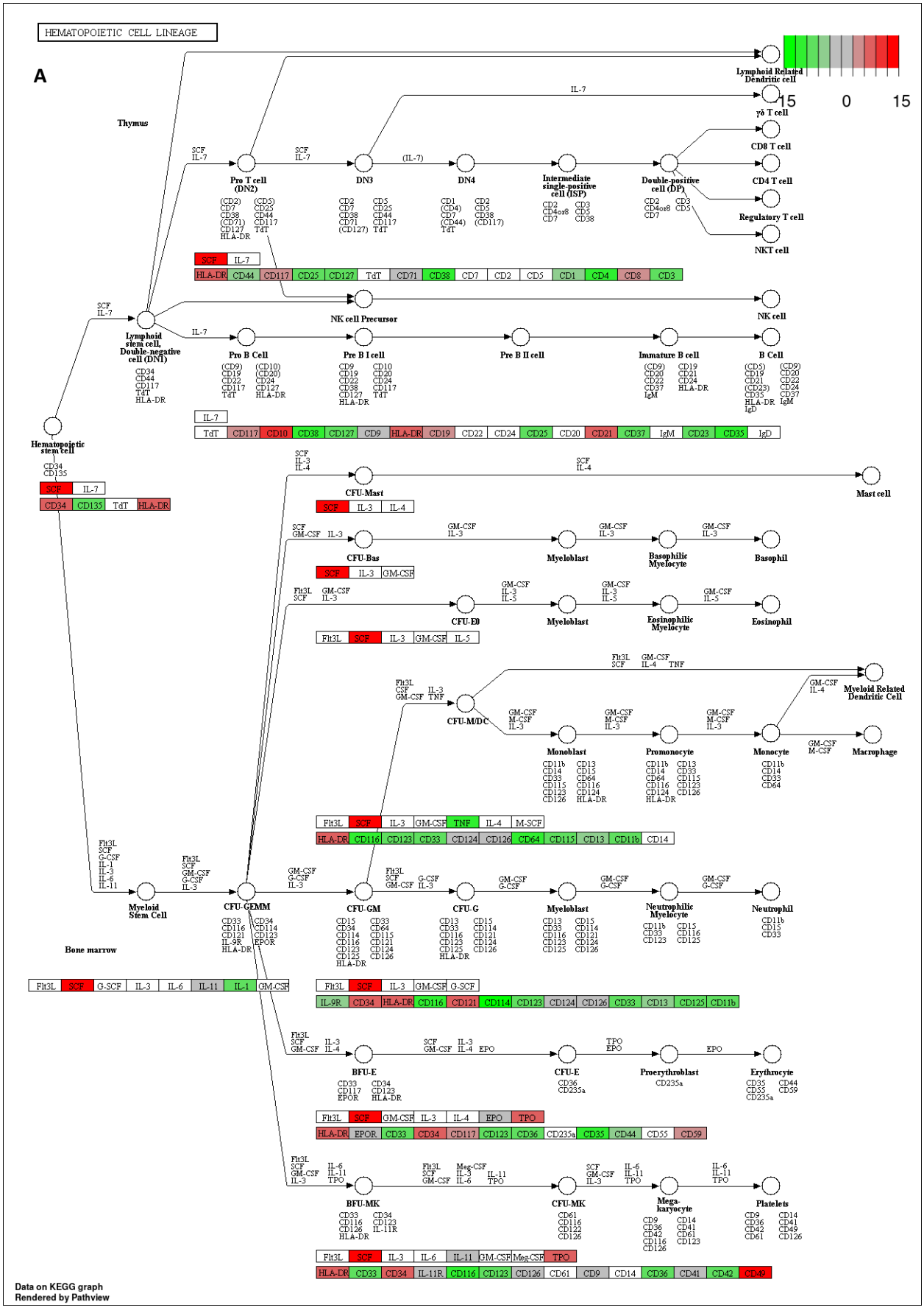
HEMATOPOIETIC CELL LINEAGE
A
15
0
15
Lymphoid Related Dendritic cell
γδ T cell
CD8 T cell
CD4 T cell
Regulatory T cell
NKT cell
Thymus
Pro T cell (DN2)
DN3
DN4
Intermediate single-positive cell (ISP)
Double-positive cell (DP)
NK cell Precursor
NK cell
Lymphoid stem cell, Double-negative cell (DN1)
Pro B Cell
Pre B I cell
Pre B II cell
Immature B cell
B Cell
Hematopoietic stem cell
CFU-Mast
Mast cell
CFU-Bas
Myeloblast
Basophilic Myelocyte
Basophil
CFU-Eo
Eosinophilic Myelocyte
Eosinophil
CFU-M/DC
Myeloid Related Dendritic Cell
Monoblast
Promonocyte
Monocyte
Macrophage
Myeloid Stem Cell
CFU-GEMM
CFU-GM
CFU-G
Neutrophilic Myelocyte
Neutrophil
Bone marrow
BFU-E
CFU-E
Proerythroblast
Erythrocyte
BFU-MK
CFU-MK
Mega-karyocyte
Platelets
Data on KEGG graph
Rendered by Pathview

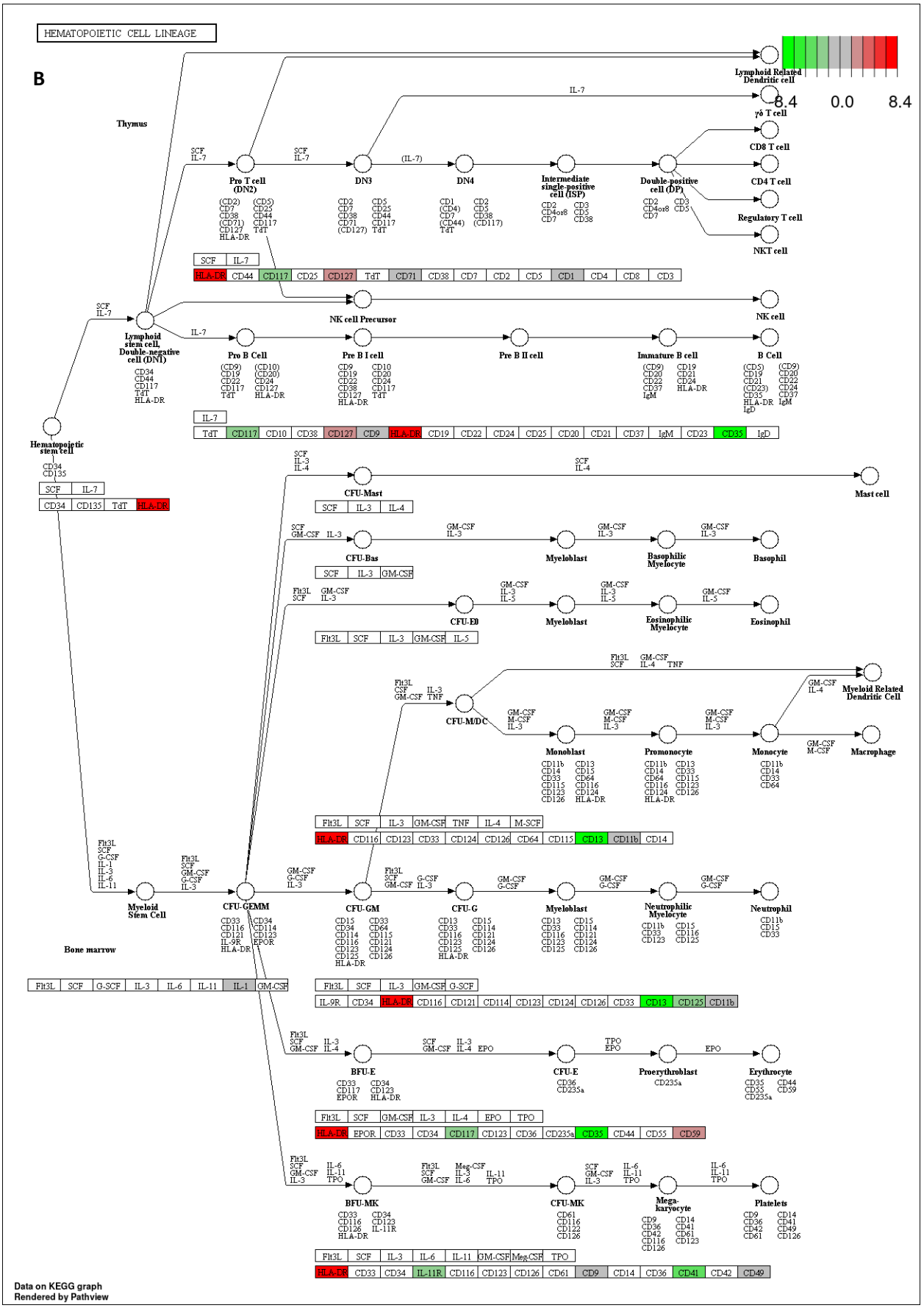
HEMATOPOIETIC CELL LINEAGE
B
-8.4
0.0
8.4
Lymphoid Related Dendritic cell
Thymus
γδ T cell
CD8 T cell
CD4 T cell
Regulatory T cell
NKT cell
Pro T cell (DN2)
DN3
DN4
Intermediate single-positive cell (ISP)
Double-positive cell (DP)
NK cell Precursor
NK cell
Lymphoid stem cell, Double-negative cell (DN1)
Pro B Cell
Pre B I cell
Pre B II cell
Immature B cell
B Cell
Hematopoietic stem cell
CFU-Mast
Mast cell
CFU-Bas
Myeloblast
Basophilic Myelocyte
Basophil
CFU-Eo
Eosinophilic Myelocyte
Eosinophil
CFU-M/DC
Myeloid Related Dendritic Cell
Monoblast
Promonocyte
Monocyte
Macrophage
Myeloid Stem Cell
CFU-GEMM
CFU-GM
CFU-G
Neutrophilic Myelocyte
Neutrophil
Bone marrow
BFU-E
CFU-E
Proerythroblast
Erythrocyte
BFU-MK
CFU-MK
Mega-karyocyte
Platelets
Data on KEGG graph
Rendered by Pathview

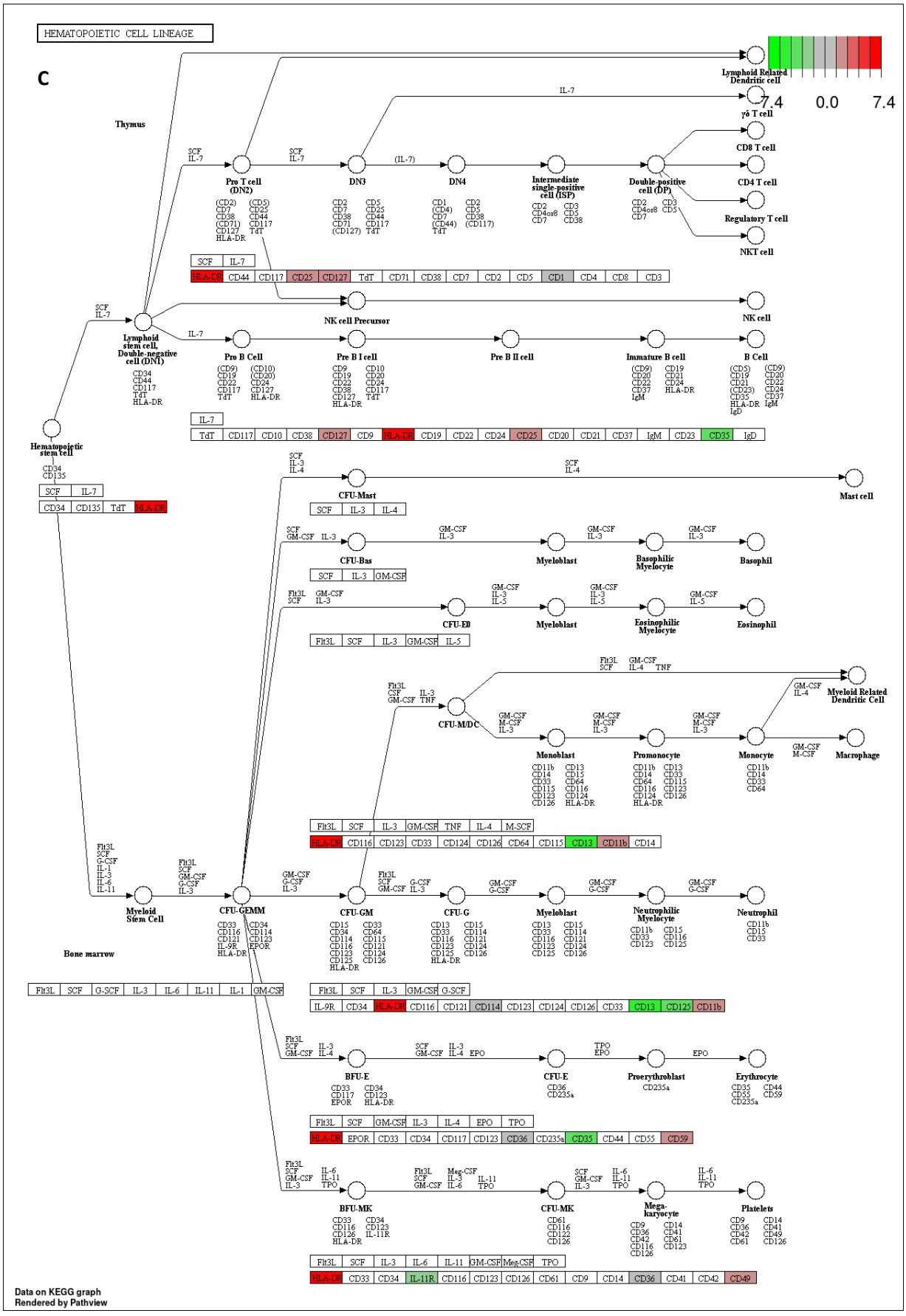
HEMATOPOIETIC CELL LINEAGE
C
7.4
0.0
7.4
Lymphoid Related Dendritic cell
Thymus
γδ T cell
CD8 T cell
CD4 T cell
Regulatory T cell
NKT cell
Pro T cell (DN2)
DN3
DN4
Intermediate single-positive cell (ISP)
Double-positive cell (DP)
NK cell Precursor
NK cell
Lymphoid stem cell, Double-negative cell (DN1)
Pro B Cell
Pre B I cell
Pre B II cell
Immature B cell
B Cell
Hematopoietic stem cell
CFU-Mast
Mast cell
CFU-Bas
Myeloblast
Basophilic Myelocyte
Basophil
CFU-Eo
Eosinophilic Myelocyte
Eosinophil
CFU-M/DC
Myeloid Related Dendritic Cell
Monoblast
Promonocyte
Monocyte
Macrophage
Myeloid Stem Cell
CFU-GEMM
CFU-GM
CFU-G
Neutrophilic Myelocyte
Neutrophil
Bone marrow
BFU-E
CFU-E
Proerythroblast
Erythrocyte
BFU-MK
CFU-MK
Mega-karyocyte
Platelets
Data on KEGG graph
Rendered by Pathview

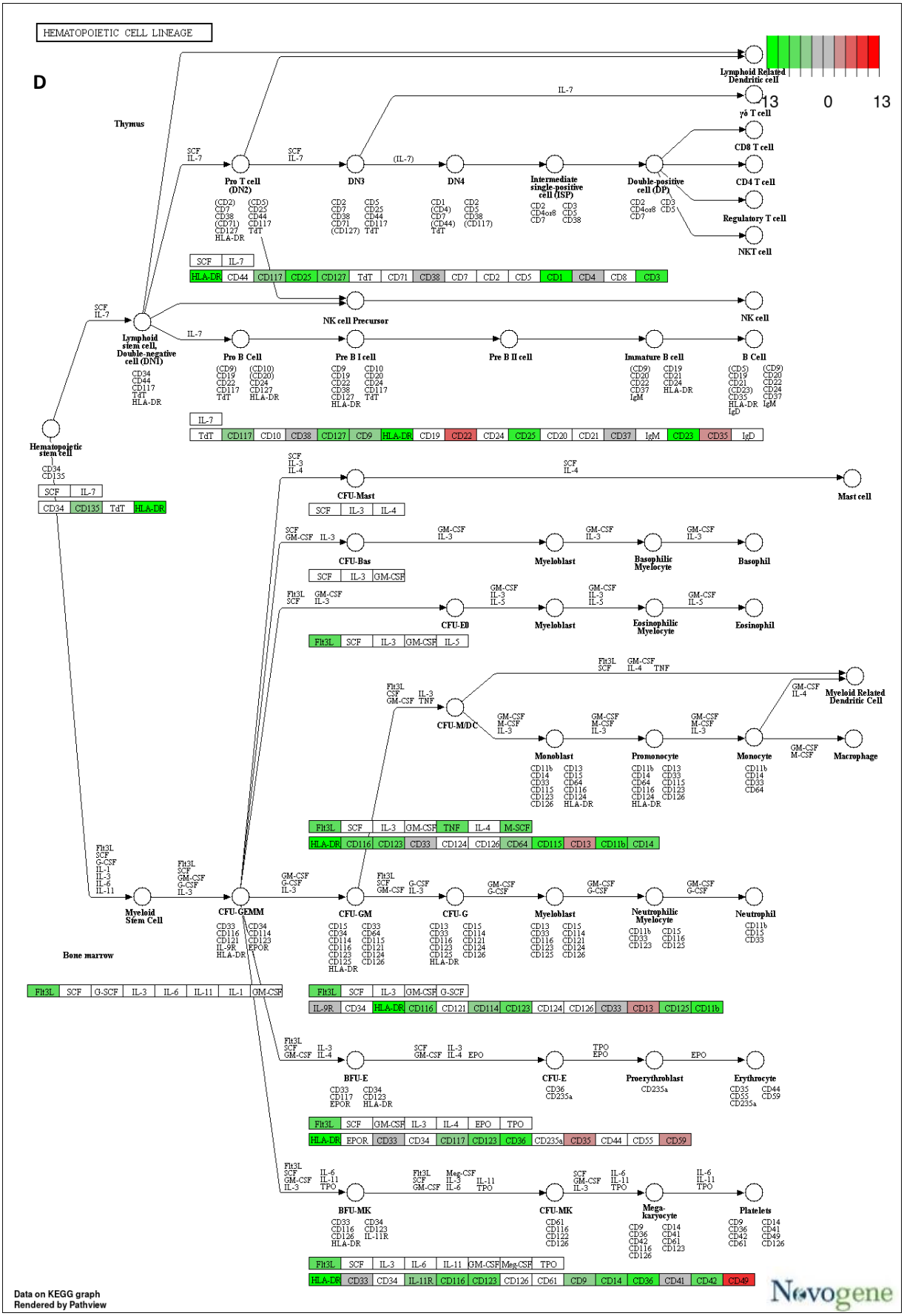
HEMATOPOIETIC CELL LINEAGE
D
13
0
13
Lymphoid Related Dendritic cell
γδ T cell
CD8 T cell
CD4 T cell
Regulatory T cell
NKT cell
NK cell
Thymus
Pro T cell (DN2)
DN3
DN4
Intermediate single-positive cell (ISP)
Double-positive cell (DP)
NK cell Precursor
Lymphoid stem cell, Double-negative cell (DN1)
Pro B Cell
Pre B I cell
Pre B II cell
Immature B cell
B Cell
Hematopoietic stem cell
CFU-Mast
Mast cell
CFU-Bas
Myeloblast
Basophilic Myelocyte
Basophil
CFU-Eo
Eosinophilic Myelocyte
Eosinophil
CFU-M/DC
Myeloid Related Dendritic Cell
Monoblast
Promonocyte
Monocyte
Macrophage
Myeloid Stem Cell
CFU-GEMM
CFU-GM
CFU-G
Neutrophilic Myelocyte
Neutrophil
Bone marrow
BFU-E
CFU-E
Proerythroblast
Erythrocyte
BFU-MK
CFU-MK
Mega-karyocyte
Platelets
Data on KEGG graph
Rendered by Pathview
Novogene

Figure 5.14. KEGG Pathway Analysis of the Haematopoietic Cell Lineage in MOLM-13 NRAS-overexpressing cell lines. Expression differences are shown for the MOLM-13-NRAS-WT over-expressing cell line, compared to the MOLM-13 parental (control) cell line. Red indicates increased gene expression, green indicates decreased. **A)** WT **B)** G12C **C)** G12D **D)** Q61K.

Given the evidence thus far regarding the potential stem properties of MOLM-13-NRAS-WT over-expressing cells, the haematopoietic stem cell state was further assessed using this RNASeq data set, as well as flow cytometry. Analysis of a 10 gene signature revealed a distinct signature of the haematopoietic stem cells in the MOLM-13-NRAS-WT cell line compared to the others, as evidenced in Figure 5.15. The *CD34* data appears negative here given its significantly lower expression compared to other genes across all cell lines. However, CD34 will be further probed and discussed below, at a gene and protein level.

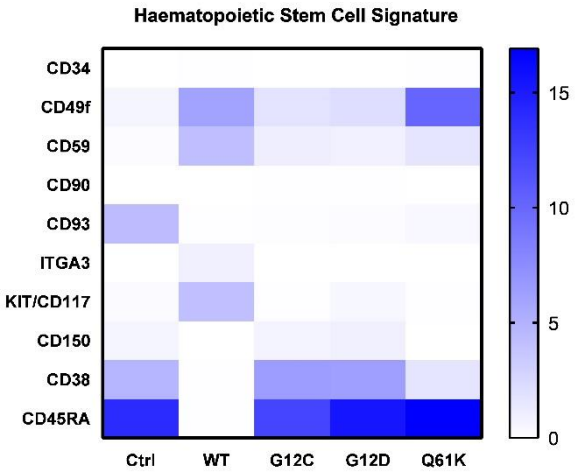

Figure 5.15. Analysis of the haematopoietic stem cell markers within MOLM-13-NRAS over-expressing cells. Markers analysed were those commonly used in HSC marker panels, and typically considered HSC markers. Heat map was constructed using mean FPKM values, in GraphPad Prism V8.0.

The CD34+/CD38- signature has long been associated with HSCs (Rix, Maduro, Bridge & Grey, 2022). Comparison of the expression of these two cell surface markers from the RNASeq data further supports the stemness state of the NRAS-WT over-expressing cells, and the lack of this in the other cell lines. This is illustrated using the bar plots in figure 5.16. Whilst *CD34* is not expressed in the Control, G12C or G12D over-expressing cell line, its expression is considerably increased (albeit to still a very low FPKM value), in the NRAS-WT and somewhat the NRAS-Q61K over-expressing cells. This pattern is inversed with regards to *CD38* (encoding cyclic ADP ribose hydrolase, also known as CD38), since there is *CD38* seen in the Control, G12C or G12D over-expressing cell lines, and not in the WT over-expressing. *CD38* expression is also considerably decreased in the MOLM-13-Q61K over-expressing cell line. Therefore, this suggests the potential for the MOLM-13-NRAS-WT over-expressing cells to have reverted back to an HSC state. Should this be the case, it may be that NRAS mutants push cells from an LSC phenotype, which could explain the emergence of a resistant subclone having emerged from a quiescent stem cell post-therapy.

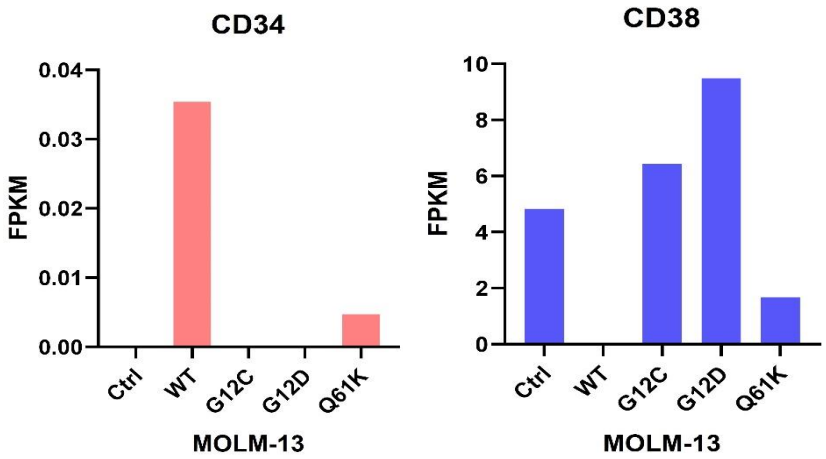

Figure 5.16. Gene expression level changes in the common HSC-associated signature, as determined by RNASeq data. Charts created using mean FPKM values, in GraphPad Prism 8.0.

Increased CD34+ expression was then validated using flow cytometry. Results are detailed in figure 5.17. The increased RNA transcript level did not correspond to an increase in CD34 expression detectable by FACS. Indeed, it appears that the CD34 expression was second lowest out of all the cell lines tested. However, none of these CD34 levels were found to be significantly different (N=3, independent samples unpaired t test). Whilst some stemness features did appear upregulated, it seems that the NRAS WT over-expressing cells do not wholly revert to an HSC phenotype.

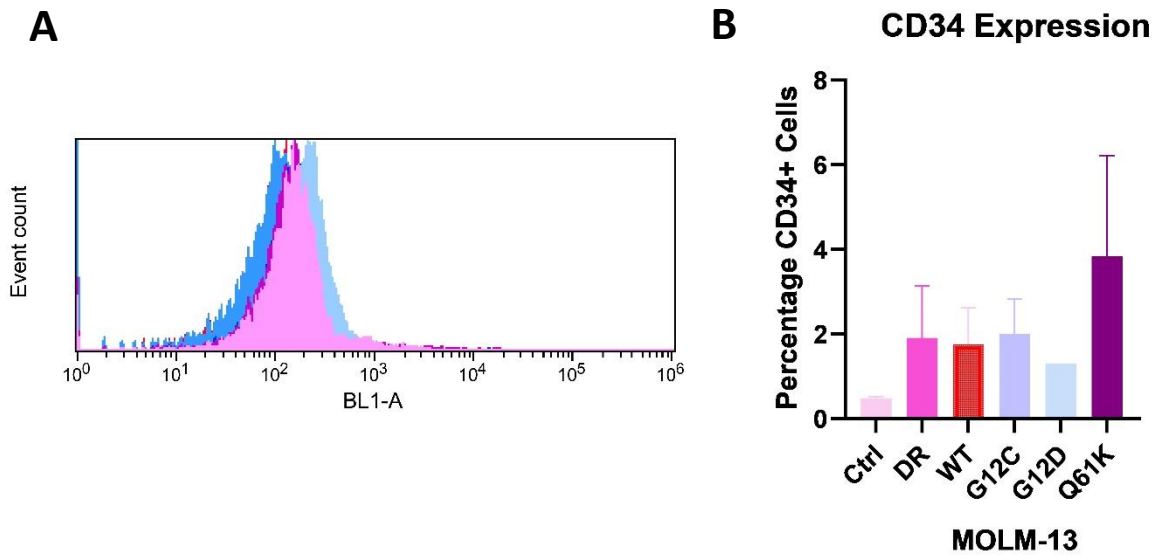

Figure 5.17. CD34 Expression in MOLM-13 NRAS-Over-expressing cell lines. Cells were fixed and stained for 1 h with anti-CD34-FITC, and quantified by flow cytometry. **A)** Histogram illustrating overlap in CD34 expression between all cell lines, which is quantified in **B**) using a bar graph. Histogram generated using FCSalyzer. Bar created in GraphPad Prism 8.0, with statistical analysis carried out using the Unpaired t test, based on N=3 independent subclones +/- SEM. *P*>0.05 in all cases, therefore no statistical significance.

The LSC17 score was determined by Ng et al., in 2016. This collection of genes was seen to be the fundamental determinants of an LSC state, and can be used diagnostically to determine risk (Ng et al., 2016). This identifies the difference between typical HSCs, and those which are leukaemic driving, LSCs. The score was used here to assess in greater detail the level of stemness seen in the MOLM-13-NRAS-WT over-expressing cells, to expand on the CD34 work carried out above. This was based on the RNASeq FPKM values. Two genes (*KIAA0125* and *NGFRAP1*) were no analysed within the RNASeq panel of genes and therefore could not be included here. However, there was not seen to be a distinct change in gene expression within this LSC17 score, as displayed in the heatmap in Figure 5.18. Therefore, based on the lack of a distinct phenotype, it could be assumed that while certain stemness features are upregulated in cells over-expressing NRAS WT compared to the mutants, this does not correlate with a full reversion back to the LSC state. Nevertheless, further work using HSCs (such as those derived from cord blood or indeed AML patients) could help elucidate the impacts of the mutants as a driver out of the LSC state.

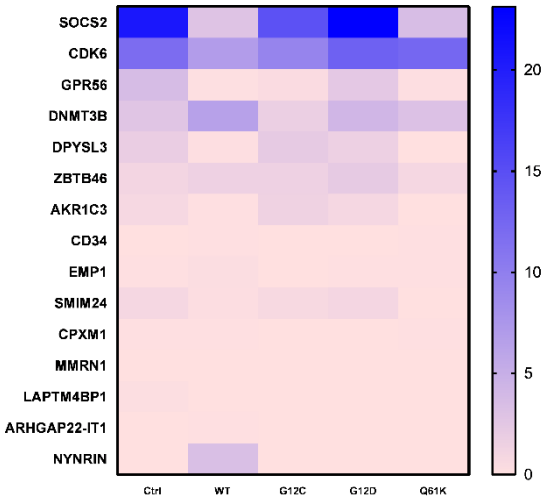

Figure 5.18. LSC17 Score Gene Expression in MOLM-13 NRAS-Over-expressing cell lines.

The list of these genes was taken from Ng et al., 2016. Heatmap created in GraphPad Prism 8.0, based on FPKM values calculated by Novogene.

5.4 Discussion

The data described in this final results chapter is wide ranging, spanning both genotypic and phenotypic alterations arising as a result of the over-expression of different NRAS mutations in a genetically identical (MOLM-13) background. The aims of this chapter included the generation and comparison of the NRAS over-expressing cells to parental and drug-resistant cells, which has been carried out.

The generation of the NRAS wild-type and over-expressing MOLM-13 cell lines resulted in a useful tool to examine the impact of clinically-relevant NRAS mutations in a genetically identical background. Whilst the overexpression model does have some drawbacks with regards to it not necessarily being wholly biologically identical to an AML patient, the comparison between cell lines remains valid. Furthermore, the methods developed to generate these cell lines and assess them phenotypically can be repeated to study other clinically relevant mutations, both within NRAS and beyond. However, this chapter should have been compared to a successful CRISPR model, which was aimed to be created in Chapter 4. Had that been successful, there would have been a more direct comparison between the impacts of the overexpression or CRISPR system, to reveal the true changes incurred by NRAS mutants compared to wild-type.

However, these models reveal that there are considerable differences between the different NRAS mutants which arise in AML. This occurs at both the phenotypic level (e.g. cell growth and cycling rates, and drug sensitivity) as well as at the genotypic level. Whilst these are largely mutation site based (i.e. position 12 or 61), there were also some differences between the G12C and the G12D mutants. This does not

necessarily explain the full drug-resistant phenotype, since over-expression of these mutants did not necessarily decrease sensitivity to FLT3 inhibitors as much as in the acquired resistance (prolonged drug exposure) model they were compared to. Given co-expression and upregulation or downregulation of other leukaemic drivers seen in the transcriptomic sequencing, it can be inferred that there is a highly complex network of genes responsible for the drug-resistant phenotype, to which NRAS contributes considerably, in unique ways associated with their individual mutations. Nevertheless, it is evident that certain NRAS mutants, particularly NRAS Q61K, do contribute to a resistant phenotype, and this could potentially be addressed through treatment stratification. Nevertheless, this is only clinically relevant if NRAS mutants are screened for at diagnosis, rather than just relapse, as is recommended (but not mandated) by the ELN 2022 guidelines (Döhner et al., 2022).

Future work will involve a deeper analysis of genes manipulated in multiple mutant over-expressing cell lines, to assess their as drug targets. Some of these pathways have been indicated in Appendix 8. Furthermore, expansion of this work to a greater panel of AML-relevant NRAS mutations, to obtain a better understanding of the NRAS mutations putting patients most at risk of treatment failure and disease relapse.

Chapter 6

Discussion

6. Discussion

The work carried out in this thesis provides a deeper understanding of the role of individual NRAS mutants within a leukaemic context. This thesis has described the development, optimisation and implementation of tools required for this study, and ultimately facilitates the study of a myriad of genes across AML. It has been possible to investigate alterations induced by NRAS at both a genotypic and phenotypic level. Much of the data described here is novel with regards to AML, which appears to be somewhat differently affected by NRAS than other cancers, such as lung cancer and melanoma. This further indicates the necessity for disease-specific studies, particularly given the advent and development of novel direct Ras-targeted therapies.

6.1 Genotype Heterogeneity in NRAS-mediated AML

As previously discussed, AML is a highly heterogenous disease, with many landscaping and driver genes underpinning the AML genotype. Patients can be stratified by these genotypes using certain classifications, such as the ELN and FAB classifications, as described in section 1.2. Whilst NRAS mutations are generally equally spread throughout each of the FAB classifications, they are starting to be used to a greater level to stratify patients within the ELN classification. In the beginning of this thesis, several different cell lines were screened for NRAS and KRAS mutations, since these are the most common Ras isoforms that are mutated in AML. As expected, the *NRAS* genotype was considerably heterogenous. Figure 3.2 and Figure 3.3 indicates there were no cell lines expressing more than one common Ras hotspot mutation, as correlates with the literature (Prior, Lewis & Mattos, 2012). This, alongside the reported genetic data already detailed in Table 2.3 aligns clearly with

the highly heterogenous landscape of AML, as depicted by the TCGA Consortium and many more besides (Papaemmanuil et al., 2016; The Cancer Genome Atlas, 2013). Whilst not all cell lines were Ras mutation positive, each cell line was reported to have a host of other leukaemic driver mutations, such as MOLM-13 and MV4-11 both being FLT3-ITD+: MOLM-13 are FLT3-ITD heterozygous, and MV4-11 are FLT3-ITD homozygous (Leibniz Institute, 2023). Further detail on the presence of other leukaemic driver mutations within the panel of cell lines originally screened can be found in Table 2.3.

Figure 3.2 indicates cell lines with acquired resistance to quizartinib gained NRAS mutations. MOLM-13-DR became NRAS Q61L homozygous and MV4-11-DR became NRAS G12D heterozygous. The parental cell lines (MOLM-13 and MV4-11) were NRAS wild-type, prior to their prolonged exposure to quizartinib. The gain of the different mutations, as well as differences in zygosity was particularly interesting. It is generally considered that Q61 mutants are generally less transforming in most cancer contexts, and this could perhaps explain why there was a difference in mutation zygosity (Killoran & Smith, 2019; Prior, Hood & Hartley, 2020).

Certain cancers are known to be largely dependent on one particular mutational hotspot in one particular Ras isoform (such as the presence of KRAS G12 mutants in 67% of cases in pancreatic adenocarcinoma) (Bailey et al., 2018; Gao et al., 2013; Gorrini, Harris & Mak, 2013). In contrast, it is known that other cancers including AML, exhibit more of a reliance on a wider variety of mutational hotspots within one isoform, as is described in Figure 1.12. Furthermore, some cancers, exhibit both an isoform

and mutational hotspot preference, such as melanoma, where NRAS Q61 mutants are 20-fold more common than G12 mutants (Burd et al., 2014).

However, given that the cells were rendered resistant to the same drug, it is interesting to further probe the reasoning for the gain in different mutations, at different hotspots. This was the research topic that was taken forwards, with the aim of being investigated using over-expression and CRISPR-Cas9 models.

An over-expression model was initially selected to study the NRAS mutants G12C, G12D and Q61K, to directly compare the differences between mutants, in an efficient manner. These mutants were chosen for differing reasons, including their presence in the drug resistance model previously developed in our lab. G12 and Q61 mutants were chosen to be compared due to their previously-reported vast differences – for example, Q61 hotspot mutants are considered to be less transforming (oncogenic) than G12 or G13 mutants in most cancers. This is, in part, due to differences in their biophysical properties: G12 and G13 mutants have a high affinity for GEF proteins thereby favouring transformation to their active GTP-bound form, whereas Q61 mutants have a decreased sensitivity to GAPs (and thereby remaining in the active form, rather than being deactivated as usual) (Smith, Neel & Ikura, 2013). This subtle difference can have various effects in cancer, with NRAS Q61 mutations being more oncogenic and more common in melanoma than any of the other hotspot mutations, whereas KRAS Q61 mutants are less oncogenic in colorectal cancer than G12 or G13 mutants (Burd et al., 2014; Smith, Neel & Ikura, 2013).

In the NRAS G12C, G12D and Q61K over-expression models, it was interesting to see the whole landscape of AML-associated (driver) mutations change. Certain AML drivers appeared to show a unique transcriptomic expression pattern depending on the NRAS mutation which was over-expressed, as shown in Chapter 5. For example, *RARA*, which commonly forms a translocation protein with PML in Acute Promyelocytic Leukaemia (APML), was over-expressed only in the MOLM-13-NRAS-G12C cell line. In contrast, the *CEBPA* transcription factor is over-expressed in the MOLM-13-NRAS-G12D cell line. Whilst this pattern was not replicated in publicly available datasets, the data available for both *CEBPA* or *RARA* expression, in conjunction with NRAS point mutations, was severely limited (N<3 for each point mutation) (The Cancer Genome Atlas, 2013; Tyner et al., 2018).

It has been recently shown that there is almost a seven-fold increase in the likelihood of there being a *CEBPA* alteration, when *NRAS* is mutated. This encompasses both expression level changes and mutations of any kind – truncating biallelic mutations are most common for *CEBPA* (Wang et al., 2020). Indeed, patients with these biallelic mutations are more likely to have a favourable outcome, just as NRAS mutations are classed as favourable risk (Zhu et al., 2017). Interestingly however, *CEBPA* truncating mutations are also associated with drug-resistance, particularly to PI3K-AKT pathway inhibition, as well as IDH inhibition (e.g. ivosidenib), which NRAS mutants also confer resistance to (Guangrong et al., 2023; Wang et al., 2020). Indeed, presence of *CEBPA* truncating mutations appear to confer resistance to FLT3 inhibitors, as seen in *ex vivo* treatment of FLT3-ITD+ patient samples with quizartinib, although the resistance mechanisms in CEBPA and NRAS mutant AML differ (McMahon et al., 2019; Sexauer et al., 2012). It would appear that a high level of *CEBPA* expression is required for

quizartinib to elicit its effects, and potentially this may overcome the oncogenic effect of the G12D activating mutant present in the MOLM-13-NRAS-G12D cell line, rendering the cells still sensitive to quizartinib, as shown in Figure 5.3. However, co-operation and antagonism of *CEBPA* and *NRAS* remains to be fully elucidated, with limited and conflicting literature available thus far.

RARA over-expression occurs in approximately 30% of AML patients (not including the FAB M3 classification of APML), and does not appear to directly affect patient prognosis i.e. it occurs with equal prevalence across the favourable, intermediate and poor risk AML patients (de Botton et al., 2023; TCGA Network, 2013). Although the PML-RARA fusion protein is successfully targetable using All-Trans Retinoic Acid (ATRA), as well as arsenic trioxide (AsO_3), these drugs would be less useful in pure *RARA* over-expressing cases only, due to their mechanism of action with need for binding to the PML segment of the fusion protein too (Martino & Welch, 2019). Instead, *RARA* over-expression has recently been shown to be an actionable target in these patients through treatment with the RARα antagonist tamibarotene. This, particularly when given with hypomethylating agents such as decitabine, generally conferred a better prognosis, with 61% patients reaching complete remission with incomplete haematologic recovery within less than two months (de Botton et al., 2023).

Previous work has shown that the presence of NRAS mutations in APML may confer resistance to ATRA therapy, since both NRAS and RUNX1 mutants were present only in patients who relapsed post-ATRA and chemotherapy (Noguera et al., 2019). However, unlike in some cases of AML, these mutations were detectable at the diagnostic stage (Iaccarino et al., 2019; Noguera et al., 2019). As with many AML

patient studies, the sites of NRAS mutations conferring this resistance were not fully described in these papers, rendering it impossible to directly link this to the presence of the G12C mutant, which was seen to uniquely affect *RARA* expression here.

Overall, the already highly heterogenous landscape of AML is recapitulated in the drug-resistant model of AML presented here, implicating NRAS mutations in the resistance phenotype. Indeed, interplay between genes appears to further affect this resistance heterogeneity and indicates the need for co-operation between leukaemic drivers to confer overall prognosis. An improved understanding of co-operation and co-expression between genes could also help determine likely patient prognosis. Whilst NRAS mutants are not routinely screened for, detection of alterations or mutations in *CEBPA* or *RARA* may further assist with therapy stratification, and the prediction of relapse. Indeed, as NRAS-targeted therapies develop, these may prove useful in patients with other leukaemic drivers, who are at a risk of relapse to conventional therapy due to the presence of NRAS mutations.

6.2 Differential NRAS Expression

Figure 3.4 and 3.5 indicated there was an increase in NRAS expression, in the drug-resistant (NRAS mutant) cells, compared to parental, at both the transcriptional and translational level. To date, this has not been deeply probed in AML, however data from melanoma and lung cancer drug resistance studies suggest NRAS transcript level suggest a potential emergence for increased NRAS transcript levels in the resistant context (Ninomiya et al., 2018; Randic et al., 2023). Indeed, this may be driven by the transcription factor P2RX7, as has been recently shown in tyrosine kinase inhibitor-resistant NRAS-mutant melanoma (Randic et al., 2023). P2RX7

expression was seen to be upregulated at the transcriptional level in the MOLM-13-NRAS-Q61K over-expressing cell line used here, which also exhibited resistance to the tyrosine kinase inhibitors trametinib, quizartinib and gilteritinib. In future, it would be interesting to probe this association further, in both the NRAS-Q61K over-expressing cell line and the DR cell line.

Some understanding can be gained from publicly available datasets with regards to NRAS expression levels in AML, though this is limited. The Human Protein Atlas reveals some correlation between NRAS mutant status and NRAS expression in various cell lines. In support of the data here, this resource reports almost a doubling of the normalised Transcript per Million (nTPM) value in THP-1 and HL-60 NRAS Q61L homozygous, compared to MOLM-13 and MV4-11 (Human Protein Atlas, 2023). As shown in Figure 3.2, THP-1 are NRAS G12D heterozygous and HL-60 are Q61L homozygous, whereas MOLM-13 and MV4-11 are NRAS WT. However, examination of transcriptomic data from the TCGA AML dataset also revealed no significant differences in *NRAS* transcript levels between NRAS wild-type and NRAS-mutant AML patients, and indeed there was no significant difference between the transcript levels in patients with mutations at each of the hotspots. Nevertheless, this must be caveated with the considerably small sample size of NRAS-mutant patients studied within the TCGA dataset, with RNASeq data only available for 11 NRAS-mutant patients overall, of whom three were G12 mutated, five were G13 mutated, and three had a Q61 mutation. Nevertheless, it seems that, despite changes seen in our model, *NRAS* transcript level does not necessarily correlate with the presence of a mutation. There was also no correlation in the TCGA data set between *NRAS* transcript level (in

patients with NRAS wild type and NRAS mutant) and overall survival (Papaemmanuil et al., 2016; The Cancer Genome Atlas, 2013).

Fluctuations in Ras isoform expression levels within the NRAS-overexpressing cell lines in Figure 5.23 suggest a redundancy between the different isoforms, and the level of overexpression of one isoform may result in a decrease in protein expression of the other isoforms. This is particular prominent in the Q61K mutant overexpressing cell lines. It is known that NRAS, KRAS and HRAS do all confer different leukaemogenic potential, however there remains some differences the myeloid disease that they are most likely to propagate, and highly likely need other mutations to induce leukaemia, as has been shown throughout section 5.7 (Parikh, Subrahmanyam & Ren, 2007).

In the FLT3 inhibitor resistance model used here, NRAS protein levels were increased in the drug-resistant cell lines, relative to their parental cell lines, determined by Western blot. This also occurred for KRAS, but not HRAS. It is known that NRAS and KRAS are the two most mutated Ras isoforms in AML, with only a very low proportion of patients expressing HRAS mutations (Hoadley et al., 2018; Tyner et al., 2018). The increased transcript and protein levels in the drug-resistant cells may explain the potential for NRAS (and indeed KRAS) mutations to occur in AML drug resistance. As proposed by Hood, Sahraoui, Jenkins and Prior (2023), the greater the abundance of a particular Ras isoform within a cell at a protein level, the greater the incidence of mutations within this isoform. Mass spectrometry revealed that total Ras protein abundance tends to positively correlate with cell size, with KRAS the predominantly expressed Ras isoform across a breadth of cell lines, and in Ras wild-type adult mice

(Hood, Sahraoui, Jenkins & Prior, 2023). This perhaps explains the reason it is the most commonly mutated isoform across a range of cancers: its greater abundance presents an increased likelihood of a point mutation occurring. The data also suggested that, in the context of heterozygous-mutated genotype, mutant Ras proteins are expressed to a greater level than the wild-type, but only in the case of some mutants and can be codon dependent (not, for example, KRAS G12C) (Hood, Sahraoui, Jenkins & Prior, 2023). Nevertheless, there were no AML cell lines studied, and given that there was shown to be a considerable difference between Ras abundance in different cancers, it would be interesting to study the MOLM-13 and MV4-11 cell lines and their drug-resistant counterparts in a similar manner. Indeed, this study focussed on G12 and G13 mutants only, and could be expanded to assess the relative difference between G12 mutant : wild-type Ras ratio and Q61 mutant : wild-type Ras ratio.

6.3 NRAS-Mediated Signalling Pathway Alterations

6.3.1 Ras Signalling in a Transiently Transfectable Context

The over-expression system was first examined in a transiently transfectable context, for simplicity of construct validation. This was carried out in HEK293T and HeLa cells. Based on the data in Figure 3.13, it appears that transfection of either NRAS wild-type, G12C, G12D or Q61K only elicit an effect on the ERK pathway in HEK293T cells. As can be determined from the two control (untransfected and EGFP) conditions, this pathway is typically inactive in HEK293T. In contrast, the AKT pathway is typically activated, and over-expression of NRAS did not have any effect on this pathway.

KRAS expression appeared to decrease in the cells transfected to over-express NRAS WT or G12D only. However, total Ras protein within the cells did increase as expected, thereby implying that the overall phenotypic effects seen in the cells after these over-expression models have been generated are as a result of increased NRAS. It is known that mutations within these two isoforms rarely co-occur in cancer (Mulligan et al., 2014; Nagakubo, Hirotsu, Amemiya, Oyama, Mochizuki & Omata, 2019). Nevertheless, it would be interesting to probe in the future if there is any true inverse relationship between NRAS and KRAS levels, and the reasoning behind this difference in mutational background.

6.3.2 Ras Signalling in AML

As previously described, the MAPK, PI3K-AKT and STAT5 pathways are all heavily involved in the pro-survival and proliferative phenotype of AML. The first two of these pathways, MAPK and PI3K-AKT, act downstream of Ras, whereas the STAT5 pathway is somewhat more independent. These have been shown to be activated in MOLM-13 and MV4-11 cell lines, with an increase in ERK signalling in the resistant counterparts (Figure 3.6). Furthermore, Figure 3.7 indicates increased NRAS activation within the drug-resistant cell lines, compared to the parental cells. This is perhaps unsurprising, given the oncogenic, activating nature of the NRAS mutations, thereby causing an increase in signalling within these proliferative pathways.

Previous work has identified MEK inhibition as a means of arresting proliferation in the AML cells in PDX mice, though this was not cytotoxic (Burgess et al., 2014). This could be due to the powerful oncogenic effect of the NRAS mutations (NRAS G12D was examined in this case), limiting the effects of MAPK pathway inhibition at a patient-

acceptable concentration. PI3K-AKT inhibition had no effect on the NRAS-mutant AML in this work either, whether used as a single agent or in conjunction with either of the MEK inhibitors (Burgess et al., 2014). A further drawback to MAPK pathway inhibition is the reliance of a vast array of cell types on ERK signalling, particularly through MEK. The lack of specificity for cancer cells renders a high potential for on-target toxicity of MEK inhibitors, as has been previously reported with cobimetinib, where there was poor tolerability and limited efficacy in part due to dose restrictions (2 patients with partial response only out of 177 dosed) (Shapiro et al., 2020). However, this is starting to be overcome by the use of more potent therapies targeting ERK instead, such as LY3214996 (Temuterkib) (Bhagwat et al., 2020; Köhler et al., 2021). There are currently several clinical trials recruiting patients for monotherapy with LY3214996, or in conjunction with standard of care. This includes an AML clinical trial, involving patients not suitable for standard therapy (Clinical Trial NCT04081259).

The alterations between PTEN expression shown in Figure 3.6 was somewhat surprising. This would typically indicate a decrease in survival and proliferative capability, since PTEN is a negative regulator of the pro-proliferative AKT pathway, and is widely known to be down-regulated in myeloid malignancies (Dahia et al., 1999; Ryu et al., 2019). This does explain the down-regulation of AKT activation in the MV4-11-DR cells compared to the parental line, suggesting that these cells exhibit a stronger reliance on the MAPK pathway to promote the drug-resistant phenotype following the increased expression and activation of NRAS, rather than the AKT pathway. This somewhat correlates with the lack of efficacy associated with AKT targeting in Burgess et al. (2014). The MOLM-13 parental and drug-resistant cells do not follow this pattern however, with an increase in both PTEN and AKT signalling

seen. However, the presence of oncogenic Ras downstream of this repressor could negate the typical downstream effects, effectively 'out-competing' the increased tumour-suppressive effects of PTEN (To, Perez-Losada, Mao & Balmain, 2005). It has been shown KRAS G12D mutations co-operate with *PTEN* loss in the generation of pancreatic ductal adenocarcinoma in mice, however studies comparing different NRAS mutants in conjunction with PTEN are yet to be reported (Kopp et al., 2018). Nevertheless, the overall increase in PTEN may ultimately explain why there is decidedly less of an increase in AKT activation compared to ERK activation – whilst both are somewhat Ras-mediated, the PI3K-AKT pathway has a stronger reliance on activation through PIP_3 presence, something which is inhibited by PTEN.

Nevertheless, given the diversity of signalling pathways as well as mutational acquisition within drug-resistant cells, these findings should be caveated with the fact there may be other genetic alterations and pathways which are also associated with the resistant phenotype. For example, the loss in STAT5 activation shown in Figure 3.6, though difficult to detect, may provide an alternative mechanism of drug resistance. It is therefore important to explore pathway alterations at a deeper level.

It is interesting to note that the transcriptomic sequencing revealed NRAS wild-type over-expressing cells exhibited more altered genes in general when compared to the control level, rather than any of the cell lines over-expressing the mutants. Many of the genes overexpressed in the NRAS G12C and G12D over-expressing MOLM-13 cells were the same, as indicated by their cross-over in the Venn diagrams in Appendix Figures 8.4-8.6. Indeed, no genes were downregulated in the MOLM-13-NRAS-G12D cell line exclusively in the PI3K-AKT and JAK-STAT pathways. Genes occurring in

multiple NRAS mutant over-expressing cases, but not in the wild-type over-expressing cells, may represent a potential therapeutic option, that could be targeted using small molecule inhibitors for example. In the case of the PI3K-AKT pathway, it could be that inhibiting the upregulation of *YWAHB,* which encodes a protein of the same name that is part of the 14-3-3 family of proteins involved in signal transduction by phospho-site recognition.

It is apparent that over-expression of different NRAS mutants appeared to affect both the MAPK and PI3K-AKT pathways considerably differently. For example, whilst AKT activation (and indeed total AKT expression) remained low at a protein level similar to the control MOLM-13 cell line (Figure 5.23), it is evident that there was a significant upregulation of this pathway at a transcript level, as indicated in Appendix Figure 8.1. As per the transcriptomic data, the PI3K-AKT pathway is most upregulated when the NRAS wild-type was over-expressed, compared to any of the mutants. This correlates with mouse protein data, comparing the impacts of all three key Ras isoforms (Parikh, Subrahmanyam & Ren, 2007). A small subset of PI3K-AKT-related genes were upregulated in the G12C and G12D over-expressing cells, with seven genes upregulated in both of these cell lines only. This indicates that perhaps AKT pathway alterations and targeting are less relevant in the case of NRAS-mutant AML. Nevertheless, no genes from the PI3K-AKT, MAPK or JAK-STAT pathways were downregulated exclusively in the G12D over-expressing cells (Appendix Figure 8.3 and 8.6), indicating that this pathway remains relatively unchanged, and not silenced by redundancy given the increase in MAPK pathway gene expression levels.

As expected, there were several genes upregulated in the MAPK pathway (Appendix Figure 8.2 and 8.5), and in the majority of over-expressing cell lines this did correlate to an increase in ERK pathway signalling, shown in Figure 5.7. The singular gene upregulated in all three mutant overexpressing cell lines, *DUSP6*, may provide an actionable target (Appendix Figure 8.5 and Section 6.12). However, there were several MAPK pathway-associated genes upregulated in the MOLM-13-NRAS-Q61K cell line only. Given that this mutation conferred significant resistance to a variety of the clinically-relevant drugs used in Figure 5.5, and has been supported by data from Ball et al. (2019), targeting genes upregulated by NRAS Q61K may help to overcome NRAS-mediated resistance, whilst sparing healthy cells, thereby reducing drug toxicities. Interestingly, the anti-apoptotic gene *BCL2* was upregulated. The BCL2 protein is clinically targetable using the BH3 mimetic venetoclax. Although venetoclax resistance has been associated with the presence of Ras mutations, these mutations were not stratified beyond their isoform (though HRAS mutants were excluded), and the site of mutation was never detailed (DiNardo et al., 2020a). Therefore, the exclusive upregulation of BCL2 here in conjunction with the literature suggests any effects of venetoclax may be restricted to cells which are NRAS Q61K mutation positive. Indeed, venetoclax resistance is associated with upregulated MCL1 stabilised by NRAS (Zhang et al., 2022b), which was seen in all overexpression cases here apart from NRAS Q61K, further supporting further exploration into the stratification of venetoclax therapy by NRAS genotype.

One gene recognised as being upregulated in NRAS mutant over-expressing cell lines is *IL7R*, the gene encoding the Interleukin 7 Receptor, also known as CD127. This gene is involved in both the PI3K-AKT and JAK-STAT pathway, as determined by

KEGG pathway mapping. This upregulation recapitulates data seen in mouse models for ALL (Cramer et al., 2018). In this case, use of IL7R antagonists may prove useful. For example, an IL7R (CD127) antagonist such as OSE-127 may have benefits in inhibiting the JAK-STAT pathway which has upregulated activity triggered by IL-7, as well as mediating detection and phagocytosis by macrophages. This, in theory, should therefore inhibit the upregulation of two of the three key AML pathways: PI3K-AKT and JAK-STAT (STAT5). Such effects have already been shown in ALL, with particular efficacy in relapsed/refractory PDX mouse models (Lenk et al., 2022).

Ultimately, the RNASeq data presented in Chapter 5 highlights putative mechanisms responsible for NRAS mutant mediated AML pathogenesis which may be actionable drug targets. However, these should be further investigated to identify druggable protein targets, for a more direct understanding of expression at both the gene and protein level.

6.4 NRAS-Mediated Proliferation

NRAS-mediated proliferative potential was initially measured in transient transfection models, both in a physiological context (HEK293T) and cancerous context (HeLa). Growth curves in Figure 3.12 indicate the difference between these contexts, since G12 Ras mutants were only able to increase the growth rate in HeLa cells relative to any other control or transfected condition. In HEK293T cells, transfection with any of these constructs did not significantly affect the growth rate. This difference implies NRAS mutants do affect proliferation rate as expected, however rely on other oncogenic mutations to elicit their effect. For example, the tumour suppressor gene *Rb* is repressed in HeLa as a result of the presence of Human Papilloma Virus (HPV)

oncoproteins, E6 and E7, conferring an oncogenic effect (Goodwin & DiMaio, 2000). Regardless of the cause of the oncogenicity however, it is important to note that the multi-faceted nature of cancer limits the potential of there only being one driver gene (in this case *NRAS*), and instead relies on a myriad of mutations. This is in line with the clonal evolution/CSC theory presented in the introduction (Section 1.3.1), suggesting the need for oncogenic landscaping mutations to co-operate with NRAS mutations to cause an oncogenic effect. It is widely known that AML is a highly heterogenous disease characterised by the diversity of driver and landscaping oncogenic mutations, so it is plausible that these mutations co-operate with NRAS mutants to confer the leukaemic phenotype.

As can be determined from Figure 5.2, the over-expression of NRAS mutants conferred a highly statistically significant increase in proliferative potential in the MOLM-13 cell line, compared to the over-expression of NRAS wild-type, or the control cell line. This correlates with the oncogenic capacity commonly associated with G12 or Q61 mutants. However, this difference is much plainer to see in Figure 5.2A, rather than B. The data for Figure 5.2A was collected manually, with 12 repeated measurements ultimately taken per cell line, every 24 h. This comprised three individual biological replicates, with four technical replicates taken each time these biological replicates were measured. Therefore, although the use of a haemocytometer could be considered somewhat more subjective than flow cytometry, the collection of the various replicates per cell line mitigated for any potential subjectivity. The less pronounced difference seen by the CFSE staining after 96 h could be due to the sensitivity of the staining, with a logarithmic scale required to illustrate unstained, 0 h stained and 96 h stained cells. However, it could be that there

was smaller difference seen in growth rate (staining intensity) after 96 h between cell lines, compared to the difference between the 0 and 96 h timepoints for each cell line, therefore rendering cell proliferation differences somewhat less apparent. Nevertheless, it remains possible to see more of a left-shift in the red peak (96 h stained) of the cells over-expressing any of the three mutants, compared to the MOLM-13 control or MOLM-13-NRAS-WT over-expressing cells. Interestingly, the peak of the MOLM-13-DR did not appear to have as much of a left-shift as the NRAS-mutant-over-expressing cells, indicating that these drug-resistant cells have less of a proliferative capacity, and in fact this remains similar to the original control cells.

Nevertheless, despite some differences in the sensitivity of the assays, the significantly increased proliferative potential conferred by NRAS mutants is apparent. This correlates with the significantly increased proliferative potential in the HeLa cells, as described in Figure 3.12. However, unlike in HeLa, there was also a significant increase in proliferative potential of the cells over-expressing NRAS Q61K, whereas in HeLa this was restricted to the G12 mutants only. This further provides evidence that the effects of NRAS mutants are disease dependent, in this case a difference between cervical cancer cells (HeLa) and AML cells (MOLM-13). Whilst NRAS Q61 mutants are generally considered to be less transforming than G12 mutants (Hobbs, Der & Rossman, 2016), the data shown here, in terms of proliferative capacity at least, seem to correlate better with research from Christin Burd's group that NRAS Q61 mutants are highly oncogenic in certain contexts (such as melanoma). Indeed, NRAS Q61 mutants are most commonly expressed in melanoma, in which they were seen to be highly leukaemogenic (Burd et al., 2014). They are also equally represented in AML as G12 or G13 mutants, as shown in Figure 1.13 (The Cancer Genome Atlas, 2013).

Based on this data, it would seem plausible that the incidence of these mutations somewhat correlate with differences in their oncogenic power in different cancers.

6.5 NRAS-mediated Cell Cycling

As demonstrated in Figure 5.3, progression through the cell cycle differed between the cells over-expressing different NRAS mutants. Cell cycle analysis was carried out by staining cells with 7AAD, which binds to DNA. This is then detected by flow cytometry. Staining progresses from left to right as cells move through the cell cycle, since DNA content increases throughout the cell cycle. However, judgement of the individual phases can be subjective, and other assays may be employed in conjunction. This may include probing for individual cyclins, for example through Western blotting.

It appears that the NRAS G12C and G12D over-expressing cells follow a similar pattern to the control cells, whereas the MOLM-13-NRAS-Q61K cell line shows a stronger resemblance to the MOLM-13-DR cell line. Indeed, these latter two cell lines appeared to progress quicker through the cell cycle than the control or G12-mutant over-expressing cell lines. In contrast, the MOLM-13-NRAS-WT cell lines appeared to be very slowly over the 96 h in comparison to the other cell lines, with only small fluctuations in the number of cells in each stage of the cell cycle at each point. Whilst these cells appeared to remain in the mitotic phase of the cell cycle, it could be that the cells are not necessarily fully dormant (where they would be expected to be in G0/SubG1 phase), but instead they progress slower through each phase. This can be further evidenced with the increase in G1 at the latter time points, which occurs in conjunction with the decrease in G2/M. Indeed, the number of cells in S phase also begins to increase after 72 h.

Studies of NRAS mutations in melanoma have previously shown its necessity in cell cycle control. ERK activation triggered by NRAS ultimately results in the formation of activator protein 1 (AP-1) complexes, facilitating transcription of cyclin D, and thus progression from G1 to S phase. Indeed, Ras-mediated PI3K signalling also facilitates progression through S phase (Benary, Bohn, Lüthen, Nolis, Blüthgen & Loewer, 2020; Randic, Kozar, Margue, Utikal & Kreis, 2021). In NRAS Q61K-mutated melanoma, cyclin D levels are seen to be increased compared to NRAS wild-type cells, and this correlates with increased activity of cyclin-dependent kinases 4 and 6 (CDK4/6). This facilitates progression from G1 to S phase, and indeed inhibition of CDK4/6 using the selective, dual inhibitor PD-033921 inhibited cell cycle. In conjunction with MEK inhibition (acting downstream of the mutated NRAS), tumours were eradicated *in vivo* (Kwong et al., 2012). This may explain the 'double peak' seen in the G1 phase for the MOLM-13-DR (NRAS Q61L-homozygous) and MOLM-13-NRAS-Q61K cell lines in Figure 5.3, although it should be appreciated that not all Q61 mutants are the same (Huynh et al., 2022). Further work could examine cyclin D and CDK4/6 levels, as well as their sensitivity to CDK4/6 inhibitors.

In contrast, transcriptomic data indicating the upregulation of *FLT4* (*VEGFR3,* encoding Vascular Endothelial Growth Factor Receptor 3) in the MOLM-13-NRAS-WT cells may explain the cell cycle arrest seen in the MOLM-13-NRAS-WT cell line. *FLT4* has been implicated in cell cycle arrest in the case of vascular growth and endothelial cell differentiation, with increased activity of the VEGFC-FLT4-ERK axis responsible for cell cycle arrest (Jerafi-Vider et al., 2021). Given that ERK was seen to be upregulated in conjunction with *FLT4* expression in the MOLM-13-NRAS-WT over-

expressing cell line, this may be responsible for the slowed cell cycling as shown in Figure 5.3.

6.6 NRAS-mediated Colony Forming Potential

As demonstrated in section 5.3.4, there is a significant increase in colony forming capacity in cells over-expressing the NRAS mutants. The significant increase in colony forming capacity in the NRAS mutant over-expressing cell lines indicates the increased leukaemogenic capacity conferred by the mutants, compared to the parental cell line. This further provides evidence for the pro-proliferative nature of NRAS-mutant AML. However, this also supports the concept of NRAS as a leukaemic driver mutation, since it drives cells to thrive from a single cell, in a way which endogenous NRAS wild-type cells do not. However, this should also be caveated with the model restrictions – artificial over-expression may introduce a 'more supportive' nature and an increased colony forming capacity. In this way, the CRISPR-Cas9 model that was desired in Chapter 4 may be a better judge of colony forming capacity, since all levels should remain (or be controlled to remain) endogenous. Nevertheless, melanoma patient data indicates copy number variations have little impact on dissemination of tumour cells into colonies (metastasis) (Werner-Klein et al., 2018). However, this study also highlights the necessity, in melanoma, for the presence of BRAF mutations to most often drive metastasis in conjunction with NRAS mutants – it was only a minor subset of mice whose primary tumours metastasised when they were NRAS-mutated only. Again, given Q61 mutations are most prevalent in melanoma, only Q61 was screened here (Werner-Klein et al., 2018).

Therefore, the work presented in this thesis provides additional evidence to the oncogenic capacity of NRAS. Whilst blood cancer does not metastasise in the same manner as solid tumours such as melanoma, its repopulating capacity remains important. Leukaemic stem cells reside in the bone marrow in small quantities, remaining in a quiescent state. They possess a greater self-renewal quality than bulk AML, with the capability of deriving multiple leukaemic cell types. Recent work has established a self-renewal role for NRAS G12V in AML cell lines and primary samples, acting in conjunction with CD69 (Antony et al., 2023). This provides support to the data presented here that G12 mutants also confer a self-renewal capacity and indicates NRAS may be important in maintaining self-renewal capacity, although perhaps the individual mutant is less important. Indeed, it seems necessary for NRAS to co-operate with other mutations and gene expression changes across a range of leukaemia. Nevertheless, it could be that the presence of these NRAS mutations facilitate the other gene alterations, given the comparisons that were made between the control and over-expression models here.

The importance of NRAS in the stemness state and colony formation also applies to other leukaemias, including chronic myelomonocytic leukaemia (CMML). In this case, NRAS and CBL mutations were able to increase colony forming capacity *in vitro*, independently from supplemented growth factors (Geissler et al., 2020). This supports the stemness nature of the two genes, and also suggests that these cells may be less dependent on the bone marrow niche typically required for leukaemia to commence and thrive. This potentially increases the risk of relapse, since ablation of the bone marrow niche may not be sufficient to kill these cells. Bone marrow niche ablation (such as through conditioning prior to stem cell transplant) is considered beneficial in

eliminating the HSC component, although can increase leukaemia development (Bowers, Zhang, Ho, Agarwal, Chen & Bhatia, 2015; Griffin, Healy, Dahal, Floisand & Woolley, 2022). Data from the literature and this thesis may explain this, through the perseverance of NRAS-mutant cells and their ability to survive in a harsh environment (Geissler et al., 2020).

6.7 Impacts of NRAS mutants on haematopoiesis

The heatmaps presented in Figure 5.11 indicate a lack of typical haematopoietic gene expression, replaced somewhat by a stem cell signature, in the MOLM-13-NRAS-WT and MOLM-13-NRAS-Q61K cell lines. There is a strong similarity between the control cell line and the G12 mutant over-expressing cell lines, suggesting that these are progressing through normal haematopoiesis. KEGG pathway analysis reveals there is a greater level of haematopoietic gene upregulation in the wild-type over-expressing cells, whereas somewhat more of a downregulation in the Q61K over-expressing cells, both compared to the control cell line. However, Figure 5.13-5.15 indicates that this does not wholly translate to a reversal to the HSC expression pattern. Indeed, Figure 5.16 appears to differ from this stemness pattern, with certain genes (such as *SOCS2*) involved in the LSC17 score seemingly downregulated in the MOLM-13-NRAS-WT and Q61K over-expressing cell lines, compared to the others. This conflicting data suggests that whilst a true HSC or LSC phenotype is not restored following WT or Q61K over-expression, there are some alterations which may contribute to somewhat more of a pluripotent stem cell state.

Progression from stem cells to AML has been somewhat associated with the presence of NRAS Q61K mutants. An increased engraftment capability of relapse AML PDX

models has been shown once an NRAS Q61K mutation had emerged at relapse, which was not initially detectable at diagnosis. This was subsequently probed further, with increased leukaemic initiating capacity evident in NRAS Q61K subclones of the patient's AML burden, compared to those with NRAS wild-type (Zeller et al., 2022).

However, the role of NRAS in the stemness state remains to be fully elucidated. Most studies have described the influence of NRAS G12D on stemness capacity, compared to other NRAS mutants. NRAS G12D overexpression has been shown to confer bimodal effects and generating a subset of HSCs with greater proliferative capacity, whilst reducing the rate at which others divided. This was proven both *in vitro* and *in vivo.* Ultimately, the rarely dividing NRAS G12D+ HSCs were able to outcompete wild-type HSCs, rather than those that had a greater proliferative potential conferred by NRAS G12D, through an induction of STAT5 signalling (Li, Balmain & Counter, 2018). This correlates with the upregulation of *STAT5B* in the MOLM-13-NRAS-Q61K cell line alone which exhibited a greater stemness capacity, however does not explain the down-regulation of *STAT5A* in the MOLM-13-NRAS-WT cells which also appeared more stem-like (Appendix 8). However, the incidence of bimodal effects themselves suggests the role of NRAS in haematopoiesis is yet to be fully elucidated, and may rely on expression of other genes. Indeed, the Li et al. paper did not investigate the individual role of each STAT5 isoform, which may determine the stemness capacity capable of being conferred by the NRAS mutant.

The down-regulation of *SOCS2* seen here, as well as the increase in *STAT5B* activation levels, correlates with a dysregulated stemness function of HSCs shown by Jin et al. (2022). However, they showed this pattern in the published data was as a

result of JAK2 activation which occurs due to *SOCS2* downregulation. However, *JAK2* expression levels were not impacted in our NRAS Q61K over-expression model, though this does not mean that they were not affected at an activation level, and would be worth probing further in the future. Nevertheless, other elements of the JAK-STAT pathway were upregulated, which may have also been upregulated as a result of *SOCS2* suppression in our model (Appendix 8).

Indeed, the co-operation of NRAS oncogenic mutants with other AML-related genes, such as the NUP98-HOX10HD fusion protein also appeared to confer an increase in HSC stemness capacity *in vitro* (Dong et al., 2019). However, this paper studied the G12D mutant, which did not show stemness capacity in the MOLM-13 over-expression models used here. Given that the NUP98-HOX10HD fusion protein was not present in our cells, it may be that this restricted the cells over-expressing certain NRAS variants from forming a full HSC phenotype, instead limiting them in a more pluripotent state. Indeed, other work has shown that NRAS G12D is unable, *in vivo,* to maintain leukaemic progenitor activity without a *DNMT3A* R882H mutation (Lu et al., 2016).

Taken together, these results suggest that whilst NRAS mutants can confer some stemness activity, it relies on co-operation with other gene alterations to fully exhibit an HSC phenotype and leukaemic repopulating capacity.

6.8 NRAS over-expression affects regulation of oxidative phosphorylation

Oxidative phosphorylation and its by-products must be carefully controlled to maintain respiratory homeostasis, and so these processes are often dysregulated in cancer,

including AML. This includes the MOLM-13-NRAS-G12D cell line studied here, as identified through transcriptomic sequencing (Figure 5.12 and Appendix 9), where oxidative phosphorylation was the most altered biological process, and multiple aspects of the mitochondrial membrane complex were dysregulated. Indeed, NAD(P)H activity was also dysregulated, as shown in Figure 5.12 and Appendix 9. There were changes in the expression of different mitochondrial membrane complexes involved in the OXPHOS process seen, as shown in Appendix 9, where expression of complexes III and IV are particularly downregulated in the G12D over-expressing cell line, compared to other cell lines.

Dysregulated oxidative phosphorylation has been shown to confer resistance to a wide range of drugs across various haematological malignancies, including resistance to cytarabine and gilteritinib (Zhang et al., 2022a). This can affect the bulk AML blast cells, or indeed the LSC (de Beauchamp, Himonas & Helgason, 2022). This can be due to the upregulation of multiple different pathways, or bone marrow environment conditions, such as the AMPK or PI3K pathways, or CD38 expression and subsequent signalling (de Beauchamp, Himonas & Helgason, 2022; Guièze et al., 2019; Mistry et al., 2021; Raimondi, Ciccarese & Ciminale, 2020). In AML, it has previously been shown that dysregulated OXPHOS, leading to an increase in reactive oxygen species (ROS) levels, can confer resistance to a myriad of therapeutics, including cytarabine and gilteritinib. In the case of gilteritinib, DHODH, CDK9 and PRMT5 activity have all been associated with increased OXPHOS activity, in lieu of typical glycolysis (Zhang et al., 2022a). This can ultimately cause an increase of reactive oxygen species (ROS), which cancer cells are more readily equipped to tolerate than healthy cells. A minimal upregulation of ROS increases signalling within proliferative and survival

pathways (such as through mTOR) to combat the extra stress on the cell (Kenny, Craig, Villanueva & Germain, 2019). Indeed, a greater upregulation of ROS can ultimately decrease the activity of the extrinsic (Fas-mediated) apoptosis pathway in cancer (Clément & Stamenkovic, 1996; Raimondi, Ciccarese & Ciminale, 2020). This is coupled with aberrant levels of the anti-oxidant response in cancer including AML, where levels of the NRF2 protein are often elevated and can induce transcription of many detoxification and cytoprotective genes, conferring resistance to various chemotherapeutics. This confers a survival advantage to the leukaemic cells, via NFκB activity (Rushworth, Zaitseva, Murray, Shah, Bowles & MacEwan, 2012).

Activated Ras (oncogenic or wild-type) is associated with mitochondrial electron transport chain activation, specifically the decrease in complex I activation (Raimondi, Ciccarese & Ciminale, 2020). Recent work has shown that mutant NRAS can increase oxidative phosphorylation and ROS output in AML, and by targeting this using pyrvinium (OXPHOS inhibitor) as well as trametinib, may provide therapeutic benefit to NRAS-G12D mutation positive, previously trametinib-insensitive patients. Interestingly, these synergistic results were also successfully recapitulated in NRAS Q61R PDX model mice, as well as CDX model mice transplanted with the HL60 cell line (which is NRAS Q61L homozygous) (Decroocq et al., 2022).

Overall, whilst the exact interplay between individual NRAS mutants and dysregulated oxidative phosphorylation and detoxification pathways remains to be fully elucidated, there is potential for therapeutic targeting of NRAS-mutant AML by targeting the increased oxidative phosphorylation. Whilst the RNASeq data presented here appears to show that it is the NRAS G12 mutant overexpressing cell lines which would be most

susceptible to oxidative phosphorylation inhibition, there is potential for these compounds to work across NRAS-mutated AML, as described in the literature (Decroocq et al., 2022).

6.9 Intracellular Localisation of NRAS Mutants

Global analysis of the RNASeq data showed changes to intracellular trafficking within the MOLM-13-NRAS-G12C cell line. It is understood that NRAS localisation is important, given its need to move from the endoplasmic reticulum, via the Golgi body to the plasma membrane. Here, it forms complexes with its activators and effectors, eliciting its downstream effects. This is controlled using post-translational modifications within the hypervariable region of the protein, as detailed in Figure 1.7. This has previously been targeted pharmacologically, using farnesyltransferase inhibitors, such as lonafarnib and tipifarnib, though this was unsuccessful due to redundant post-translational modifications (geranylgeranyltransferase). More recently, NRAS trafficking has aimed to be arrested by targeting palmitoylation, by targeting the Rab27B-ZDHHC9 complex with artemisinin (Qiu, Abegg, Guidi, Gilmore, Seeberger & Adibekian, 2022; Ren et al., 2023). This inhibits transport of NRAS to the plasma membrane. Appendix 10 attempted to analyse effects of alterations to NRAS localisation in this cell line, however encountered difficulties due to the selection of fluorescently-labelled antibodies against cell structural markers (Appendix 10). Equally, trafficking of other proteins may also be affected, including cell receptors, which may not be appropriately externalised.

6.10 The AML Therapeutic Landscape

The AML therapeutic landscape continues to advance considerably, as a means of combatting drug resistance. A subset of these compounds has been used here, to assess their utility in an NRAS-mutant context. This could help with assisting a more personalised therapy approach, with treatment stratification a potential means of treating or preventing relapse.

Cytarabine

Cytarabine is the front-line chemotherapy for AML. It is given in conjunction with an anthracycline (typically daunorubicin) in an initial high dose induction therapy (known as the 7+3 regimen), followed by lower dose maintenance therapy, in the vast majority of cases. This front-line chemotherapeutic is vital in the 'debulking' of the AML burden in patients, in conjunction with daunorubicin. Indeed, patients typically respond well to this drug. Approximately 75% of patients respond to complete remission following cytarabine therapy within a subset of (younger adult) patients, however relapse incidence is between 40 and 70%, depending on the number of treatment cycles patients receive (Bashir et al., 2015; Sekeres et al., 2009; Willemze et al., 2013). However, relapse is common, which is why more directed, targeted therapies such as FLT3 inhibitors are being developed and used as later-line treatment options. Cytarabine is a nucleoside analogue, and therefore its classification as an anti-metabolite, renders it capable of integrating into DNA to prevent synthesis (Guinan, Benckendorff, Smith & Miller, 2020). As a result, it would generally be expected that proliferative and pro-survival signalling pathway alterations would not significantly reduce the efficacy of cytarabine.

Figure 5.5 indicates some considerable differences in drug sensitivity between the differing NRAS mutants. It is promising from a patient perspective that there was no significant difference seen in any of the cell lines' response to cytarabine. The data presented here suggests *NRAS* genotype, or at least the three mutants assessed here and the wild-type, does not cause resistance to this drug directly. Indeed, this coincides with the understanding that patients with NRAS mutations typically have a more favourable prognosis, than those with, for example FLT3 mutations. This is shown in Figures 1.4 and 1.14. Previous literature suggests that NRAS mutants in conjunction with cytarabine cause differentiation of the immature myeloid blasts which constitute the bulk of the AML (Brendel et al., 2015). This therefore permits a more logical following of haematopoiesis, differentiating into cells which are more physiologically typical, with a lower proliferative capacity. Therefore, this further supports the favourable disease phenotype associated with NRAS-mutant AML.

A retrospective study of patients receiving induction chemotherapy highlighted that those with Ras mutants (NRAS or KRAS) fared poorer in response to high dose cytarabine, compared to those who were Ras WT, exhibiting an independent increased risk of death and a poorer EFS. Nevertheless, induction chemotherapy given in this manner did result in Ras mutation clearance, whereby the Ras mutations were undetectable at CR/CRi and within relapsed cases (Ball et al., 2019). However, subsequent analysis of the same dataset by the same group revealed KRAS mutants to be responsible for the changes in EFS, rather than NRAS. Nevertheless, this has been caveated with the facts that the specific mutations occurring within NRAS were not published (Ball et al., 2021).

Within the last decade, there have been many advances in the direct targeting of FLT3-ITD, the most common leukaemogenic driver (Figure 1.3). This is seen typically as a second/third line therapeutic option, following relapse after induction and consolidation chemotherapy. This has resulted in several clinical trials, as well as the approval of two small molecule therapeutics for this area: gilteritinib and midostaurin. As the most FLT3 specific of the two drugs, gilteritinib was used in this thesis to investigate cell line sensitivity, as detailed in figure 3.8. This was compared to quizartinib, a compound for which a large-scale Phase 3 clinical trial has just been completed (Erba et al., 2023).

Gilteritinib

However, it is also widely known that many patients eventually suffer AML relapse following induction chemotherapy, and subsequently targeted inhibitors are prescribed. This is also beneficial given the clinical characteristics of the majority of patients, since many are elderly and are unable to tolerate such a harsh therapy as cytarabine/daunorubicin or stem cell transplant. Therefore, targeted therapies, such as FLT3 inhibitors present a good option, to eliminate the bulk of the AML without causing excessive healthy cell toxicity.

The ADMIRAL phase 3 trial was pivotal in the approval of gilteritinib for relapsed/refractory FLT3-mutated AML. This trial included 371 patients, of which 67% received gilteritinib therapy following relapse, and the remaining 33% receiving salvage chemotherapy (standard of care). Salvage chemotherapy in this post-relapse context generally has little effect, and indeed it was gilteritinib which conferred a significantly longer median OS and EFS. Indeed, 37% of patients who received

gilteritinib were alive after one year, compared to 17% in the salvage chemotherapy arm of the trial. Grade 3+ toxicities were seen to occur less frequently in gilteritinib-treated patients than in the salvage chemotherapy-treated patients (Perl et al., 2019). Subsequent, longer term follow-up revealed a significant overall survival benefit, with a median OS of 9.3 months in the gilteritinib cohort, compared to 5.6 months in the salvage chemotherapy cohort. This further equates to a 20.6% 2-year survival in the gilteritinib cohort, compared to 14.2% in the control (Perl et al., 2022).

Within the original ADMIRAL trial dataset, approximately 15% of all of the FLT3-mutated patients also had an NRAS mutation, though this was approximately twice as common when the patient was FLT3-TKD mutation positive. These NRAS mutations were in either exon 2, 3 or 4, which were spanned by whole genome sequencing (WGS) as part of the extended molecular analysis. Indeed, there were far fewer patients who were KRAS mutation positive (approximately 8%) (Perl et al., 2019). Both of these findings are in keeping with the general understanding of Ras isoform mutation occurrence within the genetic landscape of AML (Papaemmanuil et al., 2016; Papaemmanuil et al., 2013; The Cancer Genome Atlas, 2013). However, upon relapse, activating Ras/MAPK pathway mutations were found to be one of the leading emergent mutations. Of 40 patients who had their genome sequenced by WGS at baseline and post-relapse, 18 (45%) were found to have activating Ras/MAPK pathway mutations. Of this 18, 11 had gained NRAS mutations which were not previously detectable at baseline (equating to 28% of the total relapsed cohort assessed). 8 patients had KRAS mutations, with two patients within these totals having gained both NRAS and KRAS mutations (a generally rare occurrence) (Smith, Levis, Perl, Hill, Rosales & Bahceci, 2022). Nevertheless, as with other trials and indeed the

majority of the clinical data available, the individual NRAS mutants were not described, which may have an impact.

There is a growing body of literature associating the emergence of NRAS mutations with gilteritinib resistance in AML. Temporary knockdown of NRAS using antisense oligonucleotides has been shown to restore gilteritinib sensitivity (Joshi et al., 2023). The 2019 dataset from McMahon et al. comprised 41 relapsed/refractory AML patients receiving gilteritinib, of whom 13 had NRAS mutations only detectable post-gilteritinib therapy. There was no significant difference between patient mutation seen in this dataset, with 10 different NRAS mutations seen across all patients (McMahon et al., 2019).

Based on this published data, it is plausible that the NRAS mutants found in the MOLM-13-DR and MV4-11-DR cell lines could contribute to the level of gilteritinib-resistance seen in Figure 3.8. However, it would be expected that there would be a level of resistance seen between the parental control and the NRAS mutant over-expressing lines, which was not significantly seen here. Nevertheless, there remains some difference between the mutants, with at least a 5-fold increase in the IC_{50} values between the control cell line and the G12D or Q61K mutant over-expressing cell lines. This is in line with the data from McMahon et al (2019), where there remained a variation in NRAS mutations occurring in gilteritinib patients, as previously discussed.

Quizartinib

Quizartinib is a newer FLT3 inhibitor in development, targeting specifically the ITD mutation (Marensi, Keeshan & MacEwan, 2021). Whilst gilteritinib is largely FLT3

specific, a receptor tyrosine kinase largely only found on myeloid cells, the specificity of quizartinib in theory should be even greater, given it targets the FLT3-ITD mutant only found in AML.

The QuANTUM-First trial explored the use of quizartinib in conjunction with standard chemotherapy, both with and without allogeneic haematopoietic stem cell transplant. This Phase III randomised, placebo-controlled, double-blind trial found an improved OS (17-month median) in the patient subgroup administered 40 mg/day quizartinib for 14 days, and then followed up where appropriate with a maintenance level of quizartinib and chemotherapy. Furthermore, clinically-meaningful benefits regarding EFS, as well as time to relapse and relapse incidence were also seen. Indeed, most serious adverse events (grade 3-4) were the same in both the placebo and quizartinib groups, though a subset of quizartinib-treated patients did exhibit high-grade neutropenia as well. Importantly, the QTc prolongation that has been previously associated with quizartinib was better managed in this trial, with any patients experiencing this generally doing so in an asymptomatic manner (Erba et al., 2023; Kang et al., 2021). Data from this trial thus far remains to be fully examined whether there are mutational background differences between the responder and non-responder patients, which will further contextualise this work.

Other, pre-clinical research has not directly associated NRAS with quizartinib resistance (Aikawa et al., 2020; Rosenberg, Watanabe-Smith, Tyner, Tognon, Druker & Borate, 2020), though only select mutations occurring post-establishment of midostaurin resistance were studied in depth. This paper suggested that quizartinib remains effective in KRAS G12A and NRAS G12C MOLM-14 cells, which had been

rendered resistant to midostaurin, albeit to a six-fold increased IC_{50} value (Aikawa et al., 2020). This paper does not consider other mutation sites and amino acid alterations as has been shown in Figure 5.5. Indeed, Figure 5.5 of this thesis indicates that the MOLM-13-NRAS-G12C cell line remains sensitive to quizartinib. In contrast, over-expression of NRAS Q61K renders the cells more resistant, almost on par with the cells made resistant to quizartinib through prolonged exposure. This could, potentially be due to the presence of a Q61 NRAS mutant in both of these cell lines, regardless of the amino acid it is substituted to (Leucine in the MOLM-13-DR, Lysine in the MOLM-13-NRAS-Q61K).

However, the means by which NRAS inhibits the activity of FLT3 inhibitors remains to be elucidated. Interestingly, the transcriptomic data, supported by Western blotting in Figure 5.6, revealed a decrease in both FLT3 activation and expression in the MOLM-13-NRAS-Q61K line. Should the target not be expressed, it follows that the drug cannot bind. Indeed, the fact that quizartinib is highly specific for FLT3-ITD may prove highly detrimental in NRAS Q61K mutated AML, more so than gilteritinib which has some (albeit low potent) effects on other RTKs. Figure 5.6 and Appendix 8 also indicate that FLT3 expression decreases to some degree in the MOLM-13-NRAS-WT line too. This correlates with Figure 5.5, where there is some level of decrease in drug sensitivity seen. However, over-expression of G12C or G12D did not impact FLT3 expression in the transcriptomic data, which again correlates with the maintenance of sensitivity to gilteritinib and quizartinib in the over-expression cell lines.

Trametinib

Trametinib is a MEK inhibitor, acting downstream of NRAS. It is currently approved for BRAF-mediated melanoma, and has shown promise in Ras mutant-mediated myeloid malignancies (Borthakur et al., 2016; Ragon et al., 2019). Figure 3.8 indicated that the MOLM-13-DR cells responded better than their parental counterparts to trametinib. However, subsequent data in Figure 5.5 indicates that this is not due to the presence of a Q61 mutant, since the MOLM-13-NRAS-Q61K had an IC_{50} >10 µM for trametinib, and it can be seen in Figure 5.5D that the dose response curve is far higher for the MOLM-13-Q61K cell line than the MOLM-13-DR cell line. Sensitivity seen in MOLM-13-DR may be amino acid substitution specific, although is more likely due to other mutations occurring in this DR cell line. Indeed, it could also be due to the over-expression of NRAS, which may confer a greater oncogenic capacity due to the vastly increased level of protein expression. That is to say that the increased oncogenic gene dose may outcompete the downstream pharmacological inhibitory effects of trametinib. MOLM-13 cells over-expressing G12C or G12D responded in a relatively similar manner to the controls, and in fact it was only the over-expression of NRAS wild-type that increased the IC_{50} (although this differs from the pattern shown on the graph).

A phase II trial of trametinib monotherapy in Ras-mutant myeloid malignancies did show some promise, with approximately 8% of patients reaching complete remission following daily administration of trametinib, for at least 28 days. Furthermore, 53% of Ras-mutated AML/MDS patients and 73% of CMML patients achieved stable disease, which is somewhat promising for relapsed/refractory AML (Borthakur et al., 2016). However, since there were so few patients achieving complete remission, it is likely the drug was only able to reduce the mass proliferation oncogenic effects, without

affecting cell viability. Therefore, this does not eliminate the problem of oncogenic Ras, and presents the risk of relapse, should the drug be removed. Such a concept has been shown in other cancers, such as pancreatic ductal adenocarcinoma, where stabilisation of the anti-apoptotic MCL-1 by interaction with the deubiquitinase USP9X causes resistance to trametinib (Perurena et al., 2023).

As a means of bettering outcomes seen with trametinib and increasing leukaemic cell apoptosis, trametinib has been trialled in conjunction with AKT inhibition, using uprosertib. A Phase II clinical trial did not identify an improved outcome for patients with Ras-mutated AML administered both drug classes, since no patients achieved complete response. This was despite a decrease in both ERK and S6 activation levels, as expected (Ragon et al., 2019). Nevertheless, Ras is involved in a wide range of pathways beyond the MAPK and AKT pathways, as indicated by the transcriptomic data presented here. Therefore, an alternatively Ras-mediated upregulated pathway may have conferred this resistance, which is somewhat recapitulated in the NRAS over-expression models used here. Interestingly, *USP9X* expression levels were somewhat increased in the MOLM-13-NRAS-WT and MOLM-13-NRAS-Q61K cell lines, albeit not to a significant level, however could be mediating some form of MCL-1 stabilisation and trametinib resistance. However, this may not be the only explanation for the resistance seen, particularly given that the expression level of *USP9X* can be linked to survival outcome itself (Pérez-Mancera et al., 2012).

Ultimately, the data presented in Figure 5.5 indicates differing drug sensitivities based on NRAS mutational status. Whilst the development of direct KRAS G12C inhibitors was revolutionary for the treatment of Ras-mediated cancers, the data presented here

indicates NRAS Q61K may have a stronger impact in drug resistance in AML. Therefore, there is currently an unmet clinical need for the treatment of drug-resistant AML, with outcomes potentially improved for patients should NRAS Q61K be inhibited.

Venetoclax

Many of the trials involving venetoclax are limited to older patients, partially due to their inferior survival outcomes generally, and the difficulties faced with administering highly toxic chemotherapy to patients with a greater range of co-morbidities (Kantarjian et al., 2010). Efficacy of venetoclax in AML is becoming increasingly well-proven. In a Phase Ib study reported in 2018, use of venetoclax plus decitabine or azacytidine resulted in 61% of patients reaching complete remission, or complete remission with incomplete marrow recovery (DiNardo et al., 2018). Indeed, an expanded analysis of this trial in 2020 revealed approximately a 5 month (50%) increase in overall survival, in patients administered azacytidine and venetoclax, compared to those administered azacytidine and a placebo (DiNardo et al., 2020a). This is now expanded into Phase 3 trials (NCT02993523).

The role which venetoclax can have in NRAS mutant AML still remains to be fully elucidated however. As described in section 6.3.2 with regards to the BCL2 expression in our cell lines, it may be that the efficacy of venetoclax is restricted to NRAS Q61K-mutant patients. There have been multiple reports poorer OS in NRAS-mutant patients in response to venetoclax compared to NRAS WT patients, however these have not been stratified by mutation site and amino acid change (Maiti et al., 2020; Wang et al., 2020). Indeed, it has been identified that of 12 patients who had NRAS or KRAS mutations and received venetoclax + azacytidine therapy, 10 patients relapsed. Whilst

these patients all expressed multiple mutations, the only mutated gene they had in common was NRAS or KRAS. Nevertheless, there remains the potential for other genes to be causing relapse in other ways, since not all relapsed patients expressed NRAS or KRAS mutations (Maiti et al., 2020).

As shown by our transcriptomic data here, the mutation site and amino acid substitution can affect both BCL2 expression and reliance on oxidative phosphorylation, the mechanisms by which venetoclax acts. Therefore, it would be interesting to measure the effects of venetoclax in our mutant cell lines, and assess the impacts of each mutation to the sensitivity of this more novel but highly useful AML therapy.

6.11 Ras-targeting therapeutics

BAY293

BAY293 is an investigational compound, designed to inhibit the activation of KRAS by the GEF SOS1. This small molecule inhibitor serves as a chemical probe to investigate the arrest of SOS1-mediated KRAS activation, in the case of wild-type and G12C mutated KRAS (Hillig et al., 2019). This interacts at the c-Raf binding domain on KRAS, thereby rendering it a non-GTP-competitive inhibitor. This is beneficial given the picomolar affinity with which GTP binds Ras, rendering it difficult to pharmacologically outcompete GTP binding (Stephen, Esposito, Bagni & McCormick, 2014). Since BAY293 inhibits SOS-1-mediated activation of KRAS, by interacting at a hydrophobic pocket of SOS1 adjacent to the KRAS binding site, there is potential for this compound to work against other isoforms too, through binding to the same pocket. Indeed, this hydrophobic pocket was also identified as important in the HRAS-SOS1

interaction, and pre-clinical fragments have also been discovered against this (Winter et al., 2015).

It is evident from Figure 3.8 that BAY293 has a considerably lower cytotoxic effect on any of the four cell lines tested compared to some of the other compounds used, including cytarabine. Furthermore, there was no significant difference between the parental and FLT3 inhibitor resistant cell lines. In conjunction with other data appears here, the BAY293 dose-response curves presented in Figure 3.8 suggests a lack of importance for KRAS in the AML cell lines studied here, conferring a greater role for NRAS in AML pathogenesis. However, since there are no direct NRAS targeting inhibitors, this cannot be fully elucidated using this method of comparison. Nevertheless, there remains some activity against both the MOLM-13 and MV4-11 cell lines, in line with the published data (Hillig et al., 2019).

However, as shown in Figure 5.5E, this drug was mostly ineffectual in the NRAS-mutant over-expression models used here. Therefore, this compound, and perhaps SOS1 inhibition itself, is not a viable means of eradicating NRAS-mutant AML. The transcriptomic data illustrated in Appendix Figure 8.5 showed a decrease in *SOS1* expression in all NRAS over-expressing cell lines compared to the MOLM-13 control, and therefore this may also contribute to the lack of efficacy with BAY293. A down-regulation of SOS1 following NRAS over-expression implies that there is a secondary mechanism employed by the cells (perhaps activation by an alternative GEF) responsible for the maintenance of NRAS in its active state.

MRTX849

With the advent of direct targeting, mutation-specific KRAS inhibitors such as AMG510 (Sotorasib) and MRTX849 (Adagrasib), a deeper understanding of *NRAS* genotype should be routinely screened for. Not only could this be used to stratify treatment with a variety of therapeutics currently used in AML, but also could be used to directly target mutant NRAS.

AMG510 and MRTX849 were revolutionary in the Ras-mediated disease field: they are the first direct-targeting KRAS G12C inhibitors. These compounds performed well in clinical trials, resulting in their gain of emergency approval by the FDA in 2021 (Canon et al., 2019; Govindan, 2019; Romero, 2020; Zhang et al., 2023).

The phase 1/2 KRYSTAL-1 trial was pivotal in assessing the safety and efficacy of MRTX849 (Jänne et al., 2022). This involved 112 NSCLC patients, of whom 43% had an objective response confirmed. Only three patients showed an increased tumour burden after therapy. Median OS was 12.6 months, with median PFS was 6.5 months. Whilst almost all patients (97%) suffered at least one adverse event, less than half suffered a grade three or higher event, and such an event resulted in treatment cessation in 7% patients. This drug binds covalently to KRAS G12C, thereby showing a distinct selectivity for this particular form of oncogenic Ras. Moreover, MRTX849 also relies on interaction with the H95 residue, in the recently identified Switch II Pocket (SII-P), thereby increasing its specificity for KRAS beyond the other Ras isoforms. This explains the lack of efficacy shown in the MOLM-13 and MV4-11 parental and drug resistant cell lines (Figure 3.8), since these cell lines were already deemed to be KRAS wild-type in Figure 3.3. Furthermore, this specificity explains the lack of efficacy in the NRAS over-expression model, even despite the presence of the NRAS G12C mutant. The RNASeq data indicated there were no KRAS G12C point

mutations introduced following the over-expression of NRAS G12C (or in any of the other NRAS mutant over-expressing cell lines). Given that KRAS and NRAS are rarely co-mutated in patients (largely due to phenotypic redundancy between the Ras isoforms) (The Cancer Genome Atlas, 2013), it appears that MRTX849 has little therapeutic use in NRAS-mutant AML.

AMG510

AMG510 was studied in the CodeBreaK100 trial, amongst others. Its good performance here resulted in the accelerated approval of this drug by the FDA, and is now approved in other locations worldwide (Blair, 2021; European Medicines Agency, 2022; Jaber, 2021). In this trial of 126 patients, 46% displayed an objective response, and every patient showed some level of disease control. Median response time was 11.1 months, with median PFS 6.8 months. Only 20% of patients exhibited grade 3 or higher toxicity.

This mechanism of action of this drug is similar to MRTX849, binding covalently to the mutated cysteine residue at KRAS G12. However, AMG510 does not interact as strongly with H95, thereby rendering it slightly less isoform specific. Nevertheless, the specificity for the G12C mutation explains its lack of efficacy in the four cell lines it was tested in Chapter 3 (Figure 3.8). AMG510 was seen to be useful in the MOLM-13-NRAS-G12C cell line, and suggests its potential for use in NRAS G12C mutated AML. This effect was seen to be almost wholly specific to the NRAS G12C over-expressing cell line, although it did also induce cytotoxic effects in the MOLM-13-NRAS-Q61K cell line at high doses. This could, however, be due to an off-target effect. Ultimately, both AMG510 and MRTX849 are able to interact with the recently discovered Switch II

Pocket (SII-P), which is KRAS G12C specific. However, the data presented here indicates AMG510 is less specific for this pocket, and is able to interact with NRAS G12C too.

6.12 The Future for NRAS Therapeutics in AML – Potential Novel Targets

A key issue of Ras-targeting is the abundance and importance of NRAS within almost all cells – specific targeting is required to ensure a reduction in on-target toxicity where possible. Whilst direct Ras-targeting agents are beginning to be developed, the pipeline of these remains somewhat limited with a long development process ahead, and NRAS-direct targeting agents are in their infancy. Therefore, alternative therapeutic strategies could involve targeting other genes directly associated with NRAS mutants, such as some of those identified by the transcriptomic data presented in this thesis.

As shown in Figure 5.10A, there are certain genes altered across all three different NRAS mutant overexpressing MOLM-13 cell lines, however not in the NRAS wild-type over-expressing cells. This includes *DUSP6*, a negative regulator of the MAPK pathway (Zhang et al., 2010). Over-expression of a negative MAPK regulator seems contradictory to the oncogenic effects incurred by NRAS, however this deubiquitinase appears to have conflicting tumour suppressing or promoting influences across different cancers. In lung cancer, increased expression of *DUSP6* appears to have a pro-apoptotic effect (Zhang et al., 2010), whereas in AML, increased *DUSP6* expression is known to synergise with FLT3-ITD to confer oncogenic effects (Arora et al., 2012; Zuchegna, Di Zazzo, Moncharmont & Messina, 2020). Furthermore, *DUSP6* expression was seen to be increased in NRAS Q61R-mutant melanoma cell lines,

providing further support to the RNASeq data shown in Figure 5.8 (Bloethner et al., 2005).

Based on this transcriptomic data, therapeutic targeting of *DUSP6* may reduce leukaemic survival. A DUSP6 inhibitor, (E)-2-benzylidene-3-(cyclohexylamino)-2,3-dihydro-1H-inden-1-one (BCI), has been evaluated against a wide panel of cancer cell lines, as well as *in vivo* zebrafish models, showing efficacy as an anti-cancer agent (Molina et al., 2009; Shojaee et al., 2015; Wu et al., 2018). Indeed, inhibition of the ERK feedback pathways using this same BCI compound inhibited proliferation and colony forming capacity in an NRAS G12D-mutated background, accompanied by the induction of an ROS response (Shojaee et al., 2015). Given that the oxidative phosphorylation pathway was also manipulated in the G12-mutant over-expressing cell lines as determined by the RNASeq data, a compound such as BCI may provide a therapeutic option for NRAS-mutant acute leukaemias.

However, it has since been shown that there is a co-operative/redundancy effect between *DUSP4* (which is not altered significantly in the transcriptomic data here) and *DUSP6* (Ito et al., 2021). Therefore, this raises the potential need for a dual inhibitor as a means of inhibiting the proliferative effects of these *DUSP*s in NRAS-mutant AML. Such a concept has been previously identified somewhat using CRISPR screens on *DUSP4* and *DUSP4/6* dual knockouts, where the dual knock-out showed a greater inhibition of growth than either the single knockout, or the parental cell line (Ito et al., 2021). Future work could include the use of dual DUSP inhibitors within our panel, to identify a viable therapeutic strategy.

6.13 Novel Direct Ras-Targeting Therapeutics

Having evidenced the differences in mutational effect incurred by the different Ras isoforms, as well as by the different codons and amino acid substitutions, it is clear that the field of direct Ras-targeting agents must continue to expand. Whilst the KRAS G12C inhibitors were revolutionary in opening the door to direct Ras-targeting therapeutics, this solves only a small part of the problem of Ras in cancer. As shown in Figure 1.12, there are a multitude of mutations within each of the Ras isoforms, all of which can have oncogenic effects (Miller & Miller, 2012).

The small molecule MRTX1133 is a direct KRAS G12D inhibitor. *In silico* development, biochemical optimisation and *in vitro* success of a non-G12C targeting compound indicated the possibility of targeting a greater number of mutations, rather cysteine mutants able to form covalent bonds. This compound, identified through *in silico* modelling, works through non-covalent interactions in the SII-P, in a similar (but not identical) to that seen with MRTX849 in the KRAS G12C mutant. This drug also showed efficacy *in vitro* and *in vivo* and continues to be explored, having just started recruiting patients into Phase I/II clinical trials in early 2023 (NCT05737706) (Wang et al., 2022).

However, in part thanks to advantages in computational modelling, compounds are starting to be investigated against other Ras mutations. This includes other KRAS mutations which may be applicable to a wider range of cancers, including KRAS G12R. However, whilst such a compound has been designed and co-crystallised with the KRAS G12R protein, its cellular efficacy still remains severely limited (Zhang, Morstein, Ecker, Guiley & Shokat, 2022). Indeed, a similar process utilising the SII-P

on KRAS has been exploited in the G12S mutant, with biochemical success seen with a natural β-lactone compound (Zhang, Guiley & Shokat, 2022). Targeting of NRAS Q61R and Q61K has also been explored, with the design of theoretical compound HM-561 *in silico*. However, this remains to be examined in a cellular context (Hu & Marti, 2023).

6.14 Methodological Limitations

Throughout this thesis, there were several methods applied, both in the generation of the tools to study NRAS mutants, as well as the inevitable optimisation of phenotypic assays. Although a selection of processes and experiments were unsuccessful, many of the experiments were able to generate useful, novel data. Even in the cases of failed experiments, lessons have been learned and will be described in the following section.

6.14.1 Lentiviral Component delivery

Lentiviral transduction permits stable integration or removal of genes from the genome, and was beneficial here in ensuring the prolonged, stable nature of protein expression. This approach was used for both the constitutive over-expression models and the introduction of components for inducible CRISPR-Cas9 gene editing, given the well-described difficulties transiently transfecting AML cell lines. This is evidenced in Figures 4.6-4.8, where Cas9 was introduced into the cells in an inducible manner following lentiviral transduction and puromycin selection, and has also been described throughout Chapter 5. However, this method seemed inefficient when delivering the HDR-template and guide, with <5% efficiency (as determined by EGFP-readout). In this thesis, lentiviral concentration was attempted, using ultracentrifugation. However, this did not prove effective, potentially instead damaging the lentivirus, since it is a

fragile virus, more so than other viruses such as adenovirus (Cooper, Patel, Senadheera, Plath, Kohn & Hollis, 2011; Jiang et al., 2015). Other alternatives to centrifugation could be employed, such as tangential flow filtration permits a high throughput method of lentiviral concentration, without as considerable a loss of lentiviral particles as has been seen in other centrifugation methods. This can result into up to 2000-fold increase in concentration of lentiviral particles (Cooper, Patel, Senadheera, Plath, Kohn & Hollis, 2011). However, due to equipment complexity, this method was not utilised here.

Alternative methods to improve lentiviral transduction efficiency could be employed, including the addition of salt solutions or sucrose to make the cells more amenable to transduction (Jiang et al., 2015). This is through the inclusion of amphiphilic polymers within the solution, encouraging a more fluid membrane state, by charge neutralisation on both the lentiviral particles and the cell membrane, therefore rendering it easier for the lentiviral particles to penetrate the cell membrane (Adhikari, Goliaei, Tsereteli & Berkowitz, 2016; Czeiszperger, Wang & Chung, 2020; Masiuk, Zhang, Osborne, Hollis, Campo-Fernandez & Kohn, 2019). However, these amphiphilic polymers are considered toxic to the cells, and can therefore decrease cell survival (Czeiszperger, Wang & Chung, 2020). Given that haematopoietic cell health is already generally considerably affected by lentiviral transduction, as well as the extra burden on the cell through the induction of Cas9, it was deemed unsuitable for these lentiviral transduction experiments to add yet another means of cellular stress.

In a similar way, the use of electroporation or chemical-mediated transfection (e.g. lipofection) for introduction of the HDR template sequence may also have been

beneficial in improving editing efficiency, rather than lentiviral transduction. These were not attempted here, given the harsh toxicity and low efficiency often witnessed by using this in haematopoietic cells (Kim & Eberwine, 2010; Papaioannou et al., 2023). This would involve introduction of the HDR template sequence alone as an oligonucleotide, and thus there would be no positive selection marker (as the EGFP was in the plasmid/transduction method of introduction). Given that the efficiency of CRISPR-Cas9 editing is low, even with a higher efficiency of HDR template sequence delivery, it would have therefore required a considerable larger subcloning screen to identify the positively-edited cells.

Spinoculation, the process of centrifuging the lentiviral/polybrene/cells culture, was shown to be somewhat beneficial, in Figure 4.11. This process alters cytoskeletal dynamics, specifically through actin and cofilin mobilisation. This renders the cell membrane more amenable to viral penetration (Guo, Wang, Yu & Wu, 2011). However, this is completed at a low speed, due to the fragile nature of both the lentiviral particles and the cells under viral stress, which provided some benefit here.

6.14.2 In vitro NRAS over-expression

One of the key targets from Chapter 3 was to create genetically identical AML models expressing different NRAS mutants, to directly compare the effects of these on the leukaemogenic potential and phenotypic effects seen in different NRAS-mutant contexts. The drug resistant nature of these cell lines would also be examined, since section 3.6 proved a difference in drug sensitivity between the MOLM-13 and MV4-11 cell lines, and different NRAS mutations occurring in the FLT3-inhibitor resistant forms of these cell lines. This had been attempted in Chapter 4 using CRISPR Cas9,

however this was not successfully generated. Instead, an over-expression model was used, as indicated by Figure 5.1.

To ensure there was a purely NRAS-over-expressing population of cells being used for each model (rather than a mix of cells with endogenous or exogenous levels of NRAS), transduced cells were selected using puromycin, and then subcloned from a single cell using irradiated HS5s to support their growth at such a low density. Both of these purification methods were also carried out for the CRISPR work, and will be examined in sections 6.14.8-9. Whilst this establishes a population of cells only over-expressing NRAS (or the variant introduced), this does not necessarily result in an equal level of over-expression between each subclone of cells. This could have been better accounted for by determining the Multiplicity of Infection (MOI) of the lentivirus used to transduce these cells, however this was not possible, given the already low rate of transduction (which was similar to that seen with the LeGo-iG derived lentivirus detailed in Chapter 4). This would have determined how many copies of the NRAS-encoding lentivirus would enter cells, so that the over-expression levels could be controlled (Zhang et al., 2004). However, since this was not possible, the relative expression levels of NRAS in each subcloned population were determined by qPCR and Western blotting (Figure 5.1B-C). Future assays were then carried out using clones of medium and high levels of NRAS over-expression which were similar between each mutant examined, to ensure that any differences seen were due to the individual mutant, rather than a significantly greater NRAS expression level itself.

Phenotypic effects of NRAS mutant over-expression has previously been analysed with respect to the NRAS G12V mutant, whereby NRAS G12V was over-expressed in

a doxycycline-inducible manner in the monocytic THP-1 (NRAS G12D heterozygous) cell line. It was seen that a greater level of NRAS G12V over-expression conferred self-renewal capacity, compared to those cells which expressed NRAS G12V at a lower level. In contrast, there was a greater level of apoptosis in the cells expressing a lower level of NRAS G12V, compared to either the wild-type cells, or those highly over-expressing G12V (Kurata et al., 2022). This variation correlates strongly with the concept of the Ras abundance sweet-spot model, as described in (Prior, Hood & Hartley, 2020). Given the increased self-renewal that is typically associated with a greater stemness capacity (Ge, Wang, Zhang, Li, Ye & Jin, 2022), this data suggests potential for a level of drug-resistance conferred by greater NRAS-mutant, or at least NRAS G12V, expression. The difference in expression levels will be explored in Chapter 5 with respect to a wider range of over-expressed NRAS mutants in a NRAS wild-type background, using the tools generated in section 3.7 of this chapter.

6.14.3 *In vitro NRAS* knock-out

A similar lentiviral approach was aimed to be used to knock-out *NRAS* from AML cell lines, this time using CRISPR to maintain the permanence of the knock-out. This involved the design of guide sequences around the start codon of NRAS, which were cloned into a plasmid containing Cas9. Through lentiviral transduction, these would be constitutively expressed in transduced cells, resulting in a permanent knock-out of *NRAS*.

To validate the tools necessary, this was done in HEK293T and HeLa cells. Since CRISPR-Cas9 gene editing relies heavily on guide specificity and efficiency, multiple guide pairs were designed, and tried in transient HEK293T transfections, to assess

their quality. Such work is regularly performed as validation steps, particularly in large screens, as detailed in (Suzuki, Tsukumo, Furihata, Naito & Kohara, 2020). As shown in Figure 3.16A, guide 3 did not sufficiently cut the DNA, since there was only the wild-type gene amplification evident in the agarose gel separation of the PCR product following transfection with guides 1+3 or 2+3. This correlates with the low efficiency scores seen in Table 3.4. Whereas, guides 1, 2 and 4 were deemed a success, given that there was a lower band of smaller DNA length (equal to that which should have been left following the cut). This was confirmed by sequence alignment (Figure 3.16B). These would be taken forward for transduction into AML cell lines.

The edited HEK293T were briefly characterised, by studying their proliferation rate. Whilst over-expression of NRAS mutants did not appear to confer a proliferative effect in HEK293T, knockout of NRAS did confer a significant growth disadvantage. The same pattern was seen in HeLa, which were edited using the same guides. This suggests the reliance on NRAS for proliferation in both of these cell lines, although the HEK293T seem insensitive to over-expression of the NRAS mutants.

Interestingly, *NRAS* knock-out in HEK293T appeared to increase levels of ERK activation. This challenges the concept of the essential nature of NRAS for proliferative signalling. However, ERK regulatory feedback loops and Ras-independent ERK activation pathways could explain this. For example, in keratinocytes, ERK activation was found to occur as a result of calcium signalling (Schmidt et al., 2000). Furthermore, recent work in RASless mouse embryonic fibroblasts (MEFs) has implicated the kinase suppressor of Ras (KSR1 and KSR2) proteins in the Ras-independent activation of ERK. In the case of pharmacological KRAS inhibition,

increased expression of KSR1 led to a decreased effectiveness of the KRAS inhibitor tested. KSR1 protein expression was also seen to be upregulated in AMG510-resistant pancreatic cell lines, compared to the parental cell lines (Paniagua et al., 2022). This implies KSR1 and 2 are able to increase ERK signalling independently

Indeed, the level to which *NRAS* was knocked-out was not determined here. Whilst there was clear evidence of gene editing, further analysis could be undertaken in the future to validate a total knock-out, or at least the level to which NRAS must be silenced/removed for growth to be slowed to an acceptable level, without itself causing an aberrant activation of ERK. As has been previously discussed, there is some evidence suggesting the amount of Ras in a cell can confer different phenotypic effects. Whilst this was examined in terms of over-expression, different levels of decreased NRAS levels may alter signalling and subsequent phenotype (Kurata et al., 2022).

Though it would have been physiologically interesting to investigate the pathways able to promote cell survival (if at all) following NRAS knock-out in AML cell lines, NRAS deletion in patients is rare. Although components required to make AML cell line *NRAS* knock-outs had been generated and some data gleamed from a non-cancer model, this was not taken forward into AML cell lines. This was, in part, due to difficulties in component delivery to AML cell lines, as evidenced in Chapter 4. Instead, the mutant over-expression was focussed on, with mutations rather than deletions more physiologically relevant.

6.14.4 Inducible Cas9

The transcriptionally-inducible nature of the Cas9 gene permits these cells to be widely repurposed as necessary. The restricted expression confers a reduced processing burden to the cell, by limiting continued, excess stress on the cellular intrinsic transcription and translation machinery. As proven in figure 4.3, the concentration of doxycycline used was not toxic to the MV4-11-DR cells, therefore reducing risk of excess death caused in this way. However, previous studies have shown a toxic effect of doxycycline and other tetracycline analogues on leukaemic cell lines, albeit at a greater concentration than any of those used here (Saikali & Singh, 2003; Song, Fares, Maguire, Sidén & Potácová, 2014). Nevertheless, certain pre-apoptotic/cell death pathways could have been induced, which may affect cell phenotype including proliferation rate and stress pathway activation (Wang, Xiang, Zhang & Chen, 2015). In this case, doxycycline was only used to induce Cas9 expression and subsequent editing, and so was only added to cells for 24 h prior to transduction with lentivirus encoding the guide sequence, plus the following 72 h to ensure sufficient transduction and editing. By the time any signalling dynamic assessments would have been carried out by transcriptomic analysis or Western blotting (after cell population subcloning) on the successfully-edited cells, as well as other phenotypic assays, the doxycycline would have been long-removed, and therefore effects would have been abrogated. This is shown in Figure 4.6, where the ERK activation signal is seen to be equivalent in the MV4-11-DR cells treated with either 0 or 6 µg/ml doxycycline. There is no ERK activation in the Cas9 positive control lane, since this control was a lysate from HEK293T constitutively expressing Cas9, and it was proven in Figure 3.13 that HEK293T do not show ERK activation. Moreover, the control (non-transduced) cells in Figure 4.2 were also treated with the same concentration of doxycycline, thereby further accounting for any doxycycline-mediated effects.

6.14.5 Promoter selection

Figure 4.1 highlights the benefit of using the SFFV promoter to facilitate gene expression in haematopoietic cells, with an exceedingly high EGFP transduction efficiency witnessed in a panel of AML cell lines. This supports data from the literature, in which it appears superior to the CMV or *Tet*-inducible promoters that have been used in other plasmids throughout this thesis (Almarza et al., 2007; Winiarska et al., 2017). However, its positioning before the HDR sequence may have been unnecessary. Instead, it may have been more optimal to introduce the HDR template sequence alone in the plasmid, without any promoter, and instead moved the promoter downstream, in front of the *EGFP* CDS (rather than the pre-existing IRES element). The EGFP would remain as a marker for successful transduction, given the inclusion of the guide, scaffold, HDR template sequence and EGFP all in the same plasmid. Nevertheless, given that there was no start codon for the HDR template, risk of unnecessary translation of the HDR template would be minimal.

6.14.6 Guide RNA sequences

A dual guide approach has previously been shown as a means of improving CRISPR-Cas9-mediated editing efficiency, and this was employed in chapter 3 when establishing the *NRAS* knock-out (Figure 3.14 and Figure 3.16) (Mandal et al., 2014). This was not possible in the HDR-editing context, since the editing had to occur over the particular region where the point mutation would occur, and nowhere else. To try to prevent excessive DNA cutting and incorrect repair, the HDR template had silent mutations included around the NRAS D12 edited site to identify edited cells, as well as rendering the guide designed no longer specific for that sequence, preventing

excess cutting. It would not necessarily have been feasible to do this at one or more locations of the genomic sequence, given the risk of excessive DNA damage being detected, thereby causing stress to the cells, potentially resulting in cell death. Furthermore, this would not necessarily have resulted in the desired mutation, since a greater number of off-target cuts increase the risk of repair by the NHEJ repair mechanism, despite the presence of the HDR template. Therefore, whilst cutting using one guide only relies on the guide being highly efficient, which this guide was already deemed not to be using the Doench et al. (2016) score, it seemed to remain the only feasible means of generating the desired mutation.

6.14.7 Promoting homology directed repair

The HDR template used here was >300 bp long, with at least 100 bp of direct homology on either side, as indicated in Figure 4.9. This should have resulted in a high degree of specificity for repair at the desired region, with integration of the desired mutations – both those that would cause the D12G mutation, and those which were silent but would eliminate guide specificity following editing. Effective HDR has been proven with only 40 bp homology arms on either side (Schubert et al., 2021). However, given the presence of different Ras isoforms within the cell, which can exhibit some sequence similarity, larger homology arms were used here to increase specificity for *NRAS.*

Alternative means of improving HDR-mediated CRISPR-Cas9 gene editing have been summarised in (Ferrari et al., 2021). These include the inhibition of the aforementioned

NHEJ repair using small molecules, promoting HDR using key factors bound to the Cas9 protein, as well as cell cycle synchronisation. Such techniques have been employed as a means to increase HDR in HSC editing *ex-vivo,* a notoriously difficult but clinically increasingly essential task. Below is a summary of the potential feasibility for their use in this context, as well as their limitations (Charpentier et al., 2018; Chu et al., 2015; Ferrari et al., 2021; Gutschner, Haemmerle, Genovese, Draetta & Chin, 2016; Jayavaradhan et al., 2019; Maruyama, Dougan, Truttmann, Bilate, Ingram & Ploegh, 2015).

Inhibition of NHEJ-promoting genes was demonstrated by Chu et al. (2015) where KU70, a protein mobilised in the presence of double-stranded breaks (DSBs) as a means of repairing DSBs, and DNA ligase IV were silenced, ultimately increasing HDR-efficiency up to 5-fold, whilst decreasing NHEJ-mediated repair. Such effect was further enhanced (up to 8-fold) by co-expression of adenoviral proteins E1B55K and E4orf6 (Chu et al., 2015; Fell & Schild-Poulter, 2012; Heyer, Ehmsen & Liu, 2010). This was performed using a combination of shRNA oligonucleotides, as well as the small molecule inhibitor (SCR7) to inhibit DNA ligase IV. Whilst this was successful in various human and mouse cell lines, these constructs were generally introduced using transient transfection, a technique which haematological cell lines, such as the MV4-11-DR cell line used here, are not highly amenable to. Instead, it is likely these oligonucleotides would need to be introduced using lentiviral transduction or an alternatively, yet equally cellular stressing method, and so would be unlikely to increase the HDR efficiency to the 66% seen in this paper.

Nevertheless, given that SCR7 is a small molecule inhibitor, there is potential for this to be useful in haematopoietic cell lines. This inhibitor has been shown to be successful in its own right, rather than purely in conjunction with shRNA as detailed previously (Hu et al., 2018). Whilst treatment with SCR7 did increase transduction efficiency, the overall transduction rate remained low. There was a significant decrease in the % of NHEJ-repaired cells, showing that this drug promotes repair by the HDR mechanism, however again this was in single-figure % recombination. Considerably more promising results were seen in other publications, suggesting a potential for cell line differences, with other groups showing up to 19-fold increase in HDR efficiency, after transient transfection and co-treatment with SCR7 (Maruyama, Dougan, Truttmann, Bilate, Ingram & Ploegh, 2015). A second cause for concern regarding the use of SCR7 is the lack of specificity from this drug. It has been shown to inhibit both DNA ligases I and II, to a greater degree than DNA ligase IV (Greco, Matsumoto, Brooks, Lu, Lieber & Tomkinson, 2016). This raises the question of subsequent DNA damaging effects.

Alternative techniques employed as a means of increasing HDR efficiency include manipulation of the cell cycle. As per Heyer, Ehmsen and Liu (2010), HDR is restricted to the G2/S phase. In contrast, NHEJ is the favoured repair pathway for DNA damage detected in G1 phase, although HDR can occur here. This is in part to the higher expression of KU70 and KU80, the DSB-detecting, repair-initiating proteins previously discussed, within G0 and G1, rather than the later stages of the cell cycle (Heyer, Ehmsen & Liu, 2010). Therefore, it is plausible that introduction of the HDR template whilst cells to be edited are in their G2/S phases may increase the chances of editing. Although in the experiments in this thesis the HDR template was presented to the cells

for approximately two full replications (96 h), it may be that any DSBs already introduced by Cas9 had already been repaired by NHEJ, since the cell cycle was not synchronised. In addition to this, it has been proposed that introduction of post-translational modifications of Cas9 whilst Cas9-expressing cells are in G1 phase may further enhance HDR editing efficiency, with its high expression tailored to G2/S phase by tagging it with Geminin (thereby a substrate of the E3 ubiquitin ligase complex APC/Cdh1) so that it is degraded by the proteasome when cells are in G1 phase (Gutschner, Haemmerle, Genovese, Draetta & Chin, 2016). This restricted expression may decrease the likelihood of Cas9 expression and DSBs occurring in G1, which would likely be repaired by NHEJ for the reasons detailed above. Such restricted Cas9 expression was explored in this thesis using a doxycycline inducible plasmid, although this could be further tailored by treating with doxycycline when cells are only in G2/S phase, maximising the opportunity for editing. Cell cycle could also be synchronised for all of the cells being edited, by culturing cells in serum-free media. Nevertheless, manipulation of the cell cycle carries its own risks, particularly since it is NRAS which is the gene to be edited, which is highly involved in cell proliferation.

Charpentier et al., have also manipulated the cell cycle, showing promising effects in various cell lines and iPSCs. This includes maintenance of the cells in the G2 phase by introduction of a Cas9-CtIP fusion protein. Not only is HDR most active in the G2 phase, the phase in which cells are restricted to in the presence of CtIP, but HDR is even further promoted through interaction of CtIP with the MRN protein complex already present in cells. Therefore, the HDR mechanism is even further promoted (Charpentier et al., 2018; Li et al., 2000; You & Bailis, 2010). Nevertheless, as predicted and discussed above, efficiency was considerably dependent on the site of

the guide (and therefore the DSB), which we have previously identified to be non-negotiable in our system.

6.14.8 Puromycin selection

Another key feature of the pCW-Cas9 plasmid that was used here is the puromycin resistance gene contained within it. This allowed for selection of positively-transduced cells, thereby creating an enriched population of cells with the inducible capability to express Cas9. This was vital to increase the chance of successful CRISPR-mediated gene editing, which was further enhanced by subcloning (section 4.3.2.3). Puromycin is a commonly used selective agent, as well as blasticidin, hygromycin and G418 (Geneticin). This drug inhibits protein translation within a cell, by the introduction of premature stop codons. An advantage to puromycin is its quicker action than, for example, hygromycin B or G418 (Geneticin) which must be used over a period of 10-14 days (Vandergaast, 2017). This longer time period increases the likelihood of outgrowth of the undesired cell population, should there be a proliferative advantage. Furthermore, it has been shown that recombinant protein expression following selection with blasticidin or neomycin is decreased compared to cells selected with puromycin or hygromycin (Guo, Fordjour, Tsai, Morrell & Gould, 2021).

As shown in Figure 4.4, puromycin is highly toxic to a wide range of AML cell lines, so resulting in low IC_{50} values (Table 4.1). An even lower concentration of puromycin was used to select cells, given the cells initial vulnerability post-transduction, and the fact they were also going to be subcloned. This would remove a subset of the non-transduced cells, whilst not providing too toxic an environment to the transduced (but

unhealthy) cells of interest, with as few ‘death factors’ are present in the media as possible, which may negatively affect the cell population of interest.

6.14.9 Subcloning of mutated cells

Subcloning on top of a stromal cell layer was used to isolate single populations, as well as growth in methylcellulose, as is demonstrated in Figure 4.8. These two methods were used to provide a more ‘supportive’ environment to the single cells, with their contents mimicking the bone marrow niche somewhat, where these cells would typically thrive. The means by which this happens though differs: one provides chemical support and one physical. The HS5 feeder layer is believed to do this through the secretion of key chemokines, whereas the methylcellulose provides a more physical support to keep small populations of cells that have originated from a single cell in close proximity to each other. Indeed, this concept was presented over 30 years ago by the Eaves group, supporting long term HSC colony forming assays, and is therefore highly applicable to this work (Eaves et al., 1991). Furthermore, it has been shown that irradiated HS5s can also confer a protective bone marrow niche, as has been previously shown for the growth of stem cells (Adamo et al., 2020)(Marensi et al., manuscript in progress).

An alternative method is to use limiting dilution in with cells resuspended in a mix of fresh media, with ‘conditioned media’. This conditioned media is taken from cell cultures of the same cell line, whilst the cells are in their log phase of growth. This ensures the cytokines released by the cells, which are required to sustain growth, are given at the correct dosage to the cells being subcloned – their media composition is the same as would be if they were in normal culture.

Subcloning using the HS5 stromal cell layer support method was beneficial in isolating a highly-expressing population of Cas9 cells, when in the presence of doxycycline (Figure 4.8). This served as a proof of concept for use of this method with the MV4-11-DR cell line. However, this method proved ineffective following delivery of the LeGo-iG-G5-HDR vector to the inducible Cas9 expressing MV4-11-DR cells. The lack of detection of edited cells could be explained by differences in growth rate. As a result of the low transduction efficiency and the low HDR rate within these cells, any edited cells may have been quickly out-competed before screening methods were employed. However, single cell plating and screening >9000 GFP+ cells obtained through FACS sorting was not feasible in such an experimental manner as had been conducted here, to identify an edit at such a low frequency. It is known that cell sorting can also affect cell health, and so this could further have contributed to poor cell survival when growing from a single cell. It could be possible to extract DNA at an earlier stage of the subcloning process to that which was performed here, however this was not seen as a favourable method since the yield after the extraction process would be low, and therefore there may be a risk of poor quality. Furthermore, this would result in removal of >95% of the cells from the already small colony, further putting them under 'single-cell' stress for longer as they re-grow.

It was determined in chapter 3 using the HeLa NRAS mutant over-expression model (section 3.7.2) that there is a difference in the growth rate when NRAS mutants are over-expressed compared to wild-type NRAS, thereby introducing the possibility that the G12D mutation reversal could reduce growth rate. Indeed, given that NRAS G12D is a highly oncogenic mutation and leukaemogenic driver (Hobbs, Der & Rossman,

2016), it could be that cells with NRAS G12 (therefore NRAS WT) only would have a lower proliferative capacity and decreased ability to survive in culture, particularly from the single cell stage, which already provides harsh conditions to cells. It is unlikely that there are no other mutations maintaining a leukaemogenic driver phenotype within the MV4-11-DR cells, given the high heterogeneity and complex mutational landscape attributed with the disease, yet this may provide some insight into experimental limitations. Nevertheless, the detection of *NRAS* knock-outs following editing with guide 5 (and then likely repair by the NHEJ pathway) renders this an unlikely reason, since it was proven in Figure 3.17 that *NRAS* knock-out cells have a significantly decreased proliferative capacity compared to wild-type cells. Ultimately, the efficiency of HDR needs to be improved to increase potential for HDR to be detected in a viable manner.

6.14.10 Identification of successfully edited clones

As is shown in sections 4.3.2.4-6, several methods were applied to screen for successfully mutated cells. This was initially done using basic PCR, with primers designed against the specific silent mutations that should have been introduced following successful editing. However, almost all clones showed a positive result for editing (Figure 4.14), which was highly unlikely to have happened, given the lack of efficient editing commonly associated with HDR-mediated CRISPR-Cas9. Sanger sequencing of positive clones identified in this manner revealed them to be non-edited. This was deemed to be due to a lack of sensitivity of basic PCR, and was therefore superseded by qPCR. Given that this is more sensitive, it was expected that clones with a lower Cq value than the control (non-edited) cells would be more likely to be

edited, since the primer specific to the coding and silent mutations would have more readily bound. There were differences in Cq values, as shown by Figure 4.15, however the 'positive' clones were again found to be NRAS G12D (and therefore non-mutated). Eventually, all clones were sequenced (a subset of which are shown in Figure 4.16), however none carried the correct mutations.

Other identification methods can be employed, including the use of next-generation sequencing (NGS) (Bell, Magor, Gillinder & Perkins, 2014). Despite the high cost associated with this, this can be somewhat scaled up to high throughput, using site-specific and barcoding primers, in multiple PCRs (Bell, Magor, Gillinder & Perkins, 2014).

Overall, although there were some elements which were unsuccessful in this thesis, reasons for performing experiments in the manner in which they were completed were rationale. Certain suggestions from the literature may present future avenues of exploration, but must be approached with caution, given experimental complexity and the available models.

6.14.11 Identification of Pathway Alterations by Western immunoblotting

It has been previously recognised that identification of individual Ras isoforms by Western blotting can be difficult, given the high sequence similarity between isoforms. To mitigate for this, isoform-specific antibodies were selected based on those previously selected in the literature, particularly from the thorough, seminal Waters et al. (2017). Nevertheless, the NRAS antibody remained difficult to visualise, and therefore was used at a much higher concentration to the other antibodies, and was

visualised using ultra-enhanced chemiluminescence reagents (Westar Supernova, Cynagen, Italy).

When looking at signalling and protein abundance changes, the Western blots could have been further verified by densitometry. This would have involved further processing of the images obtained on the ChemiDoc, to normalise the expression between the activated and total protein to the loading control, and assess for changes between cell lines. However, this relies on there being no background artefacts, which is difficult to achieve using the Westar Supernova ECL in some cases, due to its considerably high sensitivity, which may alter the specificity of protein identification (on the grayscale as used in densitometry calculations). Furthermore, whilst the pattern of expression is conserved between samples taken at different times, calculations based on these may be skewed so that data normalisation is difficult. Indeed, data normalisation on a Western blot may not be truly reflective of the pattern shown due to the semi-quantitative quantitation methods, which rely on scientist input for area of interest size etc. Therefore, this was not considered here, though could potentially be in the future. Indeed, alternative methods of determining active protein (such as by intracellular staining and analysis by flow cytometry) could be an option to determine pathway activation, and assess the correlation between transcriptomic abundance and protein activation data.

A further consideration for future work could be the use of cell fractionation prior to Western blotting. This would permit a greater understanding of cell trafficking, which the transcriptomic data presented here suggests is altered in the NRAS-mutant over-expressing cell lines. Indeed, it has previously been described that ERK localisation

can be instrumental in NRAS-mutant cancer, and blockade of ERK trafficking from the cytoplasm to the nucleus can inhibit proliferation (Arafeh et al., 2017; Maik-Rachline, Hacohen-Lev-Ran & Seger, 2019).

6.14.12 Understanding stemness potential

In this thesis, key stem cell markers have been successfully analysed by both transcriptomic profiling, flow cytometry and the methylcellulose-based colony forming assay. It has been apparent that there is some stemness capacity conferred by over-expression of NRAS WT only, and this is not present in the mutant over-expressing cell lines. However, the results thus far are not wholly conclusive, with regards to the full stemness capability and true repopulating capacity.

Work by the Jordan group, amongst others, has analysed the long-term repopulating capacity and associated LSC signature from different AML backgrounds by xenograft and secondary xenograft transplantations in mice. Secondary transplants have been used to identify leukaemic stem cell frequency and properties in a range of AML backgrounds, such as the recent discovery of *HSF1* as an LSC self-renewal driver in MLL-AF9-rearranged AML, as well as to identify drug resistance mechanisms and novel therapeutic targets within the LSC (Dong et al., 2022; Jones et al., 2020). In patient-derived xenograft (PDX) models, xenografts from patients with a more favourable prognosis (determined by the patient's karyotype) were less likely to engraft in the NSG mice used in this study and had a lower leukaemia initiating cell (LIC) burden. This LIC burden has been previously associated with a stem cell gene signature, and poorer patient overall survival (Eppert et al., 2011; Griessinger et al., 2016; Pearce et al., 2006). Whilst the models generated and used in this thesis are

cell line derived and therefore do not contain a mixed population of LICs as well as bulk AML cells, it would be interesting to examine the initiating capacity of these cells *in vivo*, and assess the correlation of NRAS WT over-expression with the stem cell gene signature. NRAS mutations are already associated with a more favourable prognosis as has been previously described in section 1.2.2, however NRAS WT over-expression is so far less studied.

6.14.13 Modelling the true leukaemic context

Throughout this thesis, NRAS-mutant AML has been studied in a monoculture, cell line context. This has proven useful to manipulate cells in a myriad of ways, including through exposure to drug concentrations and study of the leukaemic cell signalling. However, with the development of better co-culture systems, there is the potential to transition from this monoculture model to a more appropriate multi-cellular context. This co-culture system has started to be used in this thesis, with HS5 stromal cells used to support the MOLM-13 and MV4-11 cells growing from a single-cell stage, however could be expanded. This could be done using co-culture of multiple cell lines, or indeed co-culture of different cell types isolated from patient samples. It would, for example, permit the exploration of cytokine-induced signalling from the bone marrow niche, as was initially introduced in section 1.2.3. Indeed, the cytokine profile was shown to be altered in the MOLM-13-NRAS-Q61K cell line used throughout this thesis, and so it would be interesting to examine the alterations to this signalling in a system more similar to the leukaemic niche.

Indeed, it is well-understood that the leukaemic niche can manipulate the progression of leukaemia, such as through mitochondrial transfer from bone marrow stromal cells

within the niche to the leukaemic blasts. This increases proliferative capacity and survival of AML, through PGC-1α signalling. This however, can only happen following oxidative stress imparted on the stroma by the AML blasts (Marlein et al., 2018). In this way, it appears that the AML blasts rely on the stroma to survive.

These co-culture studies are important not purely for an understanding of leukaemic biology, but also for an understanding of drug efficacy, and high throughput compound screening programmes. For example, co-culture systems are starting to be used to identify drug resistance mechanisms, since the resistance driver could be stroma derived. In one recent study, resistance was conferred by the stroma to a range of small molecule Ras pathway inhibitors and chemotherapeutics such as cytarabine and doxorubicin (Herbst et al., 2023). Not only does this suggest previously unconsidered mechanisms of drug resistance, but moving forward, it would be interesting to test lead compounds within these co-culture systems, to better predict the risk of resistance in patients.

6.15 Final conclusions

The work completed throughout this thesis provides a comprehensive overview of the role which NRAS mutations can play in Acute Myeloid Leukaemia. As hypothesised at the beginning of this project, different mutations can confer different genotypic and phenotypic changes. This is true for both mutations occurring at different hotspots, as well as different amino acid substitutions at the same codon. The models generated here mostly recapitulated patient data, whilst suggesting other avenues to pursue further.

Future experimental work based on this thesis would involve optimisation of the CRISPR work to compare genotype and phenotype alterations in different models. CRISPR-Cas9 gene editing could be somewhat more of a higher fidelity representation of clinical AML, since there are perhaps more unknowns (particularly protein level) associated with the over-expression model. Indeed, a deeper probing of targets identified in the transcriptomic data here would provide more understanding of the feasibility of new therapeutic targets. Moreover, using techniques developed here, this work could be expanded to a greater panel of AML-relevant NRAS mutations, to further understand the picture of NRAS in AML.

The conclusions that can perhaps provide the most novel clinical and translational benefit come from the identification of pathways and genes/proteins that can be manipulated in a range of NRAS-mutant backgrounds, and not affected by NRAS wild-type presence. Therefore, pharmacological targeting of these targets can provide a less toxic but cross-patient approach. Nevertheless, in the years to come it would be most beneficial to screen AML patients at a deeper level for NRAS mutations (rather than purely at relapse), particularly given the rapid development of isoform and mutation specific Ras-targeting therapeutics.

Appendices

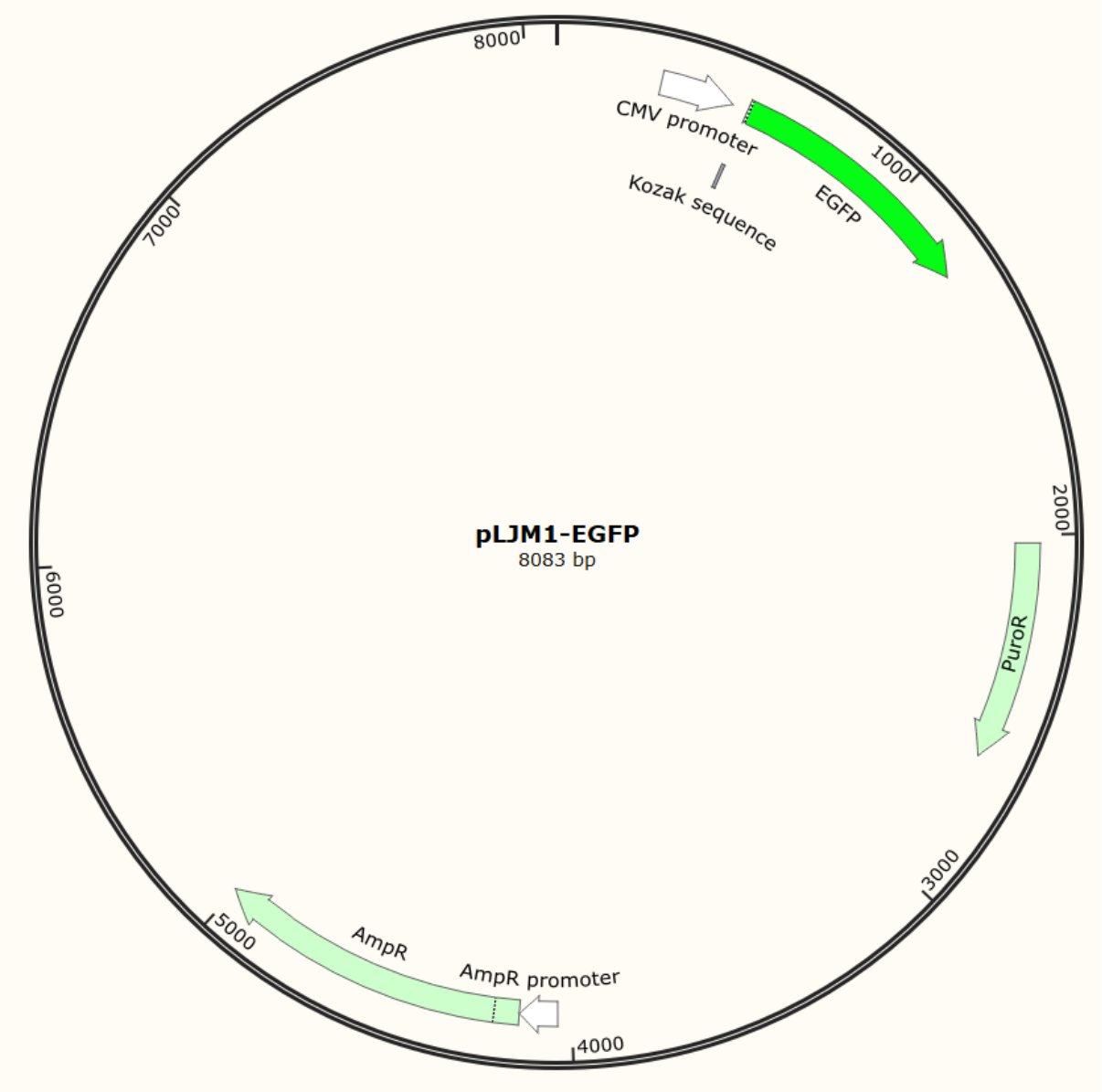

Appendix 1 pLJM1-EGFP plasmid purchased via AddGene (Cat. No. 19319). Plasmid was used as a transfection control plasmid and as the backbone for the over-expression vectors.

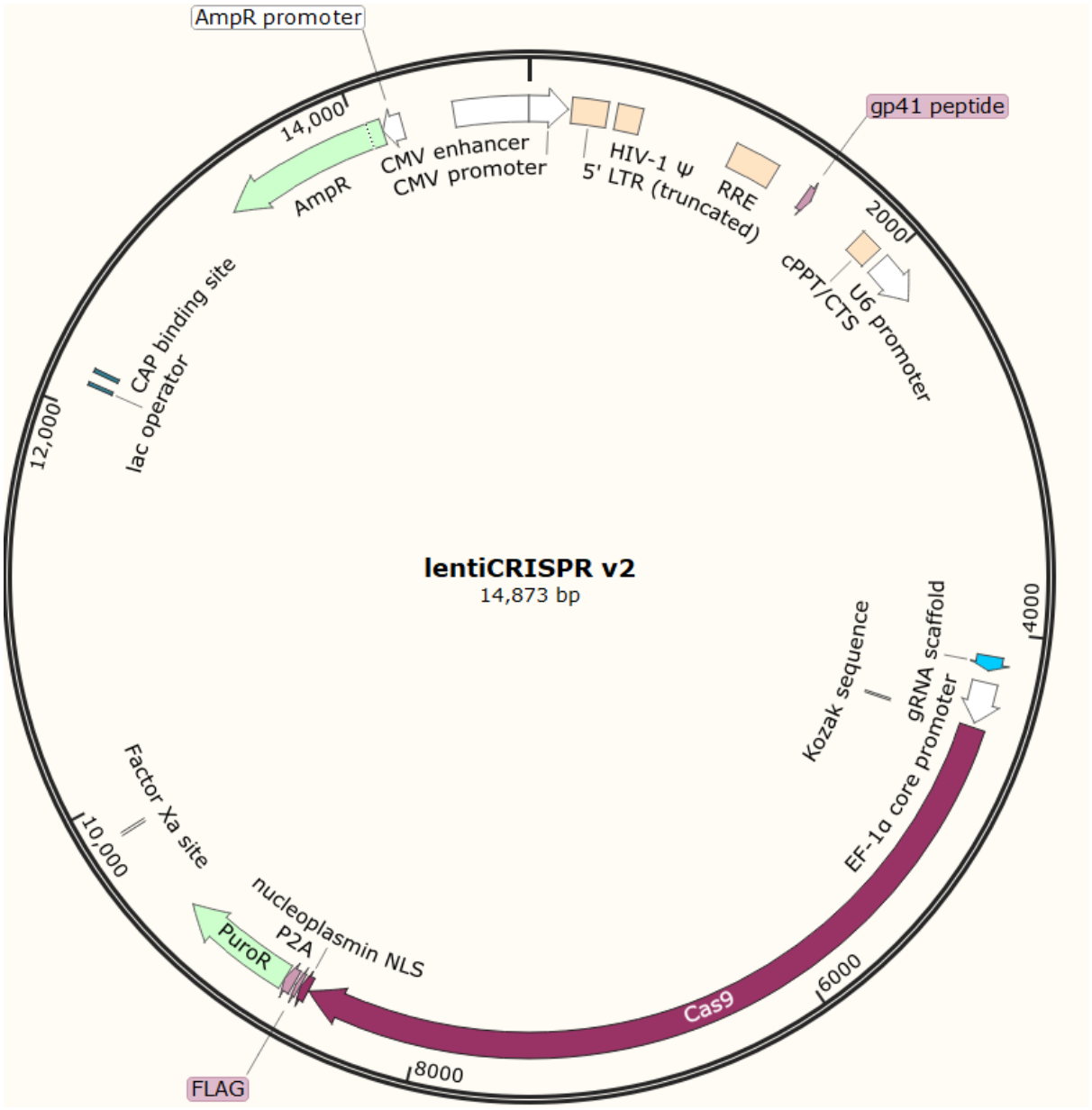

Appendix 2 Lenti-CRISPR-V2 plasmid purchased via AddGene (Cat. No. 52961). Plasmid was used to either transiently (transfection) stably (lentiviral transduction) express the Cas9 protein and a guide RNA simultaneously in various cell lines.

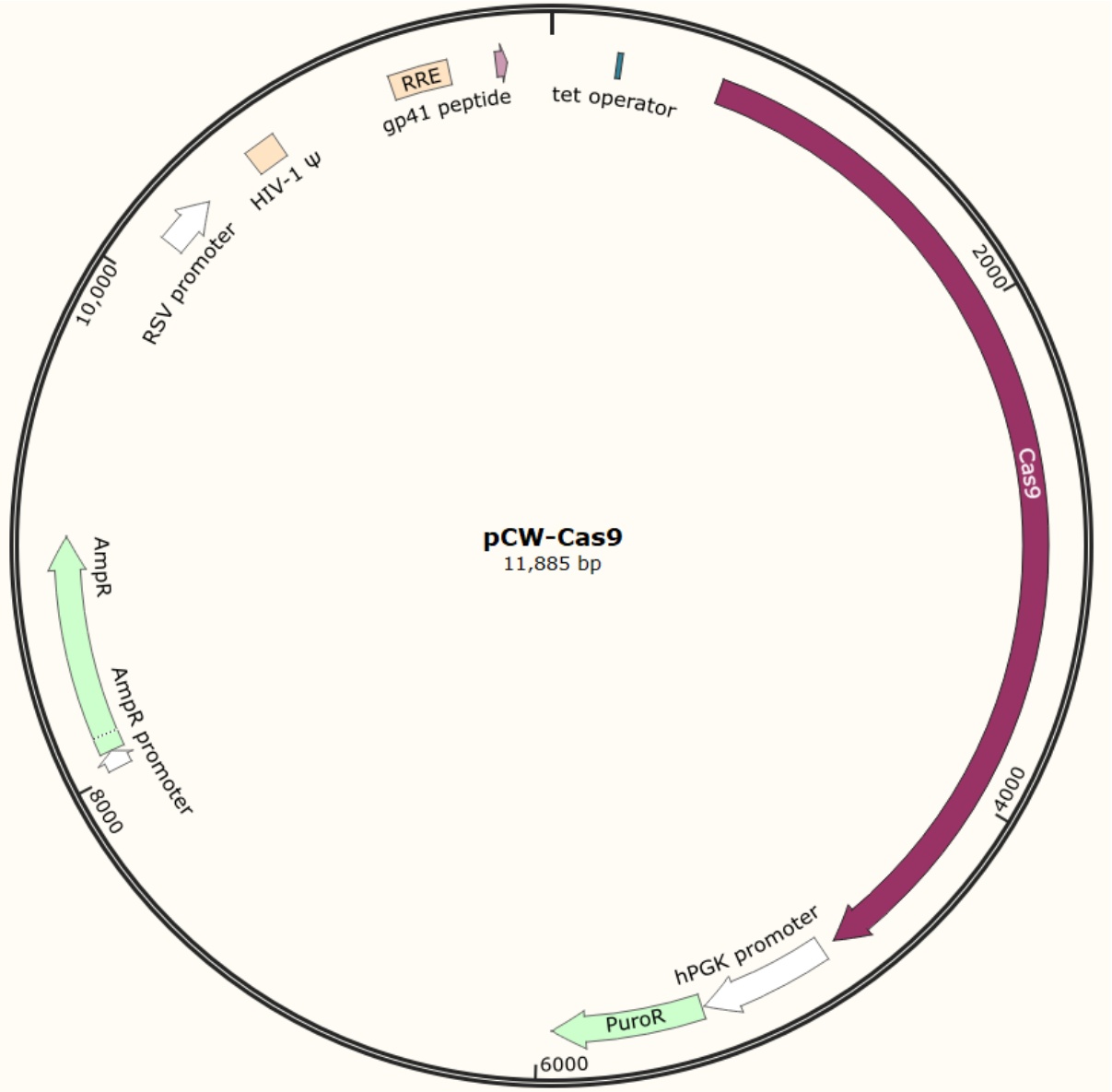

Appendix 3 pCW-Cas9 plasmid purchased via AddGene (Cat. No. 50661). Plasmid was used to stably insert the Cas9 gene into AML cell lines, which could be subsequently, selectively transcribed and thus translated in the presence of doxycycline, and then to induce gene editing in a guide RNA.

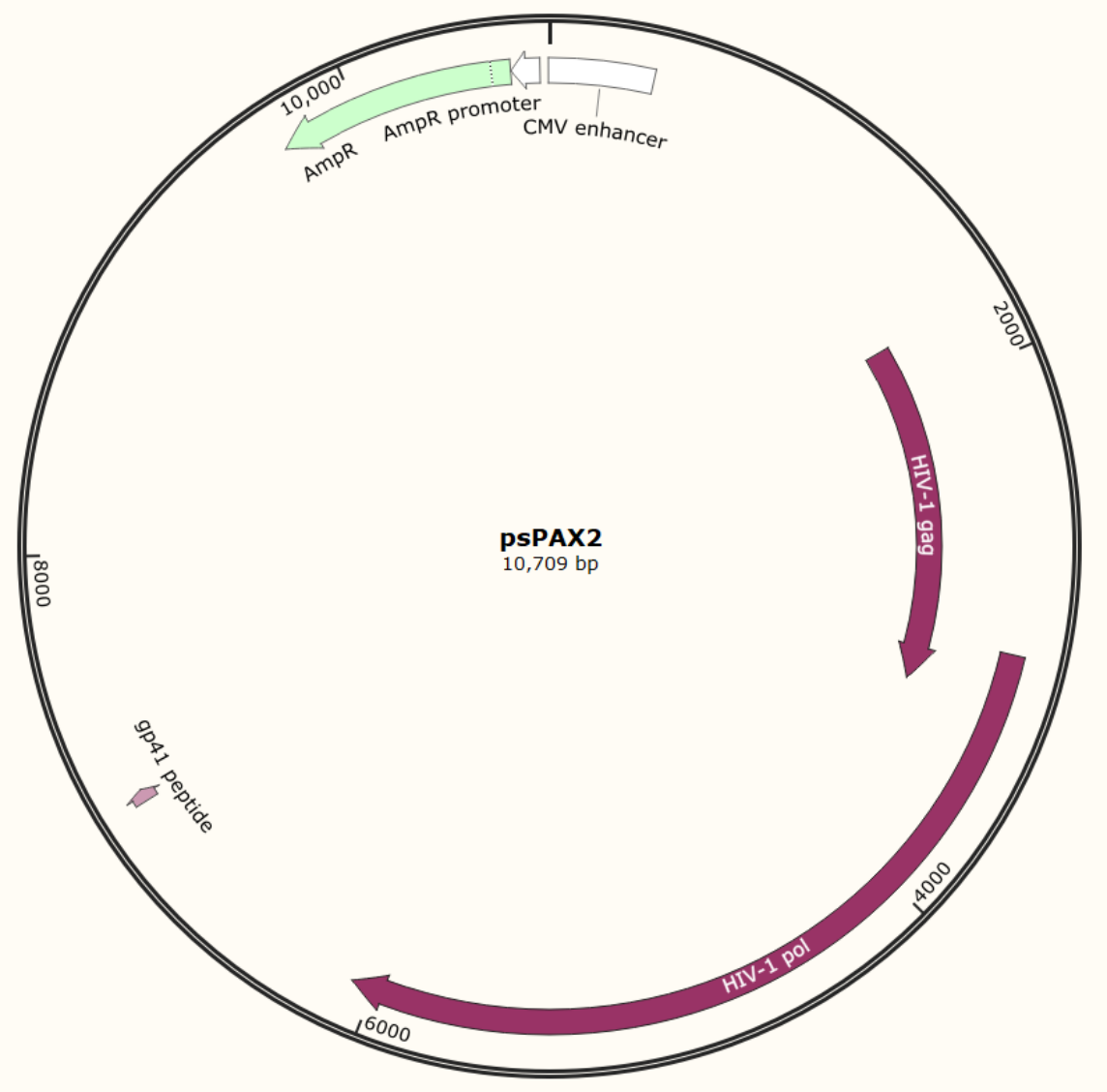

Appendix 4 psPax2 plasmid purchased via AddGene (Cat No. 12260). Plasmid was used to generate lentivirus, since it encodes the genes HIV-1 ψ and the gp41 peptide used for viral packaging.

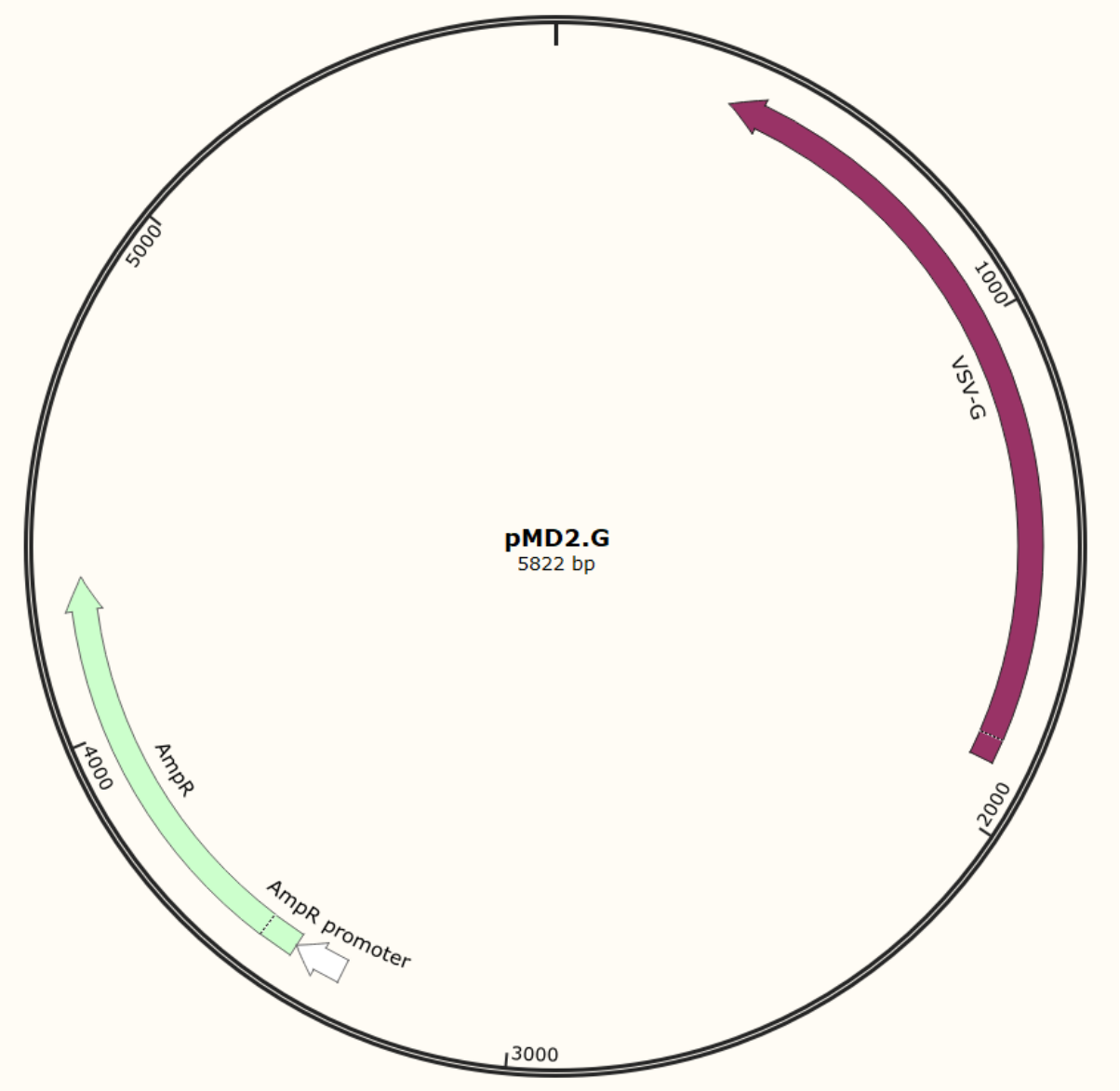

Appendix 5 pMD2.G plasmid purchased via AddGene (Cat. No. 12259). Plasmid was used to generate lentivirus, since it encodes the *VSVG* gene used for generation of a viral envelope.

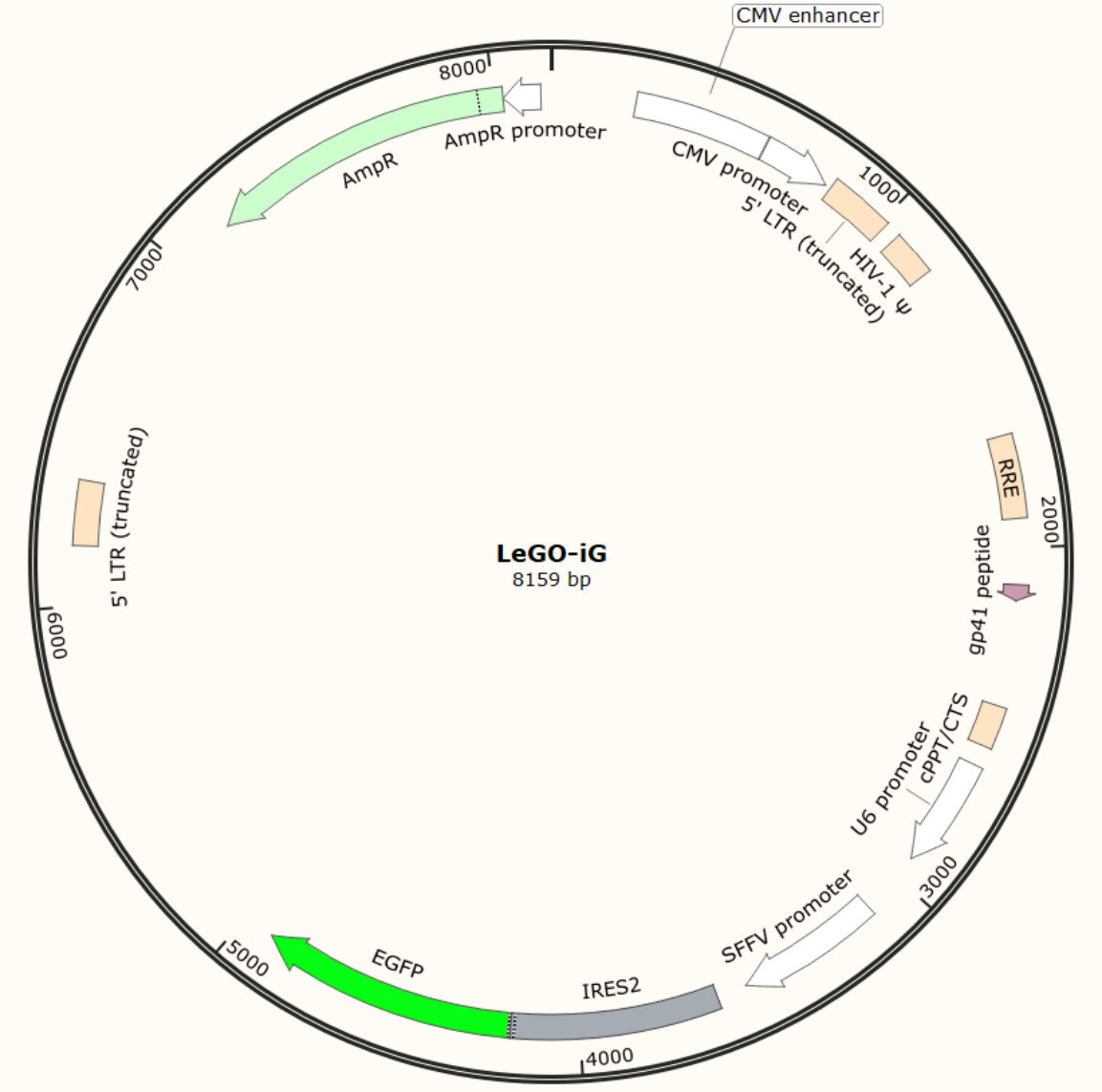

Appendix 6 LeGo-iG plasmid purchased via AddGene (Cat. No. 27358). Plasmid was used to deliver the guide RNA and HDR template to the MV4-11-DR-inducible Cas9 cell line, since it encodes the guide scaffold, U6 promoter and EGFP used for selection of positively transduced cells.

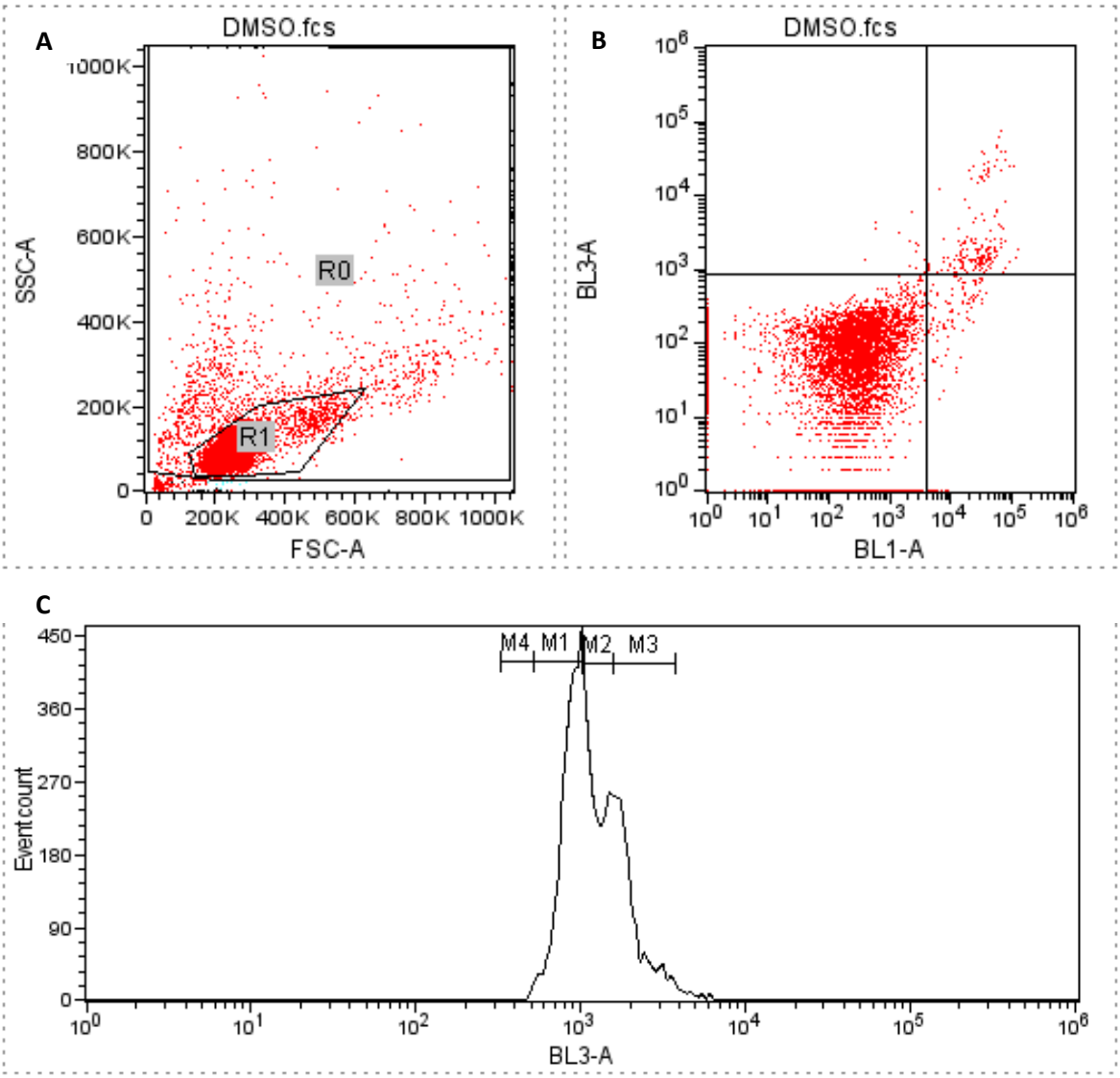

Appendix 7 Model flow cytometry plot indicating approximate gating for apoptosis (Appendix 7B) and cell cycle staging (Appendix 7C). A) FSC-A and SSC-A values were plotted initially to gate cell population of interest (non-debris). R0 represents all cells without debris. R1 represents typically healthy cells of the appropriate size (measured by FSC-A) and granularity (SSC-A). **B)** Annexin-V-FIT-C staining of externalised phosphatidylserine was quantified for those cells within the R0 population using the BL1-A laser/axis, and Propidium Iodide staining of DNA was quantified for the same population using the BL3-A laser/axis. **C)** 7AAD staining of DNA in cells in R0 was quantified using the BL3-A laser/axis, plotted on a histogram, using DNA quantity as a marker of cell cycle staging. Marker M1 represents G1 phase. Marker M2 represents S phase. Marker M3 represents G2/M phase. Marker M4 represents G0 phase.

Appendix 8 Transcriptomic Alterations in AML-relevant pathways in NRAS over-expression models

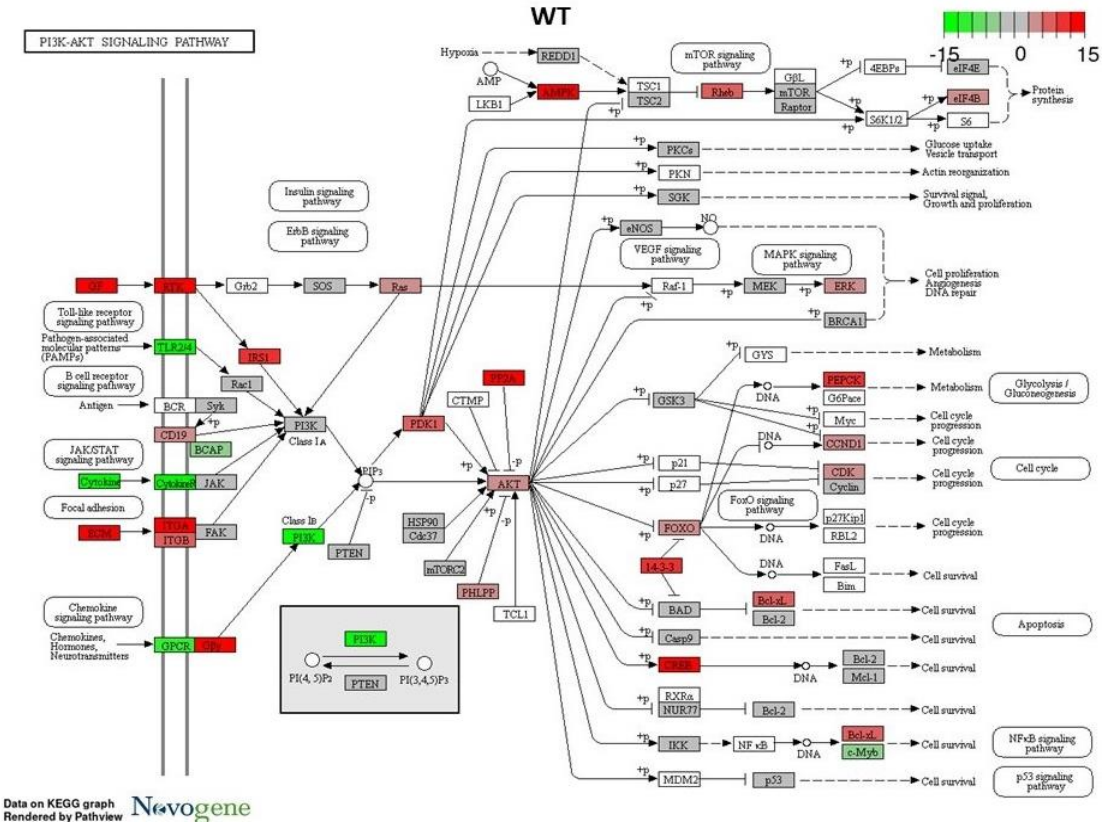

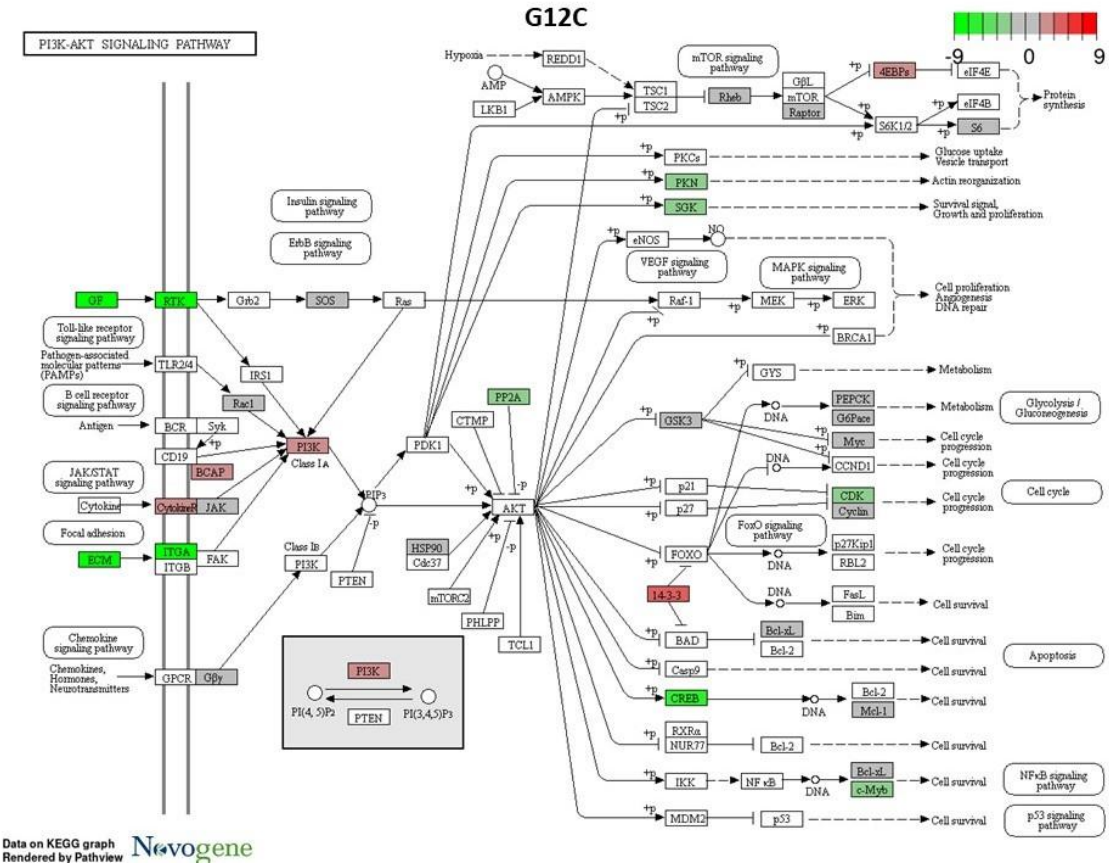

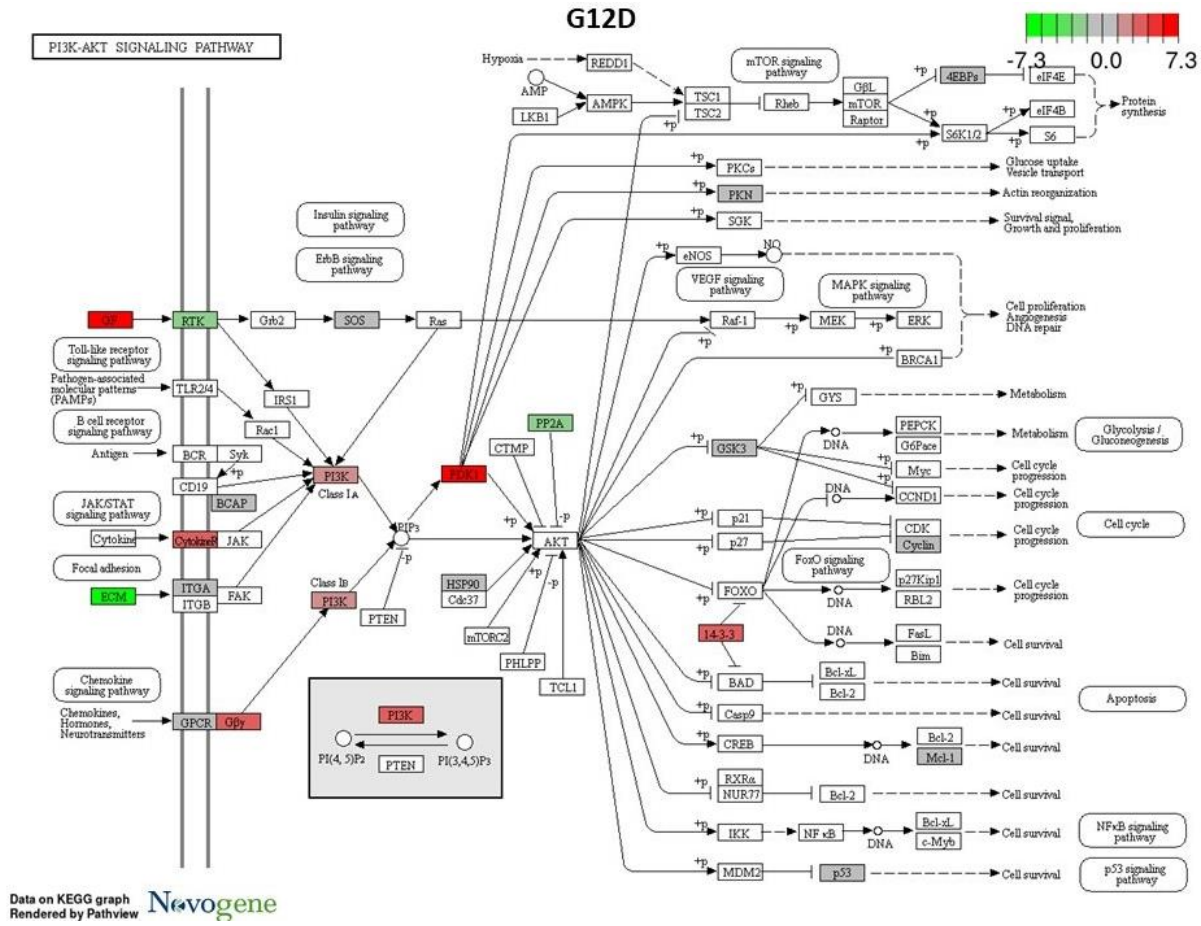
G12D
PI3K-AKT SIGNALING PATHWAY
-7.3
0.0
7.3
Data on KEGG graph
Rendered by Pathview
Novogene

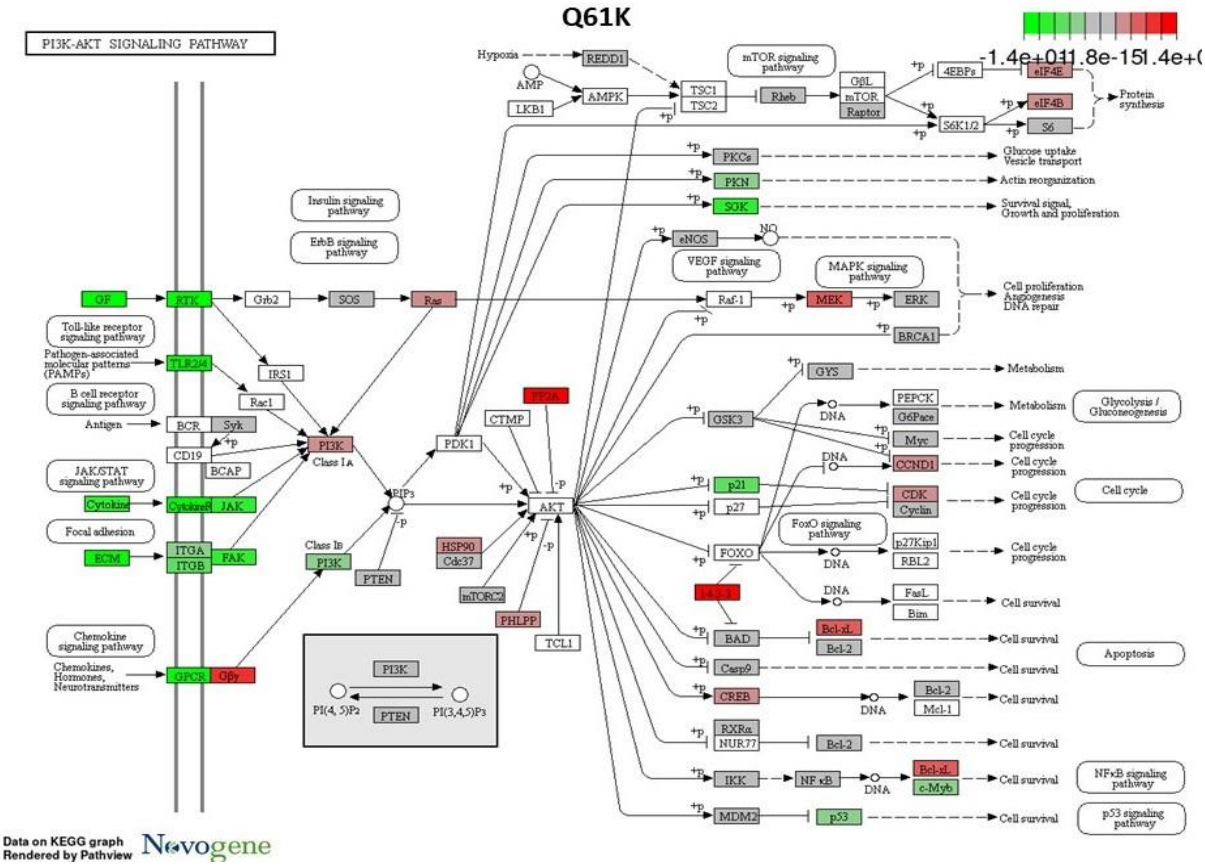
Q61K
PI3K-AKT SIGNALING PATHWAY
Data on KEGG graph
Rendered by Pathview
Novogene

Appendix Figure 8.1. KEGG Pathway mapping of the PI3K-AKT pathway in MOLM-13 NRAS-overexpressing cell lines. Map determined using transcriptomic data. Each NRAS over-expressing MOLM-13 cell line is shown here, with the transcriptomic profile compared to the MOLM-13 control cell line. Red indicates upregulated gene expression, green represents down-regulated gene expression.

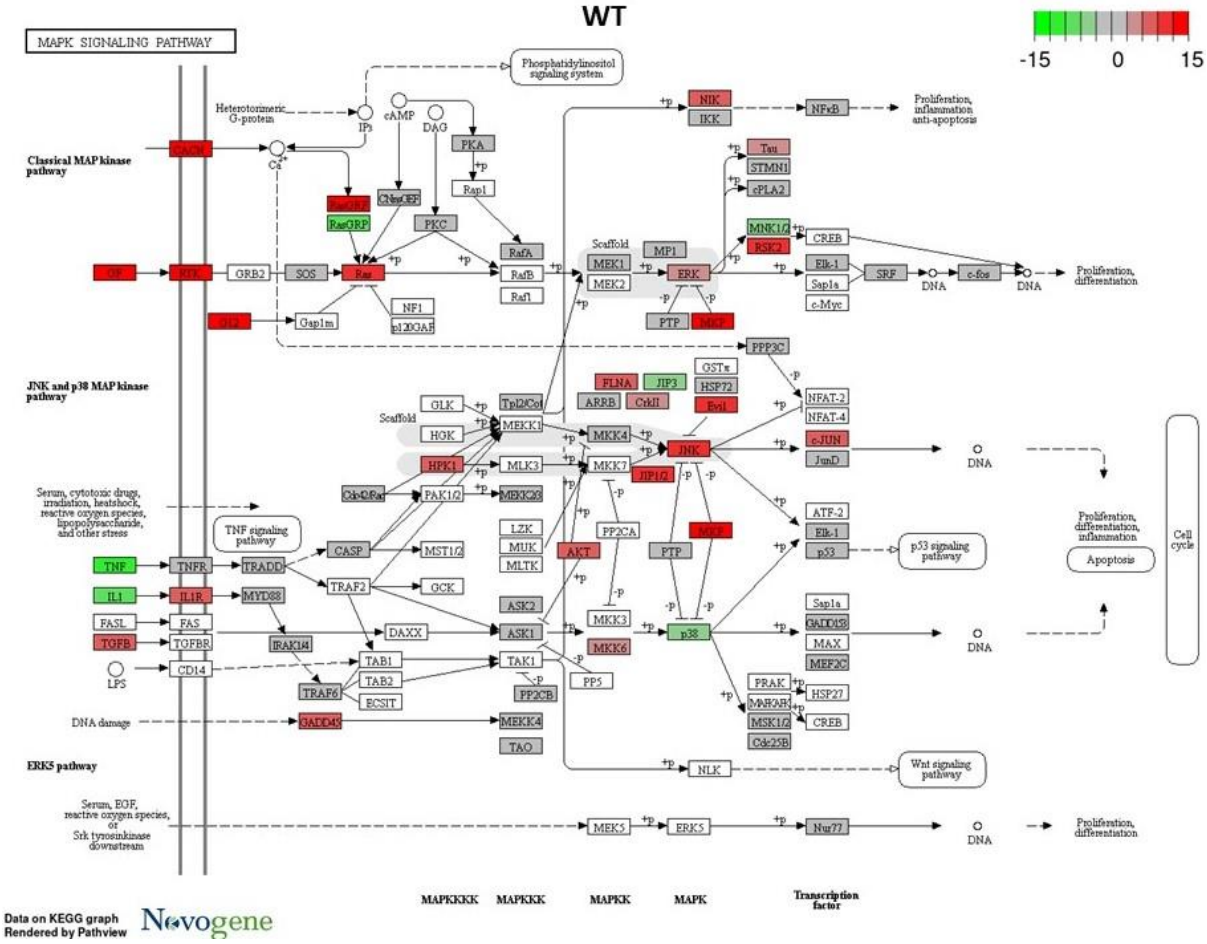

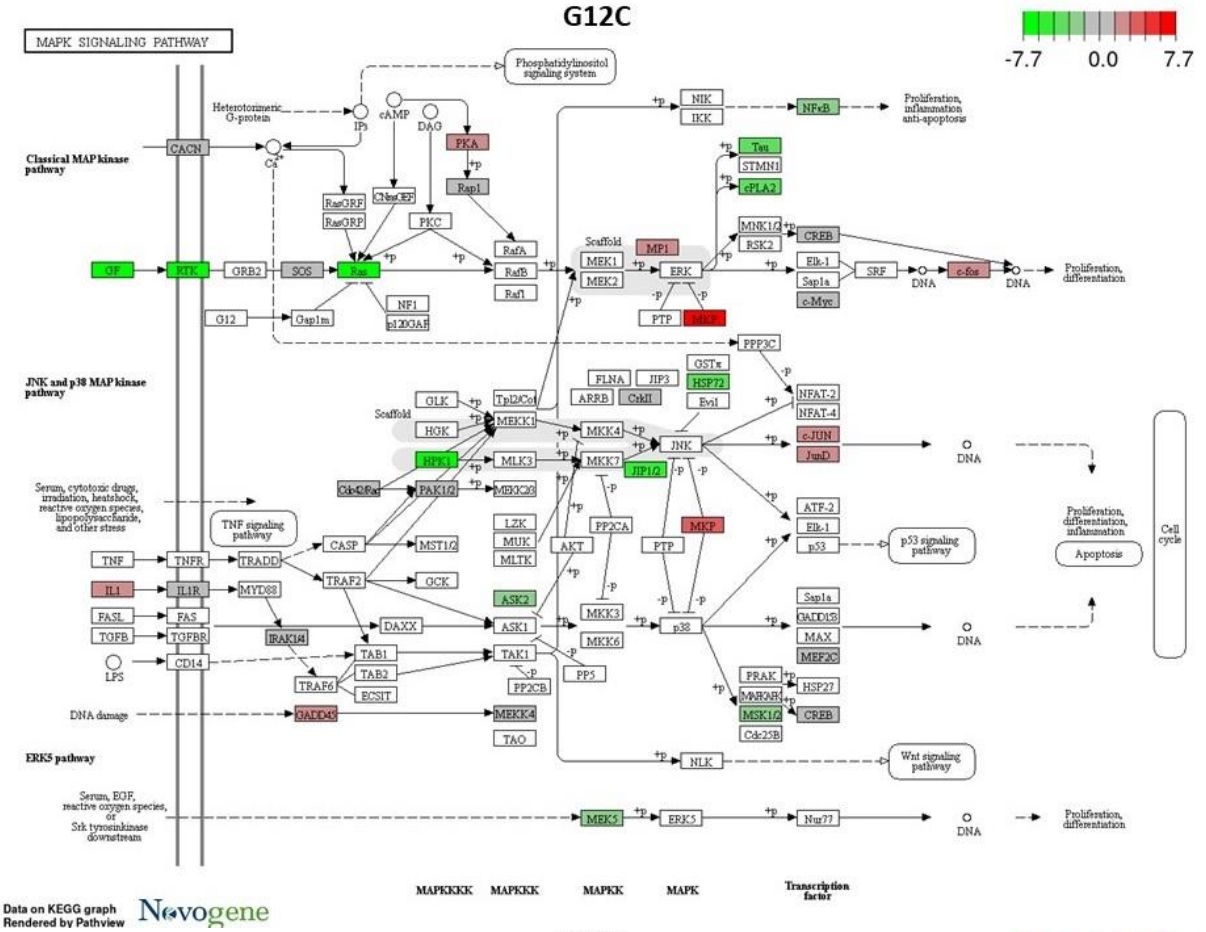
G12C
-7.7
0.0
7.7
MAPK SIGNALING PATHWAY
Phosphatidylinositol signaling system
Heterotrimeric G-protein
cAMP
DAG
IP3
PKA
NIK
IKK
NFκB
Proliferation, inflammation anti-apoptosis
Classical MAP kinase pathway
CACN
Ca2+
Rap1
RasGRF
RasGRP
CNrasGEF
PKC
Tau
STMN1
cPLA2
MNK1/2
RSK2
CREB
Scaffold
MP1
MEK1
MEK2
ERK
Elk-1
Sap1a
c-Myc
SRF
c-fos
DNA
Proliferation, differentiation
GF
RTK
GRB2
SOS
Ras
RafA
RafB
Raf1
NF1
p120GAP
G12
Gap1m
PTP
MKP3
PPP3C
GSTπ
FLNA
JIP3
HSP72
ARRB
CrkII
Evi1
NFAT-2
NFAT-4
JNK and p38 MAP kinase pathway
GLK
Tpl2/Cot
Scaffold
MEKK1
HGK
MKK4
JNK
c-JUN
JunD
HPK1
MLK3
MKK7
JIP1/2
Cdc42/Rac
PAK1/2
MEKK2/3
ATF-2
Elk-1
p53
Serum, cytotoxic drugs, irradiation, heatshock, reactive oxygen species, lipopolysaccharide, and other stress
TNF signaling pathway
LZK
MUK
MLTK
PP2CA
MKP
AKT
PTP
p53 signaling pathway
Proliferation, differentiation, inflammation
Apoptosis
Cell cycle
TNF
TNFR
TRADD
CASP
MST1/2
TRAF2
GCK
IL1
IL1R
MYD88
ASK2
Sap1a
GADD153
MAX
MEF2C
FASL
FAS
TGFB
TGFBR
IRAK1/4
DAXX
ASK1
MKK3
p38
MKK6
LPS
CD14
TAB1
TAB2
TAK1
PP5
TRAF6
ECSIT
PP2CB
PRAK
MAPKAPK
HSP27
MSK1/2
CREB
DNA damage
GADD45
MEKK4
Cdc25B
TAO
ERK5 pathway
NLK
Wnt signaling pathway
Serum, EGF, reactive oxygen species, or Src tyrosinkinase downstream
MEK5
ERK5
Nur77
MAPKKKK
MAPKKK
MAPKK
MAPK
Transcription factor
Data on KEGG graph
Rendered by Pathview
Novogene

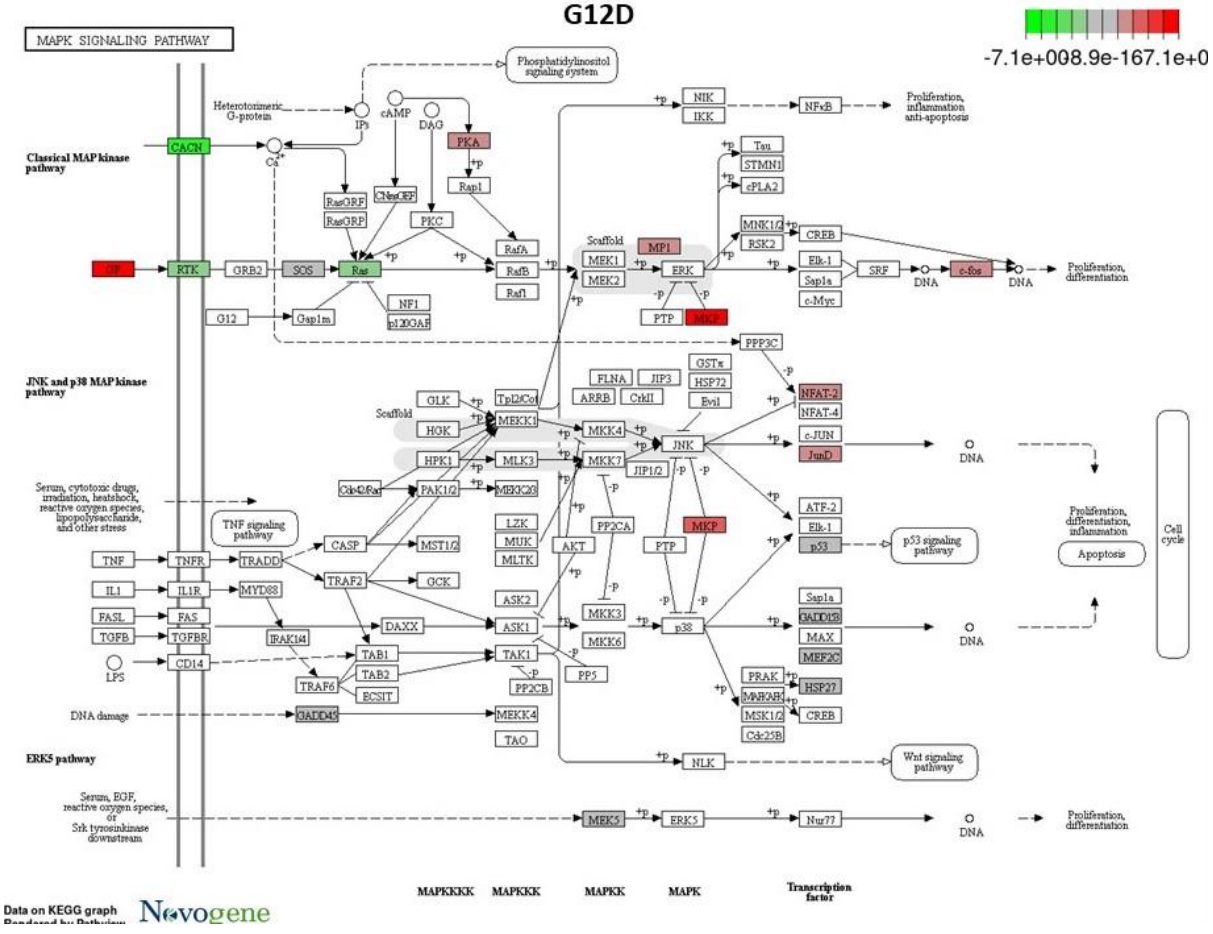
G12D
-7.1e+008.9e-167.1e+0
MAPK SIGNALING PATHWAY
Phosphatidylinositol signaling system
Heterotrimeric G-protein
cAMP
DAG
IP3
PKA
NIK
IKK
NFκB
Proliferation, inflammation anti-apoptosis
Classical MAP kinase pathway
CACN
Ca2+
Rap1
RasGRF
RasGRP
CNrasGEF
PKC
Tau
STMN1
cPLA2
MNK1/2
RSK2
CREB
Scaffold
MP1
MEK1
MEK2
ERK
Elk-1
Sap1a
c-Myc
SRF
c-fos
DNA
Proliferation, differentiation
GF
RTK
GRB2
SOS
Ras
RafA
RafB
Raf1
NF1
p120GAP
G12
Gap1m
PTP
MKP3
PPP3C
GSTπ
FLNA
JIP3
HSP72
ARRB
CrkII
Evi1
NFAT-2
NFAT-4
JNK and p38 MAP kinase pathway
GLK
Tpl2/Cot
Scaffold
MEKK1
HGK
MKK4
JNK
c-JUN
JunD
HPK1
MLK3
MKK7
JIP1/2
Cdc42/Rac
PAK1/2
MEKK2/3
ATF-2
Elk-1
p53
Serum, cytotoxic drugs, irradiation, heatshock, reactive oxygen species, lipopolysaccharide, and other stress
TNF signaling pathway
LZK
MUK
MLTK
PP2CA
MKP
AKT
PTP
p53 signaling pathway
Proliferation, differentiation, inflammation
Apoptosis
Cell cycle
TNF
TNFR
TRADD
CASP
MST1/2
TRAF2
GCK
IL1
IL1R
MYD88
ASK2
Sap1a
GADD153
MAX
MEF2C
FASL
FAS
TGFB
TGFBR
IRAK1/4
DAXX
ASK1
MKK3
p38
MKK6
LPS
CD14
TAB1
TAB2
TAK1
PP5
TRAF6
ECSIT
PP2CB
PRAK
MAPKAPK
HSP27
MSK1/2
CREB
DNA damage
GADD45
MEKK4
Cdc25B
TAO
ERK5 pathway
NLK
Wnt signaling pathway
Serum, EGF, reactive oxygen species, or Src tyrosinkinase downstream
MEK5
ERK5
Nur77
MAPKKKK
MAPKKK
MAPKK
MAPK
Transcription factor
Data on KEGG graph
Novogene

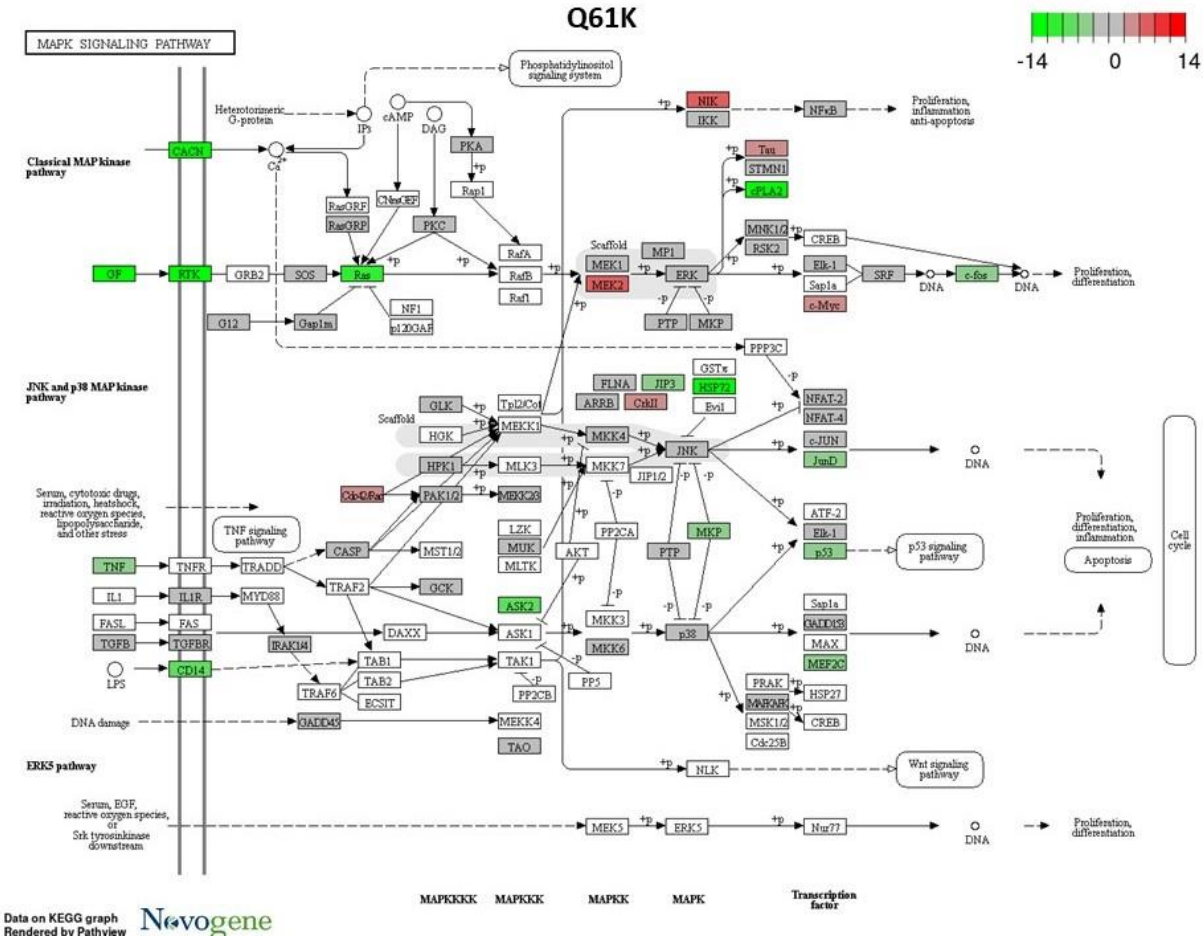

Appendix Figure 8.2. KEGG Pathway mapping of the MAPK pathway in MOLM-13 NRAS-overexpressing cell lines. Map determined using transcriptomic data. Each NRAS over-expressing MOLM-13 cell line is shown here, with the transcriptomic profile compared to the MOLM-13 control cell line. Red indicates upregulated gene expression, green represents down-regulated gene expression.

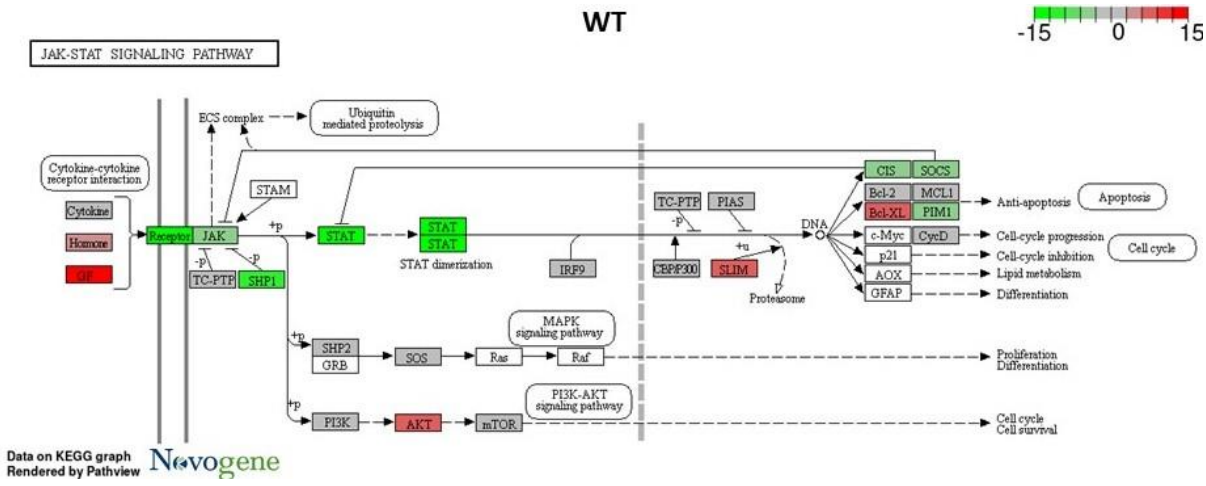

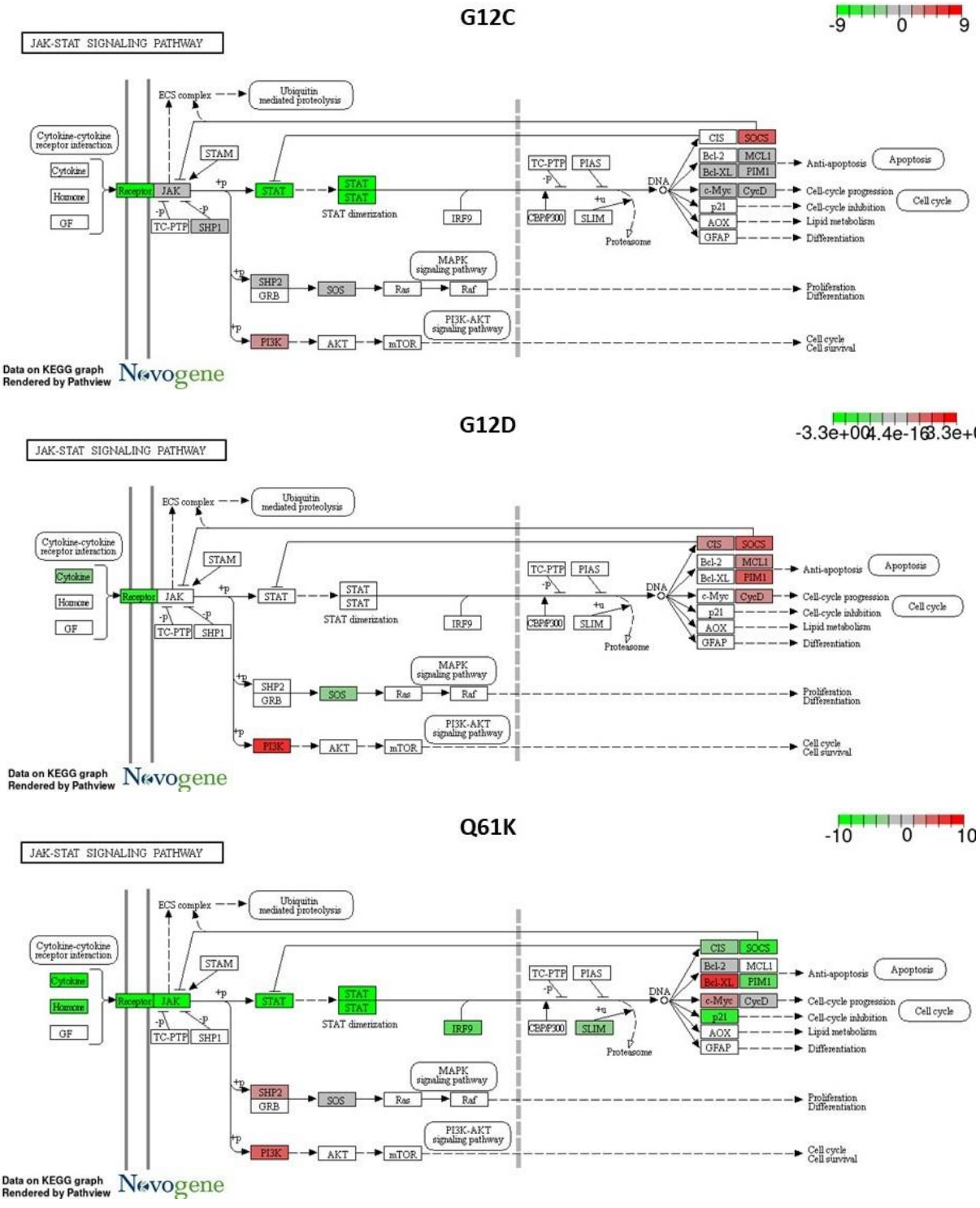

Appendix Figure 8.3. KEGG Pathway mapping of the JAK-STAT pathway in MOLM-13 NRAS-overexpressing cell lines. Map determined using transcriptomic data. Each NRAS over-expressing MOLM-13 cell line is shown here, with the transcriptomic profile compared to the MOLM-13 control cell line. Red indicates upregulated gene expression, green represents down-regulated gene expression.

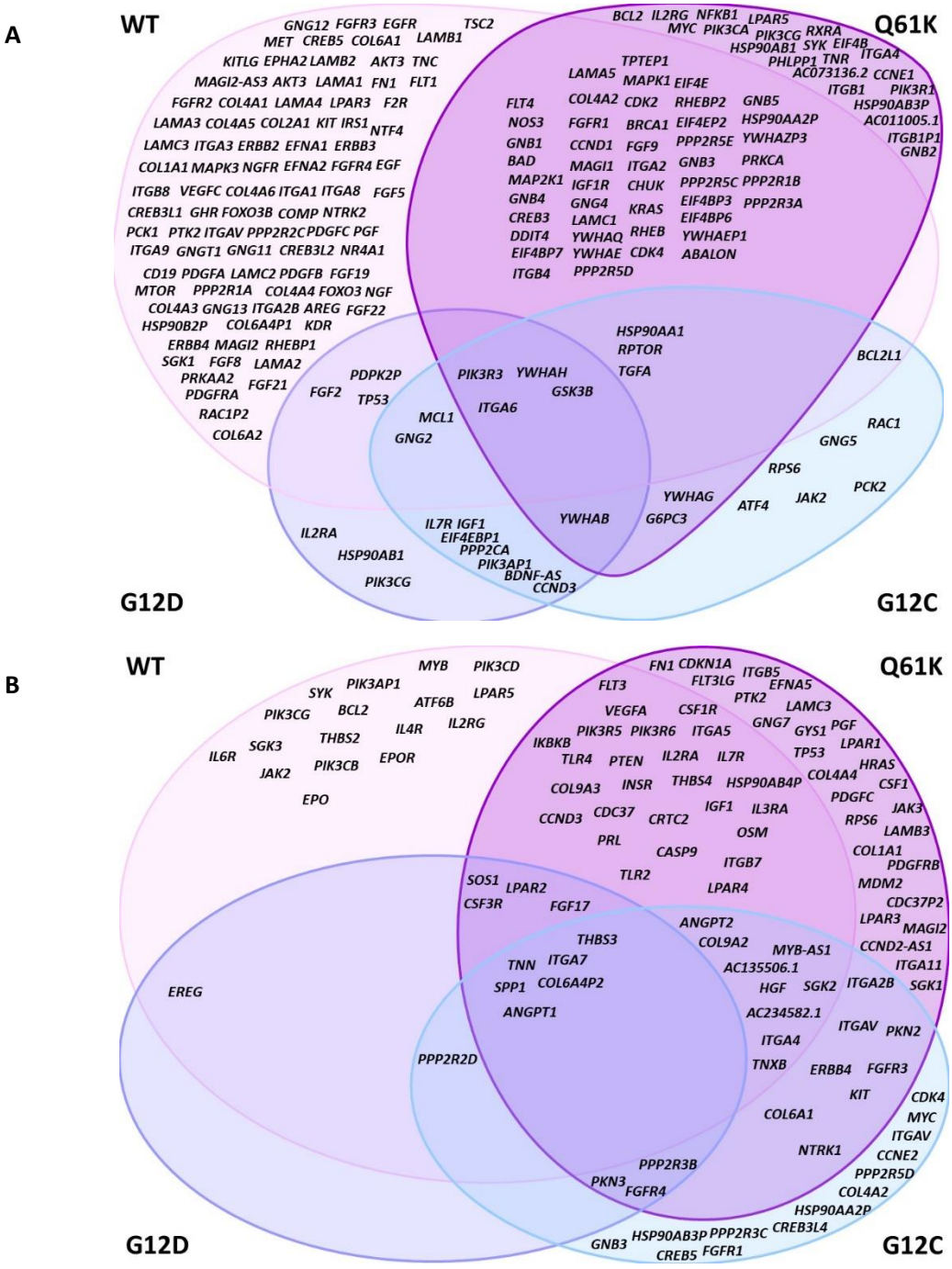

Appendix Figure 8.4. Stratification of genes altered within the PI3K-AKT pathway in MOLM-13 NRAS-overexpressing cell lines. A) Upregulated genes. **B)** Downregulated genes. Gene expression compared to MOLM-13 control cells.

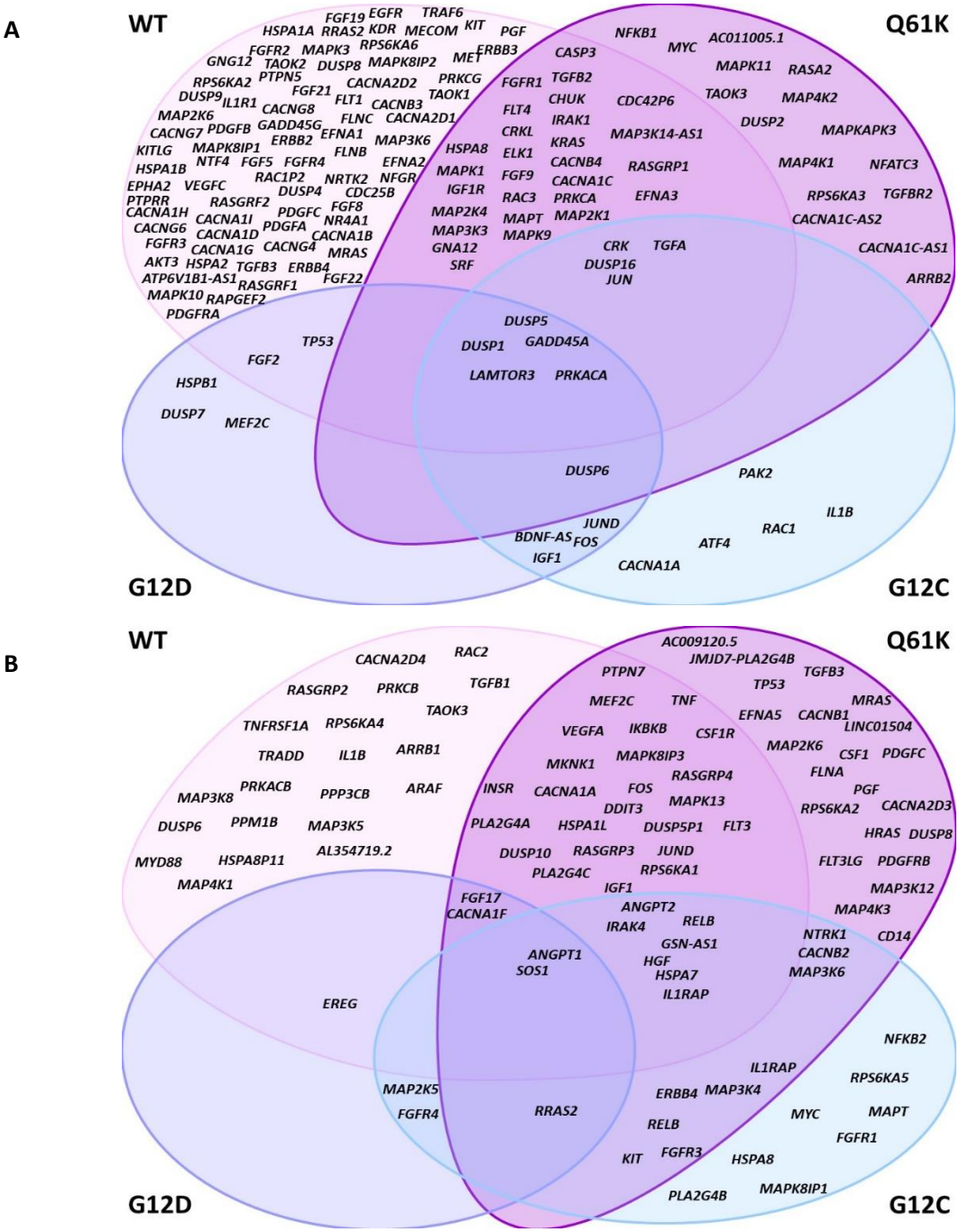

Appendix Figure 8.5. Stratification of genes altered within the MAPK pathway in MOLM-13 NRAS-overexpressing cell lines. A) Upregulated genes. **B)** Downregulated genes. Gene expression compared to MOLM-13 control cells.

A

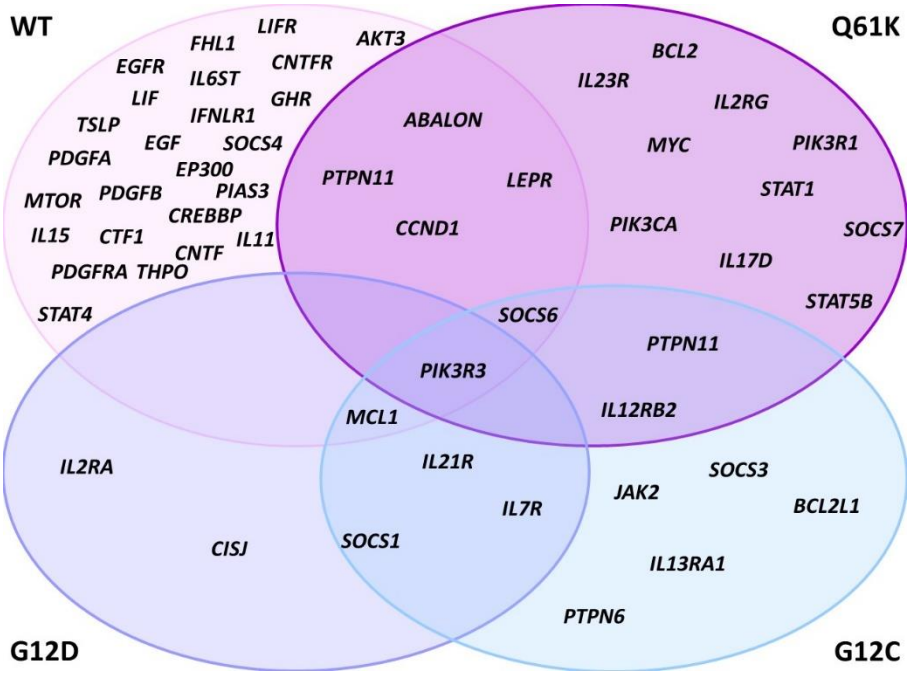

B

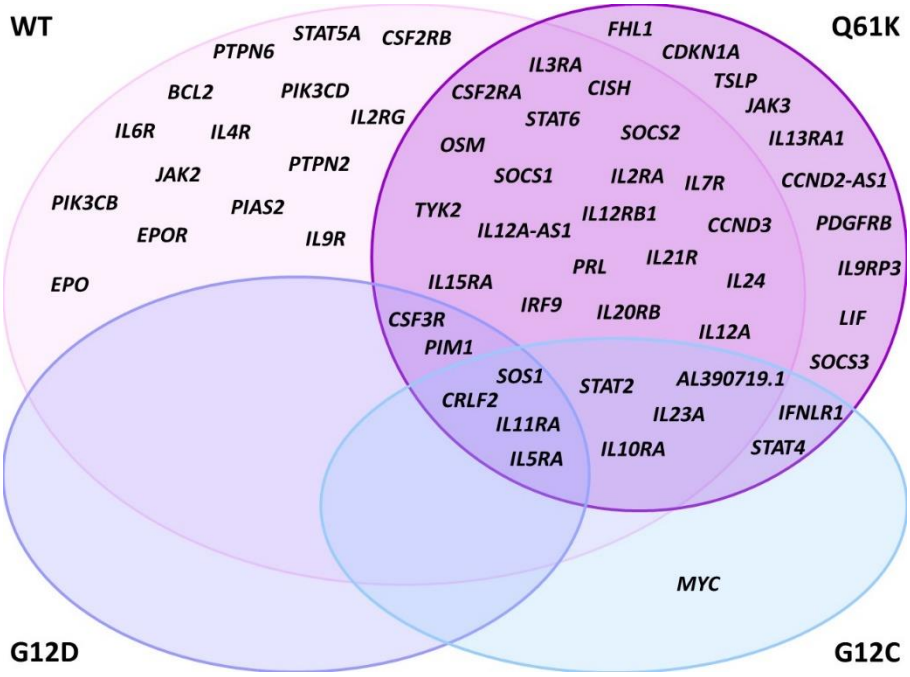

Appendix Figure 8.6. Stratification of genes altered within the JAK-STAT pathway in MOLM-13 NRAS-overexpressing cell lines. A) Upregulated genes. **B)** Downregulated genes. Gene expression compared to MOLM-13 control cells.

Appendix 9 Alterations to Oxidative Phosphorylation.

A

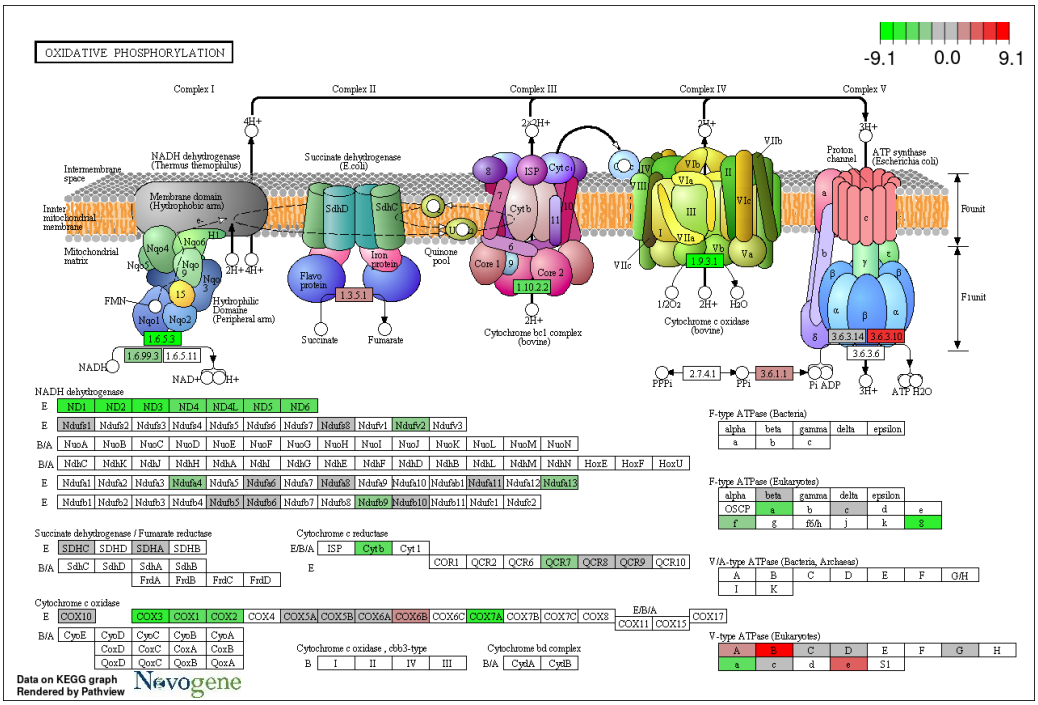

B

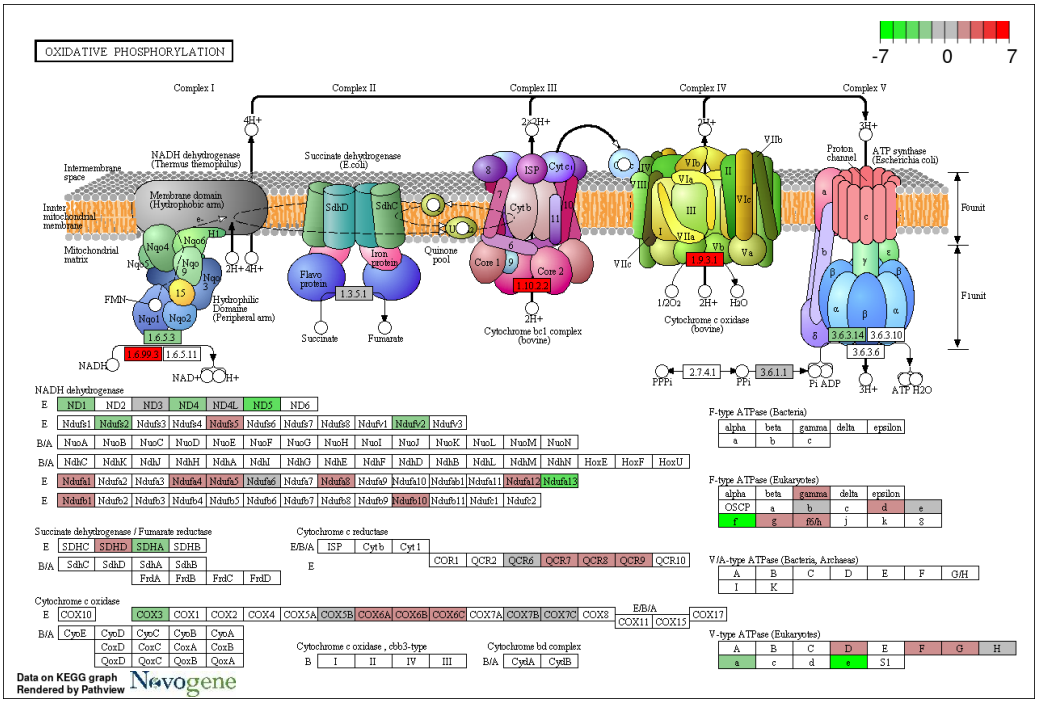

C

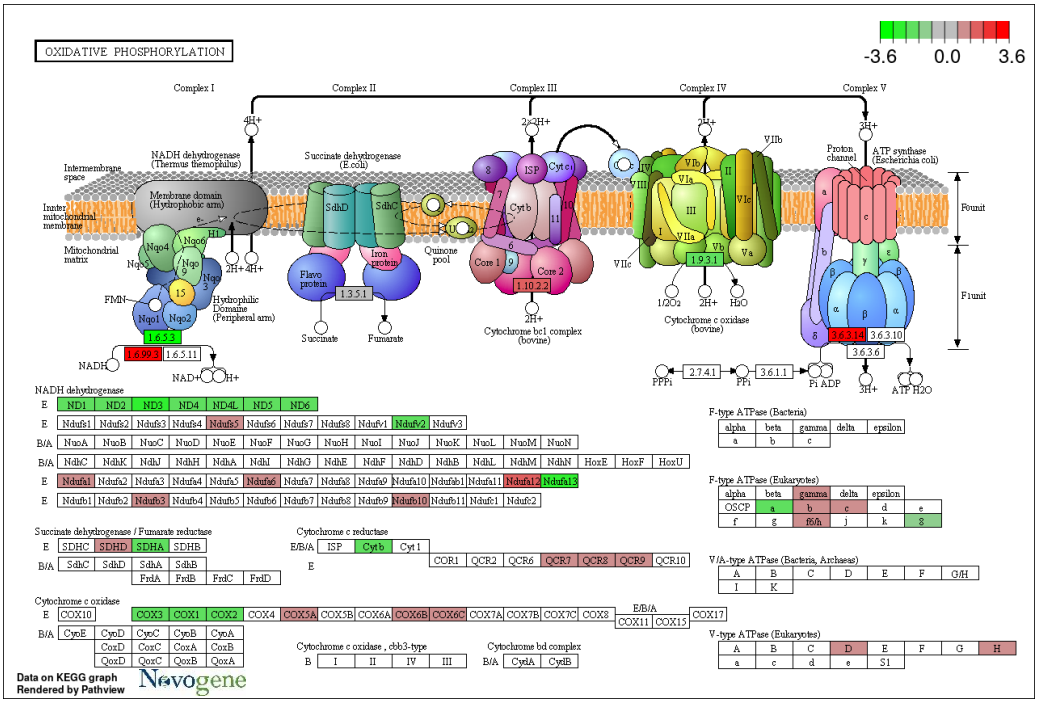

D

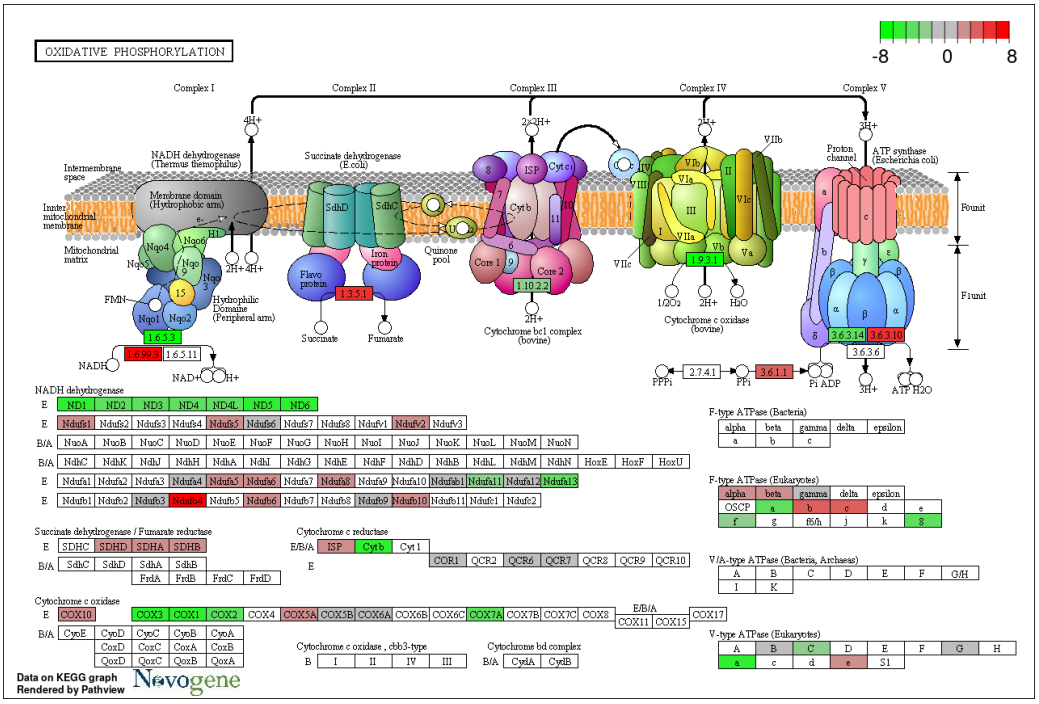

Appendix Figure 9. Dysregulated oxidative phosphorylation in NRAS over-expressing MOLM-13 cells. Data determined by transcriptomic sequencing and compared to MOLM-13 control cells. **A)** MOLM-13-NRAS-WT **B)** MOLM-13-NRAS-G12C **C)** MOLM-13-NRAS-G12D **D)** MOLM-13-NRAS-Q61K.

Appendix 10. Alterations to cell NRAS trafficking.

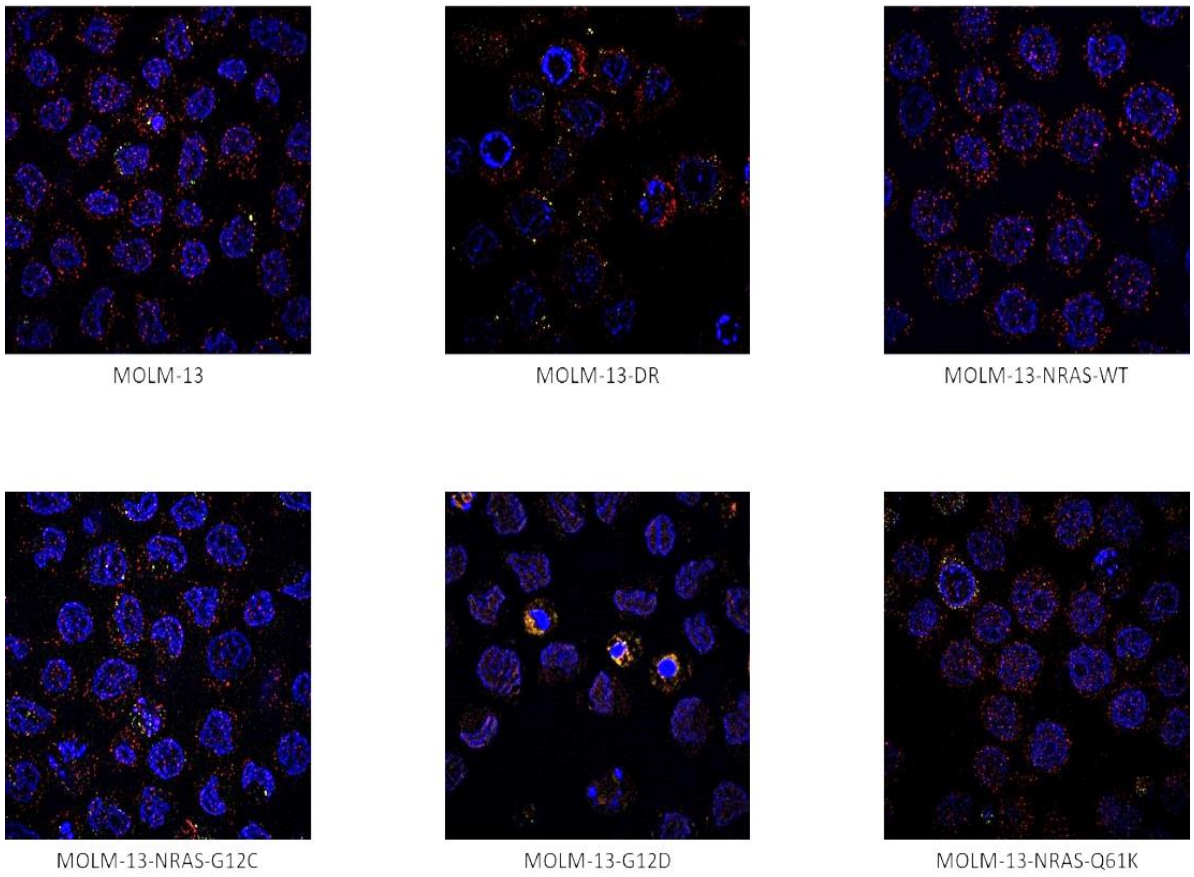

Appendix Figure 10.1. Fluorescence microscopy images detecting changes in NRAS localisation, following transcriptomic data suggestion of localisation alterations. Cells were fixed, stained and permeabilised for 24 h before being imaged using a Zeiss Elyra 7 microscope. Red represents NRAS (Coralite 647nm), blue represents (nuclear) DNA (Alexa Fluor 408nm). Yellow represents CD33 (cell surface) (Alexa Fluor 488nm) and green represents calreticulin (endoplasmic reticulum) (Alexa Fluor 555nm). These images are representative of a selection of 10 images that were taken per cell line.

A

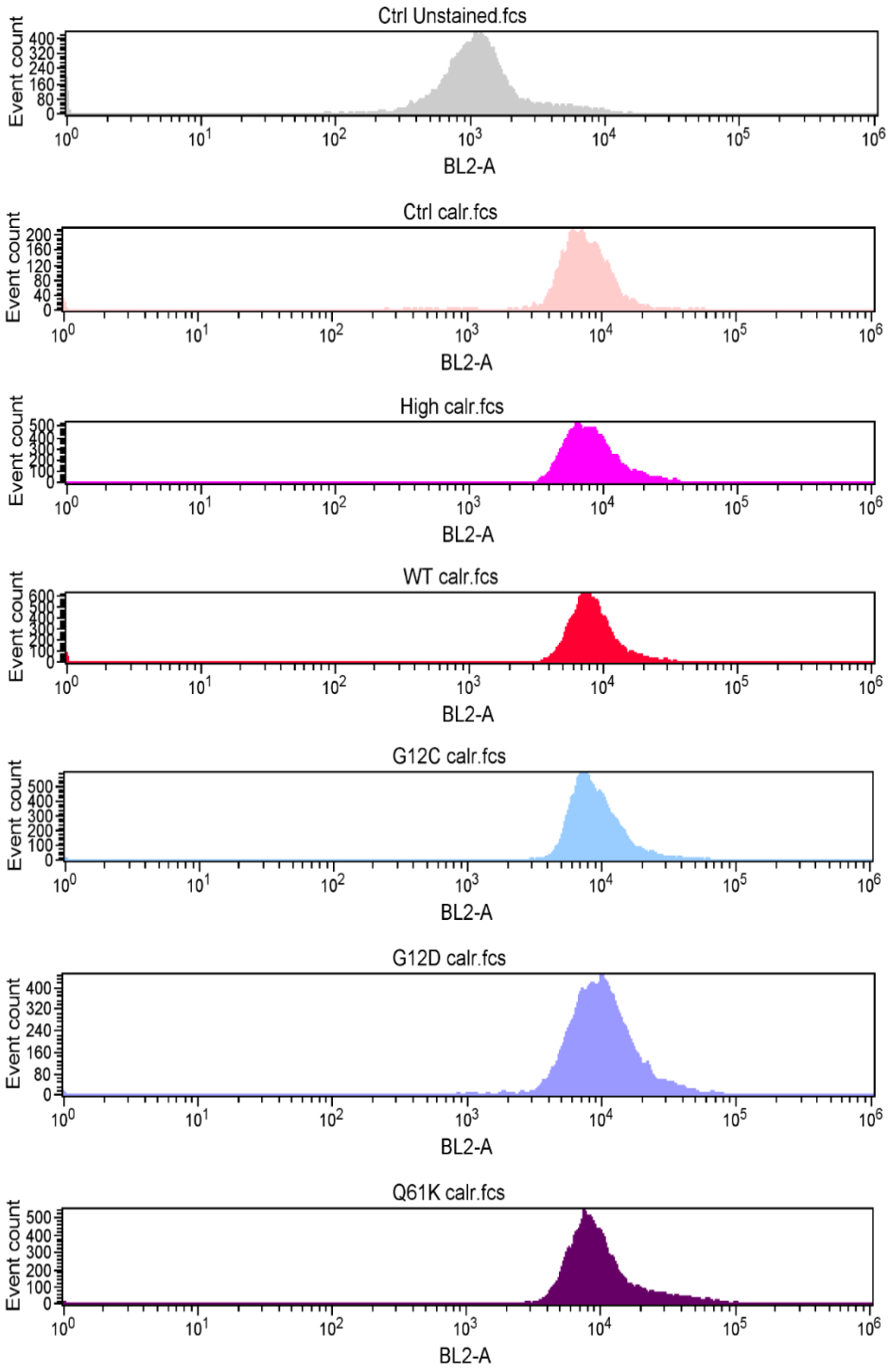
Ctrl Unstained.fcs
Ctrl calr.fcs
High calr.fcs
WT calr.fcs
G12C calr.fcs
G12D calr.fcs
Q61K calr.fcs
Event count
BL2-A

B

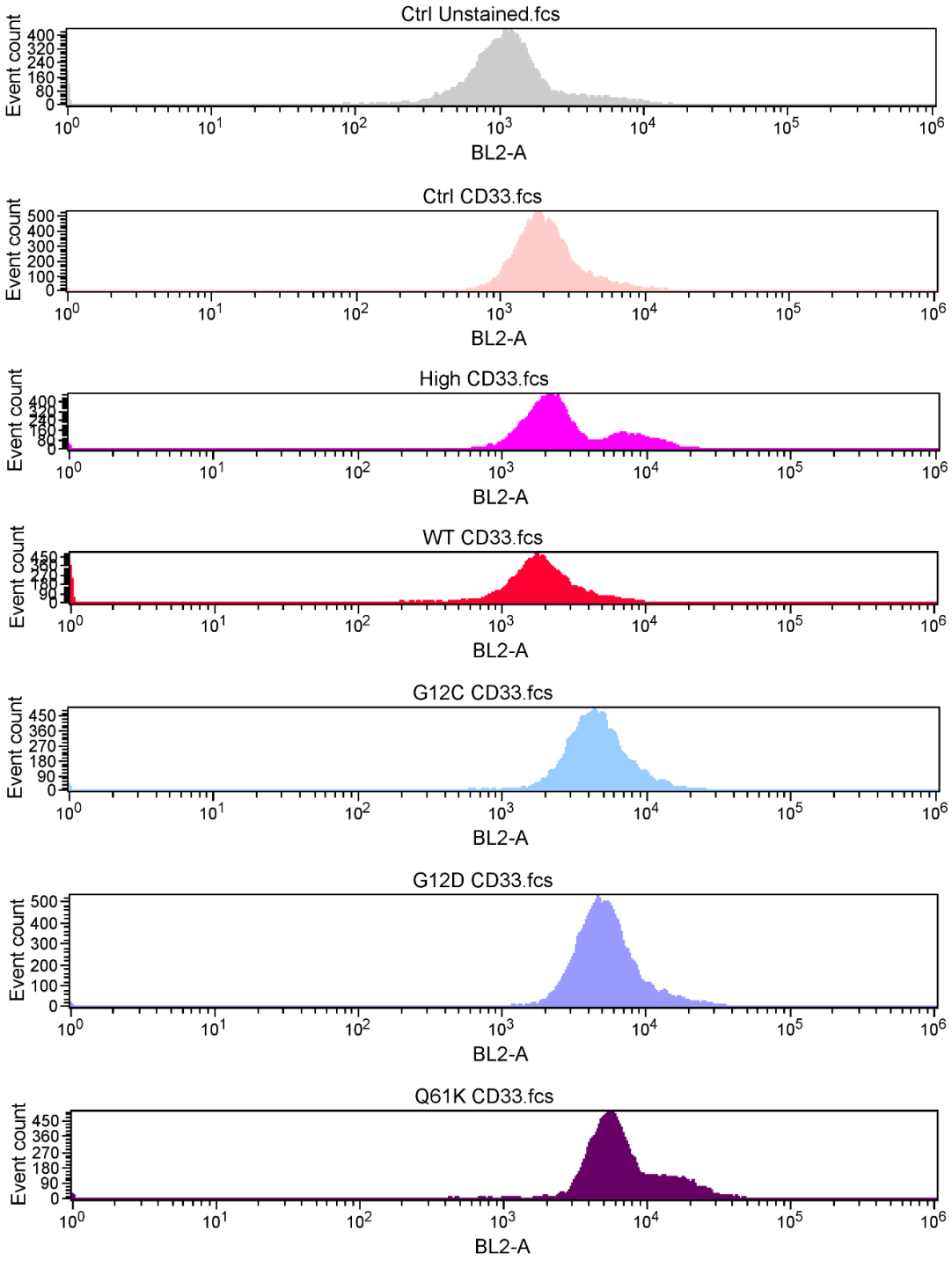

Appendix Figure 10.2. Flow cytometry plots of the cells stained for cell structure markers used in microscopy. A) Calreticulin-Alexa Fluor 555 (endoplasmic reticulum marker). **B)** CD33-Alexa Fluor 488 (cell surface marker). Plots marked as 'High' refer to the DR cell line. Data obtained using the Attune NxT flow cytometer, and analysed using FCSalyzer. Right shift compared to the grey unstained control implies positive staining for the protein of interest. Data represents N=1.

Bibliography

Abraham A, Varatharajan S, Karathedath S, Philip C, Lakshmi KM, Jayavelu AK*, et al.* (2015). RNA expression of genes involved in cytarabine metabolism and transport predicts cytarabine response in acute myeloid leukemia. Pharmacogenomics 16**:** 877-890.

Adamo A, Delfino P, Gatti A, Bonato A, Takam Kamga P, Bazzoni R*, et al.* (2020). HS-5 and HS-27A Stromal Cell Lines to Study Bone Marrow Mesenchymal Stromal Cell-Mediated Support to Cancer Development. Front Cell Dev Biol 8**:** 584232.

Adhikari U, Goliaei A, Tsereteli L, & Berkowitz ML (2016). Properties of Poloxamer Molecules and Poloxamer Micelles Dissolved in Water and Next to Lipid Bilayers: Results from Computer Simulations. The Journal of Physical Chemistry B 120**:** 5823-5830.

Aikawa T, Togashi N, Iwanaga K, Okada H, Nishiya Y, Inoue S*, et al.* (2020). Quizartinib, a selective FLT3 inhibitor, maintains antileukemic activity in preclinical models of RAS-mediated midostaurin-resistant acute myeloid leukemia cells. Oncotarget 11**:** 943-955.

Almarza E, Río P, Meza NW, Aldea M, Agirre X, Guenechea G*, et al.* (2007). Characteristics of Lentiviral Vectors Harboring the Proximal Promoter of the vav Proto-oncogene: A Weak and Efficient Promoter for Gene Therapy. Molecular Therapy 15**:** 1487-1494.

Global Bioresource Resource Centre. [Online] Available from https://pubmed.ncbi.nlm.nih.gov/1712556/. [Accessed: 22/08/2023 2023].

Anderson NR, Sheth V, Li H, Harris MW, Qiu S, Crossman DK*, et al.* (2023). Microenvironmental CXCL12 deletion enhances Flt3-ITD acute myeloid leukemia stem cell response to therapy by reducing p38 MAPK signaling. Leukemia 37**:** 560-570.

Antony ML, Chang D, Noble-Orcutt KE, Kay A, Jensen JL, Mohei H*, et al.* (2023). CD69 marks a subpopulation of acute myeloid leukemia with enhanced colony forming capacity and a unique signaling activation state. Leukemia & Lymphoma 64**:** 1262-1274.

Arafeh R, Flores K, Keren-Paz A, Maik-Rachline G, Gutkind N, Rosenberg S*, et al.* (2017). Combined inhibition of MEK and nuclear ERK translocation has synergistic antitumor activity in melanoma cells. Scientific Reports 7**:** 16345.

Arora D, Köthe S, van den Eijnden M, van Huijsduijnen RH, Heidel F, Fischer T*, et al.* (2012). Expression of protein-tyrosine phosphatases in Acute Myeloid Leukemia cells: FLT3 ITD sustains high levels of DUSP6 expression. Cell Communication and Signaling 10**:** 19.

Bahr C, Correia NC, & Trumpp A (2017). Stem cells make leukemia grow again. EMBO J 36**:** 2667-2669.

Bailey MH, Tokheim C, Porta-Pardo E, Sengupta S, Bertrand D, Weerasinghe A*, et al.* (2018). Comprehensive Characterization of Cancer Driver Genes and Mutations. Cell 173**:** 371-385.e318.

Ball BJ, Hsu M, Devlin SM, Arcila M, Roshal M, Zhang Y*, et al.* (2021). The prognosis and durable clearance of RAS mutations in patients with acute myeloid leukemia receiving induction chemotherapy. Am J Hematol 96**:** E171-e175.

Ball BJ, Hsu M, Devlin SM, Famulare C, Cai SF, Dunbar A*, et al.* (2019). RAS Mutations Are Independently Associated with Decreased Overall Survival and Event-Free Survival in Patients with AML Receiving Induction Chemotherapy. Blood 134**:** 18.

Bartram CR (1988). Mutations in ras genes in myelocytic leukemias and myelodysplastic syndromes. Blood Cells 14**:** 533-538.

Bashir Y, Geelani S, Bashir N, Mir SA, Mushtaq M, Jan MA*, et al.* (2015). Role of low dose cytarabine in elderly patients with acute myeloid leukemia: An experience. South Asian J Cancer 4**:** 4-6.

Bell CC, Magor GW, Gillinder KR, & Perkins AC (2014). A high-throughput screening strategy for detecting CRISPR-Cas9 induced mutations using next-generation sequencing. BMC Genomics 15**:** 1002.

Benary M, Bohn S, Lüthen M, Nolis IK, Blüthgen N, & Loewer A (2020). Disentangling pro-mitotic signaling during cell cycle progression using time-resolved single-cell imaging. Cell reports 31.

Bennett JM, Catovsky D, Daniel M-T, Flandrin G, Galton DAG, Gralnick HR*, et al.* (1976). Proposals for the Classification of the Acute Leukaemias French-American-British (FAB) Co-operative Group. British Journal of Haematology 33**:** 451-458.

Bertrand JY, & Traver D (2009). Hematopoietic cell development in the zebrafish embryo. Current Opinion in Hematology 16.

Bhaduri A, Di Lullo E, Jung D, Müller S, Crouch EE, Espinosa CS*, et al.* (2020). Outer Radial Glia-like Cancer Stem Cells Contribute to Heterogeneity of Glioblastoma. Cell Stem Cell 26**:** 48-63.e46.

Bhagwat SV, McMillen WT, Cai S, Zhao B, Whitesell M, Shen W*, et al.* (2020). ERK Inhibitor LY3214996 Targets ERK Pathway–Driven Cancers: A Therapeutic Approach Toward Precision Medicine. Molecular Cancer Therapeutics 19**:** 325-336.

Blackmon A, Aldoss I, & Ball BJ (2022). FLT3 Inhibitors as Maintenance Therapy after Allogeneic Stem-Cell Transplantation. Blood Lymphat Cancer 12**:** 137-147.

Blair HA (2021). Sotorasib: First Approval. Drugs 81**:** 1573-1579.

Bloethner S, Chen B, Hemminki K, Müller-Berghaus J, Ugurel S, Schadendorf D*, et al.* (2005). Effect of common B-RAF and N-RAS mutations on global gene expression in melanoma cell lines. Carcinogenesis 26**:** 1224-1232.

Bonnet D, & Dick JE (1997). Human acute myeloid leukemia is organized as a hierarchy that originates from a primitive hematopoietic cell. Nature Medicine 3**:** 730-737.

Borthakur G, Kantarjian H, Daley G, Talpaz M, O'Brien S, Garcia-Manero G*, et al.* (2006). Pilot study of lonafarnib, a farnesyl transferase inhibitor, in patients with chronic myeloid leukemia in the chronic or accelerated phase that is resistant or refractory to imatinib therapy. Cancer 106**:** 346-352.

Borthakur G, Popplewell L, Boyiadzis M, Foran J, Platzbecker U, Vey N*, et al.* (2016). Activity of the oral mitogen-activated protein kinase kinase inhibitor trametinib in RAS-mutant relapsed or refractory myeloid malignancies. Cancer 122**:** 1871-1879.

Bowers M, Zhang B, Ho Y, Agarwal P, Chen CC, & Bhatia R (2015). Osteoblast ablation reduces normal long-term hematopoietic stem cell self-renewal but accelerates leukemia development. Blood 125**:** 2678-2688.

Bowman RL, Busque L, & Levine RL (2018). Clonal Hematopoiesis and Evolution to Hematopoietic Malignancies. Cell Stem Cell 22**:** 157-170.

Brendel C, Teichler S, Millahn A, Stiewe T, Krause M, Stabla K*, et al.* (2015). Oncogenic NRAS Primes Primary Acute Myeloid Leukemia Cells for Differentiation. PLoS One 10**:** e0123181.

Brenner AK, Nepstad I, & Bruserud Ø (2017). Mesenchymal Stem Cells Support Survival and Proliferation of Primary Human Acute Myeloid Leukemia Cells through Heterogeneous Molecular Mechanisms. Front Immunol 8**:** 106.

Burd CE, Liu W, Huynh MV, Waqas MA, Gillahan JE, Clark KS*, et al.* (2014). Mutation-specific RAS oncogenicity explains NRAS codon 61 selection in melanoma. Cancer Discov 4**:** 1418-1429.

Burgess MR, Hwang E, Firestone AJ, Huang T, Xu J, Zuber J*, et al.* (2014). Preclinical efficacy of MEK inhibition in Nras-mutant AML. Blood 124**:** 3947-3955.

Burnett AK, Russell NH, Culligan D, Cavanagh J, Kell J, Wheatley K*, et al.* (2012). The addition of the farnesyl transferase inhibitor, tipifarnib, to low dose cytarabine does not improve outcome for older patients with AML. British Journal of Haematology 158**:** 519-522.

Burrell RA, McClelland SE, Endesfelder D, Groth P, Weller MC, Shaikh N*, et al.* (2013). Replication stress links structural and numerical cancer chromosomal instability. Nature 494**:** 492-496.

Burrell RA, McGranahan N, Bartek J, & Swanton C (2013). The causes and consequences of genetic heterogeneity in cancer evolution. Nature 501**:** 338-345.

Busque L, Mio R, Mattioli J, Brais E, Blais N, Lalonde Y*, et al.* (1996). Nonrandom X-inactivation patterns in normal females: lyonization ratios vary with age. Blood 88**:** 59-65.

Butrym A, Rybka J, Baczyńska D, Poręba R, Kuliczkowski K, & Mazur G (2016). Clinical response to azacitidine therapy depends on microRNA-29c (miR-29c) expression in older acute myeloid leukemia (AML) patients. Oncotarget 7**:** 30250-30257.

Campbell SL, & Philips MR (2021). Post-translational modification of RAS proteins. Current Opinion in Structural Biology 71**:** 180-192.

Acute Myeloid Leukaemia (AML) statistics [Online] Available from https://www.cancerresearchuk.org/health-professional/cancer-statistics/statistics-by-cancer-type/leukaemia-aml#heading-Zero. [Accessed: 01/11/2022 2022].

Canon J, Rex K, Saiki AY, Mohr C, Cooke K, Bagal D*, et al.* (2019). The clinical KRAS(G12C) inhibitor AMG 510 drives anti-tumour immunity. Nature 575**:** 217-223.

Carroll D (2011). Genome Engineering With Zinc-Finger Nucleases. Genetics 188**:** 773-782.

Cerami E, Gao J, Dogrusoz U, Gross BE, Sumer SO, Aksoy BA*, et al.* (2012). The cBio cancer genomics portal: an open platform for exploring multidimensional cancer genomics data. Cancer Discov 2**:** 401-404.

Chandrasegaran S (2017). Recent advances in the use of ZFN-mediated gene editing for human gene therapy. Cell Gene Ther Insights 3**:** 33-41.

Charpentier M, Khedher AHY, Menoret S, Brion A, Lamribet K, Dardillac E*, et al.* (2018). CtIP fusion to Cas9 enhances transgene integration by homology-dependent repair. Nat Commun 9**:** 1133.

Chiesa R, Georgiadis C, Syed F, Zhan H, Etuk A, Gkazi SA*, et al.* (2023). Base-Edited CAR7 T Cells for Relapsed T-Cell Acute Lymphoblastic Leukemia. N Engl J Med 389**:** 899-910.

Choe S, Wang H, DiNardo CD, Stein EM, de Botton S, Roboz GJ*, et al.* (2020). Molecular mechanisms mediating relapse following ivosidenib monotherapy in IDH1-mutant relapsed or refractory AML. Blood Advances 4**:** 1894-1905.

Choi EH, Suh S, Sears AE, Hołubowicz R, Kedhar SR, Browne AW*, et al.* (2023). Genome editing in the treatment of ocular diseases. Experimental & Molecular Medicine 55**:** 1678-1690.

Choy E, Chiu VK, Silletti J, Feoktistov M, Morimoto T, Michaelson D*, et al.* (1999). Endomembrane trafficking of ras: the CAAX motif targets proteins to the ER and Golgi. Cell 98**:** 69-80.

Chu VT, Weber T, Wefers B, Wurst W, Sander S, Rajewsky K*, et al.* (2015). Increasing the efficiency of homology-directed repair for CRISPR-Cas9-induced precise gene editing in mammalian cells. Nature Biotechnology 33**:** 543-548.

Clément MV, & Stamenkovic I (1996). Superoxide anion is a natural inhibitor of FAS-mediated cell death. The EMBO Journal 15**:** 216-225.

Concordet J-P, & Haeussler M (2018). CRISPOR: intuitive guide selection for CRISPR/Cas9 genome editing experiments and screens. Nucleic Acids Research 46**:** W242-W245.

Cooper AR, Patel S, Senadheera S, Plath K, Kohn DB, & Hollis RP (2011). Highly efficient large-scale lentiviral vector concentration by tandem tangential flow filtration. J Virol Methods 177**:** 1-9.

Cox AD, Der CJ, & Philips MR (2015). Targeting RAS Membrane Association: Back to the Future for Anti-RAS Drug Discovery? Clinical Cancer Research 21**:** 1819-1827.

Cox AD, Fesik SW, Kimmelman AC, Luo J, & Der CJ (2014). Drugging the undruggable RAS: Mission possible? Nat Rev Drug Discov 13**:** 828-851.

Cramer SD, Hixon JA, Andrews C, Porter RJ, Rodrigues GOL, Wu X*, et al.* (2018). Mutant IL-7Rα and mutant NRas are sufficient to induce murine T cell acute lymphoblastic leukemia. Leukemia 32**:** 1795-1882.

Czeiszperger TL, Wang MP, & Chung CS (2020). Membrane stabilizer Poloxamer 188 improves yield of primary isolated rat cardiomyocytes without impairing function. Physiological Reports 8**:** e14382.

Dahia PL, Aguiar RC, Alberta J, Kum JB, Caron S, Sill H*, et al.* (1999). PTEN is inversely correlated with the cell survival factor Akt/PKB and is inactivated via multiple mechanismsin haematological malignancies. Hum Mol Genet 8**:** 185-193.

Dai W, Xie S, Chen C, & Choi BH (2021). Ras sumoylation in cell signaling and transformation. Semin Cancer Biol 76**:** 301-309.

de Beauchamp L, Himonas E, & Helgason GV (2022). Mitochondrial metabolism as a potential therapeutic target in myeloid leukaemia. Leukemia 36**:** 1-12.

de Botton S, Cluzeau T, Vigil C, Cook RJ, Rousselot P, Rizzieri DA*, et al.* (2023). Targeting RARA overexpression with tamibarotene, a potent and selective RARα agonist, is a novel approach in AML. Blood Advances 7**:** 1858-1870.

de Witte T, Bowen D, Robin M, Malcovati L, Niederwieser D, Yakoub-Agha I*, et al.* (2017). Allogeneic hematopoietic stem cell transplantation for MDS and CMML: recommendations from an international expert panel. Blood 129**:** 1753-1762.

Dean M, Fojo T, & Bates S (2005). Tumour stem cells and drug resistance. Nature Reviews Cancer 5**:** 275-284.

Decroocq J, Birsen R, Montersino C, Chaskar P, Mano J, Poulain L*, et al.* (2022). RAS activation induces synthetic lethality of MEK inhibition with mitochondrial oxidative metabolism in acute myeloid leukemia. Leukemia 36**:** 1237-1252.

Dhakal P, Bates M, Tomasson MH, Sutamtewagul G, Dupuy A, & Bhatt VR (2022). Acute myeloid leukemia resistant to venetoclax-based therapy: What does the future hold? Blood Reviews**:** 101036.

Diehl JN, Klomp JE, Snare KR, Hibshman PS, Blake DR, Kaiser ZD*, et al.* (2021). The KRAS-regulated kinome identifies WEE1 and ERK coinhibition as a potential therapeutic strategy in KRAS-mutant pancreatic cancer. Journal of Biological Chemistry 297**:** 101335.

DiNardo CD, Jonas BA, Pullarkat V, Thirman MJ, Garcia JS, Wei AH*, et al.* (2020a). Azacitidine and Venetoclax in Previously Untreated Acute Myeloid Leukemia. New England Journal of Medicine 383**:** 617-629.

DiNardo CD, Pratz KW, Letai A, Jonas BA, Wei AH, Thirman M*, et al.* (2018). Safety and preliminary efficacy of venetoclax with decitabine or azacitidine in elderly patients with previously untreated acute myeloid leukaemia: a non-randomised, open-label, phase 1b study. Lancet Oncol 19**:** 216-228.

DiNardo CD, Tiong IS, Quaglieri A, MacRaild S, Loghavi S, Brown FC*, et al.* (2020b). Molecular patterns of response and treatment failure after frontline venetoclax combinations in older patients with AML. Blood 135**:** 791-803.

Doench JG, Fusi N, Sullender M, Hegde M, Vaimberg EW, Donovan KF*, et al.* (2016). Optimized sgRNA design to maximize activity and minimize off-target effects of CRISPR-Cas9. Nat Biotechnol 34**:** 184-191.

Döhner H, Dolnik A, Tang L, Seymour JF, Minden MD, Stone RM*, et al.* (2018). Cytogenetics and gene mutations influence survival in older patients with acute myeloid leukemia treated with azacitidine or conventional care. Leukemia 32**:** 2546-2557.

Döhner H, Wei AH, Appelbaum FR, Craddock C, DiNardo CD, Dombret H*, et al.* (2022). Diagnosis and management of AML in adults: 2022 recommendations from an international expert panel on behalf of the ELN. Blood 140**:** 1345-1377.

Döhner H, Weisdorf DJ, & Bloomfield CD (2015). Acute Myeloid Leukemia. New England Journal of Medicine 373**:** 1136-1152.

Dong Q, Xiu Y, Wang Y, Hodgson C, Borcherding N, Jordan C*, et al.* (2022). HSF1 is a driver of leukemia stem cell self-renewal in acute myeloid leukemia. Nat Commun 13**:** 6107.

Dong Y, Xia C, Weng Q, Wang T, Hu F, Wang K*, et al.* (2019). Synergy of NUP98-HOXA10 Fusion Gene and NrasG12D Mutation Preserves the Stemness of Hematopoietic Stem Cells on Culture Condition. Cells 8.

Drenberg CD, Hu S, Li L, Buelow DR, Orwick SJ, Gibson AA*, et al.* (2016). ABCC4 Is a Determinant of Cytarabine-Induced Cytotoxicity and Myelosuppression. Clin Transl Sci 9**:** 51-59.

Dumanski JP, Lambert J-C, Rasi C, Giedraitis V, Davies H, Grenier-Boley B*, et al.* (2016). Mosaic loss of chromosome Y in blood is associated with Alzheimer disease. The American Journal of Human Genetics 98**:** 1208-1219.

Eaves CJ, Cashman JD, Sutherland HJ, Otsuka T, Humphries RK, Hogge DE*, et al.* (1991). Molecular analysis of primitive hematopoietic cell proliferation control mechanisms. Ann N Y Acad Sci 628**:** 298-306.

Epinat JC, Arnould S, Chames P, Rochaix P, Desfontaines D, Puzin C*, et al.* (2003). A novel engineered meganuclease induces homologous recombination in yeast and mammalian cells. Nucleic Acids Res 31**:** 2952-2962.

Eppert K, Takenaka K, Lechman ER, Waldron L, Nilsson B, van Galen P*, et al.* (2011). Stem cell gene expression programs influence clinical outcome in human leukemia. Nat Med 17**:** 1086-1093.

Erba HP, Montesinos P, Kim H-J, Patkowska E, Vrhovac R, Žák P*, et al.* (2023). Quizartinib plus chemotherapy in newly diagnosed patients with FLT3-internal-tandem-duplication-positive acute myeloid leukaemia (QuANTUM-First): a randomised, double-blind, placebo-controlled, phase 3 trial. The Lancet 401**:** 1571-1583.

European Medicines Agency, 2022. *Lumykras sotorasib.* [Online] Available from https://www.ema.europa.eu/en/medicines/human/EPAR/lumykras. [Accessed: 22/08/2023 2023].

Famili F, Naber BAE, Vloemans S, de Haas EFE, Tiemessen MM, & Staal FJT (2015). Discrete roles of canonical and non-canonical Wnt signaling in hematopoiesis and lymphopoiesis. Cell Death & Disease 6**:** e1981-e1981.

Fell VL, & Schild-Poulter C (2012). Ku regulates signaling to DNA damage response pathways through the Ku70 von Willebrand A domain. Mol Cell Biol 32**:** 76-87.

Ferrari S, Vavassori V, Canarutto D, Jacob A, Castiello MC, Javed AO*, et al.* (2021). Gene Editing of Hematopoietic Stem Cells: Hopes and Hurdles Toward Clinical Translation. Frontiers in Genome Editing 3.

Florian MC, Nattamai KJ, Dörr K, Marka G, Überle B, Vas V*, et al.* (2013). A canonical to non-canonical Wnt signalling switch in haematopoietic stem-cell ageing. Nature 503**:** 392-396.

Fuster JJ (2022). Clonal hematopoiesis and cardiovascular disease in cancer patients and survivors. Thrombosis Research 213**:** S107-S112.

Gama-Norton L, Ferrando E, Ruiz-Herguido C, Liu Z, Guiu J, Islam ABMMK*, et al.* (2015). Notch signal strength controls cell fate in the haemogenic endothelium. Nature Communications 6**:** 8510.

Gao J, Aksoy BA, Dogrusoz U, Dresdner G, Gross B, Sumer SO*, et al.* (2013). Integrative analysis of complex cancer genomics and clinical profiles using the cBioPortal. Sci Signal 6**:** pl1.

Ge Y, Wang J, Zhang H, Li J, Ye M, & Jin X (2022). Fate of hematopoietic stem cells determined by Notch1 signaling (Review). Exp Ther Med 23**:** 170.

Geissler K, Jäger E, Barna A, Gurbisz M, Graf T, Graf E*, et al.* (2020). Molecular Basis and Clinical Application of Growth-Factor-Independent In Vitro Myeloid Colony Formation in Chronic Myelomonocytic Leukemia. International Journal of Molecular Sciences. doi: 10.3390/ijms21176057

Gerlinger M, Rowan AJ, Horswell S, Larkin J, Endesfelder D, Gronroos E*, et al.* (2012). Intratumor Heterogeneity and Branched Evolution Revealed by Multiregion Sequencing. New England Journal of Medicine 366**:** 883-892.

Gilardi M, Wang Z, Proietto M, Chillà A, Calleja-Valera JL, Goto Y*, et al.* (2020). Tipifarnib as a Precision Therapy for HRAS-Mutant Head and Neck Squamous Cell Carcinomas. Molecular Cancer Therapeutics 19**:** 1784.

Gillies TE, Pargett M, Silva JM, Teragawa CK, McCormick F, & Albeck JG (2020). Oncogenic mutant RAS signaling activity is rescaled by the ERK/MAPK pathway. Mol Syst Biol 16**:** e9518.

Goodwin EC, & DiMaio D (2000). Repression of human papillomavirus oncogenes in HeLa cervical carcinoma cells causes the orderly reactivation of dormant tumor suppressor pathways. Proc Natl Acad Sci U S A 97**:** 12513-12518.

Gorrini C, Harris IS, & Mak TW (2013). Modulation of oxidative stress as an anticancer strategy. Nature Reviews Drug Discovery 12**:** 931-947.

Govindan R (2019). Phase I Study of AMG 510, A Novel Molecule Targeting KRAS G12C Mutant Solid Tumours (Abstract). In ESMO 2019 Congress. Annals of Oncology, pp v159-v193.

Greco GE, Matsumoto Y, Brooks RC, Lu Z, Lieber MR, & Tomkinson AE (2016). SCR7 is neither a selective nor a potent inhibitor of human DNA ligase IV. DNA Repair (Amst) 43**:** 18-23.

Griessinger E, Anjos-Afonso F, Vargaftig J, Taussig DC, Lassailly F, Prebet T*, et al.* (2016). Frequency and Dynamics of Leukemia-Initiating Cells during Short-term Ex Vivo Culture Informs Outcomes in Acute Myeloid Leukemia Patients. Cancer Research 76**:** 2082-2086.

Griffin JM, Healy FM, Dahal LN, Floisand Y, & Woolley JF (2022). Worked to the bone: antibody-based conditioning as the future of transplant biology. J Hematol Oncol 15**:** 65.

Guangrong Q, Jin D, Sylvia C, Timothy JM, Brenda L, Quy N*, et al.* (2023). Mutation Patterns Predict Drug Sensitivity in Acute Myeloid Leukemia. bioRxiv**:** 2023.2005.2024.541944.

Guidi N, Marka G, Sakk V, Zheng Y, Florian MC, & Geiger H (2021). An Aged Bone Marrow Niche Restrains Rejuvenated Hematopoietic Stem Cells. Stem Cells 39**:** 1101-1106.

Guièze R, Liu VM, Rosebrock D, Jourdain AA, Hernández-Sánchez M, Martinez Zurita A*, et al.* (2019). Mitochondrial Reprogramming Underlies Resistance to BCL-2 Inhibition in Lymphoid Malignancies. Cancer Cell 36**:** 369-384.e313.

Guinan M, Benckendorff C, Smith M, & Miller GJ (2020). Recent Advances in the Chemical Synthesis and Evaluation of Anticancer Nucleoside Analogues. Molecules 25**:** 2050.

Guo C, Fordjour FK, Tsai SJ, Morrell JC, & Gould SJ (2021). Choice of selectable marker affects recombinant protein expression in cells and exosomes. J Biol Chem 297**:** 100838.

Guo J, Wang W, Yu D, & Wu Y (2011). Spinoculation triggers dynamic actin and cofilin activity that facilitates HIV-1 infection of transformed and resting CD4 T cells. J Virol 85**:** 9824-9833.

Guo Y, Köck K, Ritter CA, Chen ZS, Grube M, Jedlitschky G*, et al.* (2009). Expression of ABCC-type nucleotide exporters in blasts of adult acute myeloid leukemia: relation to long-term survival. Clin Cancer Res 15**:** 1762-1769.

Gutschner T, Haemmerle M, Genovese G, Draetta Giulio F, & Chin L (2016). Post-translational Regulation of Cas9 during G1 Enhances Homology-Directed Repair. Cell Reports 14**:** 1555-1566.

Han Y, Liu D, & Li L (2020). PD-1/PD-L1 pathway: current researches in cancer. Am J Cancer Res 10**:** 727-742.

Hanahan D (2022). Hallmarks of Cancer: New Dimensions. Cancer Discovery 12**:** 31-46.

Hanahan D, & Weinberg Robert A (2011). Hallmarks of Cancer: The Next Generation. Cell 144**:** 646-674.

Harousseau J-L, Martinelli G, Jedrzejczak WW, Brandwein JM, Bordessoule D, Masszi T*, et al.* (2009). A randomized phase 3 study of tipifarnib compared with best supportive care, including hydroxyurea, in the treatment of newly diagnosed acute myeloid leukemia in patients 70 years or older. Blood 114**:** 1166-1173.

Healy FM, Prior IA, & MacEwan DJ (2022). The importance of Ras in drug resistance in cancer. British Journal of Pharmacology 179**:** 2844-2867.

Herbst SA, Kim V, Roider T, Schitter EC, Bruch P-M, Liebers N*, et al.* (2023). Comparing the value of mono- vs coculture for high-throughput compound screening in hematological malignancies. Blood Advances 7**:** 5925-5936.

Heyer WD, Ehmsen KT, & Liu J (2010). Regulation of homologous recombination in eukaryotes. Annu Rev Genet 44**:** 113-139.

Hillig RC, Sautier B, Schroeder J, Moosmayer D, Hilpmann A, Stegmann CM*, et al.* (2019). Discovery of potent SOS1 inhibitors that block RAS activation via disruption of the RAS-SOS1 interaction. Proc Natl Acad Sci U S A 116**:** 2551-2560.

Hirata T, Hishimoto A, Otsuka I, Okazaki S, Boku S, Kimura A*, et al.* (2018). Investigation of chromosome Y loss in men with schizophrenia. Neuropsychiatric Disease and Treatment 14**:** 2115.

Hoadley KA, Yau C, Hinoue T, Wolf DM, Lazar AJ, Drill E*, et al.* (2018). Cell-of-Origin Patterns Dominate the Molecular Classification of 10,000 Tumors from 33 Types of Cancer. Cell 173**:** 291-304.e296.

Hobbs GA, Der CJ, & Rossman KL (2016). RAS isoforms and mutations in cancer at a glance. J Cell Sci 129**:** 1287-1292.

Hood FE, Sahraoui YM, Jenkins RE, & Prior IA (2023). Ras protein abundance correlates with Ras isoform mutation patterns in cancer. Oncogene 42**:** 1224-1232.

Hou HA, Chou WC, Kuo YY, Liu CY, Lin LI, Tseng MH*, et al.* (2015). TP53 mutations in de novo acute myeloid leukemia patients: longitudinal follow-ups show the mutation is stable during disease evolution. Blood Cancer Journal 5**:** e331-e331.

Howlader N, Noone A.M, Krapcho M, Miller D, Brest A, Yu M, Ruhl J, Tatalovich Z, Mariotto A, Lewis D.R, Chen HS, Feuer EJ, Cronin K.A. (eds) *SEER Cancer Statistics Review, 1975-2016,.* [Online] Available from https://seer.cancer.gov/csr/1975_2016/. [Accessed: 20/10/2022 2022].

Hu Z, & Marti J (2023). Molecular Dynamics simulation of NRAS-Q61 oncogenes and new strategies for in silico drug design. bioRxiv**:** 2023.2005.2025.542304.

Hu Z, Shi Z, Guo X, Jiang B, Wang G, Luo D*, et al.* (2018). Ligase IV inhibitor SCR7 enhances gene editing directed by CRISPR–Cas9 and ssODN in human cancer cells. Cell & Bioscience 8**:** 12.

Hubeek I, Stam RW, Peters GJ, Broekhuizen R, Meijerink JP, van Wering ER*, et al.* (2005). The human equilibrative nucleoside transporter 1 mediates in vitro cytarabine sensitivity in childhood acute myeloid leukaemia. Br J Cancer 93**:** 1388-1394.

NRAS Cell Line. [Online] Available from https://www.proteinatlas.org/ENSG00000213281-NRAS/cell+line#leukemia. [Accessed: 14/08/2023 2023].

Huynh MV, Hobbs GA, Schaefer A, Pierobon M, Carey LM, Diehl JN*, et al.* (2022). Functional and biological heterogeneity of KRAS(Q61) mutations. Sci Signal 15**:** eabn2694.

Iaccarino L, Ottone T, Alfonso V, Cicconi L, Divona M, Lavorgna S*, et al.* (2019). Mutational landscape of patients with acute promyelocytic leukemia at diagnosis and relapse. American Journal of Hematology 94**:** 1091-1097.

Ito T, Young MJ, Li R, Jain S, Wernitznig A, Krill-Burger JM*, et al.* (2021). Paralog knockout profiling identifies DUSP4 and DUSP6 as a digenic dependence in MAPK pathway-driven cancers. Nat Genet 53**:** 1664-1672.

Jaber N (2021). *FDA Approval of KRAS Inhibitor Sotorasib for Lung Cancer Hailed as Milestone* [Online] Available from https://www.cancer.gov/news-events/cancer-currents-blog/2021/fda-sotorasib-lung-cancer-kras. [Accessed: 22/08/2023` 2023].

Jagannathan-Bogdan M, & Zon LI (2013). Hematopoiesis. Development 140**:** 2463-2467.

Jaiswal S, & Ebert BL (2019). Clonal hematopoiesis in human aging and disease. Science 366**:** eaan4673.

Jaiswal S, Fontanillas P, Flannick J, Manning A, Grauman PV, Mar BG*, et al.* (2014). Age-Related Clonal Hematopoiesis Associated with Adverse Outcomes. New England Journal of Medicine 371**:** 2488-2498.

Janakiraman M, Vakiani E, Zeng Z, Pratilas CA, Taylor BS, Chitale D*, et al.* (2010). Genomic and Biological Characterization of Exon 4 KRAS Mutations in Human Cancer. Cancer Research 70**:** 5901-5911.

Janes MR, Zhang J, Li LS, Hansen R, Peters U, Guo X*, et al.* (2018). Targeting KRAS Mutant Cancers with a Covalent G12C-Specific Inhibitor. Cell 172**:** 578-589.e517.

Jang J, Lee J, Jang JH, Jung CW, & Park S (2019). Anti-leukemic effects of simvastatin on NRAS(G12D) mutant acute myeloid leukemia cells. Mol Biol Rep 46**:** 5859-5866.

Jänne PA, Riely GJ, Gadgeel SM, Heist RS, Ou SI, Pacheco JM*, et al.* (2022). Adagrasib in Non-Small-Cell Lung Cancer Harboring a KRAS(G12C) Mutation. N Engl J Med 387**:** 120-131.

Jayavaradhan R, Pillis DM, Goodman M, Zhang F, Zhang Y, Andreassen PR*, et al.* (2019). CRISPR-Cas9 fusion to dominant-negative 53BP1 enhances HDR and inhibits NHEJ specifically at Cas9 target sites. Nat Commun 10**:** 2866.

Jerafi-Vider A, Bassi I, Moshe N, Tevet Y, Hen G, Splittstoesser D*, et al.* (2021). VEGFC/FLT4-induced cell-cycle arrest mediates sprouting and differentiation of venous and lymphatic endothelial cells. Cell Rep 35**:** 109255.

Jiang W, Hua R, Wei M, Li C, Qiu Z, Yang X*, et al.* (2015). An optimized method for high-titer lentivirus preparations without ultracentrifugation. Scientific Reports 5**:** 13875.

Jin X, Ng V, Zhao M, Liu L, Higashimoto T, Lee ZH*, et al.* (2022). Epigenetic downregulation of Socs2 contributes to mutant N-Ras-mediated hematopoietic dysregulation. Dis Model Mech 15.

Jones CL, Stevens BM, Pollyea DA, Culp-Hill R, Reisz JA, Nemkov T*, et al.* (2020). Nicotinamide Metabolism Mediates Resistance to Venetoclax in Relapsed Acute Myeloid Leukemia Stem Cells. Cell Stem Cell 27**:** 748-764.e744.

Jones GG, del Río IB, Sari S, Sekerim A, Young LC, Hartig N*, et al.* (2019). SHOC2 phosphatase-dependent RAF dimerization mediates resistance to MEK inhibition in RAS-mutant cancers. Nature Communications 10**:** 2532.

Joshi SK, Pittsenbarger J, Luo X, Maazi H, Revenko A, Druker BJ*, et al.* (2023). Abstract B019: ASO-mediated NRAS knockdown overcomes gilteritinib late resistance in FLT3-AML. Molecular Cancer Research 21**:** B019-B019.

Kang D, Ludwig E, Jaworowicz D, Huang H, Fiedler-Kelly J, Cortes J*, et al.* (2021). Concentration-QTc analysis of quizartinib in patients with relapsed/refractory acute myeloid leukemia. Cancer Chemother Pharmacol 87**:** 513-523.

Kantarjian H, Ravandi F, O'Brien S, Cortes J, Faderl S, Garcia-Manero G*, et al.* (2010). Intensive chemotherapy does not benefit most older patients (age 70 years or older) with acute myeloid leukemia. Blood 116**:** 4422-4429.

Karimi Kelaye S, Najafi F, Kazemi B, Foruzandeh Z, Seif F, Solali S*, et al.* (2022). The contributing factors of resistance or sensitivity to epigenetic drugs in the treatment of AML. Clinical and Translational Oncology 24**:** 1250-1261.

Kenny TC, Craig AJ, Villanueva A, & Germain D (2019). Mitohormesis Primes Tumor Invasion and Metastasis. Cell Rep 27**:** 2292-2303.e2296.

Killoran RC, & Smith MJ (2019). Conformational resolution of nucleotide cycling and effector interactions for multiple small GTPases determined in parallel. J Biol Chem 294**:** 9937-9948.

Kim TK, & Eberwine JH (2010). Mammalian cell transfection: the present and the future. Anal Bioanal Chem 397**:** 3173-3178.

Köhler J, Zhao Y, Li J, Gokhale PC, Tiv HL, Knott AR*, et al.* (2021). ERK Inhibitor LY3214996-Based Treatment Strategies for RAS-Driven Lung Cancer. Molecular Cancer Therapeutics 20**:** 641-654.

Kolch W, Berta D, & Rosta E (2023). Dynamic regulation of RAS and RAS signaling. Biochemical Journal 480**:** 1-23.

Kopp JL, Dubois CL, Schaeffer DF, Samani A, Taghizadeh F, Cowan RW*, et al.* (2018). Loss of Pten and Activation of Kras Synergistically Induce Formation of Intraductal Papillary Mucinous Neoplasia From Pancreatic Ductal Cells in Mice. Gastroenterology 154**:** 1509-1523.e1505.

Koury J, Zhong L, & Hao J (2017). Targeting Signaling Pathways in Cancer Stem Cells for Cancer Treatment. Stem Cells Int 2017**:** 2925869-2925869.

Kurata M, Antony ML, Noble-Orcutt KE, Rathe SK, Lee Y, Furuno H*, et al.* (2022). Proliferation and Self-Renewal Are Differentially Sensitive to NRASG12V Oncogene Levels in an Acute Myeloid Leukemia Cell Line. Molecular Cancer Research 20**:** 1646-1658.

Kuribayashi W, Oshima M, Itokawa N, Koide S, Nakajima-Takagi Y, Yamashita M*, et al.* (2020). Limited rejuvenation of aged hematopoietic stem cells in young bone marrow niche. Journal of Experimental Medicine 218**:** e20192283.

Kwong LN, Costello JC, Liu H, Jiang S, Helms TL, Langsdorf AE*, et al.* (2012). Oncogenic NRAS signaling differentially regulates survival and proliferation in melanoma. Nature Medicine 18**:** 1503-1510.

Lai C, Bhansali RS, Kuo EJ, Mannis G, & Lin RJ (2023). Older Adults With Newly Diagnosed AML: Hot Topics for the Practicing Clinician. American Society of Clinical Oncology Educational Book**:** e390018.

Lapidot T, Sirard C, Vormoor J, Murdoch B, Hoang T, Caceres-Cortes J*, et al.* (1994). A cell initiating human acute myeloid leukaemia after transplantation into SCID mice. Nature 367**:** 645-648.

Larson RA, Mandrekar SJ, Huebner LJ, Sanford BL, Laumann K, Geyer S*, et al.* (2021). Midostaurin reduces relapse in FLT3-mutant acute myeloid leukemia: the Alliance CALGB 10603/RATIFY trial. Leukemia 35**:** 2539-2551.

Lassen A, Atefi M, Robert L, Wong DJL, Cerniglia M, Comin-Anduix B*, et al.* (2014). Effects of AKT inhibitor therapy in response and resistance to BRAF inhibition in melanoma. Molecular Cancer 13**:** 83.

Ledford, H (2020) *CRISPR gene therapy shows promise against blood diseases* [Online] Available from https://www.nature.com/articles/d41586-020-03476-x. [Accessed: 14/11/2022 2022].

Ledford, H (2022a) *CRISPR cancer trial success paves the way for personalized treatments.* [Online] Available from https://www.nature.com/articles/d41586-022-03676-7?utm_source=Nature+Briefing&utm_campaign=0f8d4b9fcf-briefing-dy-20221111&utm_medium=email&utm_term=0_c9dfd39373-0f8d4b9fcf-44413293. [Accessed: 14/11/2022 2022].

Ledford H, & Callaway E (2020) *Pioneers of revolutionary CRISPR gene editing win chemistry Nobel.* [Online] Available from https://www.nature.com/articles/d41586-020-02765-9. [Accessed: 08/11/2022 2022].

Lee HW, Sa JK, Gualberto A, Scholz C, Sung HH, Jeong BC*, et al.* (2020). A Phase II Trial of Tipifarnib for Patients with Previously Treated, Metastatic Urothelial Carcinoma Harboring HRAS Mutations. Clinical Cancer Research 26**:** 5113.

DSMZ-German Collection of Microorganisms and Cell Cultures GmbH

[Online] Available from https://www.dsmz.de/dsmz. [Accessed: 22/08/2023 2023].

Lenk L, Baccelli I, Winterberg D, Dietterle A, Corallo F, Taurelle J*, et al.* (2022). The IL7R-Antagonist OSE-127 Blocks Acute Lymphoblastic Leukemia Development Via a Dual Mode of Action. Blood 140**:** 1045-1047.

Li H, Yang Y, Hong W, Huang M, Wu M, & Zhao X (2020). Applications of genome editing technology in the targeted therapy of human diseases: mechanisms, advances and prospects. Signal Transduct Target Ther 5**:** 1.

Li S, Balmain A, & Counter CM (2018). A model for RAS mutation patterns in cancers: finding the sweet spot. Nature Reviews Cancer 18**:** 767-777.

Li S, Ting NS, Zheng L, Chen PL, Ziv Y, Shiloh Y*, et al.* (2000). Functional link of BRCA1 and ataxia telangiectasia gene product in DNA damage response. Nature 406**:** 210-215.

Loftfield E, Zhou W, Graubard BI, Yeager M, Chanock SJ, Freedman ND*, et al.* (2018). Predictors of mosaic chromosome Y loss and associations with mortality in the UK Biobank. Scientific reports 8**:** 1-10.

Loftus JP, Yahiaoui A, Brown PA, Niswander LM, Bagashev A, Wang M*, et al.* (2021). Combinatorial efficacy of entospletinib and chemotherapy in patient-derived xenograft models of infant acute lymphoblastic leukemia. Haematologica 106**:** 1067-1078.

Lu R, Wang P, Parton T, Zhou Y, Chrysovergis K, Rockowitz S*, et al.* (2016). Epigenetic Perturbations by Arg882-Mutated DNMT3A Potentiate Aberrant Stem Cell Gene-Expression Program and Acute Leukemia Development. Cancer Cell 30**:** 92-107.

Lu S, Jang H, Nussinov R, & Zhang J (2016). The Structural Basis of Oncogenic Mutations G12, G13 and Q61 in Small GTPase K-Ras4B. Scientific Reports 6**:** 21949.

Lu Y, Xue J, Deng T, Zhou X, Yu K, Deng L*, et al.* (2020). Safety and feasibility of CRISPR-edited T cells in patients with refractory non-small-cell lung cancer. Nature Medicine 26**:** 732-740.

Luis TC, Ichii M, Brugman MH, Kincade P, & Staal FJ (2012). Wnt signaling strength regulates normal hematopoiesis and its deregulation is involved in leukemia development. Leukemia 26**:** 414-421.

MacPherson L, & Dawson MA (2017). Survival of the Fittest: Darwinian Selection Underpins Chemotherapy Resistance in AML. Cell stem cell 21**:** 291-292.

Maik-Rachline G, Hacohen-Lev-Ran A, & Seger R (2019). Nuclear ERK: Mechanism of Translocation, Substrates, and Role in Cancer. Int J Mol Sci 20.

Maiti A, Rausch CR, Cortes J, E. , Pemmaraju N, Daver NG, Ravandi F*, et al.* (2020). Outcomes of relapsed or refractory acute myeloid leukemia after frontline hypomethylating agent and venetoclax regimens. Haematologica 106**:** 894-898.

Mandal PK, Ferreira LM, Collins R, Meissner TB, Boutwell CL, Friesen M*, et al.* (2014). Efficient ablation of genes in human hematopoietic stem and effector cells using CRISPR/Cas9. Cell Stem Cell 15**:** 643-652.

Marensi V, Keeshan KR, & MacEwan DJ (2021). Pharmacological impact of FLT3 mutations on receptor activity and responsiveness to tyrosine kinase inhibitors. Biochem Pharmacol 183**:** 114348.

Marlein CR, Zaitseva L, Piddock RE, Raso-Barnett L, Scott MA, Ingham CJ*, et al.* (2018). PGC-1α driven mitochondrial biogenesis in stromal cells underpins mitochondrial trafficking to leukemic blasts. Leukemia 32**:** 2073-2077.

Martino OD, & Welch JS (2019). Retinoic Acid Receptors in Acute Myeloid Leukemia Therapy. Cancers (Basel) 11.

Marusyk A, Almendro V, & Polyak K (2012). Intra-tumour heterogeneity: a looking glass for cancer? Nature Reviews Cancer 12**:** 323-334.

Maruyama T, Dougan SK, Truttmann MC, Bilate AM, Ingram JR, & Ploegh HL (2015). Increasing the efficiency of precise genome editing with CRISPR-Cas9 by inhibition of nonhomologous end joining. Nature Biotechnology 33**:** 538-542.

Masiuk KE, Zhang R, Osborne K, Hollis RP, Campo-Fernandez B, & Kohn DB (2019). PGE2 and Poloxamer Synperonic F108 Enhance Transduction of Human HSPCs with

a β-Globin Lentiviral Vector. Molecular Therapy - Methods & Clinical Development 13**:** 390-398.

Matteini F, Mulaw MA, & Florian MC (2021). Aging of the Hematopoietic Stem Cell Niche: New Tools to Answer an Old Question. Frontiers in Immunology 12.

McMahon CM, Ferng T, Canaani J, Wang ES, Morrissette JJD, Eastburn DJ*, et al.* (2019). Clonal Selection with RAS Pathway Activation Mediates Secondary Clinical Resistance to Selective FLT3 Inhibition in Acute Myeloid Leukemia. Cancer Discovery 9**:** 1050-1063.

Midic D, Rinke J, Perner F, Müller V, Hinze A, Pester F*, et al.* (2020). Prevalence and dynamics of clonal hematopoiesis caused by leukemia-associated mutations in elderly individuals without hematologic disorders. Leukemia 34**:** 2198-2205.

Miller M, & Miller L (2012). RAS Mutations and Oncogenesis: Not all RAS Mutations are Created Equally. Frontiers in Genetics 2.

Mistry JJ, Moore JA, Kumar P, Marlein CR, Hellmich C, Pillinger G*, et al.* (2021). Daratumumab inhibits acute myeloid leukaemia metabolic capacity by blocking mitochondrial transfer from mesenchymal stromal cells. Haematologica 106**:** 589-592.

Mitchell E, Spencer Chapman M, Williams N, Dawson KJ, Mende N, Calderbank EF*, et al.* (2022). Clonal dynamics of haematopoiesis across the human lifespan. Nature 606**:** 343-350.

Molina G, Vogt A, Bakan A, Dai W, Queiroz de Oliveira P, Znosko W*, et al.* (2009). Zebrafish chemical screening reveals an inhibitor of Dusp6 that expands cardiac cell lineages. Nat Chem Biol 5**:** 680-687.

Moore AR, Rosenberg SC, McCormick F, & Malek S (2020). RAS-targeted therapies: is the undruggable drugged? Nature Reviews Drug Discovery 19**:** 533-552.

Mor A, & Philips MR (2006). COMPARTMENTALIZED RAS/MAPK SIGNALING. Annual Review of Immunology 24**:** 771-800.

Moreno-Mateos MA, Vejnar CE, Beaudoin JD, Fernandez JP, Mis EK, Khokha MK*, et al.* (2015). CRISPRscan: designing highly efficient sgRNAs for CRISPR-Cas9 targeting in vivo. Nat Methods 12**:** 982-988.

Mortazavi A, Williams BA, McCue K, Schaeffer L, & Wold B (2008). Mapping and quantifying mammalian transcriptomes by RNA-Seq. Nat Methods 5**:** 621-628.

Mulligan G, Lichter DI, Di Bacco A, Blakemore SJ, Berger A, Koenig E*, et al.* (2014). Mutation of NRAS but not KRAS significantly reduces myeloma sensitivity to single-agent bortezomib therapy. Blood 123**:** 632-639.

Nagakubo Y, Hirotsu Y, Amemiya K, Oyama T, Mochizuki H, & Omata M (2019). Accurate detection of KRAS, NRAS and BRAF mutations in metastatic colorectal cancers by bridged nucleic acid-clamp real-time PCR. BMC Medical Genomics 12**:** 162.

Nemudryi AA, Valetdinova KR, Medvedev SP, & Zakian SM (2014). TALEN and CRISPR/Cas Genome Editing Systems: Tools of Discovery. Acta Naturae 6**:** 19-40.

Ng SW, Mitchell A, Kennedy JA, Chen WC, McLeod J, Ibrahimova N*, et al.* (2016). A 17-gene stemness score for rapid determination of risk in acute leukaemia. Nature 540**:** 433-437.

Ninomiya K, Ohashi K, Makimoto G, Tomida S, Higo H, Kayatani H*, et al.* (2018). MET or NRAS amplification is an acquired resistance mechanism to the third-generation EGFR inhibitor naquotinib. Scientific Reports 8**:** 1955.

Niroula A, Sekar A, Murakami MA, Trinder M, Agrawal M, Wong WJ*, et al.* (2021). Distinction of lymphoid and myeloid clonal hematopoiesis. Nat Med 27**:** 1921-1927.

Noguera NI, Catalano G, Banella C, Divona M, Faraoni I, Ottone T*, et al.* (2019). Acute Promyelocytic Leukemia: Update on the Mechanisms of Leukemogenesis, Resistance and on Innovative Treatment Strategies. Cancers. doi: 10.3390/cancers11101591

Ostrem JM, Peters U, Sos ML, Wells JA, & Shokat KM (2013). K-Ras(G12C) inhibitors allosterically control GTP affinity and effector interactions. Nature 503**:** 548-551.

Paniagua G, Jacob HKC, Brehey O, García-Alonso S, Lechuga CG, Pons T*, et al.* (2022). KSR induces RAS-independent MAPK pathway activation and modulates the efficacy of KRAS inhibitors. Molecular Oncology 16**:** 3066-3081.

Papaemmanuil E, Gerstung M, Bullinger L, Gaidzik VI, Paschka P, Roberts ND*, et al.* (2016). Genomic Classification and Prognosis in Acute Myeloid Leukemia. New England Journal of Medicine 374**:** 2209-2221.

Papaemmanuil E, Gerstung M, Malcovati L, Tauro S, Gundem G, Van Loo P*, et al.* (2013). Clinical and biological implications of driver mutations in myelodysplastic syndromes. Blood 122**:** 3616-3627; quiz 3699.

Papaioannou NY, Patsali P, Naiisseh B, Papasavva PL, Koniali L, Kurita R*, et al.* (2023). High-efficiency editing in hematopoietic stem cells and the HUDEP-2 cell line based on in vitro mRNA synthesis. Front Genome Ed 5**:** 1141618.

Parikh C, Subrahmanyam R, & Ren R (2007). Oncogenic NRAS, KRAS, and HRAS exhibit different leukemogenic potentials in mice. Cancer Res 67**:** 7139-7146.

Pattabiraman DR, & Weinberg RA (2014). Tackling the cancer stem cells - what challenges do they pose? Nat Rev Drug Discov 13**:** 497-512.

Pearce DJ, Taussig D, Zibara K, Smith LL, Ridler CM, Preudhomme C*, et al.* (2006). AML engraftment in the NOD/SCID assay reflects the outcome of AML: implications for our understanding of the heterogeneity of AML. Blood 107**:** 1166-1173.

Pérez-Mancera PA, Rust AG, van der Weyden L, Kristiansen G, Li A, Sarver AL*, et al.* (2012). The deubiquitinase USP9X suppresses pancreatic ductal adenocarcinoma. Nature 486**:** 266-270.

Perl AE, Larson RA, Podoltsev NA, Strickland S, Wang ES, Atallah E*, et al.* (2022). Follow-up of patients with R/R FLT3-mutation-positive AML treated with gilteritinib in the phase 3 ADMIRAL trial. Blood 139**:** 3366-3375.

Perl AE, Martinelli G, Cortes JE, Neubauer A, Berman E, Paolini S*, et al.* (2019). Gilteritinib or Chemotherapy for Relapsed or Refractory FLT3-Mutated AML. New England Journal of Medicine 381**:** 1728-1740.

Perurena N, Lock R, Davis RA, Raghavan S, Pilla NF, Ng R*, et al.* (2023). USP9X mediates an acute adaptive response to MAPK suppression in pancreatic cancer but creates multiple actionable therapeutic vulnerabilities. Cell Rep Med 4**:** 101007.

Pietrantonio F, Vernieri C, Siravegna G, Mennitto A, Berenato R, Perrone F*, et al.* (2017). Heterogeneity of Acquired Resistance to Anti-EGFR Monoclonal Antibodies in Patients with Metastatic Colorectal Cancer. Clin Cancer Res 23**:** 2414-2422.

Pinho S, Marchand T, Yang E, Wei Q, Nerlov C, & Frenette PS (2018). Lineage-Biased Hematopoietic Stem Cells Are Regulated by Distinct Niches. Developmental Cell 44**:** 634-641.e634.

Pollyea DA, Stevens BM, Jones CL, Winters A, Pei S, Minhajuddin M*, et al.* (2018). Venetoclax with azacitidine disrupts energy metabolism and targets leukemia stem cells in patients with acute myeloid leukemia. Nat Med 24**:** 1859-1866.

Prebet T, Sun Z, Ketterling RP, Zeidan A, Greenberg P, Herman J*, et al.* (2016). Azacitidine with or without Entinostat for the treatment of therapy-related myeloid neoplasm: further results of the E1905 North American Leukemia Intergroup study. Br J Haematol 172**:** 384-391.

Prior IA, Hood FE, & Hartley JL (2020). The Frequency of Ras Mutations in Cancer. Cancer Res.

Prior IA, Lewis PD, & Mattos C (2012). A comprehensive survey of Ras mutations in cancer. Cancer Res 72**:** 2457-2467.

Qiu N, Abegg D, Guidi M, Gilmore K, Seeberger PH, & Adibekian A (2022). Artemisinin inhibits NRas palmitoylation by targeting the protein acyltransferase ZDHHC6. Cell chemical biology 29**:** 530-537. e537.

Ragon BK, Odenike O, Baer MR, Stock W, Borthakur G, Patel K*, et al.* (2019). Oral MEK 1/2 Inhibitor Trametinib in Combination With AKT Inhibitor GSK2141795 in Patients With Acute Myeloid Leukemia With RAS Mutations: A Phase II Study. Clin Lymphoma Myeloma Leuk 19**:** 431-440.e413.

Raimondi V, Ciccarese F, & Ciminale V (2020). Oncogenic pathways and the electron transport chain: a dangeROS liaison. British Journal of Cancer 122**:** 168-181.

Ramirez M, Rajaram S, Steininger RJ, Osipchuk D, Roth MA, Morinishi LS*, et al.* (2016). Diverse drug-resistance mechanisms can emerge from drug-tolerant cancer persister cells. Nature Communications 7**:** 10690.

Ran FA, Hsu PD, Wright J, Agarwala V, Scott DA, & Zhang F (2013). Genome engineering using the CRISPR-Cas9 system. Nature Protocols 8**:** 2281-2308.

Randic T, Kozar I, Margue C, Utikal J, & Kreis S (2021). NRAS mutant melanoma: Towards better therapies. Cancer Treatment Reviews 99**:** 102238.

Randic T, Magni S, Philippidou D, Margue C, Grzyb K, Preis JR*, et al.* (2023). Single-cell transcriptomics of NRAS-mutated melanoma transitioning to drug resistance reveals P2RX7 as an indicator of early drug response. Cell Reports 42**:** 112696.

Rees HA, & Liu DR (2018). Base editing: precision chemistry on the genome and transcriptome of living cells. Nat Rev Genet 19**:** 770-788.

Ren J-G, Xing B, Lv K, O'Keefe RA, Wu M, Wang R*, et al.* (2023). RAB27B controls palmitoylation-dependent NRAS trafficking and signaling in myeloid leukemia. Journal of Clinical Investigation 133**:** e165510.

Reya T, Morrison SJ, Clarke MF, & Weissman IL (2001). Stem cells, cancer, and cancer stem cells. Nature 414**:** 105-111.

Rix B, Maduro AH, Bridge KS, & Grey W (2022). Markers for human haematopoietic stem cells: The disconnect between an identification marker and its function. Frontiers in Physiology 13.

Robinson MD, McCarthy DJ, & Smyth GK (2010). edgeR: a Bioconductor package for differential expression analysis of digital gene expression data. Bioinformatics 26**:** 139-140.

Rocks O, Peyker A, Kahms M, Verveer PJ, Koerner C, Lumbierres M*, et al.* (2005). An Acylation Cycle Regulates Localization and Activity of Palmitoylated Ras Isoforms. Science 307**:** 1746-1752.

Romero D (2020). Two new agents target KRAS G12C. Nature Reviews Clinical Oncology 17**:** 6-6.

Rosenberg MW, Watanabe-Smith K, Tyner JW, Tognon CE, Druker BJ, & Borate U (2020). Genomic markers of midostaurin drug sensitivity in FLT3 mutated and FLT3 wild-type acute myeloid leukemia patients. Oncotarget 11**:** 2807-2818.

Roy L, & Cowden Dahl KD (2018). Can stemness and chemoresistance be therapeutically targeted via signaling pathways in ovarian cancer? Cancers 10**:** 241.

Rushworth SA, Zaitseva L, Murray MY, Shah NM, Bowles KM, & MacEwan DJ (2012). The high Nrf2 expression in human acute myeloid leukemia is driven by NF-κB and underlies its chemo-resistance. Blood 120**:** 5188-5198.

Russo M, Crisafulli G, Sogari A, Reilly NM, Arena S, Lamba S*, et al.* (2019). Adaptive mutability of colorectal cancers in response to targeted therapies. Science 366**:** 1473.

Russo M, Lamba S, Lorenzato A, Sogari A, Corti G, Rospo G*, et al.* (2018). Reliance upon ancestral mutations is maintained in colorectal cancers that heterogeneously evolve during targeted therapies. Nature Communications 9**:** 2287.

Ryu MJ, Han J, Kim SJ, Lee MJ, Ju X, Lee YL*, et al.* (2019). PTEN/AKT signaling mediates chemoresistance in refractory acute myeloid leukemia through enhanced glycolysis. Oncol Rep 42**:** 2149-2158.

Saikali Z, & Singh G (2003). Doxycycline and other tetracyclines in the treatment of bone metastasis. Anti-Cancer Drugs 14.

Santini V, & Ossenkoppele GJ (2019). Hypomethylating agents in the treatment of acute myeloid leukemia: A guide to optimal use. Crit Rev Oncol Hematol 140**:** 1-7.

Santoni-Rugiu E, Melchior LC, Urbanska EM, Jakobsen JN, Stricker Kd, Grauslund M*, et al.* (2019). Intrinsic resistance to EGFR-Tyrosine Kinase Inhibitors in EGFR-Mutant Non-Small Cell Lung Cancer: Differences and Similarities with Acquired Resistance. Cancers 11**:** 923.

Saygin C, Matei D, Majeti R, Reizes O, & Lathia JD (2019). Targeting Cancer Stemness in the Clinic: From Hype to Hope. Cell Stem Cell 24**:** 25-40.

Schiffer CA SR (2003). Morphologic Classification and Clinical and Laboratory Correlates. In Holland-Frei Cancer Medicine 6th edition. BC Decker: Hamilton (ON).

Schlenk RF, Kayser S, Bullinger L, Kobbe G, Casper J, Ringhoffer M*, et al.* (2014). Differential impact of allelic ratio and insertion site in FLT3-ITD-positive AML with respect to allogeneic transplantation. Blood 124**:** 3441-3449.

Schmidt M, Goebeler M, Posern G, Feller SM, Seitz CS, Bröcker E-B*, et al.* (2000). Ras-independent Activation of the Raf/MEK/ERK Pathway upon Calcium-induced Differentiation of Keratinocytes*. Journal of Biological Chemistry 275**:** 41011-41017.

Schubert MS, Thommandru B, Woodley J, Turk R, Yan S, Kurgan G*, et al.* (2021). Optimized design parameters for CRISPR Cas9 and Cas12a homology-directed repair. Scientific Reports 11**:** 19482.

Sekeres MA, Elson P, Kalaycio ME, Advani AS, Copelan EA, Faderl S*, et al.* (2009). Time from diagnosis to treatment initiation predicts survival in younger, but not older, acute myeloid leukemia patients. Blood 113**:** 28-36.

Seth S, Li C-Y, Ho IL, Corti D, Loponte S, Sapio L*, et al.* (2019). Pre-existing Functional Heterogeneity of Tumorigenic Compartment as the Origin of Chemoresistance in Pancreatic Tumors. Cell Reports 26**:** 1518-1532.e1519.

Sexauer A, Perl A, Yang X, Borowitz M, Gocke C, Rajkhowa T*, et al.* (2012). Terminal myeloid differentiation in vivo is induced by FLT3 inhibition in FLT3/ITD AML. Blood 120**:** 4205-4214.

Shallis RM, Wang R, Davidoff A, Ma X, & Zeidan AM (2019). Epidemiology of acute myeloid leukemia: Recent progress and enduring challenges. Blood Reviews 36**:** 70-87.

Shapiro GI, LoRusso P, Kwak E, Pandya S, Rudin CM, Kurkjian C*, et al.* (2020). Phase Ib study of the MEK inhibitor cobimetinib (GDC-0973) in combination with the PI3K inhibitor pictilisib (GDC-0941) in patients with advanced solid tumors. Invest New Drugs 38**:** 419-432.

Shin S-M, Kim J-S, Park S-W, Jun S-Y, Kweon H-J, Choi D-K*, et al.* (2020). Direct targeting of oncogenic RAS mutants with a tumor-specific cytosol-penetrating antibody inhibits RAS mutant–driven tumor growth. Science Advances 6**:** eaay2174.

Shlush LI (2018). Age-related clonal hematopoiesis. Blood 131**:** 496-504.

Shlush LI, Mitchell A, Heisler L, Abelson S, Ng SWK, Trotman-Grant A*, et al.* (2017). Tracing the origins of relapse in acute myeloid leukaemia to stem cells. Nature 547**:** 104-108.

Shojaee S, Caeser R, Buchner M, Park E, Swaminathan S, Hurtz C*, et al.* (2015). Erk Negative Feedback Control Enables Pre-B Cell Transformation and Represents a Therapeutic Target in Acute Lymphoblastic Leukemia. Cancer Cell 28**:** 114-128.

Short NJ, Rytting ME, & Cortes JE (2018). Acute myeloid leukaemia. Lancet 392**:** 593-606.

Silver AJ, Bick AG, & Savona MR (2021). Germline risk of clonal haematopoiesis. Nature Reviews Genetics 22**:** 603-617.

Siravegna G, Mussolin B, Buscarino M, Corti G, Cassingena A, Crisafulli G*, et al.* (2015). Clonal evolution and resistance to EGFR blockade in the blood of colorectal cancer patients. Nature medicine 21**:** 795-801.

Smith CC, Levis MJ, Perl AE, Hill JE, Rosales M, & Bahceci E (2022). Molecular profile of FLT3-mutated relapsed/refractory patients with AML in the phase 3 ADMIRAL study of gilteritinib. Blood Advances 6**:** 2144-2155.

Smith MJ, Neel BG, & Ikura M (2013). NMR-based functional profiling of RASopathies and oncogenic RAS mutations. Proceedings of the National Academy of Sciences 110**:** 4574-4579.

Song H, Fares M, Maguire KR, Sidén A, & Potácová Z (2014). Cytotoxic effects of tetracycline analogues (doxycycline, minocycline and COL-3) in acute myeloid leukemia HL-60 cells. PLoS One 9**:** e114457.

Staal FJT, Chhatta A, & Mikkers H (2016). Caught in a Wnt storm: Complexities of Wnt signaling in hematopoiesis. Experimental Hematology 44**:** 451-457.

Stahl M, Menghrajani K, Derkach A, Chan A, Xiao W, Glass J*, et al.* (2021). Clinical and molecular predictors of response and survival following venetoclax therapy in relapsed/refractory AML. Blood Advances 5**:** 1552-1564.

Stephen Andrew G, Esposito D, Bagni Rachel K, & McCormick F (2014). Dragging Ras Back in the Ring. Cancer Cell 25**:** 272-281.

Stone RM, Mandrekar SJ, Sanford BL, Laumann K, Geyer S, Bloomfield CD*, et al.* (2017). Midostaurin plus Chemotherapy for Acute Myeloid Leukemia with a FLT3 Mutation. New England Journal of Medicine 377**:** 454-464.

Sun N, Petiwala S, Wang R, Lu C, Hu M, Ghosh S*, et al.* (2019). Development of drug-inducible CRISPR-Cas9 systems for large-scale functional screening. BMC Genomics 20**:** 225.

Sutherland H, Blair A, & Zapf R (1996). Characterization of a hierarchy in human acute myeloid leukemia progenitor cells. Blood 87**:** 4754-4761.

Suzuki T, Tsukumo Y, Furihata C, Naito M, & Kohara A (2020). Preparation of the standard cell lines for reference mutations in cancer gene-panels by genome editing in HEK 293 T/17 cells. Genes Environ 42**:** 8.

Tan E, Chin CSH, Lim ZFS, & Ng SK (2021). HEK293 Cell Line as a Platform to Produce Recombinant Proteins and Viral Vectors. Front Bioeng Biotechnol 9**:** 796991.

Tate JG, Bamford S, Jubb HC, Sondka Z, Beare DM, Bindal N*, et al.* (2019). COSMIC: the Catalogue Of Somatic Mutations In Cancer. Nucleic Acids Research 47**:** D941-D947.

TCGA Network (2013). Genomic and Epigenomic Landscapes of Adult De Novo Acute Myeloid Leukemia. New England Journal of Medicine 368**:** 2059-2074.

The Cancer Genome Atlas (2013). Genomic and Epigenomic Landscapes of Adult De Novo Acute Myeloid Leukemia. New England Journal of Medicine 368**:** 2059-2074.

The ICGC/TCGA Pan-Cancer Analysis of Whole Genomes Consortium (2020). Pan-cancer analysis of whole genomes. Nature 578**:** 82-93.

Thompson DJ, Genovese G, Halvardson J, Ulirsch JC, Wright DJ, Terao C*, et al.* (2019). Genetic predisposition to mosaic Y chromosome loss in blood. Nature 575**:** 652-657.

To MD, Perez-Losada J, Mao JH, & Balmain A (2005). Crosstalk between Pten and Ras signaling pathways in tumor development. Cell Cycle 4**:** 1185-1188.

Tomellini E, Fares I, Lehnertz B, Chagraoui J, Mayotte N, MacRae T*, et al.* (2019). Integrin-α3 Is a Functional Marker of Ex Vivo Expanded Human Long-Term Hematopoietic Stem Cells. Cell Rep 28**:** 1063-1073.e1065.

Turajlic S, Sottoriva A, Graham T, & Swanton C (2019). Resolving genetic heterogeneity in cancer. Nature Reviews Genetics 20**:** 404-416.

Tyner JW, Erickson H, Deininger MW, Willis SG, Eide CA, Levine RL*, et al.* (2009). High-throughput sequencing screen reveals novel, transforming RAS mutations in myeloid leukemia patients. Blood 113**:** 1749-1755.

Tyner JW, Tognon CE, Bottomly D, Wilmot B, Kurtz SE, Savage SL*, et al.* (2018). Functional genomic landscape of acute myeloid leukaemia. Nature 562**:** 526-531.

Uy GL, Rettig MP, Motabi IH, McFarland K, Trinkaus KM, Hladnik LM*, et al.* (2012). A phase 1/2 study of chemosensitization with the CXCR4 antagonist plerixafor in relapsed or refractory acute myeloid leukemia. Blood 119**:** 3917-3924.

Valent P, Kern W, Hoermann G, Milosevic Feenstra JD, Sotlar K, Pfeilstöcker M*, et al.* (2019). Clonal Hematopoiesis with Oncogenic Potential (CHOP): Separation from CHIP and Roads to AML. Int J Mol Sci 20.

Van Cutsem E, van de Velde H, Karasek P, Oettle H, Vervenne WL, Szawlowski A*, et al.* (2004). Phase III trial of gemcitabine plus tipifarnib compared with gemcitabine plus placebo in advanced pancreatic cancer. J Clin Oncol 22**:** 1430-1438.

Vandergaast R (2017). *Which antibiotic selection gene? Unnatural selection: using antibiotic selection genes with reporter-expressing eukaryotic cells.* [Online] Available from https://imanislife.com/sciencetalk/antibiotic-selection-gene/. [Accessed: 21/08/2023 2023].

Wang X, Allen S, Blake JF, Bowcut V, Briere DM, Calinisan A, et al. (2022). Identification of MRTX1133, a Noncovalent, Potent, and Selective KRASG12D Inhibitor. Journal of Medicinal Chemistry 65: 3123-3133.

Wang C, Xiang R, Zhang X, & Chen Y (2015). Doxycycline inhibits leukemic cell migration via inhibition of matrix metalloproteinases and phosphorylation of focal adhesion kinase. Mol Med Rep 12**:** 3374-3380.

Wang F, Morita K, DiNardo CD, Furudate K, Tanaka T, Yan Y*, et al.* (2021). Leukemia stemness and co-occurring mutations drive resistance to IDH inhibitors in acute myeloid leukemia. Nat Commun 12**:** 2607.

Wang S, Wu Z, Li T, Li Y, Wang W, Hao Q*, et al.* (2020). Mutational spectrum and prognosis in NRAS-mutated acute myeloid leukemia. Sci Rep 10**:** 12152.

Waters AM, & Der CJ (2018). KRAS: The Critical Driver and Therapeutic Target for Pancreatic Cancer. Cold Spring Harb Perspect Med 8.

Waters AM, Ozkan-Dagliyan I, Vaseva AV, Fer N, Strathern LA, Hobbs GA*, et al.* (2017). Evaluation of the selectivity and sensitivity of isoform- and mutation-specific RAS antibodies. Sci Signal 10.

Werner-Klein M, Scheitler S, Hoffmann M, Hodak I, Dietz K, Lehnert P*, et al.* (2018). Genetic alterations driving metastatic colony formation are acquired outside of the primary tumour in melanoma. Nature Communications 9**:** 595.

Westermann L, Neubauer B, & Köttgen M (2021). Nobel Prize 2020 in Chemistry honors CRISPR: a tool for rewriting the code of life. Pflugers Arch 473**:** 1-2.

Whyte DB, Kirschmeier P, Hockenberry TN, Nunez-Oliva I, James L, Catino JJ*, et al.* (1997). K- and N-Ras Are Geranylgeranylated in Cells Treated with Farnesyl Protein Transferase Inhibitors*. Journal of Biological Chemistry 272**:** 14459-14464.

Willemze R, Suciu S, Meloni G, Labar B, Marie J-P, Halkes CJM*, et al.* (2013). High-Dose Cytarabine in Induction Treatment Improves the Outcome of Adult Patients Younger Than Age 46 Years With Acute Myeloid Leukemia: Results of the EORTC-GIMEMA AML-12 Trial. Journal of Clinical Oncology 32**:** 219-228.

Winiarska M, Nowis D, Firczuk M, Zagozdzon A, Gabrysiak M, Sadowski R*, et al.* (2017). Selection of an optimal promoter for gene transfer in normal B cells. Mol Med Rep 16**:** 3041-3048.

Winter JJ, Anderson M, Blades K, Brassington C, Breeze AL, Chresta C*, et al.* (2015). Small molecule binding sites on the Ras:SOS complex can be exploited for inhibition of Ras activation. J Med Chem 58**:** 2265-2274.

Wright DJ, Day FR, Kerrison ND, Zink F, Cardona A, Sulem P*, et al.* (2017). Genetic variants associated with mosaic Y chromosome loss highlight cell cycle genes and overlap with cancer susceptibility. Nature Genetics 49**:** 674-679.

Wu Q, Zhang J, & Lucas D (2021). Anatomy of Hematopoiesis and Local Microenvironments in the Bone Marrow. Where to? Frontiers in Immunology 12.

Wu QN, Liao YF, Lu YX, Wang Y, Lu JH, Zeng ZL*, et al.* (2018). Pharmacological inhibition of DUSP6 suppresses gastric cancer growth and metastasis and overcomes cisplatin resistance. Cancer Lett 412**:** 243-255.

Yao Q, Chen Y, & Zhou X (2019). The roles of microRNAs in epigenetic regulation. Curr Opin Chem Biol 51**:** 11-17.

Yeh C-H, Moles R, & Nicot C (2016). Clinical significance of microRNAs in chronic and acute human leukemia. Molecular Cancer 15**:** 37.

You Z, & Bailis JM (2010). DNA damage and decisions: CtIP coordinates DNA repair and cell cycle checkpoints. Trends Cell Biol 20**:** 402-409.

Young AL, Challen GA, Birmann BM, & Druley TE (2016). Clonal haematopoiesis harbouring AML-associated mutations is ubiquitous in healthy adults. Nat Commun 7**:** 12484.

Yu G, Wang LG, Han Y, & He QY (2012). clusterProfiler: an R package for comparing biological themes among gene clusters. Omics 16**:** 284-287.

Zeller C, Richter D, Jurinovic V, Valtierra-Gutiérrez IA, Jayavelu AK, Mann M*, et al.* (2022). Adverse stem cell clones within a single patient's tumor predict clinical outcome in AML patients. Journal of Hematology & Oncology 15**:** 25.

Zhang B, Metharom P, Jullie H, Ellem KA, Cleghorn G, West MJ*, et al.* (2004). The significance of controlled conditions in lentiviral vector titration and in the use of multiplicity of infection (MOI) for predicting gene transfer events. Genet Vaccines Ther 2**:** 6.

Zhang H, Savage S, Schultz AR, Bottomly D, White L, Segerdell E*, et al.* (2019). Clinical resistance to crenolanib in acute myeloid leukemia due to diverse molecular mechanisms. Nature Communications 10**:** 244.

Zhang J, Johnson M, Barve M, Bazhenova L, McCarthy M, Schwartz R*, et al.* (2023). Practical Guidance for the Management of Adverse Events in Patients with KRASG12C-Mutated Non-Small Cell Lung Cancer Receiving Adagrasib. Oncologist 28**:** 287-296.

Zhang P, Brinton LT, Gharghabi M, Sher S, Williams K, Cannon M*, et al.* (2022a). Targeting OXPHOS de novo purine synthesis as the nexus of FLT3 inhibitor-mediated synergistic antileukemic actions. Sci Adv 8**:** eabp9005.

Zhang Q, Riley-Gillis B, Han L, Jia Y, Lodi A, Zhang H*, et al.* (2022b). Activation of RAS/MAPK pathway confers MCL-1 mediated acquired resistance to BCL-2 inhibitor venetoclax in acute myeloid leukemia. Signal Transduction and Targeted Therapy 7**:** 51.

Zhang Z, Gao R, Hu Q, Peacock H, Peacock DM, Dai S*, et al.* (2020). GTP-State-Selective Cyclic Peptide Ligands of K-Ras(G12D) Block Its Interaction with Raf. ACS Cent Sci 6**:** 1753-1761.

Zhang Z, Guiley KZ, & Shokat KM (2022). Chemical acylation of an acquired serine suppresses oncogenic signaling of K-Ras(G12S). Nat Chem Biol 18**:** 1177-1183.

Zhang Z, Kobayashi S, Borczuk AC, Leidner RS, LaFramboise T, Levine AD*, et al.* (2010). Dual specificity phosphatase 6 (DUSP6) is an ETS-regulated negative feedback mediator of oncogenic ERK signaling in lung cancer cells. Carcinogenesis 31**:** 577-586.

Zhang Z, Morstein J, Ecker AK, Guiley KZ, & Shokat KM (2022). Chemoselective Covalent Modification of K-Ras(G12R) with a Small Molecule Electrophile. J Am Chem Soc 144**:** 15916-15921.

Zhu Y-M, Wang P-P, Huang J-Y, Chen Y-S, Chen B, Dai Y-J*, et al.* (2017). Gene mutational pattern and expression level in 560 acute myeloid leukemia patients and their clinical relevance. Journal of Translational Medicine 15**:** 178.

Zuchegna C, Di Zazzo E, Moncharmont B, & Messina S (2020). Dual-specificity phosphatase (DUSP6) in human glioblastoma: epithelial-to-mesenchymal transition (EMT) involvement. BMC Research Notes 13**:** 374.